UNIVERSITÀ DEGLI STUDI DI TRIESTE

XXXII CICLO DEL DOTTORATO DI RICERCA IN NANOTECNOLOGIE

SUPRAMOLECULAR NANOSTRUCTURES OF SULFUR-CONTAINING TRIPEPTIDES IN WATER

Settore scientifico-disciplinare: CHIM/06

DOTTORANDO / A
MARIA CRISTINA CRINGOLI

COORDINATORE
PROF. ALBERTO MORGANTE

SUPERVISORE DI TESI
PROF. SILVIA MARCHESAN

CO-SUPERVISORE DI TESI
PROF. PAOLO FORNASIERO

ANNO ACCADEMICO 2018/2019

Contents

List of Abbreviations

AFM	Atomic Force Microscopy
Ala	Alanine
Asn	Asparagine
Asp	Aspartic Acid
ATP	Adenosine Triphosphate
CD	Circular Dichroism
$CDCl_3$	Deuterated Chloroform
Cys	Cysteine
DCM	Dichloromethane
DIPEA	*N*, *N*-Diisopropylethylamine
DMF	Dimethylformamide
DMSO-d_6	Deuterated Dimethyl Sulfoxide
DNA	Deoxyribonucleic Acid
DSC	Differential Scanning Calorimetry
DTNB	5,5'-dithio-bis-(2-nitrobenzoic acid), Ellman's reagent
DTT	Dithiothreitol
EDT	1,2-Ethanedithiol
EDTA	Ethylenediaminetetraacetic Acid
EDX	Electron Dispersive X-Ray
ESEM	Environmental Scanning Electron Microscopy
ESI-MS	Electrospray Ionization Mass Spectrometry
Eth D-1	Ethidium Homodimer Dye
Fmoc	Fluorenylmethyloxycarbonyl
FTIR	Fourier Transform Infrared Spectroscopy
G'	Elastic or storage modulus
G"	Viscous or loss modulus
Gln	Glutamine
Glu	Glutamic Acid
Gly	Glycine

HBTU	*N,N,N′,N′*-Tetramethyl-*O*-(1*H*-benzotriazol-1-yl)uronium hexafluorophosphate
HFIP	Hexafluoroisopropanol
HOAt	1-Hydroxy-7-azabenzotriazole
IR	Infrared
LC-MS	Liquid Chromatography-Mass Spectrometry
Leu	Leucine
m.p.	Melting Point
MD	Molecular Dynamics
MeCN	Acetonitrile
MeOH	Methanol
Met	Methionine
Mg^{++}	Magnesium Divalent Cation
MTS	Methane Thiosulfonate
NMDAR	*N*-Methyl-D-Aspartic Acid
NMR	Nuclear Magnetic Resonance
NSAID	Nonsteroidal Anti-Inflammatory Drugs
PBS	Phosphate Buffered Saline
PEG	Polyethylene Glycol
Phe	Phenylalanine
pI	Isoelectric Point
Pro	Proline
RP-HPLC	Reverse Phase-High Performance Liquid Chromatography
SAM	Self-Assembled Monolayer
SD	Standard Deviation
SEM	Scanning Electron Microscopy
Ser	Serine
$SOCl_2$	Thionyl chloride
SPPS	Solid Phase Peptide Synthesis
STEM	Scanning Transmission Electron Microscopy
STM	Scanning Tunnelling Microscopy
tBuSH	Tert-butylthiol
TCEP	Tris(2-carboxyethyl)phosphine

TEM	Transmission Electron Microscopy
TEMPO	2,2,6,6-Tetramethyl-1-piperidinyloxy
TFA	Trifluoroacetic Acid
THF	Tetrahydrofuran
ThT	Thioflavin T
TIPS	Triisopropylsilane
TLC	Thin-Layer Chromatography
Tm	Melting Temperature
TMP	2,2,6,6-Tetramethylpiperidine, Collidine
TMS	Tetramethylsilane
TNB	2-nitro-5-thiobenzoic Acid
TPPTS	Triphenylphosphine-3,3′,3″-trisulfonic Acid Trisodium Salt
UV	Ultraviolet Radiation
UV-Vis	Ultraviolet-visible Radiation
VA-044	2,2’-azobis[2-(2-imidazolin-2-yl)propane]dihydrochloride
Val	Valine
XRD	X-Ray Diffraction

Abstract

Nanomaterials have attracted attention in several research fields, such as chemical catalysis, medicine, and engineering. Among the broad range of nanostructured materials that have been developed in recent years, self-assembling short peptides are attractive minimalistic bioactive motifs and low-cost building blocks for supramolecular nanostructured hydrogels. They are inherently biocompatible and biodegradable functional nanomaterials, useful to the creation of novel therapeutic paradigms in nanomedicine.

This PhD thesis studied the self-assembly of heterochiral tripeptides, where the presence of both D- and L-amino acids at specific positions along the sequences is evaluated as a useful tool to obtain supramolecular nanostructured hydrogels at physiological conditions. These sequences typically contain two phenylalanine residues for self-assembly, and thus far those reported to form supramolecular hydrogels were composed of hydrophobic amino acids devoid of functional groups in the side chain. However, the presence of a sulfur atom in the peptide sequence could give interesting added properties, such as the possibility to undergo redox cycles, metal coordination, or sulfur-based reversible chemistry.

In this PhD thesis, new self-assembling heterochiral tripeptides that contain two phenylalanine residues (to drive the process) and either methionine or cysteine are described in ***Chapter 3*** and ***Chapter 4***, respectively. Peptides were synthesized *via* a standard Fmoc-based solid-phase peptide synthesis and then purified by reverse-phase HPLC. ESI–MS, ^{1}H-NMR, and ^{13}C-NMR have been carried out to have a spectroscopic characterisation of the molecules. After having obtained nanostructured hydrogels from peptide self-assembly, supramolecular behaviour of these materials has been characterised performing rheology analysis, circular dichroism analysis (CD), Fourier-transform infrared spectroscopy (FT-IR) and Thioflavin T fluorescence assay. Moreover, nanomorphology of the hydrogels, which are mainly composed of nanofibers, has been assessed by means of transmission electron microscopy (TEM). Single-crystal X-ray diffraction (XRD) studies on self-assembling peptides showed the ability of these peptides to form water channels, thanks to a clear segregation of the hydrophilic part (peptide backbone) and the hydrophobic part (side chains) of the tripeptides. Their biocompatibility was tested in fibroblast cell culture *in vitro*. After 72 hours, the cells presented a good viability and the hydrogels did not lead to cytotoxicity.

The possibility to disassemble such nanostructured hydrogels, using an external stimulus to create new smart materials, has been discussed in ***Chapter 5***. In particular, thermoreversibility has been investigated as a useful tool to disassemble a hydrogel by heating it up. The re-assembly has been easily achieved by cooling down the system. Moreover, sulfur-based chemistry has been exploited to induce selective disassembly of a hydrogel deriving from a cysteine containing peptide, by means of reaction with bromomaleimide. A photo-triggered desulfurization protocol in water has been reported to irreversibly disassemble a nanostructured hydrogel for its final disposal after use, by converting an assembling peptide into a non-assembling one. The reaction was followed by ^{1}H-NMR, ^{31}P-NMR, LC-MS, and Raman analyses. The use of light as trigger allowed spatial patterning by using a photomask.

Riassunto

Negli ultimi anni si è assistito ad un crescente sviluppo di materiali nanostrutturati in diversi campi applicativi, tra cui catalisi chimica, medicina e ingegneria. Tra le numerose tipologie di nanomateriali identificati, piccoli peptidi capaci di auto-assemblarsi in idrogel nanostrutturati hanno ottenuto un peculiare interesse in particolar modo nel campo della nanomedicina, grazie alle loro proprietà uniche, quali biocompatibilità e biodegradabilità.

In questa tesi di dottorato, tripeptidi eterochirali, contenenti, cioè, sia amminoacidi D che L nella stessa sequenza, sono stati studiati per le loro capacità di auto-organizzarsi in condizioni fisiologiche in idrogel nanostrutturati. I peptidi con questo design riportati finora sono generalmente costituiti da amminoacidi idrofobici e aromatici con lo scopo di favorirne l'autoassemblaggio; tuttavia, la presenza di gruppi funzionali nelle catene laterali degli amminoacidi, potrebbe fornire nuove prospettive applicative. Ad esempio, la presenza dello zolfo potrebbe essere sfruttata per integrare nuove proprietà dinamiche nel nanomateriale, come la possibilità di coordinare metalli o indurre reazioni di ossido-riduzione.

In questo studio, dunque, sono stati individuati nuovi tripeptidi eterochirali in grado di auto-assemblare in idrogel. Le sequenze peptidiche sono costituite da due residui di fenilalanina e un terzo residuo amminoacidico contenente l'atomo di zolfo in catena laterale, ossia la metionina (***Capitolo 3***) o la cisteina (***Capitolo 4***). Il lavoro è iniziato con la sintesi in fase solida dei tripeptidi, che sono stati poi purificati mediante HPLC a fase inversa. L'identità e la purezza dei composti sintetizzati sono state verificate tramite studi di massa, ^{1}H-NMR e ^{13}C-NMR. L'organizzazione supramolecolare di materiali ottenuti è stata poi analizzata e caratterizzata mediante l'utilizzo di diverse tecniche, tra cui analisi di reologia, dicroismo circolare (CD), spettroscopia infrarossa e saggi di fluorescenza amiloide. Studi di microscopia a trasmissione elettronica hanno inoltre permesso di analizzare la nano-morfologia dei materiali ottenuti, che sono risultati essere costituiti principalmente da fibre di diametro dell'ordine dei nanometri. Le analisi di diffrazione ai raggi X sul singolo cristallo hanno inoltre mostrato come le molecole peptidiche sono in grado di organizzarsi in maniera altamente ordinata a formare interessanti strutture canalari, in cui la catena peptidica identifica la cavità idrofilica del canale, completamente separata dall' ambiente idrofobico esterno, in cui le catene amminoacidiche laterali sono immerse. Inoltre, saggi di tossicità cellulare *in vitro* effettuati su fibroblasti hanno evidenziato una buona biocompatibilità degli idrogel nanostrutturati.

Nel ***Capitolo 5***, infine, sono state discusse tre diverse strategie utilizzabili per indurre un disassemblaggio controllato degli idrogel identificati, in modo da ottenere materiali intelligenti in grado di rispondere a stimoli esterni di tipo fisico, chimico o fotochimico. In particolare, la termoreversibiltà dei materiali è stata studiata per un approccio reversibile e indipendente dalla presenza dello zolfo. Quest'ultima è stata invece sfruttata per garantire un disassemblaggio esclusivo di peptidi contenenti cisteina, grazie alla loro selettiva reattività con bromomaleimide. Infine, un approccio fotochimico ha permesso di individuare un nuovo protocollo basato sulla desulfurizzazione della cisteina per garantire un disassemblaggio spazialmente controllato e irreversibile dell'idrogel nanostrutturato. L'andamento della reazione è stato seguito attraverso studi di ^{1}H-NMR, ^{31}P-NMR, LC-MS, e spettroscopia Raman.

Chapter 1: General Introduction

1.1. Chirality and Amino Acids

In 1848, the French chemist and microbiologist L. Pasteur identified the existence of two different crystals of tartaric acid. He noticed that they were both optically active, but they rotated the polarised light in opposite directions.[1] This was the earliest observation of chirality. Now it is known that those two types were the enantiomeric form of the same molecule, it means that they were non-superimposable mirror images of each other, because they adopted opposite spatial arrangement.

Chirality plays a key role in living systems and it is transferred from subatomic scale (neutrino) to macroscale (*e.g.*, snail shells, plants, animals, and galaxies), passing through molecular (chiral molecules, such as amino acids, carbohydrates) and supramolecular levels (nanosized biomacromolecules, such as DNA, proteins, and viruses), as shown in **Figure 1.1.**[2] Asymmetry is necessary to determine the three-dimensional architecture and, thus, the functionality of many biomacromolecules, such as the selective interactions of small molecules with receptors and enzymes.

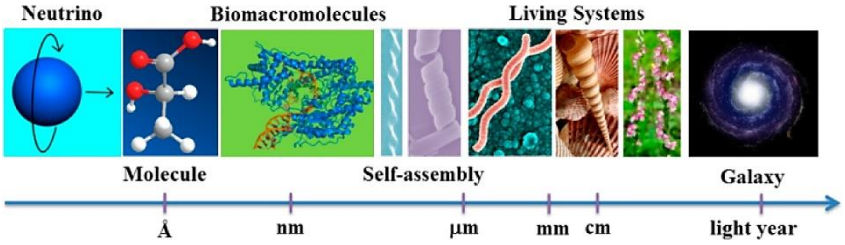

Figure 1.1. Chiral architectures at various scales. Reprinted with permission from ref. 2[Note] © 2015 American Chemical Society.[2]

The presence of four different types of atoms or functional groups (*i.e.*, a carboxyl group, an amine group, a hydrogen, and an aromatic or aliphatic side chain) bonded to the α-carbon of amino acids makes them chiral molecules, except from glycine (Gly), which is achiral

[Note] The picture of a protein structure was obtained from Wikipedia (http://upload.wikimedia.org/wikipedia/commons/f/f3/T7RNA_polymerase_at_work.png) and reprinted under the "fair use" under Wikipedia's license. Pictures are obtained from the following Web sites and apply to "fair use": bacteria (http://tech.sina.com.cn/d/2010-01-29/10113816919.shtml), seashell (http://news.hainan.net/hainan/yaowen/tupian/2014/08/14/2016639.shtml), and flower (http://www.chla.com.cn/htm/2011/0403/80069.html). The picture of a galaxy is a free stock graphic obtained from http://www.rgbstock.com/bigphoto/mVErmjU%2FSpiral+Galaxy.

because it displays two hydrogen atoms on α-carbon.[3] The absolute configurations of chiral amino acids are named D- or L-, according to the system proposed by E. Fischer for glyceraldehyde, the smallest carbohydrate with an asymmetric carbon atom.[4] All common amino acids, except glycine, have L- and D-enantiomers, depending on the relative spatial arrangement surrounding the α-carbon.

Although amino acids present in nature were commonly considered to occur only in L-form, D-amino acids have been detected in many biological organisms, where they exhibit several physiological functions.[5] Nevertheless, their distribution and regulation are completely different from those of L-enantiomers.[6]

1.1.1. D-Amino Acids in Living Systems

D-amino acids, as free forms or contained in peptides, have been widespread isolated from a considerable variety of living organisms. For example, they own a fundamental role in bacteria, to protect them from protease degradation. Actually, peptidoglycans, present in bacterial cell wall, contain D-aspartic acid (^{D}Asp), D-asparagine (^{D}Asn), D-glutamic acid (^{D}Glu), D-glutamine (^{D}Gln) and D-alanine (^{D}Ala).[7, 8]

D-chirality is also necessary in many insects, such as fireflies and luminous beetles, whose bioluminescence is exclusively attributed to the D-enantiomer of firefly luciferin, and not to its L-enantiomer. Luciferase enzyme, in presence of adenosine triphosphate (ATP), magnesium divalent cation (Mg^{++}), and molecular oxygen (O_2), catalyses the bioluminescence reaction, in which the D-enantiomer of luciferin is activated to emit visible photons.[9] D-Luciferin can be synthesized using 2-cyano-6-hydroxybenzothiazole and the amino acid D-cysteine (^{D}Cys), as reported in **Scheme 1.1**. If L-cysteine is used for the synthesis, L-luciferin was obtained, but no light emission was observed. This suggests the presence of ^{D}Cys in such insects.[10]

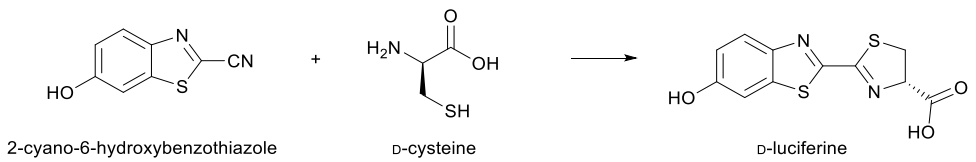

Scheme 1.1 Synthesis of D-firefly luciferin starting from ^{D}Cys.

Moreover, many invertebrates, such as molluscs and marine shellfishes, present D-amino acids (mainly ^{D}Asp and ^{D}Ala).[10 11, 12] They were also found in numerous plants, as tobacco leaves, rice and seeds.[13]

Peptides containing D-amino acids were also detected in several vertebrate animals. For instance, the heptapeptide dermorphin, isolated from the skin secretions of frog *Phyllomedusa sauvage*, contains a D-methionine (^{D}Met). Dermorphin binds to mammalian μ-type opiate receptors, inducing an analgesic effect that is stronger than that induced by morphine.[14] Similarly, deltorphin presents a ^{D}Ala, instead of the ^{D}Met, it is isolated from skin secretions of frogs *Phyllomedusa bicolor*, and it binds to mammalian δ-type opiate receptors, causing hallucinogenic effects.[15]

Free D-serine (^{D}Ser) has been found in species ranging from bacteria to mammals. D-Ser is a co-agonist of the *N*-methyl-D-aspartate subtype of glutamate receptor (NMDAR). Enzymes involved in its synthesis and degradation, as well as its receptors, were all found to be expressed in the central nervous system, where it is involved in neurotransmission regulation.[16] Moreover, the presence of ^{D}Ser in gastrointestinal system suggested its functional role, in combination with glia cells, to regulate sleep, through the NMDAR.[5]

Moreover, ^{D}Cys has been identified to have a crucial role in protecting cerebellum and kidney cells from oxidative stress, thanks to its involvement into the pathway for the production of hydrogen sulphide, a cytoprotective and signalling molecule.[17]

Such widespread presence of D-amino acids in living organisms' proteins has been explained by three theory: 1) free D-amino acids produced by racemases are directly incorporated into the peptide chain; 2) enzymatic post-translational modifications convert L-amino acids into its D-enantiomers; 3) non-enzymatic racemisation processes take place in ageing human proteins.[18]

1.2. Effect of Chirality on Peptide Secondary Structures

Natural peptides and proteins are folded in well-defined and stable architectures that allow them to exploit their functions. Spatial arrangement is due to the peptide primary sequences, disulfide bridge formations,[19] and the presence of metal binding centres, where metal cations stabilise the functional structures.[20] In synthetic peptides the introduction of one or more D-amino acids into the peptide sequence can induce significant changes in the secondary

structure because of the different interactions that can be established between the amino acids at supramolecular level. Carrying out a D-amino-acid scan (replacing each L-amino acid of a sequence with its corresponding D-enantiomer) can give important information about the relative importance of a particular amino acid in the folding and, consequently, in the biological activity of a peptide.[21]

1.2.1. Beta-Hairpins

A study by Imperiali and collaborators that dates back almost 30 years ago revealed for the first time the effect of the presence of a single D-amino acid on the secondary conformation of a peptide.[22] The authors demonstrated how the introduction of a D-proline (^{D}Pro) in a polypeptide contributed to a beta hairpin formation. Importantly, the homochiral control peptide was not able to give neither the hairpin nor the tertiary structure observed for the heterochiral one.[23] Further studies confirmed that the presence of ^{D}Pro facilitates the formation of extended β-turn sheets and β-hairpins,[24] corroborating the importance of torsion angles of D-residues in peptide folding.[25] Taking advantage of this findings, Schneider, Pochan, and co-workers used a ^{D}Pro-^{L}Pro to obtain a β-hairpin conformation, for self-assembly of a polypeptide into a biocompatible nanostructured hydrogel (as shown in **Figure 1.2**),[26, 27] which also exhibits broad-spectrum antibacterial activity.[28] Other derivates of this heterochiral peptide are reported to have possible applications as injectable drug delivery vehicle,[29] and as scaffold for automated cell-based high-throughput screening.[30]

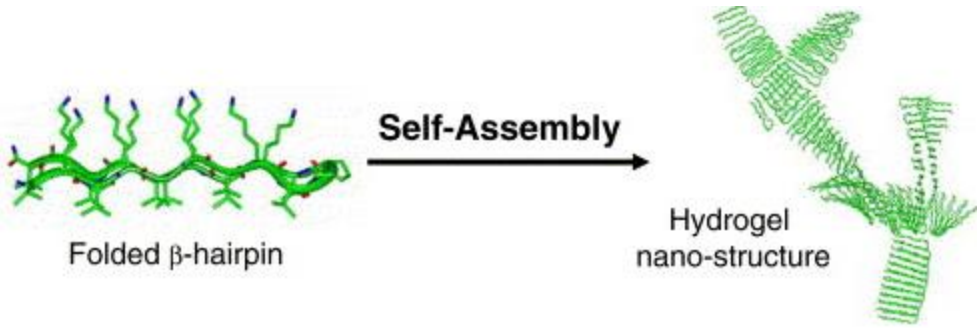

Figure 1.2. Schematic self-assembly process of a beta hairpin structure into nanostructured hydrogel. Adapted with permission from ref. 27 © 2005 Elsevier.[27]

Further NMR studies showed that the introduction of N-acetylated ^{D}Leu at the N-terminus of a peptide sequence could be a useful strategy to stabilise short β-hairpins (induced by an

internal ^{D}Pro residue), due to the noteworthy backbone stabilization, resulting from the formation of terminal hydrophobic interactions.[31]

1.2.2. Beta-Sheets

Understanding the mechanisms behind the assembly of peptides and proteins into β-sheet-fibril nanostructures is an hot topic in biochemical and biophysical research because of their association with neurodegenerative diseases, such as Creutzfeldt-Jacob and Alzheimer.[32, 33] For these reasons many researchers are studying, among the other, the effect of chiral amino acids on beta-secondary structures, in order to offer insights into the pathogenesis of, and therapeutics for, such diseases.

Substitution of all L-amino acids with all D-relative analogues in a peptide sequence brings to the formation of the peptide enantiomer, which usually displays the same conformation. Thus, if a L-homochiral peptide is organised in beta-sheet secondary structures, its D-enantiomer is expected to show the same behaviour in an achiral environment, which could be assessed by means of circular dichroism (CD) and infrared spectroscopy (IR) analysis. The CD spectra of the two enantiomers should be the perfect mirror images of each other.[34-36] However, the β-sheet conformation stability of two enantiomers at different pH or temperature could show some differences. For instance, the two enantiomers of an antimicrobial self-assembling peptide had displayed different pH dependence and evolution of secondary structures. In particular, increasing the pH from neutral to alkaline, the L-peptide conformation in solution reversibly changed from unordered to β-sheets structures. In the case of the D-enantiomer, the process was faster (hours instead of days) and resulted also in higher antimicrobial potency. The authors related the faster self-assembly of the D-peptide to different orientation of the polar side chains and to the lower values of pKa, compared to those of the L-enantiomer.[37]

Furthermore, a study reported that a protected L-octapeptide and its D-enantiomer were able to assemble into respectively left- and right-handed twisted fibrils, based on β-sheet secondary structures. Surprisingly, the co-assembly of the two enantiomeric peptides brought to the formation of nanoribbons, which contained alternating L- and D-peptides in a rippled β-sheet orientation (**Figure 1.3**).[38]

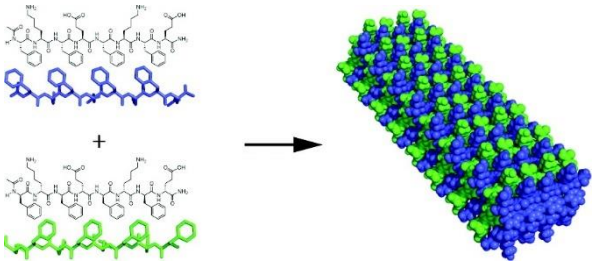

Figure 1.3. Co-assembly of enantiomeric amphipathic peptides into rippled β-sheet fibrils (L-enantiomer is represented in blue, D-enantiomer in green). Reprinted with permission from ref. 38 © 2012 American Chemical Society.[38]

A similar behaviour was displayed by L- and D-enantiomers of an amphiphilic oligopeptide, assembling into β-sheets with left- and right-handed nanofibers, respectively. On the other hand, the mixture of the two enantiomers formed globular aggregates instead of nanofibers in the same conditions, as revealed by atomic force microscopy analyses (AFM), reported in **Figure 1.4**.[39]

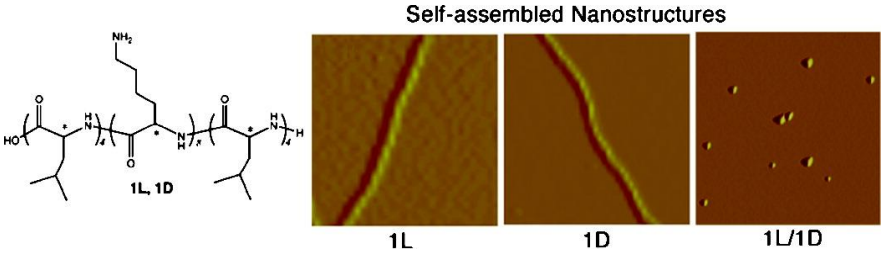

Figure 1.4. Tapping-mode AFM images of 1L, 1D, and 1L/1D equimolar mixture. Reprinted with permission from ref. 39 © 2005 American Chemical Society.[39]

However, mixing L- and D- amino acids into the same sequence could have an unpredictable effect on the peptide secondary structure. Indeed, some studies described the positive effect that a D-amino acid had on the self-assembly of a short peptide. For instance, Marchesan *et al.* investigated the supramolecular behaviour of all the possible stereoisomers of the tripeptide Phe-Phe-Val, and they identified well-defined β-sheet conformations only in those heterochiral peptides containing a D-amino acid at the N-terminus of the sequence.[40]

Other authors, moreover, synthesised an heterochiral polypeptide containing a ^{D}Pro and two residues of Cys that was able to form parallel β-sheets in aqueous solutions. They

demonstrated, moreover, that inter-strand disulfide bridges stabilised and specified the length of the parallel β-sheet secondary structure (**Figure 1.5**).[41]

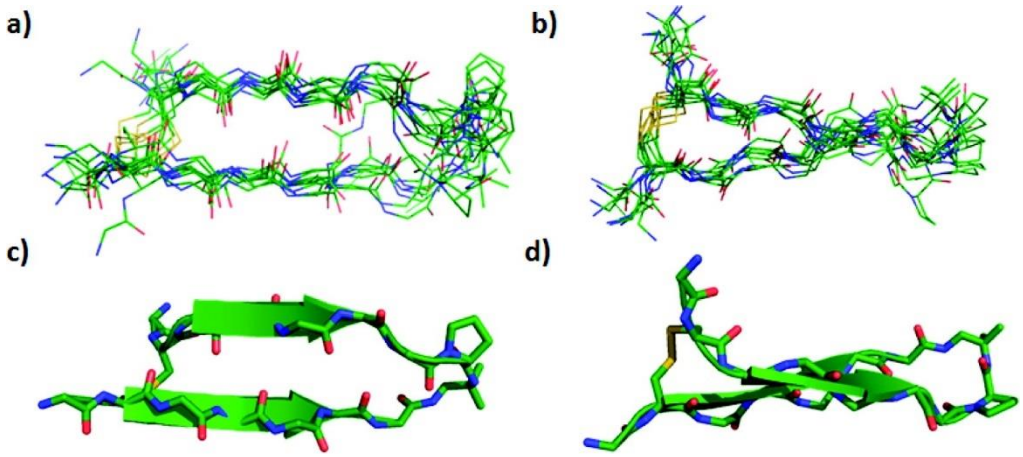

Figure 1.5. Parallel β-sheet secondary structure is stabilized and terminated by inter-strand disulfide cross-linking. Reprinted with permission from ref. 41 © 2012 American Chemical Society.[41]

Typically, the formation of β-sheets is favoured by amphiphilic moieties, induced by alternation of hydrophobic and hydrophilic amino acids in a peptide sequence: hydrophobic amino acid side chains drive the aggregation and the self-assembly, while the hydrophilic ones favour the interactions with water.[42] However, it has been recently reported that amphiphilic β-conformation can also be adopted by tripeptides containing only hydrophobic amino acids, with alternating L- and D- chirality, where the peptide backbone depicts the hydrophilic content.[43] In this case, heterochiral tripeptides belonged to the general sequence ^{L}Phe-^{D}Xaa-^{L}Phe (where ^{D}Xaa is an aliphatic D-amino acid), and they were reported to form nanostructured hydrogels in physiological conditions. Supramolecular β-sheets were identified by CD, IR analyses and single-crystal XRD structures, confirming also the prediction of molecular dynamics (MD) simulations in explicit water.[44] The homochiral stereoisomers of these peptides showed dramatic packing differences, being not able to self-assemble.[43]

In conclusion, amyloid-like behaviour and self-assembly into defined nanostructures can be tuned also by the chirality and the positions of amino acids in the peptide primary structure. Although design principles are finally emerging, they are still far from the delineation of a general framework because of the vast variety of chemical diversity encoded by amino acids,

and the fact that self-assembly is typically the result of a cooperative behaviour that amplifies subtle differences at the molecular structure level.

1.2.3. Alpha-Helices

While D-amino acid residues are known to induce turn structures, sequences containing all L-amino acids prefer an extended conformation. Indeed, substitution of a L-amino acid by the D-analogue into an assembling coiled coil sequence was reported by DeGrado and collaborators to destabilise α-helices, increasing the free energy of helix formation, compared to the homochiral peptide.[45] In an elegant work, the authors performed several conformational analysis (CD, NMR, liquid chromatography) to determine the helix destabilising effect of the D-enantiomer of the all 19 proteogenic chiral amino acids. Because of an induction into turn-like structures, all the D-amino acids decreased the helicity content, compared to the L-analogues. This effect was highly related to the type of amino acid side chains and their steric effects. In particular, β-branched amino acids and both L- and D-forms of proline showed highest disrupting effect, while histidine and aspartic acid displayed the highest propensity to form α-helical structure.[46] A recent computational study, employing all-atom molecular dynamics in explicit water, has systematically studied the influence of mixed L- and D- amino acids on helix-folding polyalanine peptides. The authors reported that even a single insertion of a ^{D}Ala completely broke the α-helix. An increase of the number of D-Ala residues in the chain altered the helical orientation towards the opposite chirality (**Figure 1.6**).[47]

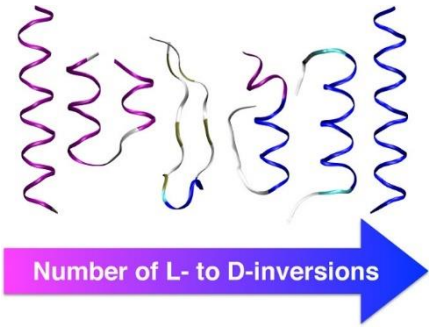

Figure 1.6. Chiral inversion of α-helix induced by D-amino acids. Reprinted with permission from ref. 47 © 2018 American Chemical Society.[47]

On the other hand, the introduction of D-amino acids in peptide adopting a helical conformation has been studied by Clayden and co-workers, who described the importance

of D-amino acids in the helix handedness. Indeed, the homochiral peptide assumed interconverting mixture of helical screw-sense conformers, while the presence of a D-amino acid stabilised the preferential formation of the left- or the right- handed helix, depending on its relative position in the sequence.[48] Other studies confirmed this assumption: polypeptides rich in L-residues gave rise to right-handed alpha-helix that then self-assembled in clock-wised spiral particles in toluene/water emulsions; on the other hand, polypeptides rich in D-residues formed left-handed spiral particles, which were based on alpha helix with the same handedness (**Figure 1.7**).[49]

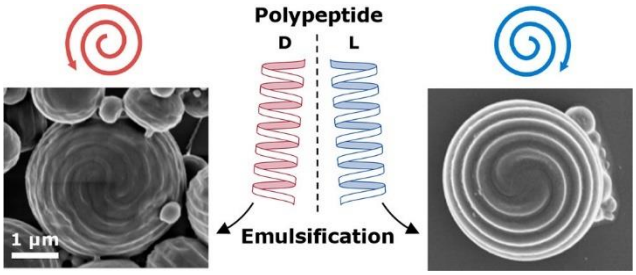

Figure 1.7. Spiral microparticles with opposite screw directions. Reprinted with permission from ref. 49 © 2018 American Chemical Society.[49]

The effects of D-amino acids on the stability of α-helices become extremely important when such conformation is involved in biological functions, such as metal binding ability of metalloproteins. Indeed, a study investigated the impact that a ^{D}Cys residue had on cadmium binding ability of a peptide able to self-assemble in three strand coiled coil structures. D-chirality of cysteine induced a different rearrangement that changed the metal binding pocket (**Figure 1.8**). These findings highlighted the possibility of using D-amino acid residues to change the coordination chemistry of a metal centre to tune its structural and catalytic properties.[50]

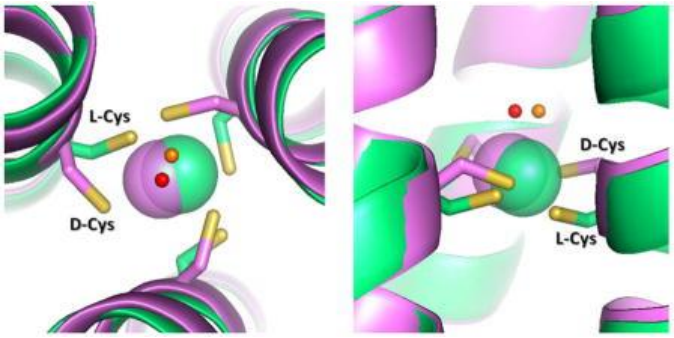

Figure 1.8. D-Cysteine ligands control metal geometries in metalloproteins. Reprinted with permission from ref. 50 © 2017 John Wiley and Sons.[50]

1.3. Self-Assembled Peptide Nanostructures

Nanomaterials have attracted attention in several research fields, such as chemical catalysis, medicine, and engineering. Among the broad range of nanomaterials that have been developed in recent years, self-assembling peptides are attractive minimalistic bioactive motifs and low-cost building blocks for supramolecular nanostructures. In particular, supramolecular nanostructured hydrogels based on hierarchical self-organisation of ultra-short peptides are attractive for the development of soft biomaterials, since they are inherently biocompatible and biodegradable functional nanomaterials, useful to the creation of novel therapeutic paradigms in nanomedicine.[51] Non-covalent π–π interactions play a special role for self-assembly, since they facilitate the supramolecular association of low-molecular-weight gelators (LMWGs), for this reason the presence of aromatic moiety is fundamental.[52] An often-used approach is introducing aromatic N-capping group, such as fluorenylmethyloxycarbonyl (Fmoc) group, largely used in peptide synthesis and commercially available, which assists self-assembly in water.[53] Alternatively, Phe-Phe derivatives, dissolved in a small amount of organic solvent, when diluted in water, they will self-assemble in several nanostructures (*e.g.*, nanotubes, nanofibers, nanowires, nano-vescicles).[54]

1.3.1. Role of Chirality in the Self-Assembly of Peptide Nanostructures

If we consider all the above described effects that could arise from the introduction of even a single D-amino acid on peptide secondary conformation, we will foresee the potential impact of using an heterochiral peptide – as opposed to a homochiral analogue - for self-assembly into well-defined nanostructures. It is remarkable that chirality can definitely be

used as an innovative means to fine-tune the self-assembly behaviour and the viscoelastic properties of the resulting supramolecular nanomaterials. Moreover, the low susceptibility to the enzyme activities of hydrogels based on heterochiral peptides increased widespread their interest and the possible applications in biomedical field, thanks to their unusual self-assembling behaviours.[55] In 2012, indeed, the first systems based on unprotected hydrophobic tripeptides, containing both L- and D-amino acids in the same sequence, were reported by Marchesan and collaborators to self-assemble in nanostructured hydrogels, at physiological conditions. In particular, the authors demonstrated that, starting from an homochiral sequence that was not able to form a hydrogel, the simple replacement with the D-enantiomer of the N-terminally amino acid converted the non-gelling peptide into a gelling one.[56, 57] Further studies provided more comprehensive insights into the role of chirality in the self-assembly of hydrophobic tripeptides. showed that the position of the D-amino acid along the sequence can be a discriminating factor to achieve self-assembly and hydrogelation, while self-assembling stereoisomers with the same amino acid sequence maintained analogous nanomorphologies (*e.g.*, twisted fibers or nanotapes).[40, 58]

The reasons for the divergent path through self-assembly between homochiral (L-L-L) and heterochiral L-D-L hydrophobic tripeptide analogues was elucidated only recently. While both systems in the non-assembled state showed a population of analogous conformations distribution in terms of relative orientation of the dipole moments of the peptide bonds, the L-D-L stereochemistry stabilised a kinked backbone with all side hydrophobic side chains on one side. As a result, heterochiral peptides could self-assemble in supramolecular amphiphilic structures, whereby the hydrophilic component (constituted by the peptide backbone) and the hydrophobic part (constituted by the amino acid side chains) were completely segregated. In this way, self-assembly into hydrogels was achieved.[44] Combined studies based on single X-ray analysis and MD simulations demonstrated a characteristic backbone rearrangement only for heterochiral sequences. The backbone orientation efficiently segregated hydrophobic regions, necessary to drive the self-assembly, from hydrophilic channels, essential to entrap the water molecules for the establishment of the hydrogel. Comparison with corresponding homochiral peptides showed that in this case hydrophobic side chains impinged into the hydrophilic areas, hindering correct self-assembly into hydrogels (**Figure 1.9**). [43]

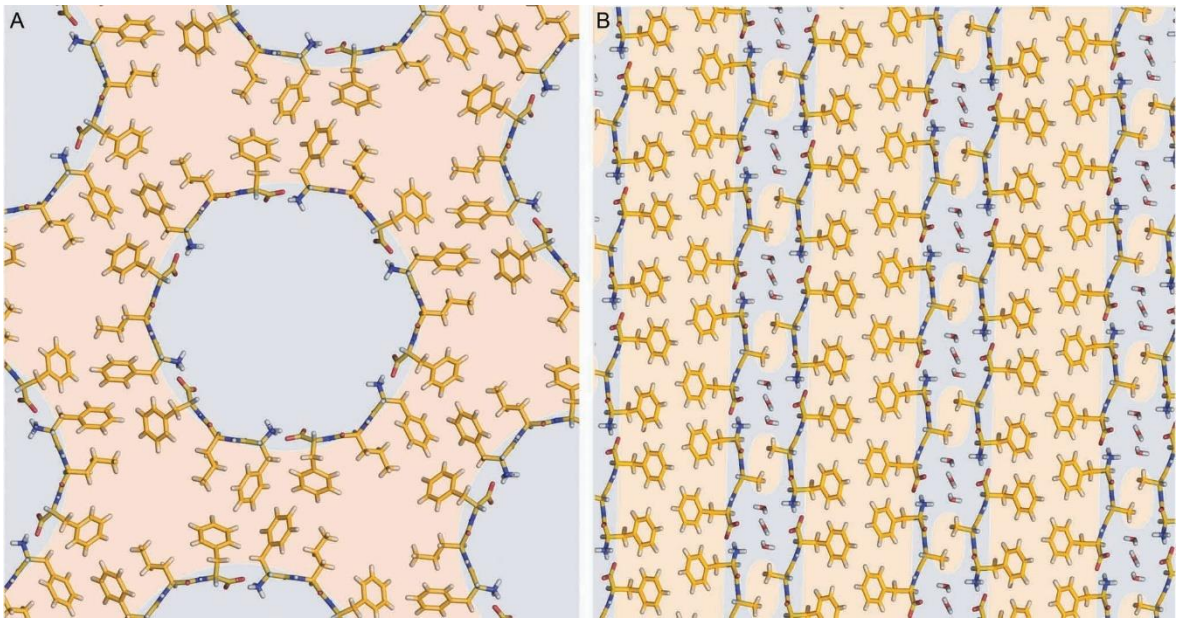

Figure 1.9. Single-crystal XRD data reveal very different packing for (**A**) heterochiral tripeptide showing a net segregation between hydrophilic (blue) and hydrophobic (orange) components, and (**B**) homochiral tripeptide. Reprinted with permission from ref. 43 © 2018 Elsevier.[43]

Moreover, the alternation of chirality exhibited interesting behaviour when applied on cyclic peptides. Indeed, Montenegro and Perrier employed cyclic octapeptides containing alternating L- and D- amino acids as building blocks for hydrogel assembly. They showed that such peptides oriented the amide bonds perpendicular to the peptide plane by the formation of hydrogen-bonded antiparallel β-sheets. In this way, vertical stacks of peptides were established to form hollow nanotubes that could further interact to give rise to soft hydrogels (**Figure 1.10**).[59, 60]

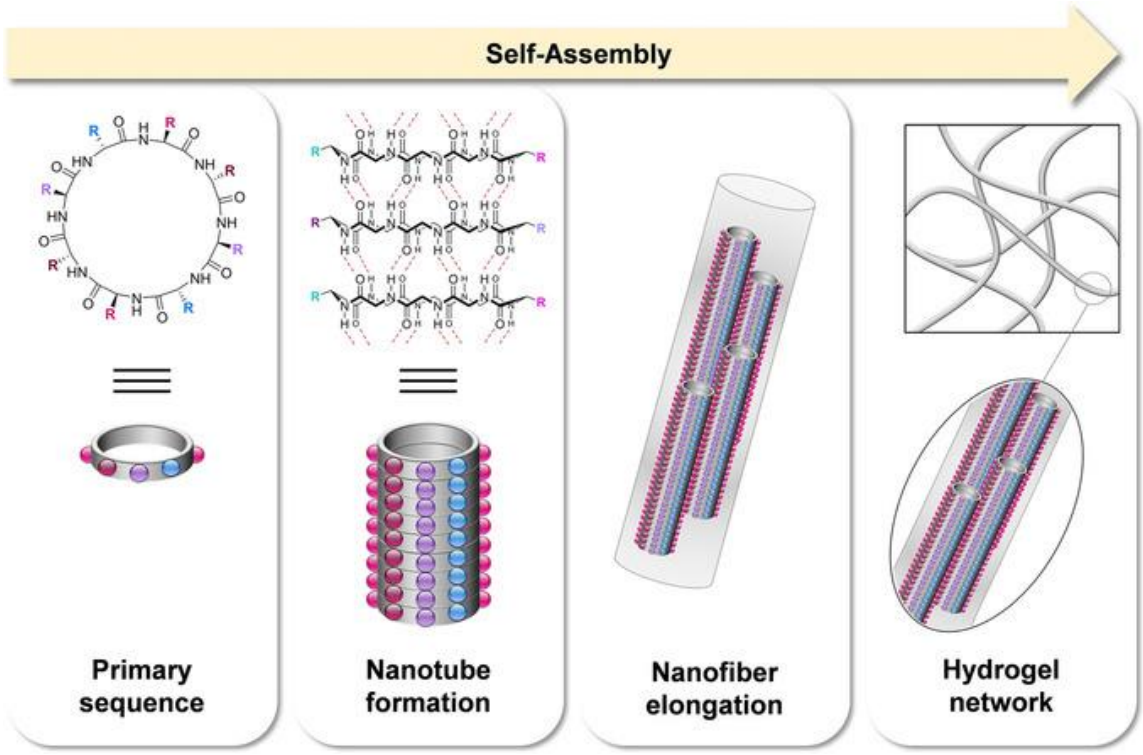

Figure 1.10. Hierarchical self-assembly process involved in hydrogel formation from D-, L- cyclic peptides. Reprinted with permission from ref. 60 © 2018 John Wiley and Sons.[60]

Several studies investigated the possibility to incorporate amino acids with different chirality into the same sequence, with the aim to describe useful prediction rules for the formation of supramolecular hydrogels. For instance, Yang and collaborators demonstrated that replacing two ^{L}Phe with two ^{D}Phe converted a peptide that only formed suspension at neutral pH, in a gelling peptide, suitable for cell culture.[61] Adam's group tested the ability to self-assemble in water of all the possible stereoisomers of naphthalene-protected di-phenylalanine. All of them successfully formed hydrogels, whose nano-morphologies and viscoelastic properties were related to the different position of the D-amino acid.[62] All these studies undoubtedly proved the significance of D-amino acids in heterochiral peptides to assist their gelling process in water.[63]

In literature N-capped heterochiral tripeptides were successfully used for the development of smart supramolecular hydrogels, which could be disassembled by external stimuli. The introduction of an azobenzene moiety (Azo) as N-capping group allowed the creation of peptides that underwent reversible conformational switches after UV irradiation. In particular, either the homochiral (L-L-L and D-D-D) and the heterochiral (D-L-L and L-D-D) stereoisomers of the sequence Azo-Lys-Phe-Ala formed hydrogels, whose mechanical

stability strictly depended on the number and the position of the D-amino acids. Remarkably, the D-homochiral tripeptide showed the best viscoelastic properties. Amongst the hydrogels obtained, the one based on the peptide containing an N-terminally amino acid with opposite chirality relative to the rest of the sequence showed multiple responses to heat, light and ligand–receptor interaction with the antibiotic vancomycin.[64] Moreover, another study also confirmed the different UV-triggered disassembly behaviours of the gels based on two enantiomers, where the D-peptide showed the slowest gel-sol transition.[65]

1.3.2. Techniques Typically Employed to Characterise Peptide Nanostructures

Heterochiral peptides are valuable candidates to be used as nanomaterial building blocks. Actually, their self-assembling behaviour could bring to the formation of supramolecular nanomorphologies, of a size range that is 1-100 nm in at least one dimension. Objects on the nanometer scale include, for example, viruses (30-50 nm), DNA (2.5 nm), fullerenes (~1 nm in diameter), single-walled carbon nanotubes (~1 nm in diameter). To characterise materials of such dimensions, the use of specific techniques is mandatory, as described in Figure **1.11**.

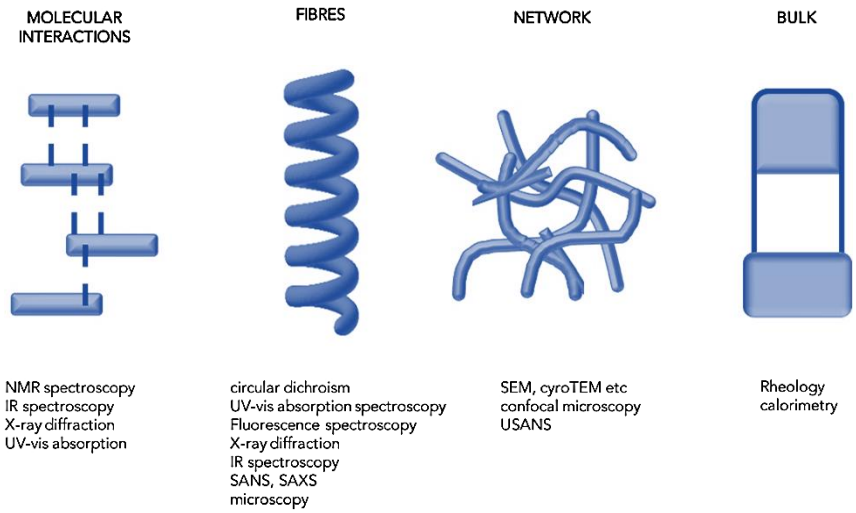

Figure 1.11. Hierarchical assembly across length scales and different techniques appropriate for analysing the structures formed at each length scale. Adapted with permission from ref. 66 © 2017 Elsevier.[66]

In particular, the most popular approach to study nanomorphologies is based on microscopy techniques that ensure high resolution. Considering the limited resolution power that corresponds to ca. 400-700 nm, according to the Abbe's law reported as Equation (1) of optical microscopes[67] (such as confocal microscopes and micro-Raman), their use has to be

combined with other techniques, such as electron microscopy (SEM and TEM, and combination of them in scanning transmission electron microscopy, namely STEM), and scanning probe microscopy (*i.e.*, atomic force microscope, AFM, and scanning tunnelling microscope, STM).

$$\text{Abbe's law: } d = \lambda / (2\, n \sin \alpha) \qquad (1)$$

Equation (1). Abbe's law of limiting resolution: d is the resolvable feature size, λ is the wavelength of light, n is the index of refraction of the medium being imaged in, and α is the half-angle subtended by the optical objective lens.

In particular, scanning electron microscopy (SEM) is a useful technique for surface topography of nanomaterials and is based on an electron beam source that generates electrons towards the anode. Condenser lens allow scanning of sample surface, thanks to the detection of secondary electrons. On the other hand, the system is more complex in the case of a transmission electron microscope (TEM), where the aim is to obtain an electron beam able to pass through the sample, to allow the detection of transmitted electrons (**Figure 1.12**).

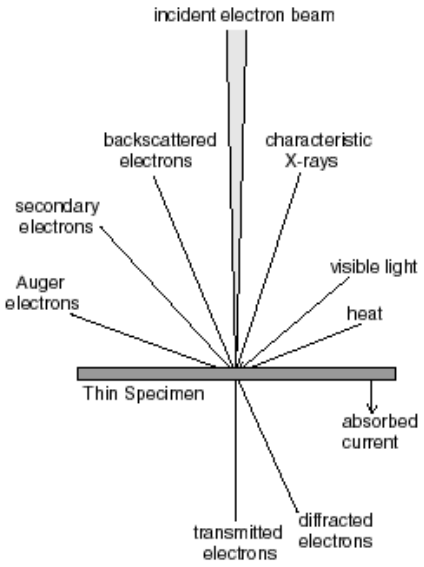

Figure 1.12. Electron beam-sample interactions.

Finally, the image is displayed on the camera and collected. Both SEM and TEM instruments require high vacuum level, in order to align and focus the electron beam. Consequently, water-based biomaterials, such as hydrogels, need to be dried before the analyses.

SEM analysis of peptide-based nanomaterials, which are non-conductive, requires an additional metal coating (with, for example, gold, palladium, iridium or a thin carbon film) to minimise charging effects. However, coating thickness could significantly affect resolution, limiting the information derived from this technique. An alternative approach is based on decreasing the vacuum inside the system; the resulting technique is named environmental scanning electron microscopy (ESEM) and allows topographic studies of non-conductive nanomaterials without additional metal coating. The main drawback of this technique is the low resolution that can be achieved, if compared to that of high-resolution SEM in high vacuum.

In the case of TEM, the required electron beam energy needs to be higher (100 KV) than that used in SEM (30KV). Such energy values could induce damages and decomposition of peptide-based nanomaterials, for these reasons, spectroscopists have to pay particular attention during analyses. On the other hand, noteworthy advances in cryo-electron microscopy that brought the Nobel Prize in chemistry to Jacques Dubochet, Joachim Frank, and Richard Henderson in 2017,[68] allow the use of cryo-TEM, which, operating at cryogenic temperature, guarantees high-resolution determination of nanostructures in water environment (**Figure 1.13**).

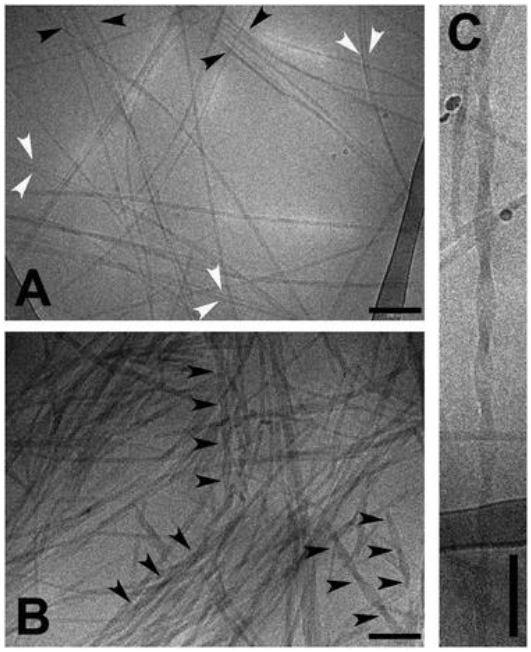

Figure 1.13. Cryo-TEM of (**A**) ^{D}Val-Phe-Phe hydrogel and (**B**) ^{D}Phe-Phe-Val hydrogel in higher magnification (**C**). Scale bar = 200 nm. Reproduced from ref. 57 with permission from The Royal Society of Chemistry.[57]

Moreover, appropriate devices (STEM) are able to both focus the electron beam and control its scanning. Electron microscopes, nevertheless, can be used as analytical techniques when they are equipped with X-ray detector, for example in the case of energy dispersive X-ray spectroscopy (EDX), allowing simultaneously elemental and morphological analyses of the nanomaterials.

1.4. Potential Biomedical Applications

The enhanced stability towards protease digestion, as previously mentioned, displayed by supramolecular nanomaterials based on peptides containing D-amino acids, allows them to be excellent candidates for use in biomedical field.[55] Because of their improved lifetime in living systems and their unexpected advantages and properties, these self-assembled materials have been studied for several kind of bio-applications, such as drug delivery and regenerative medicine.

1.4.1. Drug Delivery for Diagnostics and Therapeutics

Incorporation of drug molecules inside the nanostructures obtained by the self-assembly of peptides is a process that can be achieved through three different pathways: i) simple

physical entrapment of cargo molecules inside the carrier network; ii) non-covalent interactions between peptide and drug molecules; iii) covalent interactions between drugs and peptide building blocks.[69] In all these cases, the presence of D-amino acids could impact on the delivery process, because of their effects on peptide backbone and, consequently, on the interactions that can be established with the entangled molecules.[70] Several studies have investigated the possible use of supramolecular nanomaterials based on heterochiral peptides assembly for this purpose.

For example, Young's group studied the delivery properties of an heterochiral assembling peptide comparing it with its homochiral analogue. They designed an octapeptide with cancer-targeting moiety RGD (Arg-Gly-Asp) to use it as carrier of an anticancer drug, 10-hydroxycamptothecin. They synthesised the L-homochiral peptide and a stereoisomer containing 3 D-amino acids. Both peptides displayed self-assembling properties and the ability to entrap the drug. However, the use of the heterochiral sequence showed several advantages over the homochiral control peptide: it demonstrated higher resistance to protease digestion, improved storage stability, better controlled drug release ability, and superior cancer cell selectivity. All these factors resulted in higher antitumor activity of the D-containing peptide nanocarrier. Moreover the two peptides also showed different biodistribution, leading to the possibility of using different chirality to preferentially direct the drug on a specific site of the body.[71] Another study investigated the self-assembly of heterochiral ^{D}Leu-Phe-Phe in the presence of 5-fluorouracil. A hydrogel was obtained with loaded drug amounts within a useful range for therapeutic application. However, the hydrophilic nature of the drug resulted in rather rapid release in aqueous media, since the drug engaged in only transient interactions with the peptide.[72]

Supramolecular hydrogels have been also studied in immunotherapy, as delivering agent of antigenic proteins constituting vaccines. They could boost body immune responses, creating a valuable alternative to typically employed immunological adjuvants that are developed so far (such as nanoparticles, liposomes, polymers).[73] In this contest, nanostructured hydrogels based on the self-assembly of D-amino acid containing peptides are favoured thanks to their enhanced stability towards enzyme degradation.[74] Yang and collaborators, indeed, assessed the *in vivo* immunogenicity of a hydrogel obtained by the self-assembly of a short D-peptide in presence of ovalbumin, a model protein commonly used as antigen in immune response studies. Surprisingly, the gel showed an excellent performance, extending, moreover, antigen accumulation times in lymph nodes, compared to control experiments. These results

suggested that nanostructured hydrogels based on the self-assembly of D-peptides induced a controlled release of antigens, enhancing the antibody production and the successful immune response.[74] Further studies, performed on different peptide gelators[75] and triggers, confirmed the suitability of this innovative approach for treatment of infectious diseases and cancers.[76-78]

1.4.2. Tissue Engineering and Regenerative Medicine

Design of self-assembly peptides is an excellent technique to produce synthetic nano-biomaterials mimicking the nanofibrous network of extracellular matrix, because of their well-known properties, such as biocompatibility, biodegradability, low cytotoxicity and immunogenicity.

D-peptide based scaffolds have been used in 3D cell culture, enabling cell attachment, viability and proliferation. In particular, in 2013 nanofibers arisen from the self-assembly of a D-amino acid containing peptide have been reported as scaffold for cell culture, with several advantages relative to those derived from L-enantiomeric peptide. Cells were entangled in the network of fibers that ensured a good viability and a low degree of apoptosis enabling the formation of a healthy microenvironment for mutual interactions and cell proliferation. Moreover, proteolytic enzymes secreted by the cells didn't destroy the scaffolds, thanks to the high resistance to protease degradation conferred by D-amino acids.[79]

Further analyses also showed a relationship between supramolecular chirality of the nanofibers and cell density. Indeed, a study assessed stem cell differentiation in a hydrogel based on a Fmoc protected tripeptide containing a cysteine residue. Cysteine was used to crosslink the peptide with a poly-ethylene glycol (PEG) polymer *via* thiol-ene photopolymerization, in order to enhance the mechanical resistance of the hydrogels: the longer the light exposure time, the stiffer the hydrogel. Both the enantiomeric forms of the PEG-peptide were synthesised, and their relative hydrogel were used to encapsulate stem cells. L-gel was found to favour cell spreading and proliferation better than the D-gel. The different response to chiral supramolecular 3D environment displayed by stem cells could be a useful tool to take advantage from, for the development of biomaterials to overcome some issues related to stem cell transplants, such as tumorigenesis and undesirable too fast differentiation (**Figure 1.14**).[80]

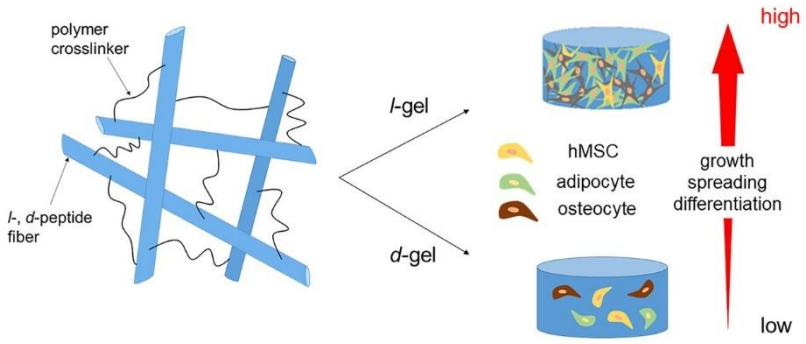

Figure 1.14. Schematic representation of the chirality effect on stem cells fate. Reprinted with permission from ref. 80 © 2018 American Chemical Society.[80]

Neuronal cells have been reported to show an intense chiral recognition, as identified by a work that examined the neuronal viability on chiral self-assembled monolayers (SAMs) based on cysteine enantiomers. The use of cysteine was justified by the observations that this amino acid has a crucial role in neuronal tissue, since the L-form is a neuromodulator and it is involved in the synthesis of glutathione, a tripeptide necessary for neuroprotection from oxidative stress. Actually, high values of ^{L}Cys have been related with severe events, such as brain ischemia. The study aimed to evaluate the effect of amino acid chirality on neuronal cell growth, testing it with both the enantiomers as free molecules and as SAMs, whereby the cysteine molecules were linked to a gold surface through thiol-gold interactions. When cell medium was enriched with free ^{L}Cys, cell growth was hindered, while the addition of ^{D}Cys didn't led to significative difference relative to control experiments, performed in absence of such amino acid. Such preliminary results showed a chiral sensitiveness by neuronal cell. The same trend was identified on SAMs. ^{D}Cys SAM induced better adhesion and optimised branching tree for neurones, than ^{L}Cys SAM, as shown in the HR-SEM reported in **Figure 1.15**.[81]

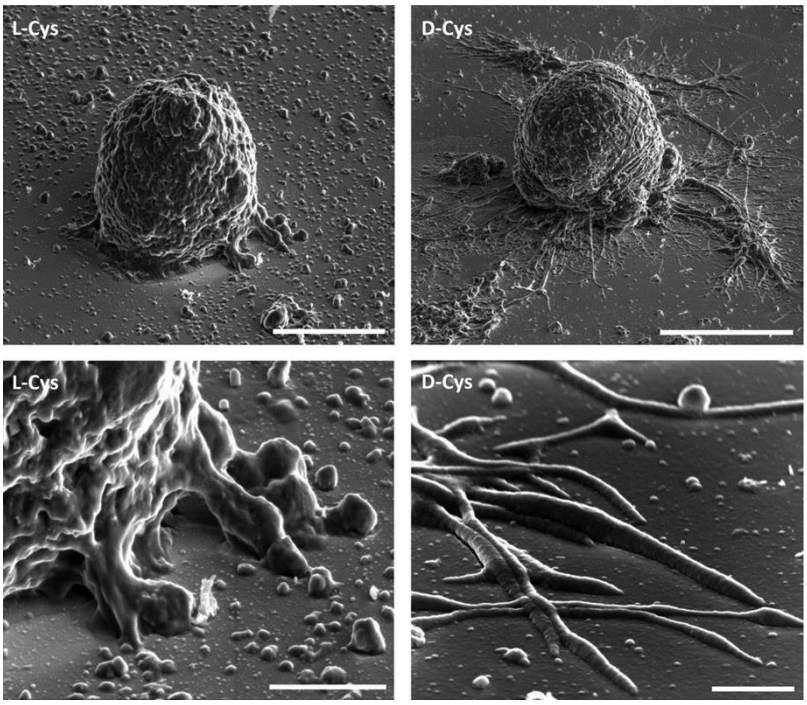

Figure 1.15. HR-SEM images of neurons growing atop ^{L}Cys (left panels) and ^{D}Cys (right panels) SAM surfaces. Lower panels show zoomed-in images of the neurite region in the upper panels. Scale bars are 3 μm (left) and 1 μm (right). Reprinted with permission from ref. 81 © 2014 American Chemical Society.[81]

Remarkably, superior neuronal growth on ^{D}Cys assemblies was found to be contrasting with the results obtained by viability experiments performed on other cells, such as fibroblasts and mesenchymal stem cells. In those cases, enhanced adhesion was obtained on ^{L}Cys coated surfaces.[81] It means that different cells could have different adhesion pathways that could be enhanced or minimised using supramolecular nanomaterials with different chirality.

Chapter 2: Aim of Project

The possibility to tailor peptide sequences by introducing sulfur-containing amino acids, *i.e.* methionine and cysteine (see **Figure 2.1**), in order to achieve 3D self-assembled nanostructures has not been deeply investigated thus far in the case of minimalistic self-assembling peptides.

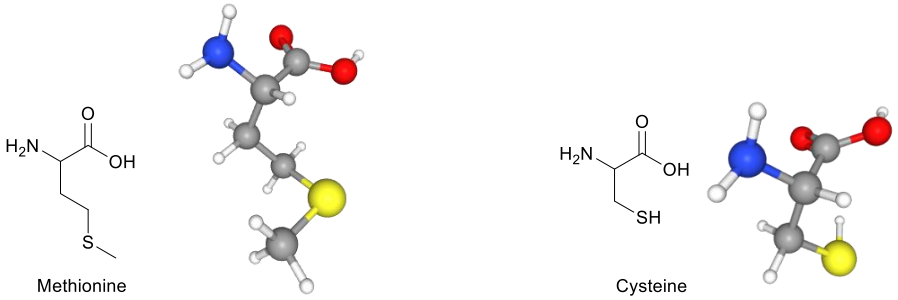

Figure 2.1. Chemical structures and ball-and-stick models of methionine and cysteine.

However, the presence of sulfur-bearing functional groups could confer interesting features to be used for the design of new functional nanomaterials. First of all, as described in the introduction, a good balance between hydrophobic and hydrophilic components in the peptide sequence is necessary to drive the self-assembly in water solution. In this context, sulfur atoms play an important role to maintain the right level of hydrophobicity. Indeed, both methionine and cysteine are non-polar and hydrophobic amino acids, since sulfur has a low propensity to establish hydrogen bonds. Methionine is considered to be highly hydrophobic and, actually, it is typically found to be present into hydrophobic pockets of proteins.[82]

Therefore, the aim of this project is to synthesise unprotected self-assembling tripeptides composed of both D- and L-amino acids at specific positions, and that display two Phe residues to drive self-assembly, and either Met or Cys as a third amino acid. Such peptides will be prepared via solid-phase peptide synthesis, purified by HPLC, characterised by a variety of spectroscopic and microscopic methods, and probed for self-assembly into hydrogels at physiological conditions. Different triggers will be assessed to drive assembly/disassembly cycles in a reversible and irreversible manner. Finally, live/dead assays will be performed *in vitro* to gain the first insights into the biocompatibility of these systems.

Chapter 3: Methionine Containing Peptides: Self-Assembly into Nanostructured Hydrogels

3.1. Introduction

3.1.1. Oxidation and Self-Assembly

The thioether functional group present in the side chain of Met can undergo a pH independent oxidation to sulfoxide. Methionine, thus, is an important physiological modulator of oxidative stress in living cells, typically linked to the presence of reacting oxygen species (ROS) in inflammation processes. The oxidative response of Met to ROS could be valuably used for the development of self-assembled nanomaterials, whose disassembly could be chemically guided. For example, Besenius and co-workers have recently reported a protocol for the assembly of transient hydrogels with tuneable lifetime, which was defined by the oxidation rate of Met thioether group. In particular, they synthesised a PEGylated oligopeptide containing two Met residues that was able so self-assemble into a hydrogel, which was based on nanorods of antiparallel β-sheets. Thus, during the self-assembly process, they introduced glucose and glucose oxidase (GOx), which catalyses the conversion of glucose to gluconolactone, releasing water peroxide (H_2O_2) into the hydrogel environment. H_2O_2 induced the oxidation of thioether groups into the corresponding sulfoxide derivatives, which were not able to self-assemble. In this way, the disassembly process was induced (see **Figure 3.1**).[83] Controlling the amount of glucose and glucose oxidase, the lifetime of the nanostructured hydrogel was tuned from 1 to 12 hours.

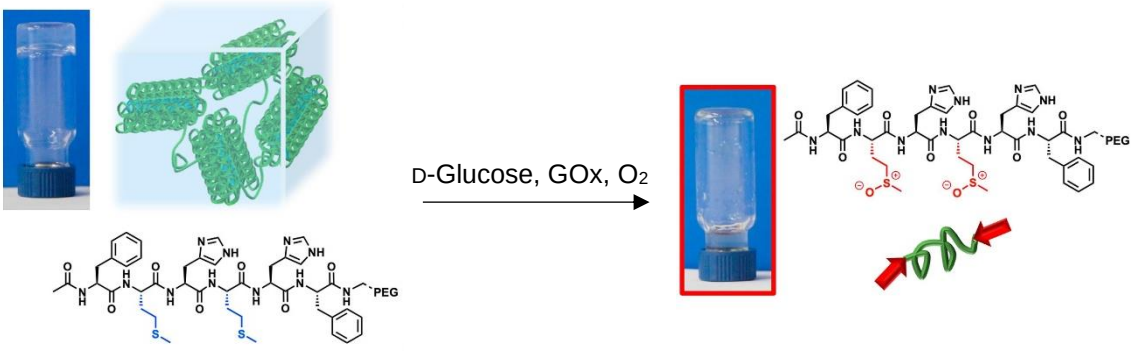

Figure 3.1. Schematic representation of the oxidation-mediated disassembly of supramolecular hydrogel. Adapted with permission from ref. 83 © 2019 Elsevier.[83]

3.1.2. Metal Coordination and Catalytic Activity

Met shows unique and very interesting properties in terms of metal binding ability and, consequently, catalytic activity. In fact, Met has an overall low metal-affinity that allows it to transport copper and other metals and is not dependent on pH; multiple Met residues can induce an additive effect to enhance the metal binding affinity; moreover, a higher affinity has been identified to Cu(I) over Cu(II).[84] Taking advantage from these fascinating features, a series of peptides containing Met has been synthesised with the aim to coordinate Cu(I). The peptide-Cu(I) complex was successfully employed for the asymmetric homogeneous catalysis of the Henry condensation in green conditions, as reported in **Figure 3.2**.[85]

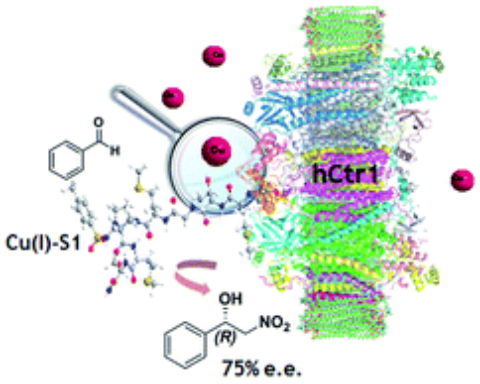

Figure 3.2. Henry reaction catalysed by peptide ligand–Cu(I) complexes. Reproduced from ref. 85 with permission from The Royal Society of Chemistry.[85]

3.2. Results and Discussion

3.2.1. Design of Selected Peptide Sequences

Three peptide sequences were designed to assess the effect of the methionine position on self-assembly behaviour, as reported in **Table 3.1.**

Peptide Sequence	**^{D}Met**-Phe-Phe	Phe-^{D}**Met**-Phe	^{D}Phe-Phe-**Met**
Chemical Structure	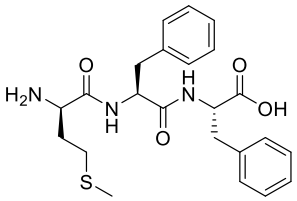	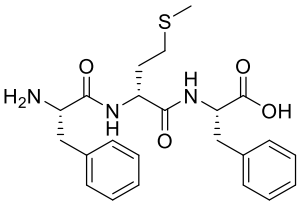	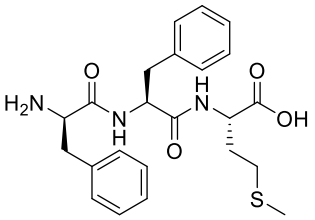

Table 3.1. Selected Met-containing tripeptides synthesised.

The rational design of these sequences derived from previous studies reported by our group. ^{D}Met-Phe-Phe and ^{D}Phe-Phe-Met feature D-L-L stereoconfiguration, which proved successful to achieve gelators based on hydrophobic sequences Xaa-Phe-Phe or Phe-Phe-Xaa, where Xaa is a aliphatic hydrophobic amino acid, such as Val.[57] The different stereoconfiguration at one chiral centre allowed different side-chain orientations that favoured engagement of peptide molecules in ordered stacks, which could interdigitate by means of Phe zippers.[40, 56, 58] Phe-^{D}Met-Phe is based on gelators that feature L-D-L stereoconfiguration and Phe-Xaa-Phe amino acid sequence, where Xaa is a hydrophobic aliphatic amino acid, such as Val or Leu.[43, 44] These two described design rules are tested here to validate and extend their applicability for the self-assembly of sequences that display one methionine residue at any position along the tripeptide sequence.

3.2.2. Peptide Synthesis and Characterisation

The selected peptide syntheses were manually carried out accordingly to standard Fmoc-based solid phase peptide synthesis (SPPS). To avoid possible side reactions related to the oxidation of methionine residue, the syntheses were performed in inert environment, introducing argon flow into the glass funnel, equipped with a fritted disk. The gas bubbling also has the double function of allowing resin stirring and solvent filtration. 2,2-chlorotrityl chloride resin was selected as solid support, because its steric hindrance is known to limit side reactions. Orthogonal protection was possible thanks to the different cleaving susceptibility of the Fmoc group and 2,2-chlorotrityl chloride resin to basic (piperidine) or acidic (TFA) conditions, respectively. (Benzotriazole-1-yl) tetramethyluronium hexafluorophosphate (HBTU) was selected as coupling agent to convert the Fmoc-protected

amino acid into the active ester in the presence of the base, diisopropylethylamine (DIPEA), and of the additive 1-hydroxy-7-aza-benzotriazole (HOAt), which was used to accelerate the acylation reaction.

In this manner, the tripeptide was prepared from the C- to the N-terminus on the resin, and each synthetic step was monitored by standard colourimetric tests, based on bromophenol blue or chloranil. Final cleavage of the unprotected tripeptide from the resin was achieved in acidic conditions with the addition of a reducing agent to avoid methionine oxidation. In particular, two popular cleavage cocktails are *Reagent K* (composed by trifluoroacetic acid, phenol, water, thioanisole, and 1,2-ethanedithiol (EDT)) and *Reagent L* (composed by trifluoroacetic acid, water, triisopropylsilane (TIPS) and dithiothreitol (DTT)) .[86] In this case, reagent L was chosen because of the absence of toxic phenol and a lower pungent odour compared to that of reagent K. During the reaction, highly reactive carbocations could be generated, for this reason scavengers (in this case, water, DTT, and TIPS) have to be added to trap them and avoid side alkylation reactions on the sensitive amino acid methionine. Evaporation of the cleavage cocktail under argon flow was followed by purification by reverse-phase HPLC. Peptide identity and purity were assessed by means of spectroscopic techniques, *i.e.*, NMR and LC-MS. Spectroscopic characterisation data of each peptide are reported in **Appendix**.

3.2.3. Peptide Self-Assembly into Nanostructured Hydrogels

The synthesised peptides were tested for their ability to self-assemble into nanostructured hydrogels. Among the different triggers that can be used to induce the self-assembly (*e.g.*, solvents, pH, temperature, sonication), the one selected for this set of peptides was the pH switch. This is a well-established procedure,[43, 44, 56] which allows the peptides to be rapidly dissolved in a alkaline buffer (pH 12), and then assembled at physiological conditions (pH 7.2 ± 2), after the addition of an acidic buffer (pH 5.8).

3.2.3.1. Tube Inversion Test

A very simple test to screen gelation conditions is based on the inversion of the test tube; if it resists gravity, it is likely a hydrogel. Although this test is not accurate, it is simple and quick, thus it often represents a first convenient option to undertake this kind of studies.

All the three heterochiral peptides effectively self-assembled into self-supportive hydrogels in a similar range of MGC (*i.e.*, the minimum gelling concentration, which in this study was limited to 1 hour), as shown in **Table 3.2**. Thus, the design rules applied to the study of these tripeptides were successful. In particular, the tripeptides containing methionine residue in the middle or at the C-terminus of the sequence, formed hydrogels at 10 mM, while the presence of methionine at the N-terminus required 15 mM peptide concentration to gel.

Peptide Sequence	^{D}**Met**-Phe-Phe	Phe-^{D}**Met**-Phe	^{D}Phe-Phe-**Met**
Photographs of the tube inversion test	 15 mM	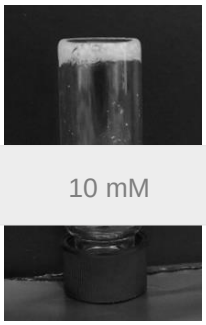 10 mM	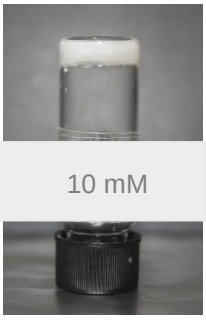 10 mM

Table 3.2. Self-supported hydrogels obtained by the self-assembly of Met-containing peptides.

3.2.3.2. Hydrogel Characterisation by Rheology

The word rheology derives from the Greek "*rheo*" that means flowing, and it studies how a material flows or is being deformed by the application of stress. The relationship between applied stress and induced strain allows the identification of a certain material as viscous (*i.e.*, liquid) or elastic (*i.e.*, solid). Hydrogels are positioned in between these two categories, as they are viscoelastic materials, whose properties are characterised by the elastic or storage modulus (G') and the viscous or loss modulus (G"). In particular, a material can be defined as gel when G' is higher than G" and both are independent from the frequency of the applied stress (*i.e.*, they are measured in linear viscoelastic regime).

Oscillating rheometers are ideal instruments to assess the viscoelastic properties of a sample. The hydrogel is placed between two plates, and only the top one oscillates, thus applying

stress onto the sample. Three parameters can be modified to give different information about the gelling nature of the material tested. A *frequency sweep* experiment is based on the application of a constant stress varying the frequency and allows to determine whether the material tested is a gel or not. In a *time sweep* measurement, the time of applied stress is changed in order to study the kinetics of gelation. Finally, a *stress sweep* applies an increasing stress at constant frequency to assess the mechanical resistance of the material.

The three tests mentioned above were performed for each hydrogel at MGC. In particular, frequency sweep experiments showed similar viscoelastic properties for all the three materials confirming their gel nature, as reported in **Figure 3.3**. Comparable values of G' (20 kPa) and G" (1 kPa) were observed for the peptides containing the D-amino acid at the N-terminus of the sequence (*i.e.*, ^{D}Met-Phe-Phe and ^{D}Phe-Phe-Met), despite the different peptide concentration at MGC. By contrast, Phe-^{D}Met-Phe showed lowest values of both viscous (7 kPa) and elastic (0.6 kPa) moduli.

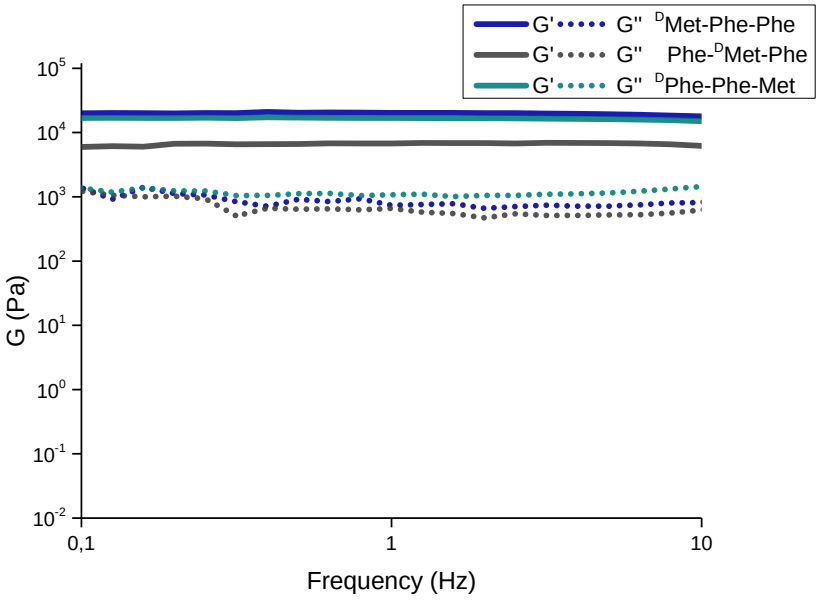

Figure 3.3. Frequency sweep analyses of Met-containing peptides.

The latter peptide also displayed the slowest gelation kinetics, as indicated by time sweep analyses shown in **Figure 3.4**. Actually, it needed almost 20 minutes to give rise to a stable hydrogel, while the other two regioisomers efficiently gelled in less than 3 minutes.

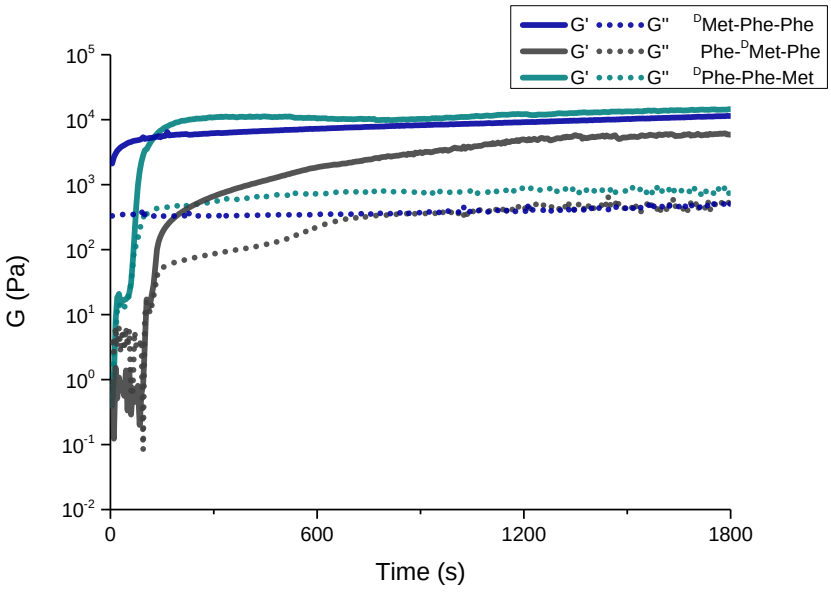

Figure 3.4. Time sweep analyses of hydrogels derived from Met-containing peptides.

Finally, stress sweep measurements were performed to evaluate the ability of each hydrogel to resist after an increasing mechanical stress. Data reported in **Figure 3.5** showed that in this case the peptide ^{D}Met-Phe-Phe revealed the highest mechanical stability, maintaining its gel nature upon applied stress up to 45 Pa, while the two isomers were disrupted by an applied stress of 30 Pa. If the stress was further increased, the hydrogels underwent to a gel-sol transition, detectable by the inversion of G' and G" values.

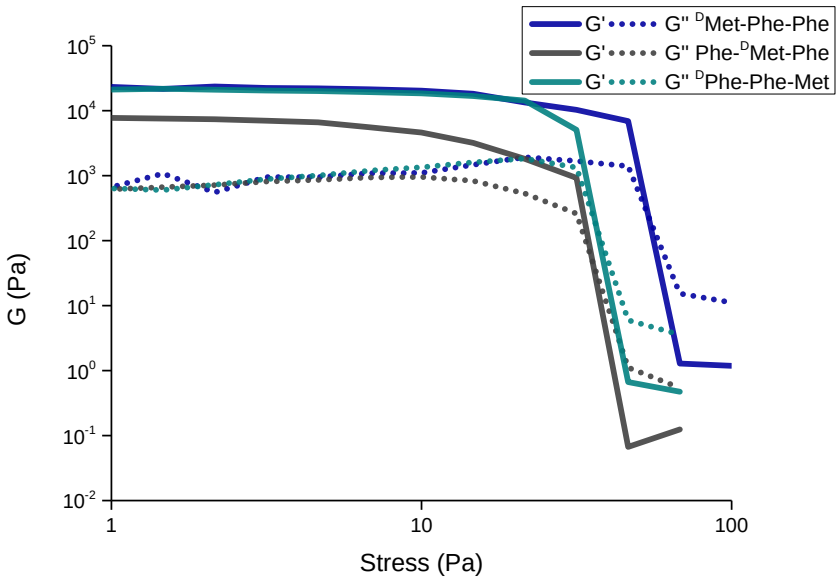

Figure 3.5. Stress sweep analyses of Met-containing peptides.

3.2.4. Hydrogel Nanomorphology: TEM Analyses

TEM analyses were performed by Dr. Slavko Kralj, from Jožef Stefan Institute in Ljubljana, Slovenia, to assess each hydrogel nanomorphology.

As shown in **Figure 3.6 A, B**, and **C**, all the three methionine-containing peptides self-assembled in anisotropic nanostructures that formed the hydrogel network.

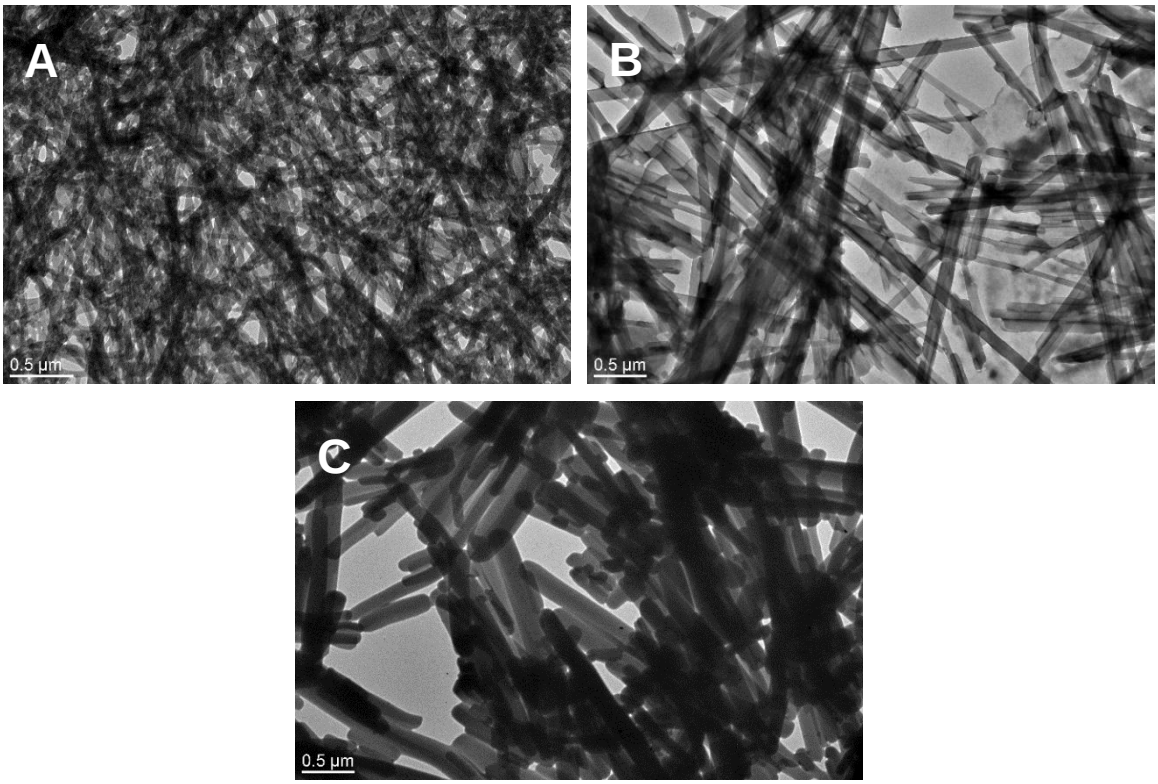

Figure 3.6. TEM micrographs of nanostructured hydrogels obtained from the self-assembly of (**A**) ^{D}Met-Phe-Phe, (**B**) Phe-^{D}Met-Phe, and (**C**) ^{D}Phe-Phe-Met.

Noteworthy differences can be detected analysing the data showed by TEM images. First of all, an increasing of average nanofiber diameters was observed when methionine position was changed from the N-terminus (27 nm) towards the C-terminus (109 nm), passing through the middle of the sequence (72 nm), as highlighted in **Figure 3.7**.

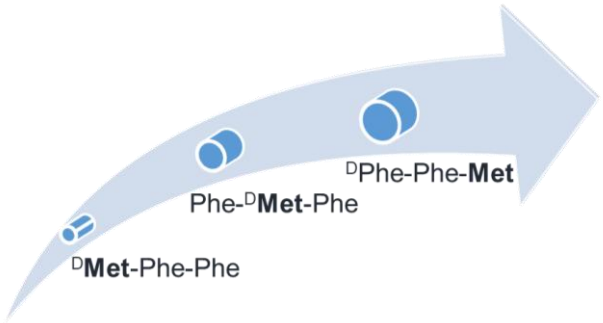

Figure 3.7. Schematic representation of nanofiber diameters of methionine-containing gelling peptides.

The same trend was also noticed about homogeneity of the materials. The presence of a methionine at the N-terminus of the sequence led to narrower nanofiber diameter distribution compared to the other hydrogels analysed, as reported in **Figure 3.8**. Although there is no evident relation between the nanomorphology and the rheological behaviour described above, it is possible that the thin fibril network of ^{D}Met-Phe-Phe allowed for more contact points between fibrils, thus rendering the material overall more resistant against applied stress.

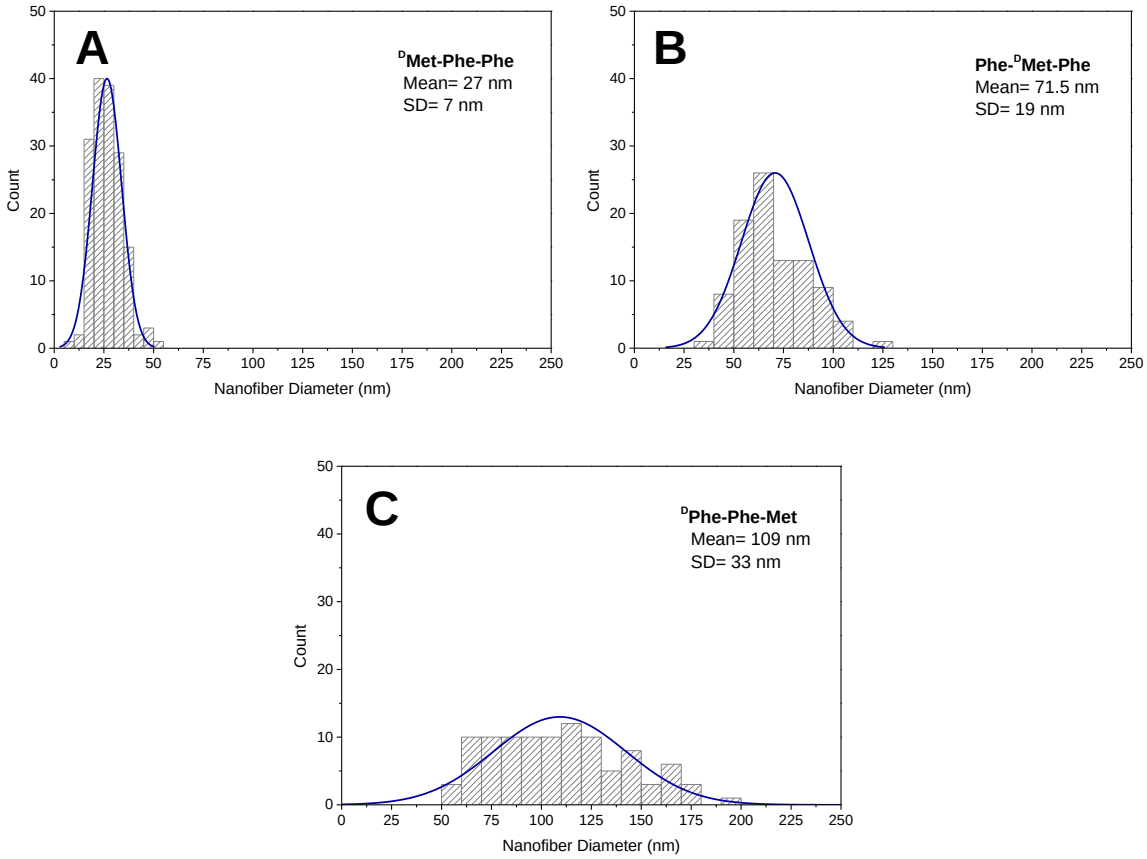

Figure 3.8. Gaussian distributions of nanofiber diameter hydrogels obtained from the self-assembly of **(A)** ^{D}Met-Phe-Phe, **(B)** Phe-^{D}Met-Phe, and **(C)** ^{D}Phe-Phe-Met.

Heterogeneity of nanostructure dimensions is a known issue that is due to the hierarchical mechanism of self-assembly, which proceeds uncontrolled from fibrils to their bundling into fibers of various thicknesses. Our previous study revealed that introduction of external

elements, such as carbon nanodots, during the self-assembly of an heterochiral tripeptide, could be a successful approach to hinder bundle formation and achieve homogeneous nanostructured hydrogels.[87] On the other hand, these new outcomes suggest that merely a change in the position of the sulfur-bearing amino acid along the peptide sequence is sufficient to access different fibril diameters, both in terms of average size and distribution width.

3.2.5. Circular Dichroism Analyses

Circular dichroism (CD) is a spectroscopic technique related to UV spectroscopy and employed to study chiral molecules. It can give important structural information since it is based on sample absorption of UV-Vis radiation (typically in 200-500 nm wavelength range), although recent developments in this field allowed the use of infrared radiations in vibrational circular dichroism (VCD).[88] In CD analyses, the radiation is a linearly polarised UV light, which is made of two components: a left-handed and a right-handed circularly polarised light. A chiral chromophore can absorb such components with different intensity, thus altering the circular polarised light in an elliptical polarised one, where the difference between the two absorbance values gives rise to circular dichroism spectrum (in molar ellipticity, Θ), related to wavelength.

CD is a widely used technique for conformational studies of peptides and proteins. In this case, the possible chromophores are associated with:

- amide bonds, whose possible electronic transitions are $\pi \rightarrow \pi^*$ at 180-200 nm and $n \rightarrow \pi^*$ at 210-230 nm;
- side chains of aromatic amino acids (*e.g.*, Phe, Tyr, Trp), whose electronic transitions are related $\pi \rightarrow \pi^*$ at 250-300 nm.

Establishments of non-covalent interactions between peptide molecules that involve amide bonds and their environment induce typical CD spectra, which can help the identification of secondary arrangement adopted by short peptides into supramolecular nanostructures.

In order to better assess the self-assembly process of methionine containing peptides, CD analyses were performed for each peptide following the evolution from the non-assembled

state towards the supramolecular assembled one. To ensure the former working conditions, CD spectra were acquired over time (to monitor for the lack of spectral changes due to assembly) at low concentration (1 mM, 10 times below the MGC), and in alkaline conditions, at which the peptides are typically dissolved.

In their non-assembled states, the three peptides displayed similar spectra (as reported in **Figure 3.9**) with two positive maxima at 198 nm and 216 nm, which were due to the above-described transitions of amide bonds. The lack of CD features above 270 nm suggests that the aromatic side chains do not influence the CD spectra.

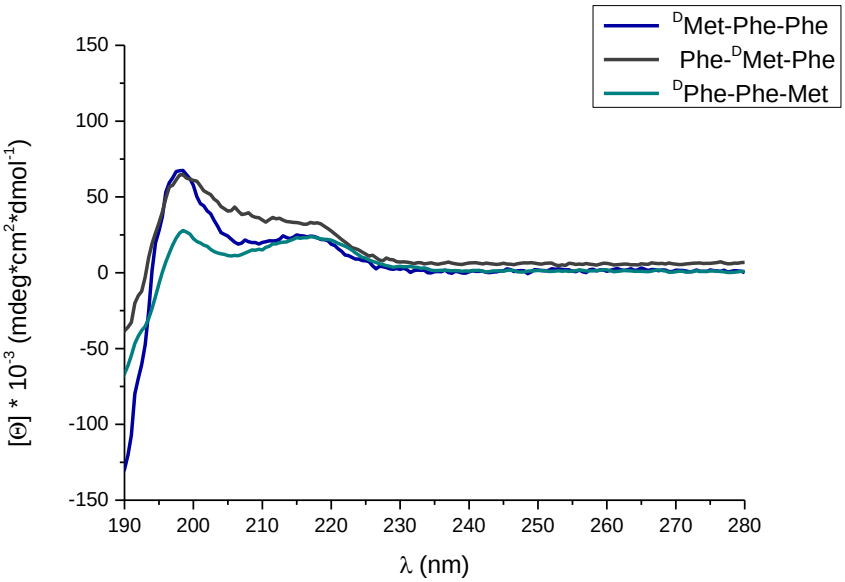

Figure 3.9. CD spectra of Met-containing peptides in solution.

Although such spectra cannot be ascribed to the most common conformations typically adopted by peptides (such as α-helices or β-sheets), they are consistent with our recent studies on the self-assembly of L-D-L tripeptides based on Phe-Xaa-Phe sequence (where Xaa = Val, Leu, Ile, etc.). In that case, a combined approach, based on theoretical and experimental CD analyses, molecular dynamic (MD) simulations, and single-crystal XRD data, revealed that all tripeptides visited a population of conformations in solution, as expected for such flexible molecules, whereas the most stable peptide conformations for the L-D-L tripeptides populated the region of the Ramachandran plot where type II β-turns were found.[43] Although classical turn definition is based on sequences that feature at least four

amino acids, these conformations can be considered turns also based on the requirements of overall change of direction of the peptide backbone, and $C\alpha_1$-$C\alpha_3$ distance being less than 7 Å.[89]

In order to study the evolution of peptide self-assemblies and their kinetics, the heterochiral peptides were analysed by CD spectroscopy at their minimum gelling concentrations at neutral pH, similarly to what was done for rheology time-sweep measurements. CD spectra of assembled states in hydrogels displayed dramatic differences relative to those in solution. In particular, in the case of ^{D}Met-Phe-Phe and Phe-^{D}Met-Phe, CD signals gave negative values, showing both an intense minimum at 222 nm that suggested important peptide conformational changes during the self-assembly process. The presence of noise below 220 nm did not allow to visualise the fine details of the spectra in that region.

Accordingly to rheological results previously discussed, almost instantaneous self-assembling behaviour was observed for ^{D}Met-Phe-Phe, as reported in **Figure 3.10**. Instead, the peptide containing Met residue in the middle of the sequence showed slower assembling kinetics (**Figure 3.11**).

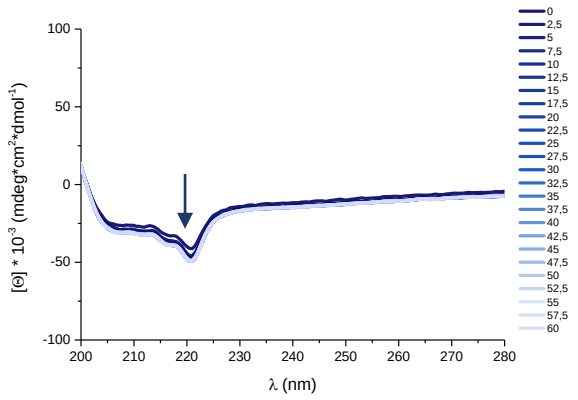

Figure 3.10. Evolution of CD spectra of peptide ^{D}Met-Phe-Phe during the assembly. Arrow indicates direction of signal evolution over time.

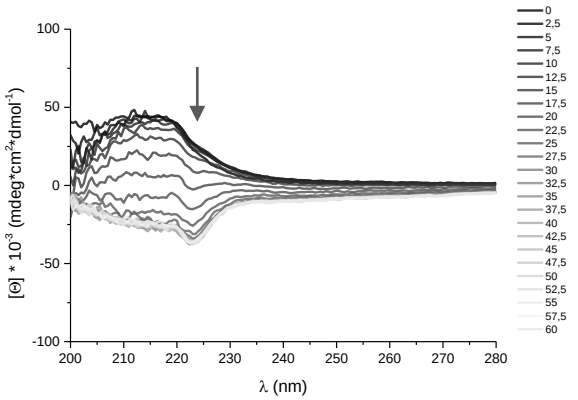

Figure 3.11. Evolution of CD spectra of peptide Phe-^{D}Met-Phe during the assembly. Arrow indicates direction of signal evolution over time.

CD spectra of the peptide containing Met residue at the C-terminus of the sequence, surprisingly, showed a different profile relative to the other two peptides of the series (**Figure 3.12**). CD spectra at MGC displayed a minimum at 222 nm (as observed also for

the assembled state of the other two peptides) and a positive maximum at 199 nm. However, over 1 hour, the CD signal displayed continuous changes, whereas both maximum and minimum decreased their intensity to finally give, after 15 minutes, a stable positive spectrum, whose features are similar to the non-assembled state. This evolution of the CD signature suggested that peptide molecules immediately self-organised themselves, but they reached a kinetically stabile state after a series of rearrangements that took place in the first 15 minutes.

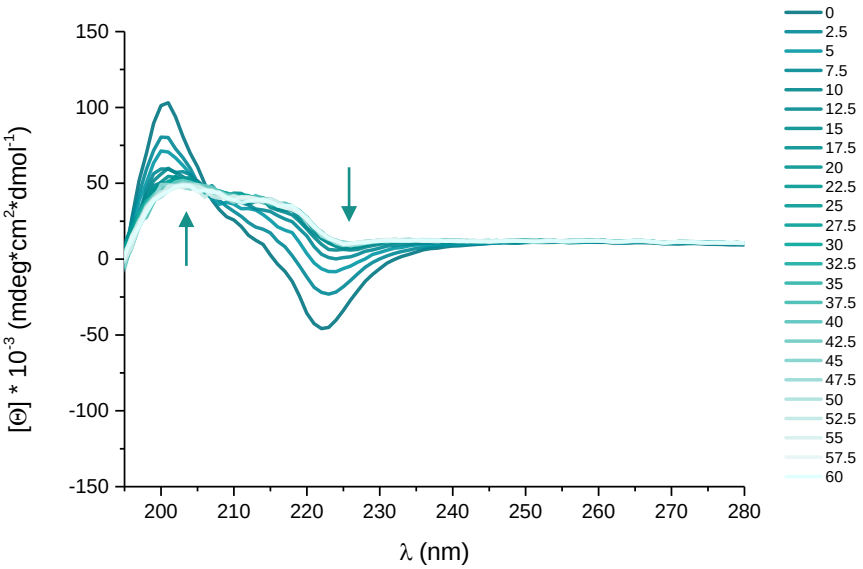

Figure 3.12. Evolution of CD spectra of peptide ^{D}Phe-Phe-Met during the assembly. Arrows indicate direction of signal evolution over time.

CD spectroscopy was also used to test the thermal stability and, eventually, the thermoreversibility of conformations adopted by peptides in the assembled nanostructures. After 1 hour of self-assembly, a heating ramp was applied to the systems and CD spectra were collected. In **Figure 3.13**, evolution of CD spectra of ^{D}Met-Phe-Phe is reported as an example to show how gradual heating induced changes in the supramolecular structures until 80 °C, at which temperature the CD signature matched that of the non-assembled state, thus confirming complete disassembly.

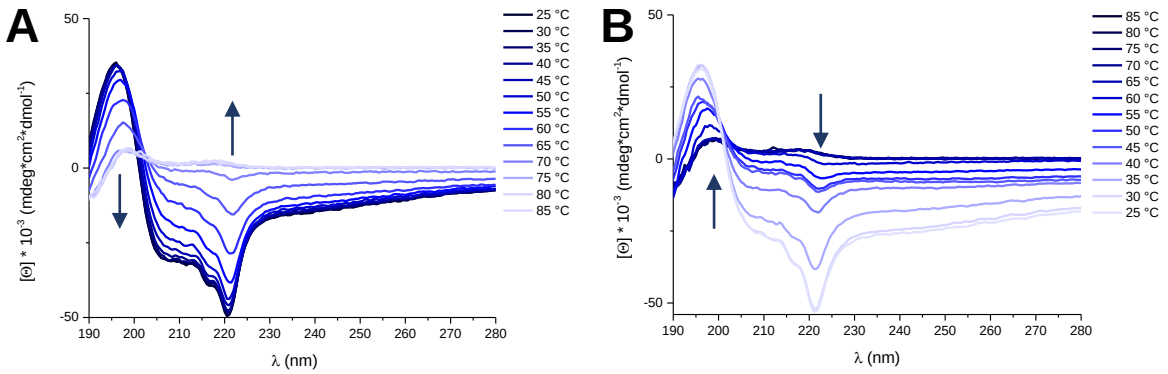

Figure 3.13. Evolution of CD spectra of peptide ^{D}Met-Phe-Phe during a (**A**) heating and (**B**) cooling ramp. Arrows indicate direction of signal evolution over temperature.

To assess the melting temperature (Tm) of each nanostructured hydrogel, the values of molar ellipticity at 223 nm were plotted against temperature and they are reported in **Figure 3.14**. The hydrogel based on the peptide containing methionine at the N-terminus showed the highest thermal stability, with a melting temperature of 60 °C, relative to 50 °C for the other two. This data is in agreement with the mechanical stability trend against applied stress observed by rheometry and discussed above.

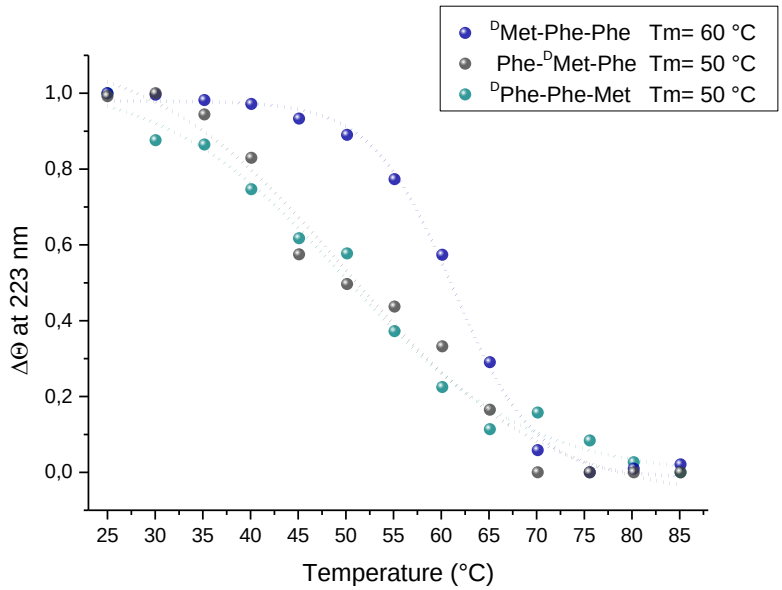

Figure 3.14. Evolution of CD spectra of peptide hydrogels over heating.

All the three nanostructured hydrogels exhibited thermoreversibility, verified also through visual observations reported in **Table 3.3**. The hydrogels disassembled with heating and re-assembled after cooling to room temperature.

Peptide Sequence	**^{D}Met**-Phe-Phe	Phe-**^{D}Met**-Phe	^{D}Phe-Phe-**Met**
Melting Temperature	 60 °C	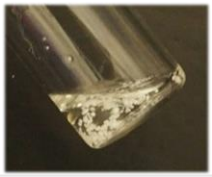 50 °C	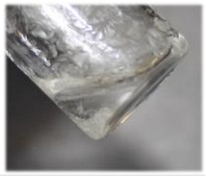 50°C
Thermoreversed hydrogel	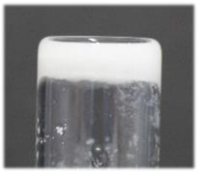	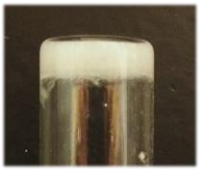	

Table 3.3. Photographs of disassembling hydrogels at their melting temperatures and thermoreversed hydrogels.

3.2.6. Infrared Spectroscopy

Although infrared radiation (IR) is defined to be in the area between visible (< 700 nm) and microwave (> 1mm) radiations, the region typically employed in IR spectroscopy is in the frequency range of 2.5-25 μm, which corresponds to 4000-400 cm^{-1} wavelength number. These energy values are associated to vibrational transitions. Considering that bonds of all molecules that constitute matter are constantly vibrating and the number of possible vibration modes (*e.g.*, symmetric and asymmetric stretching, bending in and out of plane, scissoring, rocking, wagging, twisting) in a non-linear molecules are 3N-6 (where N is the number of atoms), the intensity of IR absorption depends on dipole moment changes upon vibrating. IR spectroscopy can be used to evaluate secondary conformations of peptides and proteins, looking at bands related to amide bond vibration modes:

- Stretching N-H: 3500 - 3200 cm^{-1};
- Stretching C=O (amide I): 1700 cm^{-1};
- Bending N-H (amide II): 1650 - 1500 cm^{-1}.

Establishment of non-covalent interactions (*e.g.*, hydrogen bonds, salt bridges) that involve amide bonds and induce different peptide supramolecular packing (such as beta sheet, alpha helix or random coil), can be detected by IR spectroscopy due to shifting of such bands.

Xerogels were analysed using Fourier-transformed IR (FTIR) to better assess supramolecular behaviour of Met-containing peptides. Spectra are reported in **Figure 3.15**.

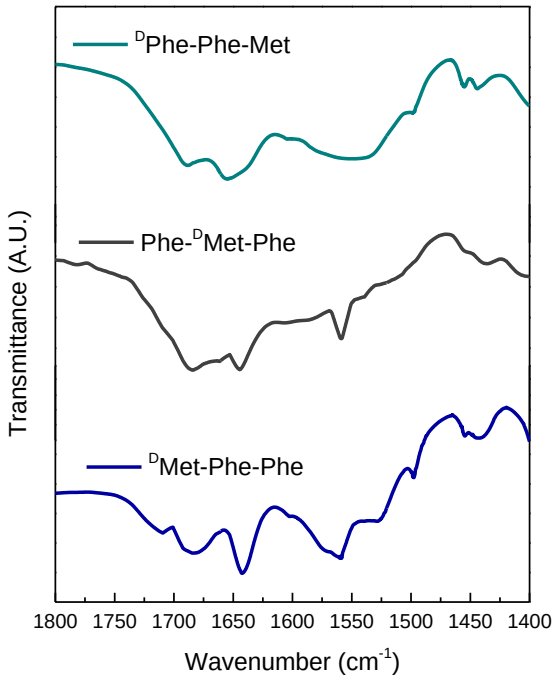

Figure 3.15. FTIR spectra of xerogels obtained by methionine containing tripeptides.

All the three xerogels displayed a band at ca. 1688 cm^{-1}, which is compatible with the presence of trifluoracetic (TFA) counterion, derived from HPLC purification. The gel based on the assembly of the peptide that contains Met at the C-terminus of the sequence revealed an intense band at 1653 cm^{-1}, which is the region assigned to α-helices, accompanied by a shoulder in the beta-sheet region. The other two samples showed a blue-shift to 1644 cm^{-1}, the region where β-sheet or random coil conformations are generally found. To better

evaluate peptide conformation, it appeared necessary to perform further analysis as described below.

3.2.7. Thioflavin T Fluorescence Assay

Amongst the several fluorescent dyes (*i.e.*, Congo Red, Nile Blue, Thioflavin T) that are reported to study amyloid fibrillization process of polypeptides and proteins, Thioflavin T (ThT) is probably the most employed because it is able to emit an intense fluorescence when it binds to fibrils. In particular, the ThT binding to at least four hydrophobic beta-strands induces an increase of fluorescence emission that allows to assess the presence of hydrophobic grooves into the assembled state.[90] Fluorescence of ThT in solution is quenched by the free rotation of the bond between two aromatic moieties (*i.e.*, benzothiazole and the dimethylanilino units reported in **Figure 3.16**). Thus, fluorescence occurs when ThT binding to amyloid fibrils hampers such rotation.[91, 92]

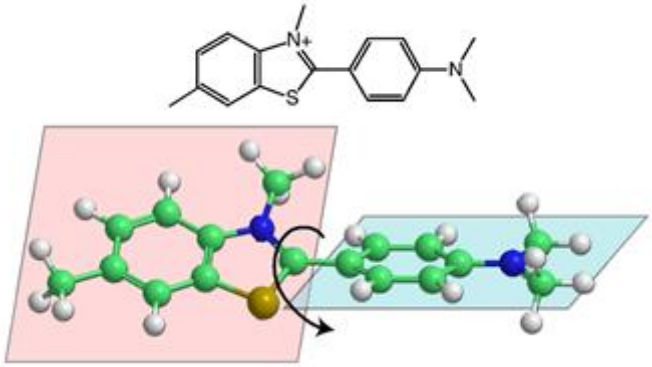

Figure 3.16. Chemical structure and the two planer segments of ThT. Rotational immobilization of ThT preserves the excited state, resulting in a high quantum yield of fluorescence. Adapted with permission from ref. 92 © 2010 Elsevier.[92]

In the case of the three nanostructured hydrogels, ThT fluorescence assay was performed to gain more insights into the supramolecular arrangement of tripeptides. As reported in **Figure 3.17**, all the hydrogels positively responded to ThT test, even though with different intensity. In particular, Phe-^{D}Met-Phe gave rise to highest fluorescence values, while the isomer bearing the Met at the C-terminus was weakly fluorescent upon ThT binding.

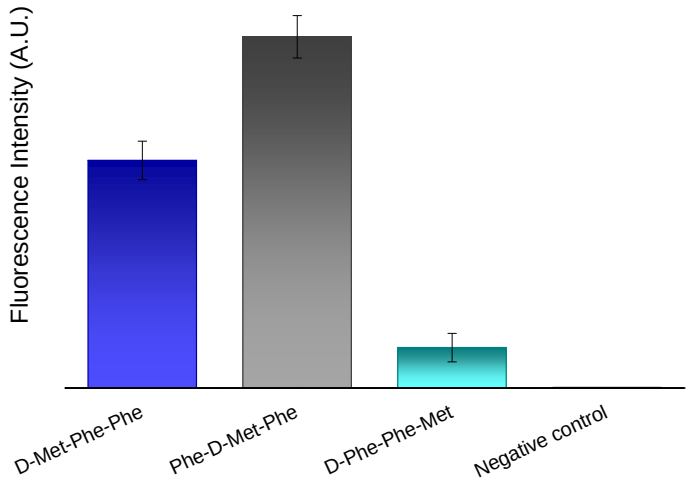

Figure 3.17. ThT fluorescence intensity assay of nanostructured hydrogels, based methionine containing tripeptides.

These differences in fluorescence responses to ThT are in agreement with the FTIR data, since ^{D}Met-Phe-Phe and Phe-^{D}Met-Phe gels both display significant fluorescence as well as an IR signature corresponding to beta sheets. On the contrary, ^{D}Phe-Phe-Met gel displayed a FTIR signature in the amide I region corresponding mainly to an α-helix, which is not expected to bind ThT, and only a minor shoulder in the beta-sheet region, and indeed only weak fluorescence was observed. However, a fine correlation between fluorescence emission intensity and supramolecular organisation was not evident. Several factors have to be taken in consideration, including hydrophobicity of supramolecular assemblies, spatial extension of grooves, permeability of the dye through the hydrogel phase. Certainly, each peptide is able to bind to ThT molecules with different affinity, whereby the two nanostructured hydrogels that showed narrower fibril diameter distributions forming more homogenous networks (*i.e.*, ^{D}Met-Phe-Phe and Phe-^{D}Met-Phe) offered extensive surfaces to bind to ThT molecules.[87]

3.2.8. Single Crystal X-Ray Diffraction

Single-crystal X-ray diffraction (XRD) data were collected by Prof. Rita De Zorzi and her team at the University of Trieste, using the facilities of Elettra Synchrotron (Area Science Park, Basovizza, Trieste, XRD1 beamline).

3.2.8.1. Single-Crystal XRD Data of ^{D}Met-Phe-Phe

The asymmetric unit contains a molecule of the peptide in its zwitterion form, a molecule of ethanol, and two molecules of water (ethanol and water have been used as solvents in the crystallization experiment). A total of 2 molecules of peptide, related by symmetry operators of the $P2_1$ space group, are present in the unit cell (**Figure 3.18A-C**).

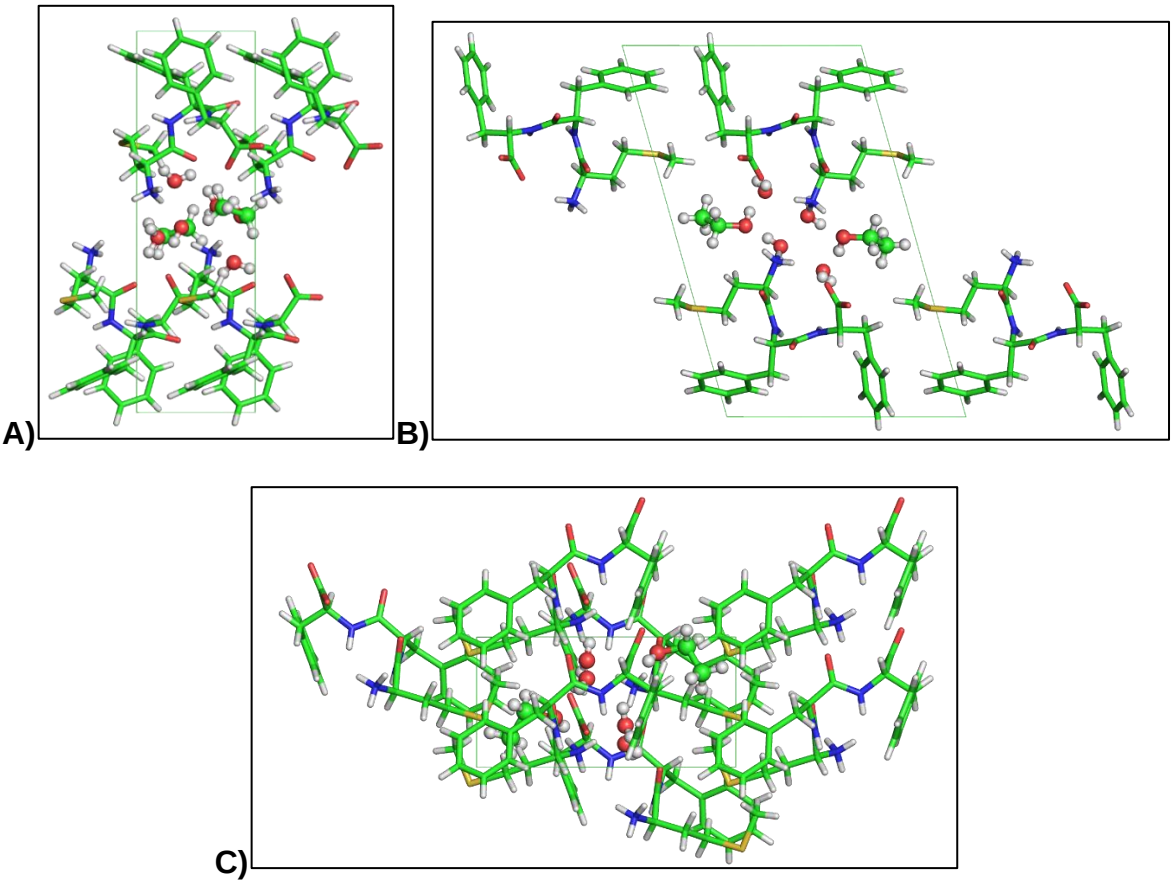

Figure 3.18. Unit cell of crystals of ^{D}Met-Phe-Phe. Crystal packing in the crystal of the peptide ^{D}Met-Phe-Phe, grown in ethanol and water. Views along (**A**) the *a* crystallographic axis, (**B**) the *b* crystallographic axis and (**C**) the *c* crystallographic axis. Peptide molecules are shown as sticks, solvent molecules are shown as spheres. Carbon atoms are shown in green, oxygen atoms in red, nitrogen atoms in blue, sulfur atoms in yellow, hydrogen atoms in white.

The crystal packing shows channels based on hydrophilic interactions involving the backbone of the peptides and the solvent molecules, surrounded by a prevalence of hydrophobic groups, *i.e.* the phenyl moieties (**Figure 3.19**).

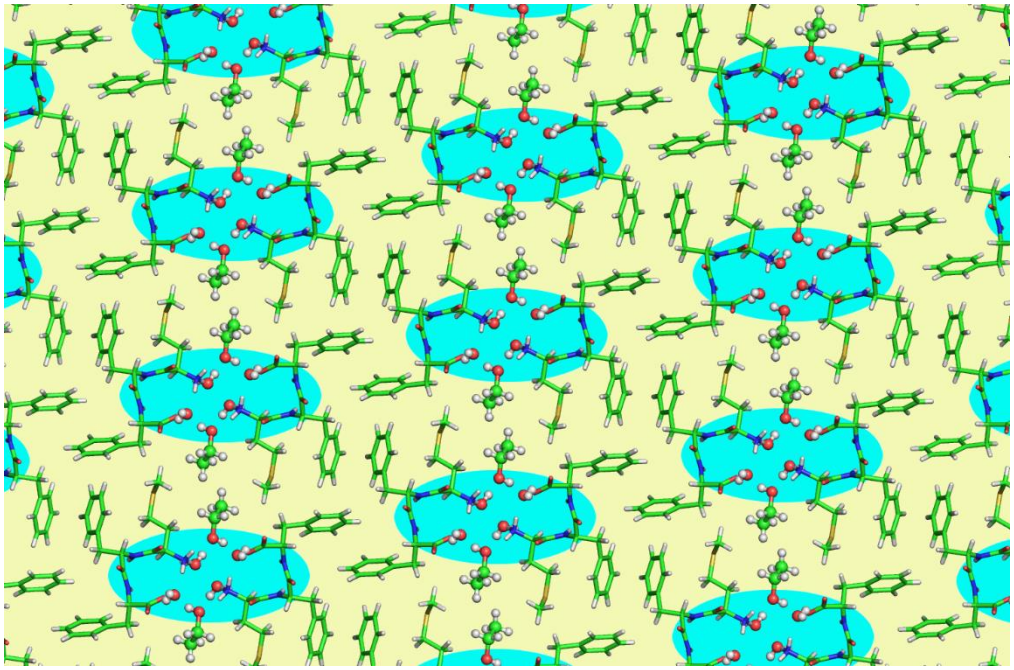

Figure 3.19. Packing of peptide and solvent in the structure of ^{D}Met-Phe-Phe. Hydrophilic channels in the crystal of ^{D}Met-Phe-Phe. Hydrophobic components are shown with a yellow background, hydrophilic channels with a blue background. Crystal packing is shown along the *b* crystallographic direction.

In particular, in the hydrophilic channels interactions between the peptide molecules are mediated by solvent (**Figure 3.20**).

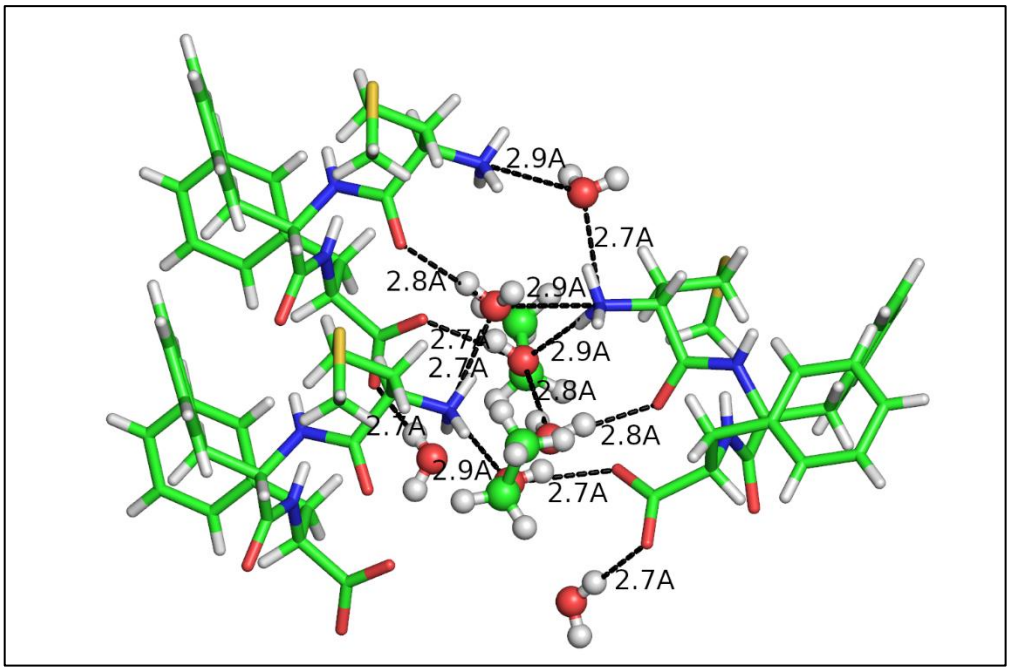

Figure 3.20. Hydrogen bond and salt bridge interactions in the hydrophilic channels
Within the hydrophilic channels, interactions between peptides are mediated by hydrogen bond and salt bridge interactions between solvent molecules and peptide moieties, *i.e.* carboxylate groups, amino groups and amide groups. Donor-acceptor distances are reported.

In the crystallographic direction *b*, peptides forming piles are held together by hydrophilic interactions (**Figure 3.21**), most of which are mediated by solvent molecules (black dashes in **Figure 3.21**).

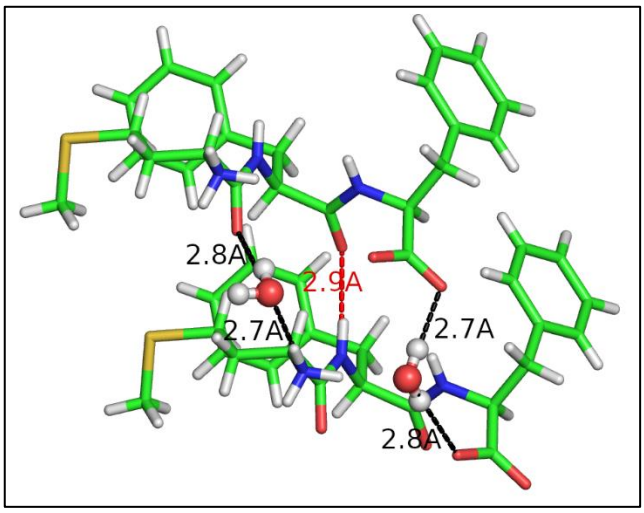

Figure 3.21. Peptide-peptide and peptide-solvent interactions along the *b* crystallographic direction.

Hydrophilic interactions hold together peptide molecules in piles along the *b* crystallographic direction. Most of the peptide-peptide contacts are mediated by interactions with solvent molecules (water), shown in black dashes, while fewer are direct hydrogen bonding interactions between peptides, shown in red dashes.

Crystallographic details of $^{D-}$Met-Phe-Phe are reported in ***Chapter 6*** **(Materials and Methods)** and further crystallographic data in **Appendix** (**Tables A.3.1 and A.3.2**).

3.2.8.2. Single-Crystal XRD Data of ^{D}Phe-Phe-Met

The asymmetric unit contains three molecules of the peptide in its zwitterion form, and 7 molecules of water. The three crystallographically independent molecules of peptide have a similar conformation of the backbone and side chains of the first and third residue, but they differ for the N-Cα-Cβ-Cγ torsion angle and the Cα-Cβ-Cγ-Cδ torsion angle of the second residue (**Figure 3.22**). A total of 12 molecules of peptide are present in the unit cell, each related to the others by the symmetry elements of the *C2* space group (**Figure 3.23**).

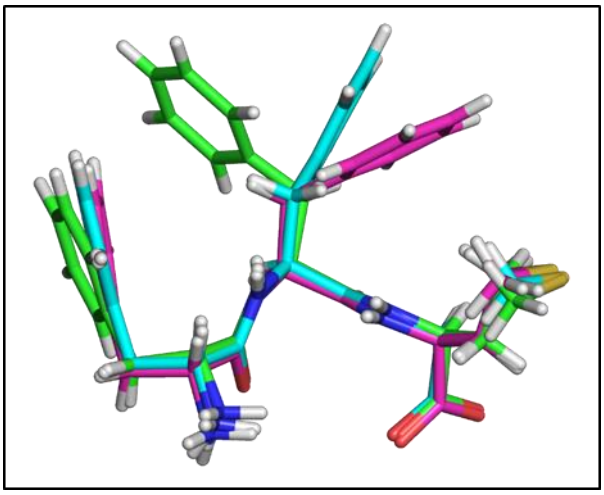

Figure 3.22. Comparison between crystallographically independent molecules in the structure of ^{D}Phe-Phe-Met.

The three crystallographically independent molecules of ^{D}Phe-Phe-Met show a similar backbone conformation, a similar side chain rotamer for the first and third residue, but a marked difference in

the side chain of the second, phenylalanine residue. In particular, torsion angles N-Cα-Cβ-Cγ and Cα-Cβ-Cγ-Cδ have following couple of values for the three independent molecules: (-76.72°, 126.25°), (-156.69°,25.66°), and (90.09°, 95.69°), considering the positive Cα-Cβ-Cγ-Cδ torsion angle. The independent molecules are shown with different colours.

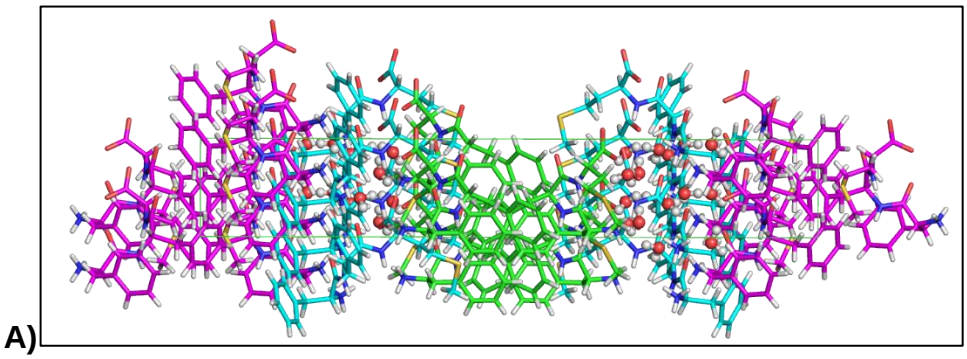

A)

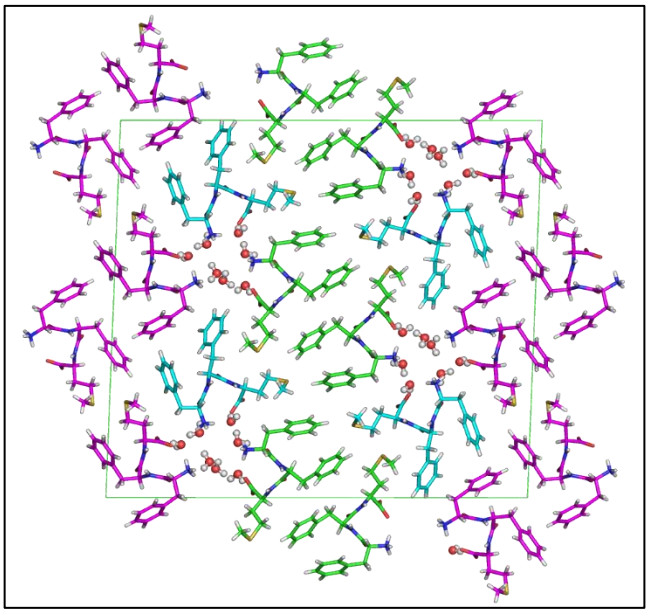

B)

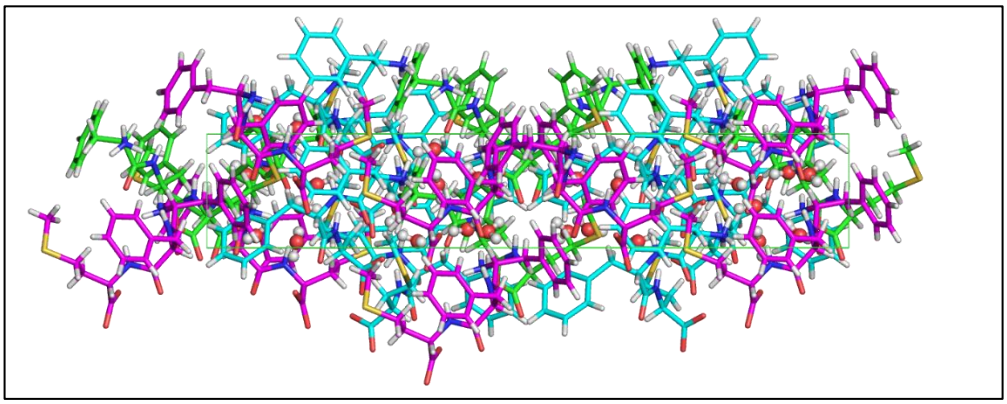

C)

Figure 3.23. Unit cell of crystals of ^{D}Phe-Phe-Met**.** Crystal packing in the crystal of the peptide ^{D}Phe-Phe-Met. Views along (**A**) the *a* crystallographic axis, (**B**) the *b* crystallographic axis and (**C**) the *c* crystallographic axis. Crystallographically independent molecules are shown with different colours.

In the crystal packing (**Figure 3.24**), molecules of ^{D}Phe-Phe-Met form channels along the b crystallographic direction, filled with solvent (water) molecules.

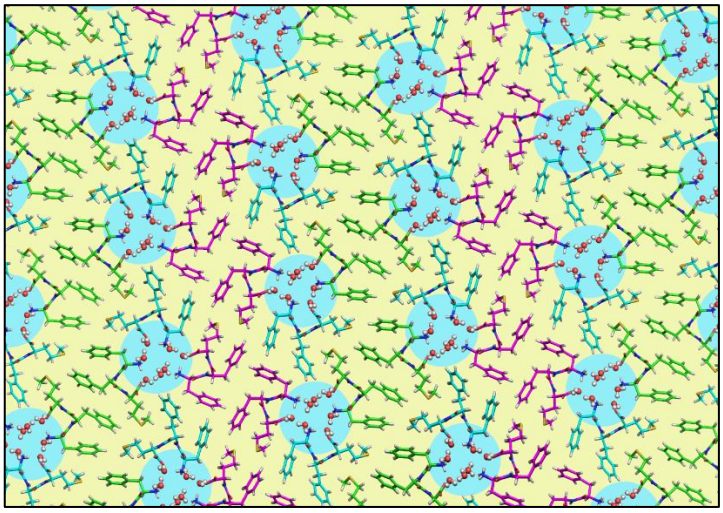

Figure 3.24. Hydrophobic and hydrophilic regions in the crystal packing of ^{D}Phe-Phe-Met**.** Areas with mainly hydrophobic character are depicted with a yellow background colour, channels with water molecules surrounded by the polar groups of the peptide (N- and C- termini and backbone amides) are depicted with a blue background.

The channels have an irregular shape and an average diameter of about 6 Å. The walls of the solvent-filled channels are constituted by the hydrophilic moieties of the peptides, *i.e.* N- and C- termini and amide groups of the backbone, while water molecules inside the channel interact with salt bridges and hydrogen bonds with peptide molecules (**Figure 3.25**). Most of the hydrophilic interactions present in the structure, *i.e.* hydrogen bonds and salt bridges, involve solvent molecules, bridging together the peptide molecules that constitute the crystal. **Figure 3.25** highlights such interactions with black dashes, while peptide-peptide hydrophilic interactions are represented with red dashes. The number of peptide-solvent and peptide-peptide interactions and their donor-acceptor distances show the importance of the solvent molecules in the crystal structure of ^{D}Phe-Phe-Met: interactions involving solvent molecules are in larger number and are shorter than those involving only peptide molecule, indicating that the presence of water molecules is crucial in the formation of the peptide network. In addition, hydrophobic interactions involving the phenylalanine side chains,

contribute to the close packing of the structure (**Figure 3.26**): CH-π interactions and π-π interactions.

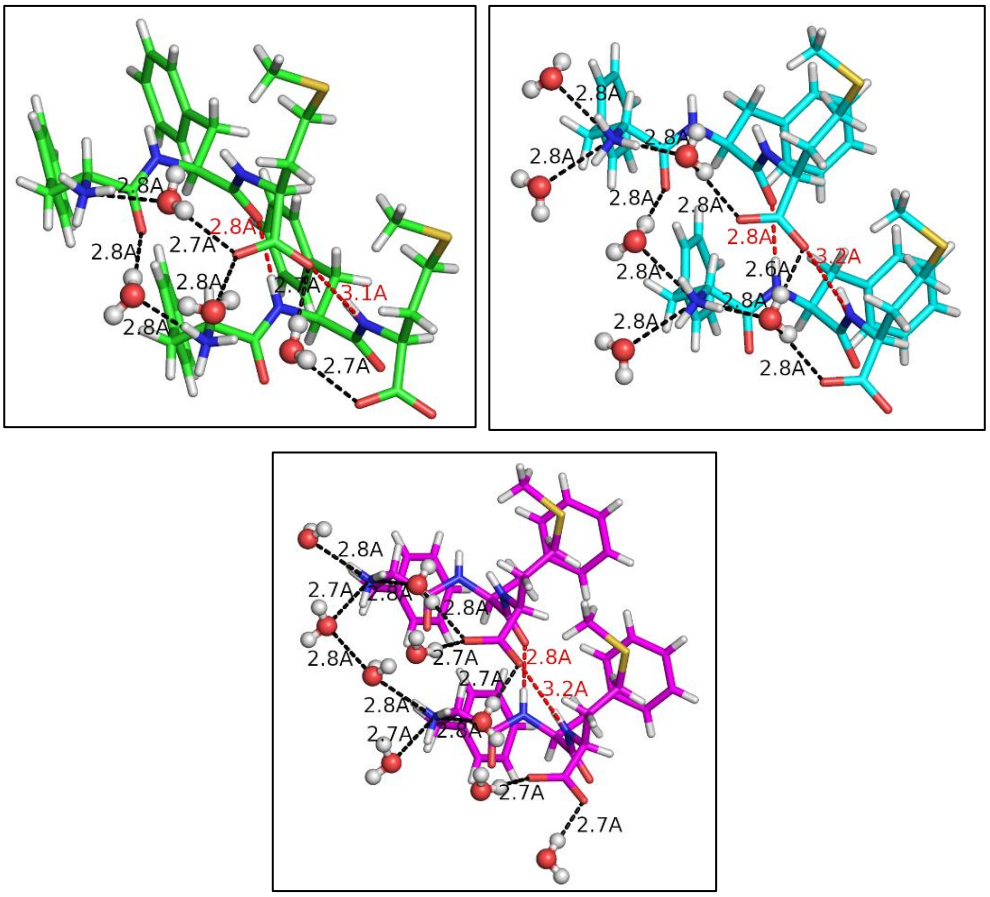

Figure 3.25. Hydrophilic interactions. Pattern of hydrophilic interactions, namely hydrogen bonds and salt bridges. Interactions between peptide molecules and solvent are marked with black dashes and distances between the donor and the acceptor atom are reported. Interactions involving only peptide molecules are marked with red dashes and distances between the donor and the acceptor atom are reported. Crystallographically independent molecules are represented with different colours.

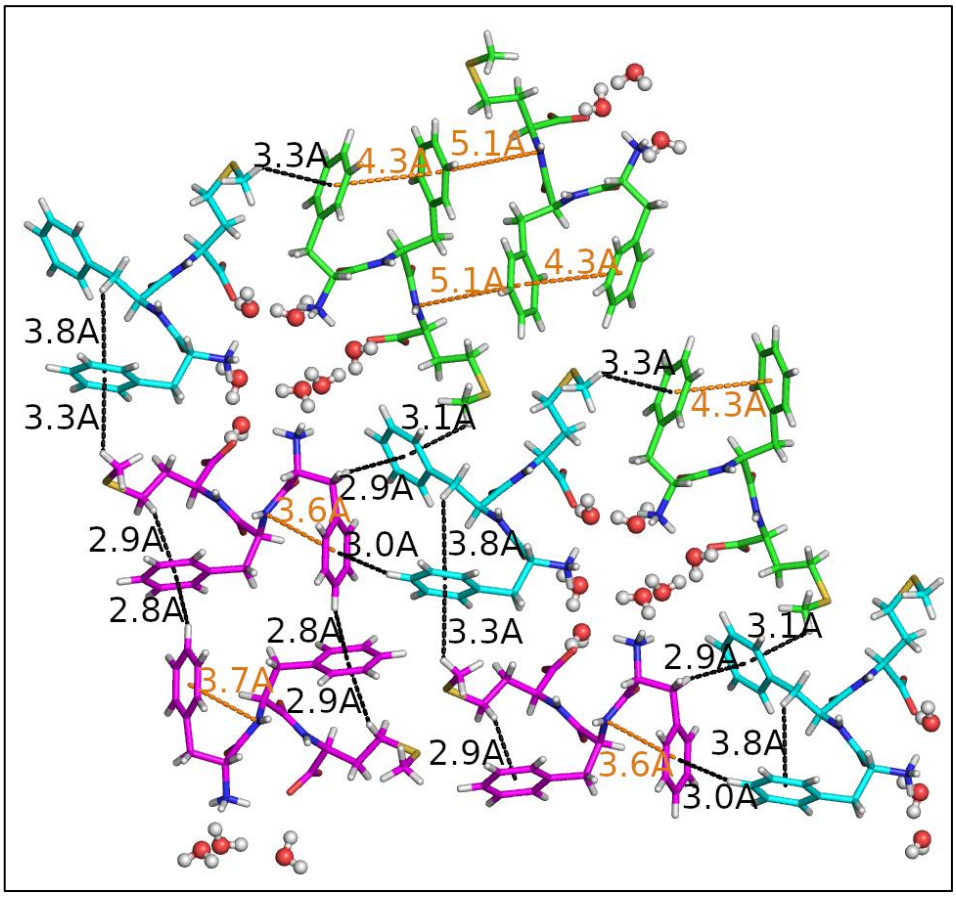

Figure 3.26. Hydrophobic interactions involving phenylalanine side chains. Numerous hydrophobic interactions are present in the structure of ^{D}Phe-Phe-Met and contribute to the crystal packing. Among them, CH-π interactions, shown as black dashed, involve phenyl rings as π aromatic systems, and methyl and methylene groups of the methionine residues, methylene groups and hydrogens of the phenyl ring of phenylalanine residues, as hydrogen atom donors. Distances between the hydrogen atom and the center of the phenyl ring are reported. π-π interactions, reported in orange dashes, involve phenyl rings or π-delocalized systems of the peptide backbone. Distances between the centers of the phenyl rings, or between the center of the phenyl ring and a nitrogen atom of the backbone are reported.

Crystallographic details of ^{D}Phe-Phe-Met are reported in ***Chapter 6*** **(Materials and Methods)** and supplementary data are reported in **Appendix** (**Tables A.3.1 and A.3.2**).

3.2.9. Cytocompatibility Tests

Nanostructured hydrogels could find several bio-applications, such as scaffolds for cell growth, tissue engineering, or drug delivery in nanomedicine. For these reasons, two out of three hydrogels (*i.e.*, those based on the self-assembly of ^{D}Met-Phe-Phe and ^{D}Phe-Phe-Met) were tested for their cytotoxicity in fibroblast cell culture *in vitro*. After 72 hours, the cells presented a good viability and the hydrogels did not lead to cytotoxicity. These experiments were performed by Dr. Evelina Parisi in collaboration with Prof. Mikaela Grönholm at Helsinki University. Biocompatibility assays on the third hydrogel (based on the self-assembly of Phe-^{D}Met-Phe peptide) are currently ongoing.

Two types of tests were performed on hydrogels in order to assess their potential cytotoxicity:

- LIVE/DEAD viability/cytotoxicity tests;
- MTS (3-(4,5-dimethylthiazol-2-yl)-5-(3-carboxymethoxyphenyl)-2-(4-sulfophenyl)-2H-tetrazolium, inner salt) cell proliferation assays.

The cell line that was selected to perform biocompatibility assays is murine fibroblast cells, because of their manageable ability to spread and grow in a short period of time. ^{D}Val-Phe-Phe hydrogel was used as a gel control, since it was previously reported to lead to good cell viability and spreading.[58]

3.2.9.1. LIVE/DEAD Viability/Cytotoxicity Assay

The test is based on the use of two fluorescent dyes, *i.e.* calcein AM and ethidium homodimer (Eth D-1). Calcein AM is a molecule that is able to permeate cell membranes. It doesn't emit fluorescence itself, but it is able to emit an intense green fluorescence, when its ester groups are hydrolysed by ubiquitous esterase enzymes present in living cells. For this reason, it is used as marker of living cells. On the other hand, Eth D-1 is able to intercalate nucleic acids emitting, thus, a red fluorescence. Since it doesn't have membrane permeation ability, its red fluorescence emission is an indicator of the presence of dead cells, whose broken membranes allow the exhibition of nucleic acid to Eth D-1 binding. The combined use of the two dyes gives complementary information about the viability and the spreading ability of cells in hydrogel scaffolds. Microscopy images were collected every 24 hours over three days of cell culture and they are reported in **Figures 3.27-3.29**.

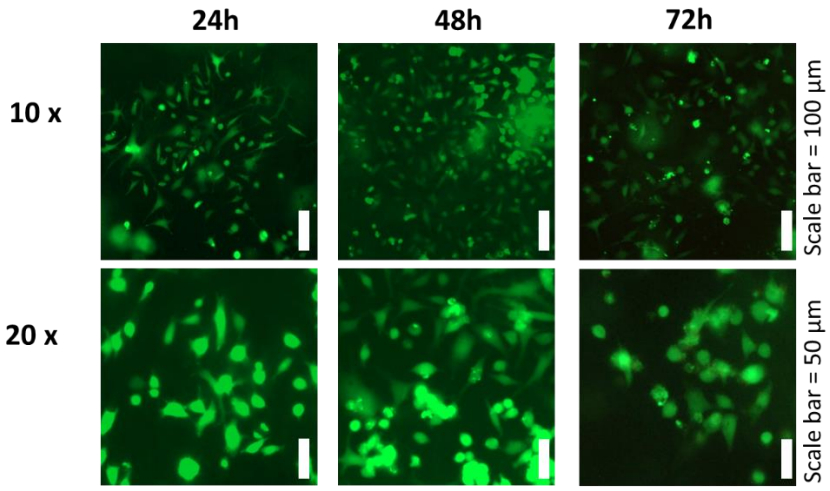

Figure 3.27. Images of live/dead staining ^{D}Val-Phe-Phe hydrogel control over 3 days of fibroblast cell culture.

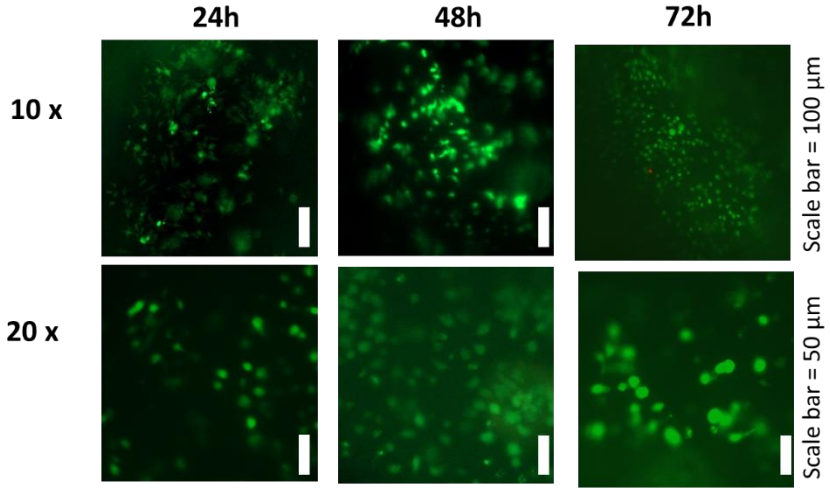

Figure 3.28. Images of live/dead staining ^{D}Met-Phe-Phe hydrogel over 3 days of fibroblast cell culture.

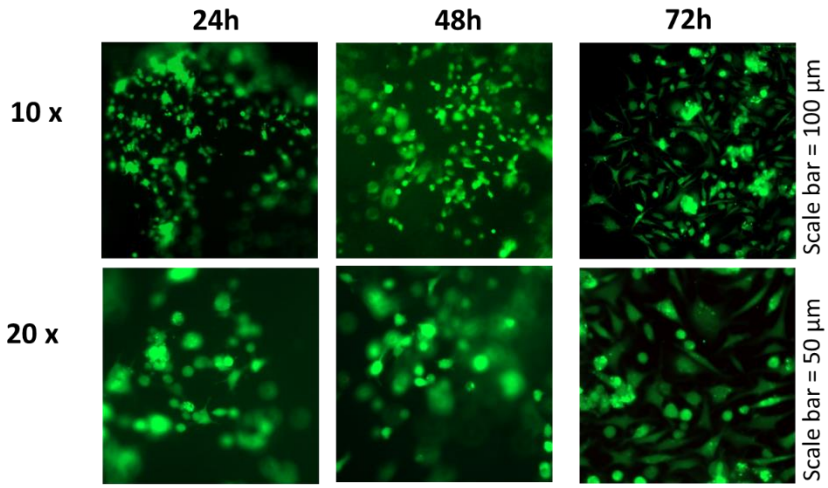

Figure 3.29. Images of live/dead staining ^{D}Phe-Phe-Met hydrogel over 3 days of fibroblast cell culture.

All the three hydrogels led to high cell viability and comparable cell density. ^{D}Phe-Phe-Met led to a higher degree of cell spreading, however, this was also the stiffer gel as showed by rheometry, and it is well known that harder surfaces promote fibroblast spreading. Importantly, after 72 hours, the hydrogels maintained their gel nature, demonstrating their ability to successfully incorporate cells into their nanostructured networks of fibrils, as reported in **Figure 3.30A-C**.

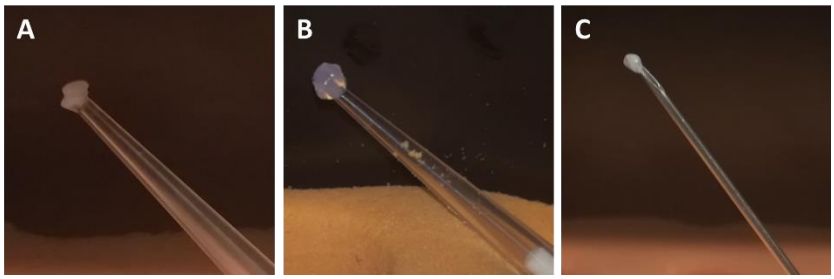

Figure 3.30. Images of hydrogels based on tripeptides (**A**) ^{D}Val-Phe-Phe, (**B**) ^{D}Met-Phe-Phe, and (**C**) ^{D}Phe-Phe-Met after 72 hours of cell culture.

3.2.9.2. MTS Cell Proliferation Assay

The test is established on the ability of living cells to reduce MTS through the action of NAD(P)H-dependent dehydrogenase enzymes. The absorbance of the reduced MTS measured at 490 nm is directly related to the presence of metabolically active cells.

Also in this case, the hydrogel based on ^{D}Val-Phe-Phe was used as a control to normalise the absorbance intensity showed by the two tested nanostructured hydrogels. As reported in **Figure 3.31**, in this test both the hydrogels based on methionine containing peptides apparently performed worse than the control. However, it is highly possible that this test suffered interference from the opaque nature of the hydrogels, which leads to scattering phenomena. In addition, diffusion through the hydrogel phase could be hindered by stiffness, and indeed both hydrogels are stiffer than the control.[58]

Overall, this data did not agree with live-dead fluorescence assay, revealing that MTS results should be treated with caution and other assays should be accurately performed to lead to a comprehensive cytotoxicity analysis of the new 3D nanobiomaterials.

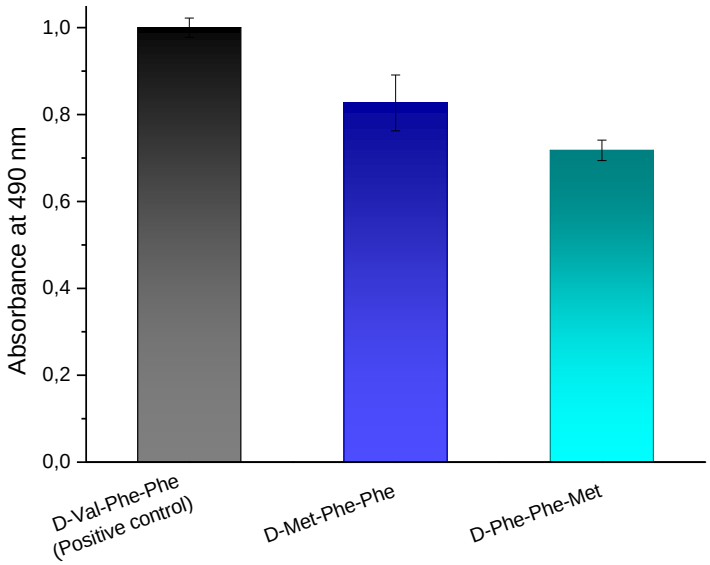

Figure 3.31. MTS assay results for hydrogels based on methionine containing tripeptides.

3.3. Conclusions

All the three peptides containing a methionine residue in a different position along the sequence were successfully synthesised, purified, and characterised. They were all able to self-assemble into self-supporting and nanostructured hydrogels, with good and similar viscoelastic properties. Such results were consistent to those previously reported based on heterochiral hydrophobic gelling peptides, demonstrating not only that the design rules identified by our group successfully correlated chirality and amino acid sequence to an efficient self-assembly, but also they extended the applicability of such prediction rules to peptides containing sulfur bearing amino acids. The thioether moiety, thus, does not alter the self-assembly of short heterochiral peptides and can effectively be used for the creation of new nano-biomaterials, with potential applications as cell scaffolds. Indeed, promising results about their biocompatibility have been provided by cell viability assays, although further studies need to be performed.

Moreover, XRD analyses revealed elegant organisation in water channels, whose dimension and shape are depending on the position of methionine along the sequence. Such findings open the possibility to fine tune supramolecular structures *ad hoc* accordingly for the planned purpose.

Chapter 4: Cysteine-Containing Peptides: Self-Assembly into Nanostructured Hydrogels

4.1. Introduction

4.1.1. Oxidation and Self-Assembly

Cysteine contains a thiol group in the side chain that can be ionised as the negatively charged thiolate ion, which is much more reactive than neutral thiol. The intrinsic pKa of this moiety is around 8.6, however, this value could be remarkably shifted (from 9 to 3) depending on the structure and the environment surrounding the cysteine residue.[93] Moreover, the sulfur atom in cysteine can undergo several oxidative modifications (as shown in **Figure 4.1**) that are pH dependent, since the thiolate is easier to oxidase than the thiol form.[94]

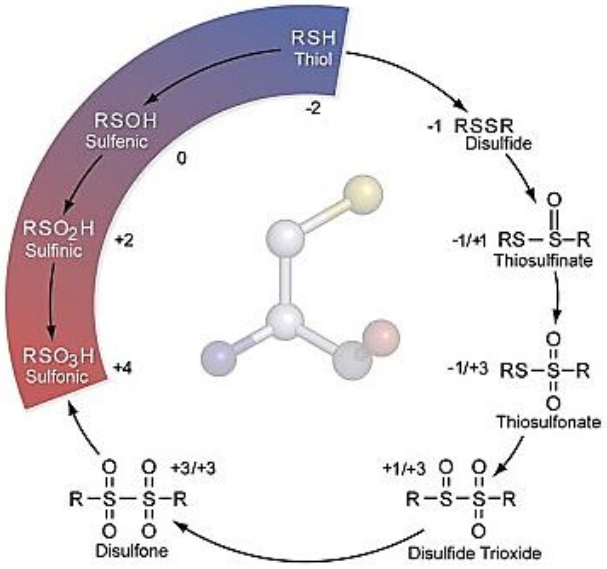

Figure 4.1. Oxidative modifications of cysteine. Reprinted with permission from ref. 94 © 2008 Elsevier.[94]

Amongst the different oxidation states that sulfur atom can display, the most energetically stable is the disulfide form (-1), which is fundamental for the stabilisation of protein folding. Although the other oxidation states (from -2 to +4) are less favoured, they confer cysteine the possibility to exert several biochemical functions, such as catalysis, redox switches, metal binding, and involvement in regulatory and signalling pathways.[94]

All these properties allow Cys to be considered as an amino acid with unique features that can be exploited for the design of new smart and functional nanomaterials. For example,

Dodero and co-workers have recently identified a redox mechanism to modulate amyloid fibril formation, based on a Cys-containing peptide. In particular, they noticed that the self-assembly behaviour of a N-protected tripeptide was dependent on the oxidative state of the Cys sulfur atom (see **Figure 4.2**). Indeed, in reducing conditions (generated by the presence of a reducing agent), the peptide was only able to form nanospheres with a 60 nm diameter, after a solvent switch. Oxidative conditions (pH 8) induced the oxidation to the disulfide that was associated with the formation of elongated nanofibrils with 20 nm diameter. The addition of reducing agent on the formed fibrils brought to their disruption into spherical nanoparticles. Thus, they not only demonstrated the importance of disulfide bond in the formation of amyloid fibrils, but, moreover, they also identified a redox switch for the assembly of the same peptide in different nanostructures.[95]

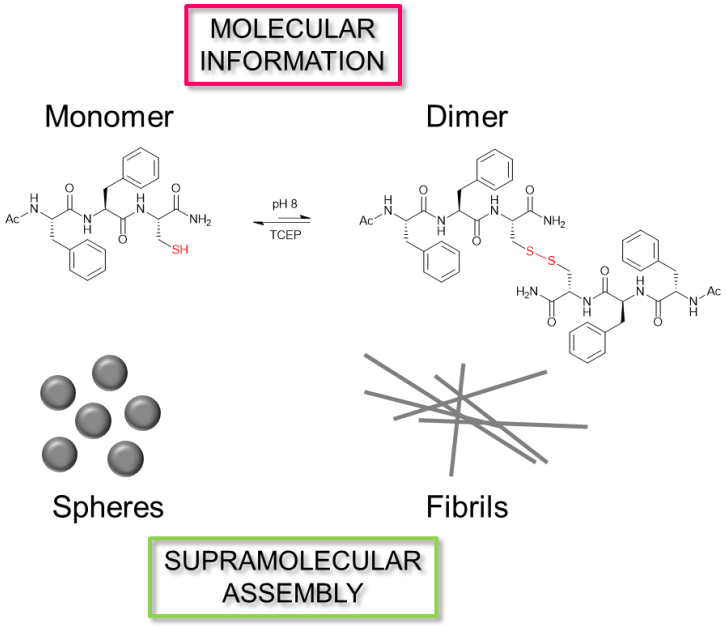

Figure 4.2. Modulating amyloid fibrillation by intermolecular disulfide chemical reduction. Adapted from ref. 95 with permission from the PCCP Owner Societies.[95]

4.1.2. Metal Coordination and Catalytic Activity

The chemistry of sulfur-metal bond has been widely investigated especially in relation with gold binding. Cys-containing peptides, indeed, have been largely reported to be excellent candidates for the production of supramolecular hybrid gold-nanoparticles, with strong chiroptical properties.[96, 97]

Recently, Heddle and collaborators used the intrinsic ability of cysteine to bind gold atoms to develop a synthetic protein able to self-assemble into an ultra-stable gold protein cage with spherical shape. The building block used was a cysteine-containing protein ring, whose self-assembly was triggered by a gold(I)-phosphine compound. The reversible assembly and disassembly (induced by reducing agents) of such 3D architecture was tailored by metal ion coordination, in particular by Cys-Au-Cys bonds, at the interface between two adjacent proteins, as reported in **Figure 4.3.** Surprisingly, the flexibility typical of proteins allowed the unprecedented stabilisation of this particular cage with unusual geometry, *i.e.* Archimedean snow cube, otherwise impossible to be formed: actually, this architecture has never been observed in nature. Moreover, the cages revealed intense stability to chemical and thermal treatments. The hollow cavity formed by such "paradoxical" geometry adopted by protein nanocages conferred them unique properties that can be valuable if used as innovative and smart nanomaterials for intracellular drug delivery, which can be modulated upon external stimuli.[98]

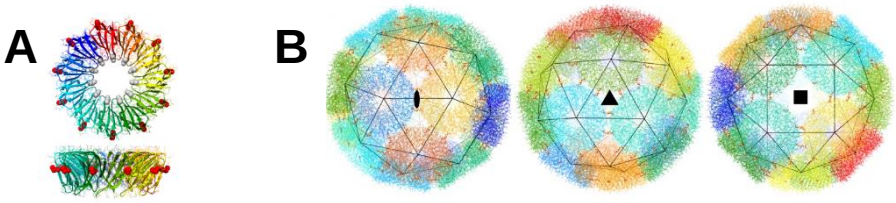

Figure 4.3. Structure of (**A**) Cys-containing protein building block, shown in two orthogonal views and (**B**) three cage models, consisting of 24 protein rings, centred on the (from left to right) two-, three- and four-fold symmetry axes. Adapted from ref. 98 by permission from Springer Nature.[98]

Nevertheless, also ultra-short peptides that contain cysteine residues could have the ability to coordinate metals. For example, the Mansy group reported the possibility of glutathione, a simple tripeptide containing Glu, Cys and Gly, to stabilise iron-sulfur clusters, showing redox catalytic activity. Considering the wide presence of iron-sulfur in many enzymes, the authors envisaged the importance of short peptides in prebiotic environment for the evolution to more complex enzymes (**Figure 4.4**) and opened the door to the possibility of using such simple systems for enzyme mimicry.[99]

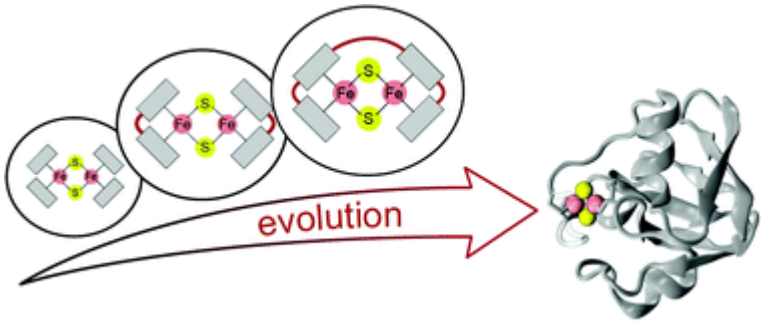

Figure 4.4. Duplications of an iron–sulphur tripeptide lead to the formation of a protoferredoxin. Reproduced from ref. 99 published by The Royal Society of Chemistry, CC BY 3.0.[99]

4.2. Results and Discussion

4.2.1. Design of Selected Peptide Sequences

Previous studies about the self-assembling ability of tripeptides with general designer sequence Phe-Xaa-Phe (where Xaa was an aliphatic amino acid) have been investigated only in the L-D-L stereoconfiguration, alternating, thus, amino acids with opposite chirality,[44] and compared against their homochiral analogues (L-L-L).[43] A comprehensive study about other chirality of the stereocenters in tripeptides, where an aliphatic amino acid was positioned in the middle of the sequence as well as based on cysteine residue, was not reported so far.

Therefore, effects of chirality on the self-assembly of Cys-containing tripeptides have been here systematically investigated, by synthesising four stereoisomers of heterochiral tripeptides containing two Phe residues separated by a Cys, whose chemical structures are reported in the **Table 4.1**. The four enantiomeric forms of these peptides were not taken in consideration, since their supramolecular behaviour in an achiral environment is expected to be the same of their mirror images, as described in **Section 1.2.2**. Therefore, the four compounds depicted below represent the chiral space of Phe-Cys-Phe stereoisomers.

Peptide Sequence	Phe-Cys-Phe	**^{D}Phe**-Cys-Phe	Phe-**^{D}Cys**-Phe	Phe-Cys-**^{D}Phe**
Chemical Structure	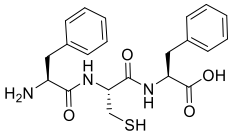	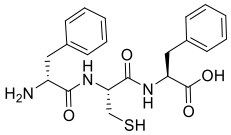	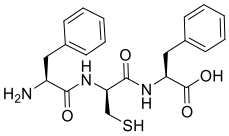	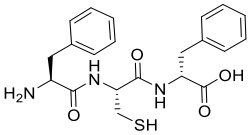

Table 4.1. Selected Cys-containing tripeptides synthesised.

4.2.2. Peptide Synthesis and Characterisation

The peptide syntheses were manually carried out accordingly to standard Fmoc-based solid phase peptide synthesis (SPPS), analogously to Met-containing peptides (**Section 3.2.2**), with some differences due to the presence of Cys, which is more sensitive to side reactions than Met. To avoid the oxidation of Cys, the syntheses were performed into fritted glass funnel under continuous argon stream, which was also bubbled into solvents before their use. Cys derivatives are highly susceptible to base catalysed racemisation reactions that could occur during activation and coupling steps. For this reason, 2,2-chlorotrityl chloride resin was selected as solid support and trityl was selected as protecting group for the sulfhydryl moiety of Cys, since their steric hindrance limits racemisation reactions. With the attempt to avoid epimerisation, Cys coupling was carried out in less polar solvents, using a mixture of dichloromethane (DCM) and *N*, *N*-dimethylformamide (DMF), instead of only DMF used for other amino acid couplings. For the same reason, the use of collidine (TMP), as weaker base than DIPEA, was preferred during coupling reactions.[100]

As reported for Met-containing peptides, also in this case the cleavage was performed treating the resin with reagent L (trifluoroacetic acid, water, TIPS and DTT) that simultaneously cleaved cysteine-protecting group and tripeptide from the solid support. The reaction was carried out for 90 minutes, instead of 120, to limit acid catalysed side reactions.

After having successfully synthesised and purified through reverse phase HPLC the peptides, their purity was assessed by means of spectroscopic techniques, *i.e.*, NMR and LC-

MS. Complete spectroscopic characterisation data of each peptides are reported in the **Appendix**.

4.2.3. Peptide Self-Assembly

The four peptides synthesised were tested for self-assembly into supramolecular materials. The trigger method selected to induce self-assembly was a temperature switch, unlike to what was done for Met-containing tripeptides (***Chapter 3***), whereas a pH switch (from alkaline to neutral pH) was employed. In this case, dissolution of Cys-containing peptides in alkaline buffer with pH > pKa of thiol group have been preferentially avoided, in order to prevent possible oxidation reactions (described in **Section 4.1.1**). For this reason, peptides were dissolved at 15 mM concentration in a neutral buffer by heating up and manually shaking the samples. When completely dissolved, the samples were left to cool down gradually to room temperature.

4.2.3.1. Tube Inversion Test

Formation of supramolecular materials was visually monitored and reported in **Table 4.2**.

Peptide Sequence	Phe-Cys-Phe	^{D}**Phe**-Cys-Phe	Phe-^{D}**Cys**-Phe	Phe-Cys-^{D}**Phe**
Photographs of the tube inversion test (15 mM)				

Table 4.2. Supramolecular materials obtained by the self-assembly of Cys-containing peptides.

Apparently, all the four peptides seemed to self-assemble into self-supporting and quite homogeneous supramolecular materials in physiological conditions, with the exception of Phe-Cys-^{D}Phe peptide that showed white and dense aggregates surrounded by liquid solution. In particular, both homochiral and N-terminus containing D-amino acid peptides

gave rise to opaque self-supportive materials, while a transparent and translucent hydrogel was observed for the isomer containing ^{D}Cys residue.

4.2.3.2. Hydrogels Characterisation: Rheological Analyses

Rheological analyses are necessary and essential to validate whether the self-assembly process led to a hydrogel or not. Similarly to what was done for Met-containing tripeptides (***Chapter 3***), the supramolecular materials obtained by the self-assembly of Cys-containing isomers were tested for they hydrogel nature, by means of rheology studies that revealed interesting features.

Homochiral sequence has been previously reported to self-assemble at higher concentration (almost 100 mM) into a translucent gel upon a solvent switch trigger (from 1,1,1,3,3,3-hexafluoro-2- propanol (HFIP) to deionised water 1:1), although rheology and microscopy characterisation were not performed.[42] Effectively, such peptide gave a self-supportive opaque hydrogel in physiological conditions and at lower concentration (15 mM), as confirmed by rheological analyses, reported in **Figure 4.5**, although its viscoelastic properties were not remarkably good: indeed G' and G'' showed low values, 800 and 12 Pa, respectively.

Moreover, other two stereoisomers were confirmed to be hydrogels, as shown in **Figure 4.5**. In particular, tripeptide that contains ^{D}Cys in the middle of the sequence gave rise to a hydrogel with superior viscoelastic properties, exhibiting higher values for G' and G'', respectively 115 kPa and 8 kPa, relative to those shown by the hydrogel based on the isomer with ^{D}Phe at the N-terminus of the sequence (*i.e.*, 3 kPa and 0.25 kPa).

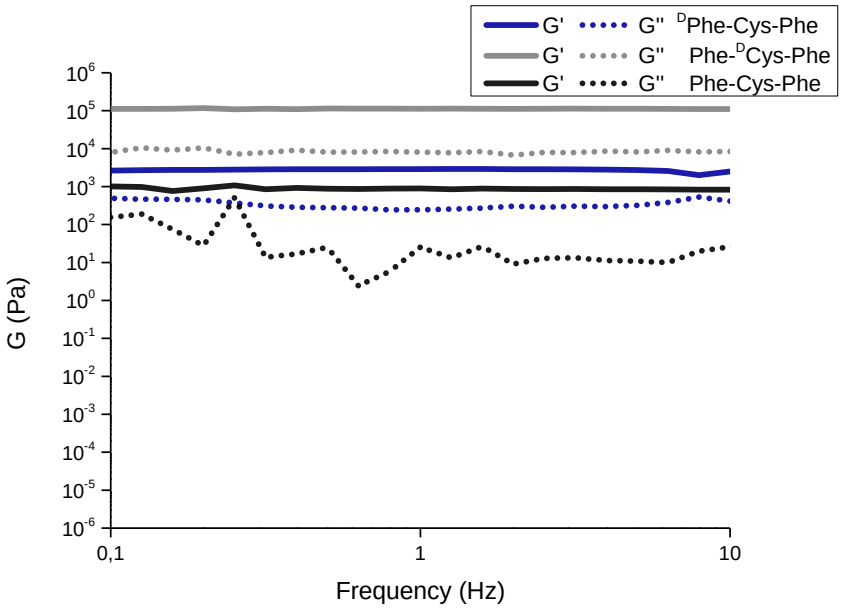

Figure 4.5. Frequency sweep measurements of supramolecular hydrogels obtained by the self-assembly of homochiral peptide Phe-Cys-Phe (black), and heterochiral peptides ^{D}Phe-Cys-Phe (blue) and Phe-^{D}Cys-Phe (grey).

The aggregates observed after the self-assembly test for the peptide containing D-amino acid at the C-terminus, that is Phe-Cys-^{D}Phe, were confirmed by rheology as not being a hydrogel (**Figure 4.6**), in line with previous reported results[58] and as supposed by visual observations.

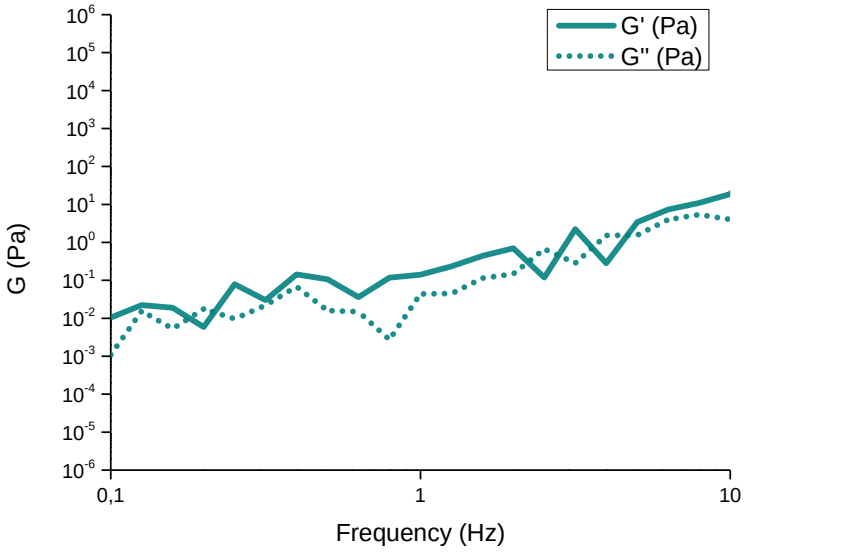

Figure 4.6. Frequency sweep measurement of aggregates obtained by the self-assembly of heterochiral peptide Phe-Cys-^{D}Phe.

The kinetics of self-assembly were overall fast for all the three hydrogels, which were formed within few minutes, as shown in **Figure 4.7**.

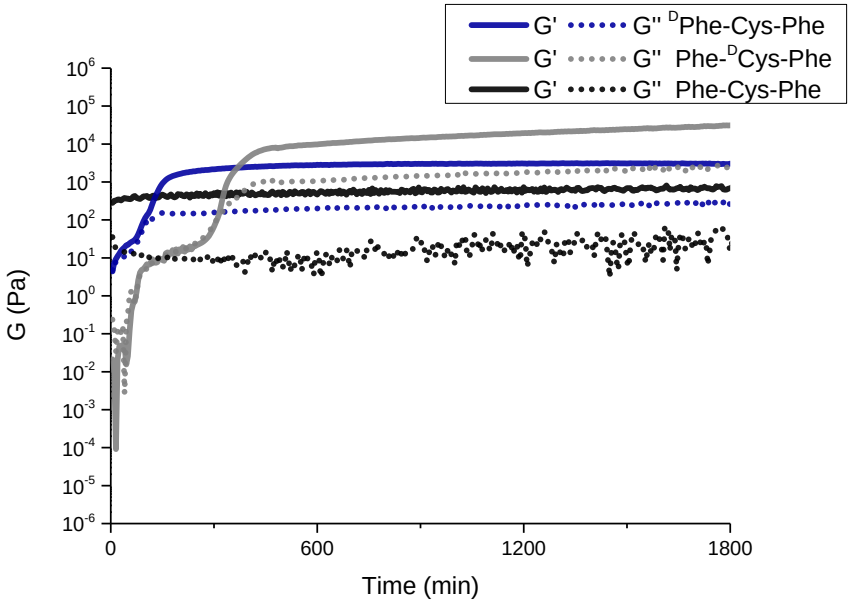

Figure 4.7. Time sweep analyses of supramolecular hydrogels obtained by the self-assembly of homochiral peptide Phe-Cys-Phe (black), and heterochiral peptides ^{D}Phe-Cys-Phe (blue) and Phe-^{D}Cys-Phe (grey).

Moreover, the hydrogels deriving from Phe-^{D}Cys-Phe demonstrated also an excellent and higher mechanical resistance upon the induction of an increasing stress, if compared to its analogues, as reported in **Figure 4.8**. Indeed, the hydrogel was stable up to 300 Pa applied stress, whilst the hydrogel based on the assembly of peptide ^{D}Phe-Cys-Phe started to lose its integrity already at 4 Pa, to be completely destroyed at 10 Pa. The worst mechanical resistance was showed by the hydrogel formed by the homochiral peptide, which was broken with as little as 1.6 Pa applied stress.

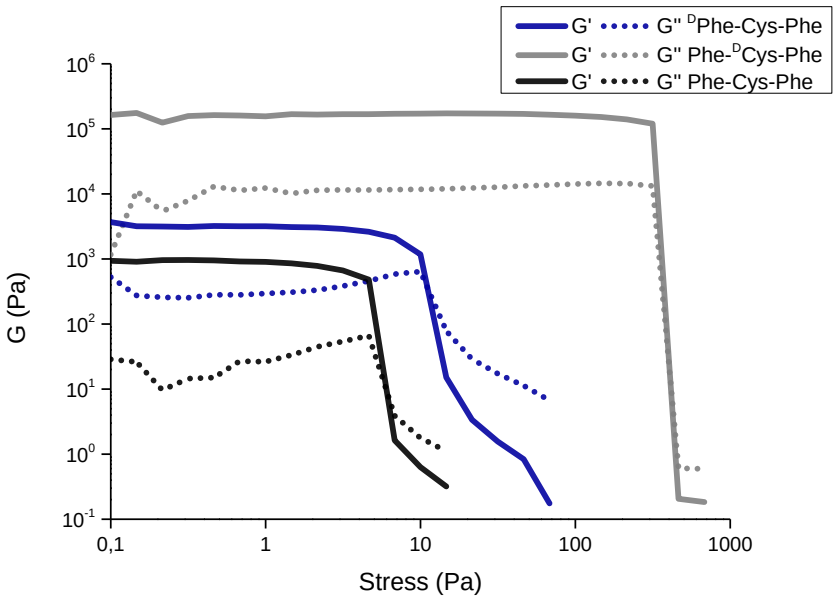

Figure 4.8. Stress sweep measurements of supramolecular hydrogels obtained by the self-assembly of homochiral peptide Phe-Cys-Phe (black), and heterochiral peptides ^{D}Phe-Cys-Phe (blue) and Phe-^{D}Cys-Phe (grey).

These findings corroborated and extended to Cys-containing tripeptides the prediction rules previously identified about the effect of chirality on hydrogelation processes, whereby tripeptides with chirality L-D-L demonstrated better performance than homochiral (L-L-L) isomers.[40, 43, 58]

However, prediction of self-assembling propensity of tripeptides is not so trivial, because of the inherent flexibility and chemical diversity of tripeptides. This is exemplified by an elegant study by Ulijn and Tuttle that correlated hydrophobicity with aggregation propensity in water for all 8,000 combinations of L-amino acids in tripeptides in the search for new hydrogelators, yet only 4 gelling sequences were described. Thus, hydrogel formation could be ascribed to the establishment of a good balance between the hydrophilic and the hydrophobic content of peptides, although this is not the only factor that has to be taken in account. LogP (defined as the partition coefficient of a molecule between n-octanol and water) could be a useful parameter that allows to estimate the hydrophobicity of peptides based on their sequence. However, logP predictions don't consider chirality as a key element for hydrophobicity, although different chirality of stereocentres induces different side chain

orientations, thus, different way of peptide interactions with water or organic solvents. Indeed, logP of the all four stereoisomers was found to be 1.3 ± 0.3.[101, 102]

In order to get some insights into the gelling ability of this set of Cys-containing tripeptides, analytical RP-HPLC was used to assess their hydrophobicity. Retention times, reported in **Table 4.3**, revealed that non gelling sequence was too hydrophilic to self-organise in a network of fibrils and thus generate hydrogel. On the contrary, the higher retention time displayed by the gelling heterochiral peptides suggested their good hydrophobic/hydrophilic balance to gel in physiological conditions. Furthermore, the homochiral sequence displayed a low hydrophobicity, even though it was able to form a hydrogel with weak and low viscoelastic properties.

Peptide Sequence	***LogP***	***Retention time (min)***	***Gel***
Phe-Cys-Phe	1.3 ± 0.3	13.6	✓
^{D}Phe-Cys-Phe	1.3 ± 0.3	14.1	✓
Phe-**^{D}Cys**-Phe	1.3 ± 0.3	14.6	✓
Phe-Cys-**^{D}Phe**	1.3 ± 0.3	13.5	✗

Table 4.3. Hydrophobicity, based on logP and experimental HPLC retention time, and gelling ability for Cys-containing tripeptides.

4.2.4. Nanostructures: TEM and SEM analyses

TEM is an essential and indispensable technique to assess the nanomorphology of the new materials obtained by the self-assembly of the cysteine containing isomers, in order to gain insights into the effect of chirality on nanoscale level. TEM analyses have been performed on all the supramolecular materials using the same conditions and the same concentration for each peptide, as discussed in **Section 4.2.3**: in this way every difference eventually observed in nanostructures could be directly related to the different chirality of each sequence. In order to study the evolution of nano- and microstructure formation over time, samples were analysed after 1 hour and after 24 hours of self-assembly, in collaboration with

Dr. Daniel Iglesias (from the University of Trieste) and Dr. Slavko Kralj (from the Jožef Stefan Institute in Ljubljana, Slovenia). SEM analyses have been performed at the Department of Physics of the University of Tartu, in Estonia, under the supervision of Prof. Sergei Vlassov, during a training school supported by a grant from COST Action 15216.

Each peptide gave rise to different kinds of nano- and micro-morphologies. In particular, the homochiral peptide formed sheet-like structures (reported in **Figure 4.9**) that appeared as crystal needles and plates, similar to those previously identified into the assembly of another homochiral tripeptide Leu-Phe-Phe.[56] Such structures were already formed after 1 hour of self-assembly, as shown in **Figure 4.9A**. SEM analysis confirmed the presence of prevalently flat surface and few elongated structures (**Figure 4.10**).

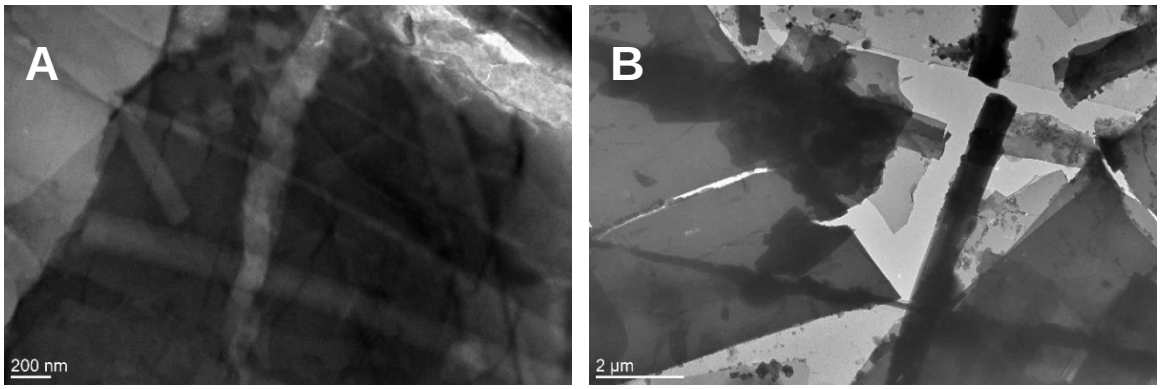

Figure 4.9. TEM micrographs of nanostructures obtained from homochiral peptide Phe-Cys-Phe after (**A**) 1 hour and (**B**) 24 hours of self-assembly.

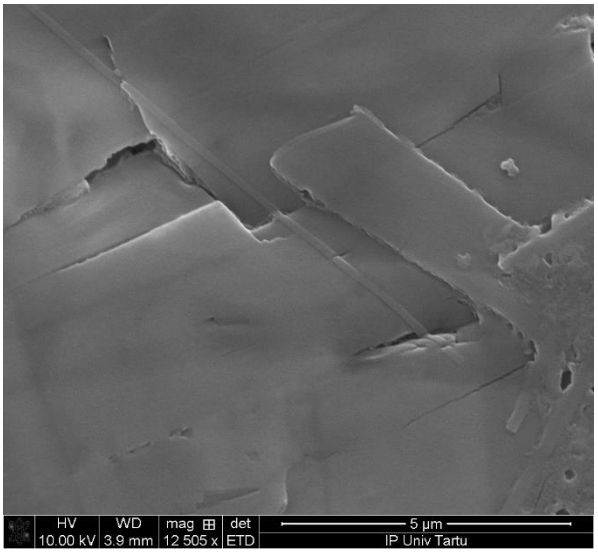

Figure 4.10. SEM micrographs of nanostructures obtained from homochiral peptide Phe-Cys-Phe.

The heterochiral peptide that contains a ^{D}Phe at the N-terminus of the sequence, self-assembled in a network of thin nanofibers (**Figure 4.11A**) with an average diameter of 50 nm ± 18 nm. After 24 hours, the nanofibers grew into thicker tube-like structures (average diameter 208 nm ± 60 nm), as shown in **Figure 4.11B**. These elongated anisotropic structures were confirmed by SEM imaging (**Figure 4.12**).

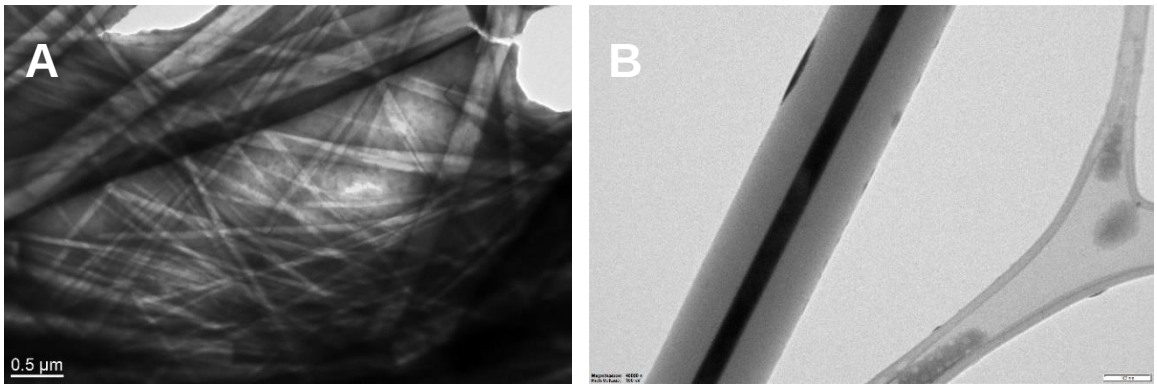

Figure 4.11. TEM micrographs of nanostructures obtained by homochiral peptide ^{D}Phe-Cys-Phe after (**A**) 1 hour and (**B**) 24 hours of self-assembly.

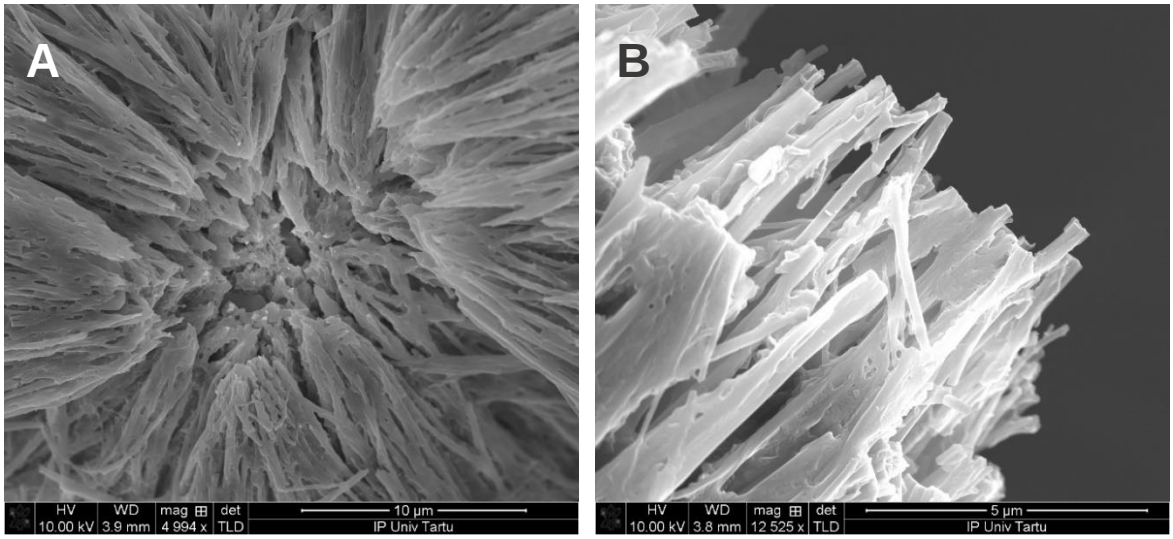

Figure 4.12. SEM micrographs of nanostructures obtained by homochiral peptide ^{D}Phe-Cys-Phe after (**A**) 1 hour and (**B**) 24 hours of self-assembly

Heterochiral peptides containing the ^{D}Cys in the middle of the sequence, formed truly thin nanofibrils with anisotropic behaviour and diameter of 2.2 nm ± 0.5 nm that run in parallel to form, within one hour, thicker nanofibers with average diameter of 23 nm ± 5 nm (**Figure 4.13A**). These nanofibers grew, thus, into microfibers with diameter 171 nm ± 67 nm within 24 hours of assembly (**Figure 4.13B**). For this sample, the resolution of SEM didn't allow the possibility to distinguish such thin fibrils, for which TEM is more meaningful, although the vulnerability of sample to the electron beam-induced damages required high expertise and precision.

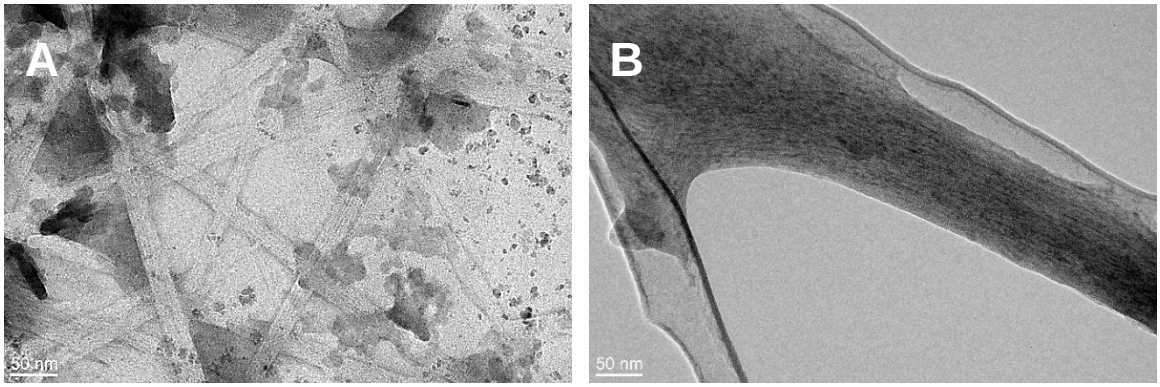

Figure 4.13. TEM micrographs of nanostructures obtained by homochiral peptide Phe-^{D}Cys-Phe after (**A**) 1 hour and (**B**) 24 hours of self-assembly.

Finally, heterochiral peptide, Phe-Cys-^{D}Phe, the only one that was not able to self-assemble into hydrogel, revealed within 1 hour the presence of microcrystals, partially damaged due to their high sensitivity to the electron beam (**Figure 4.14A**) and amorphous and not well-organised aggregates after 24 hours (**Figure 4.14B**).

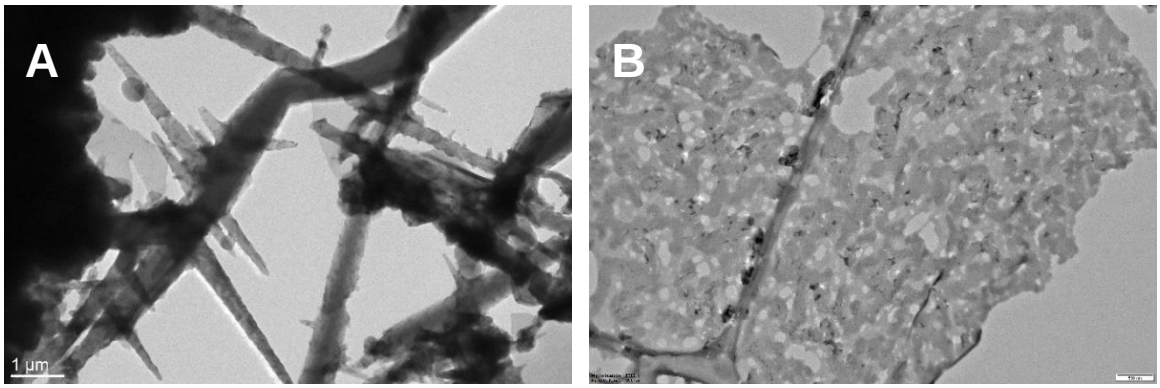

Figure 4.14. TEM micrographs of nanostructures obtained by homochiral peptide Phe-Cys-^{D}Phe after (**A**) 1 hour and (**B**) 24 hours of self-assembly.

Electron microscopy, thus, revealed that merely changing the position of the D-amino acid from the N-terminus to the middle position of a sequence can be used as a simple and efficient strategy to fine tune the dimensions of nano and micro-fibers. Considering that the only difference was chirality amino acids, the fact the diverse nanostructures were observed at TEM suggested that chirality remarkably affected assembly. To gain deeper understandings concerning supramolecular behaviour, more analyses have been performed.

4.2.5. Circular Dichroism Analyses

To assess conformations cysteine containing peptides adopt in solution, they were dissolved at 1 mM in phosphate buffer at neutral pH and CD spectra were collected (**Figure 4.15**). Three peptides out of four displayed the same CD signature discussed above for Met-containing tripeptides, with positive values and two maxima at 197 nm and 216 nm, corresponding respectively to the π→π* and n→π* transition of peptide bonds.

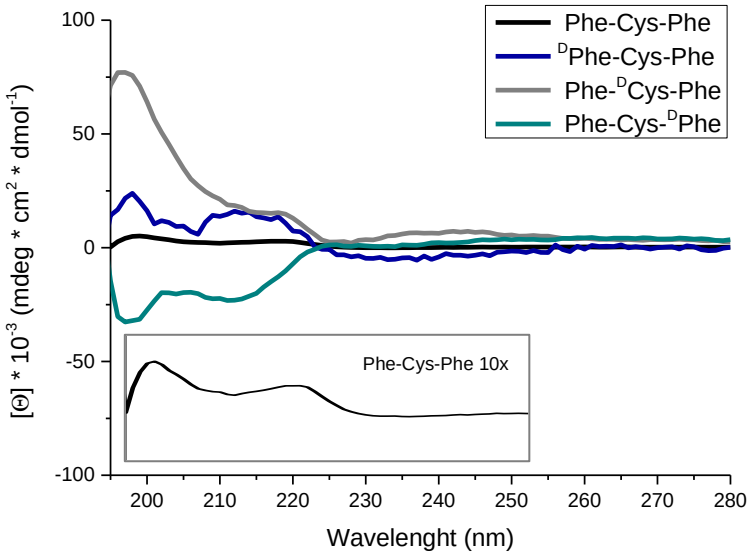

Figure 4.15. CD spectra of Cys-containing tripeptides in solution. Inset shows magnified CD spectra of homochiral tripeptide.

Surprisingly, the peptide that contains ^{D}Phe at the C-terminus of the sequence, *i.e.* Phe-Cys-^{D}Phe, showed an opposite trend, giving a spectrum that seemed to be the mirror image of the other ones, with negative values and two minima at 197 nm and 216 nm. Typically, two CD spectra that are mirror images of each other refers to two enantiomeric peptides, but this was not the case. The observation that the peptide showed a negative CD signature in solution might be related to the presence of the D-amino acid at the C-terminus of the sequence, in line with some studies that correlated the chirality of this residue to the supramolecular chirality induced by heterochiral peptide derivatives. In particular, CD signals of the self-assembled states of gelling lipopeptides containing a di-alanine motif were dictated by the chirality of the amino acid at the C-terminus of the lipopeptide sequence.[103] Other studies on self-assembling tetrapeptide Ile-Ile-Ile-Lys demonstrated the importance of stacked hydrogen bonds between carbonyl groups of the amino acids at the C-terminus, whose chirality guided the screw sense of the twisted fibers regardless of the chirality of all the other amino acids.[104] Additional studies on a larger library of tripeptides containing a D-amino acid in this position are, however, necessary to define and corroborate the trend reported thus far.

Concerning the three tripeptides that formed stable nanostructured hydrogels (*i.e.*, Phe-Cys-Phe, ^{D}Phe-Cys-Phe and Phe-^{D}Cys-Phe), CD analyses of their kinetics over 1 hour confirmed the fast self-assembly process identified through rheology time sweep measurements, as reported in **Figure**s **4.16**, **4.17**, and **4.18**, respectively. CD signatures of assembled states were overall similar to those displayed by tripeptides in solutions, suggesting that nano- and microstructure formation was mostly related to a higher level of peptide molecule organisation rather than conformational changes in peptide backbones. CD signals of the assembled heterochiral peptide ^{D}Phe-Cys-Phe was extremely weak due to the fact that the hydrogel was opaque, importantly affecting spectroscopy measurement.

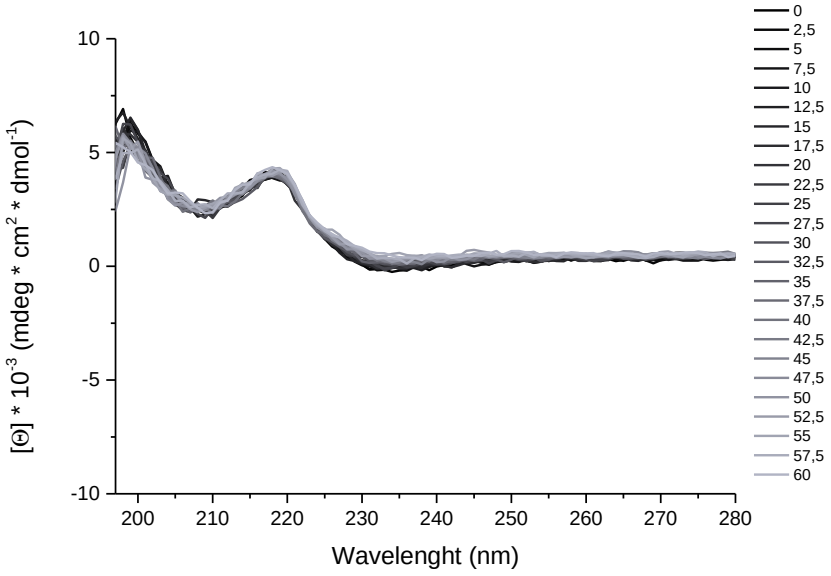

Figure 4.16. Evolution of CD spectra of peptide Phe-Cys-Phe during the assembly over time (indicated in minutes). No significant changes in CD spectra are identified.

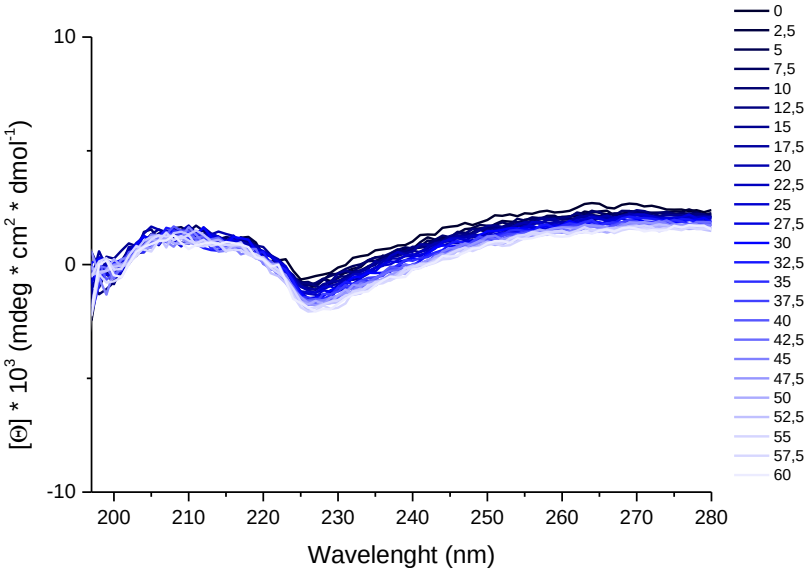

Figure 4.17. Evolution of CD spectra of peptide ^{D}Phe-Cys-Phe during the assembly over time (indicated in minutes). No significant changes in CD spectra are identified.

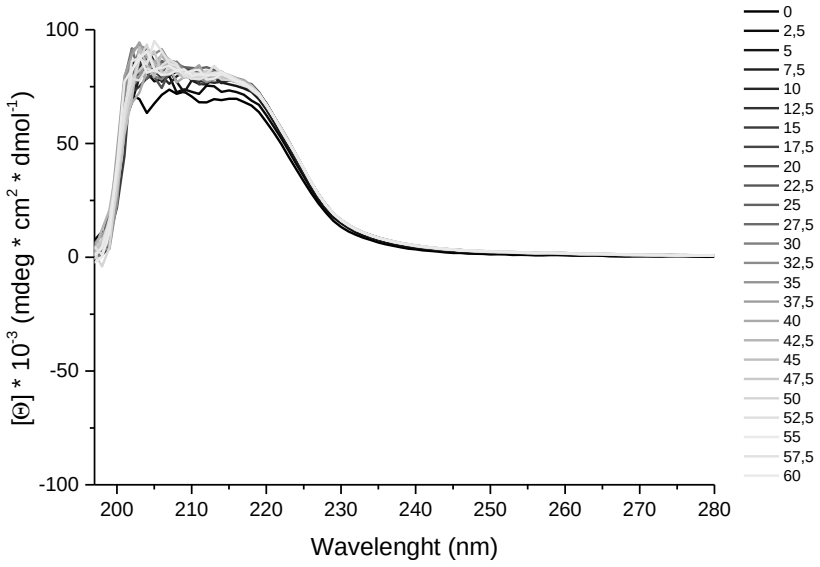

Figure 4.18. Evolution of CD spectra of peptide Phe-^{D}Cys-Phe during the assembly over time (indicated in minutes). No significant changes in CD spectra are identified.

4.2.6. Infrared Spectroscopy Analyses

Xerogels obtained drying the hydrogels were analysed using Fourier-transformed IR (FTIR) to better assess supramolecular behaviour of cysteine containing tripeptides. Spectra are reported in **Figure 4.19**. Considering the requirement to dry the sample and its preparation procedure through KBr pellet method, obtaining useful results from IR spectroscopy on this kind of samples is not so trivial. Indeed, xerogel that derived from peptide containing ^{D}Cys in the middle of the sequence gave a broad and low meaningful band in the interested region that didn't allow to assess useful supramolecular information. Both the heterochiral peptide containing the D-amino acid at the N-terminus of the sequence and the homochiral peptide revealed an intense band at 1650 cm^{-1}, which is the region were α-helix conformations are typically found.

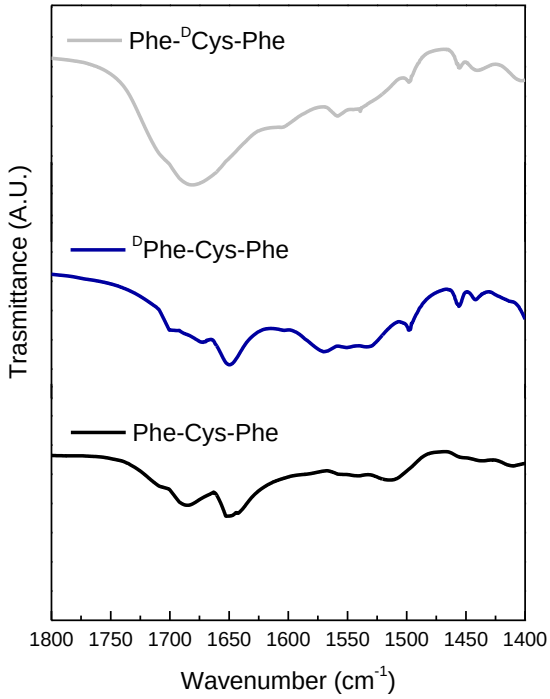

Figure 4.19. FTIR spectra of xerogels obtained by cysteine containing tripeptides.

4.2.7. Amyloid Fluorescence Assays

As already described in **Section 3.2.7**, ThT was used to assess the supramolecular arrangement of materials obtained by the self-assembly of the cysteine containing peptides, with the aim to implement the poor results obtained by IR spectroscopy. The three hydrogels analysed gave positive results for their ThT binding ability, although with different intensity, whilst amorphous aggregates deriving from peptide that contain ^{D}Phe at the C-terminus of the sequence induced the emission of low fluorescence whose intensity was comparable to that emitted by the negative control (buffer solution without peptide), as expected. Results are shown in **Figure 4.20**.

Some considerations could be done about the intensity of fluorescence emission from ThT into the hydrogels. Surprisingly, hydrogels that gave IR bands related to α-helix behaviour induced high fluorescence intensity emission and, in particular, hydrogel based on the self-assembly of peptide containing the ^{D}Phe at the N-terminus of the sequence displayed the highest fluorescence values. On the other hand, heterochiral peptide with L-D-L chirality gave only a weak fluorescence.

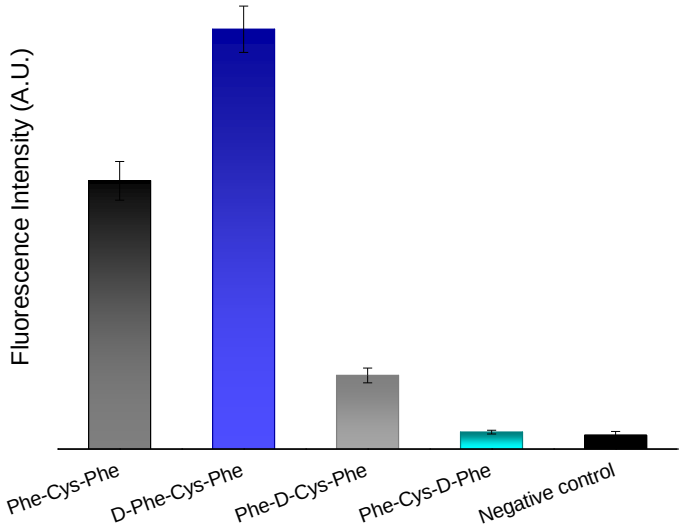

Figure 4.20. ThT fluorescence intensity assay of nanostructures obtained from cysteine containing tripeptides.

If is true that ThT is largely reported to follow the formation of amyloid fibrils thanks to its ability to bind to four consecutive β-sheets, it is also true that ThT is actually a dye that positively interact with hydrophobic grooves. Probably, the high fluorescence emitted by the hydrogel derived from the peptide with chirality D-L-L could be ascribed to the high affinity of the organic dye to the hydrophobic grooves formed in this case, more effective than those formed by the other assembled tripeptides, and in particular by the peptide containing ^{D}Cys in the middle of the sequence.

In order to better understand the supramolecular behaviour of heterochiral tripeptide Phe-^{D}Cys-Phe, other fluorescence assays were performed employing another dye, Nile Blue instead of ThT.[105] In this case, three different concentrations of peptides were tested and compared to a negative control, based on the phosphate buffer, in absence of peptide. Fluorescence emission was noticed, even though the intensity was, once again, quite low, as reported in **Figure 4.21**.

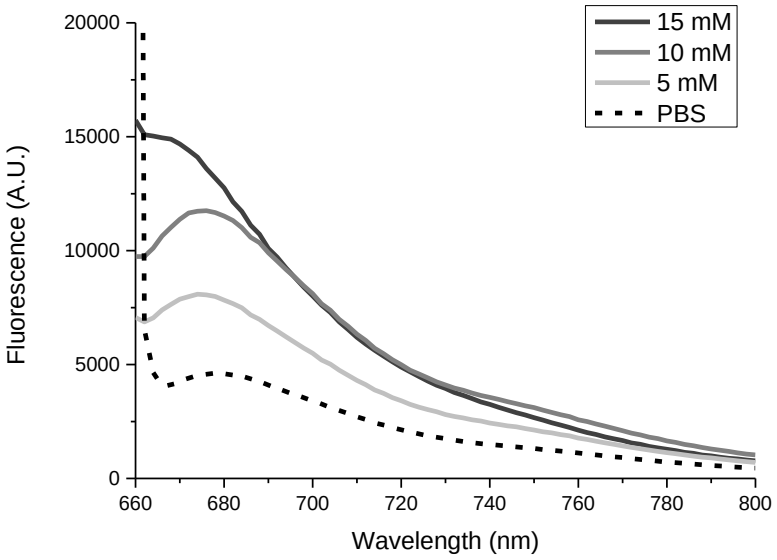

Figure 4.21. Nile Blue A fluorescence emission of nanostructures obtained from different concentration of Phe-^{D}Cys-Phe.

4.2.8. Single Crystal X-Ray Diffraction

Single-crystal X-ray diffraction (XRD) data were collected by Prof. Rita De Zorzi and her team at the University of Trieste, using the facilities of Elettra Synchrotron (Area Science Park, Basovizza, Trieste, XRD1 beamline).

4.2.8.1. Single Crystal XRD Data of ^{D}Phe-Cys-Phe

The asymmetric unit contains two molecules of the peptide in its zwitterion form, with the thiol group in the reduced form. In the residual electron density, a molecule of methanol at 50% occupancy, two molecules of water at full occupancy, a molecule of water at 70% occupancy and three molecules of water at 50% occupancy were recognized. The two crystallographically independent molecules of peptide have a similar conformation of the backbone and side chains. **Figure 4.18** shows the comparison between the two peptides, considering the 65% occupancy position of the disordered thiol group. A total of 8 molecules of peptide are present in the unit cell, each related to the others by the symmetry elements of the $P2_12_12$ space group (**Figure 4.19**).

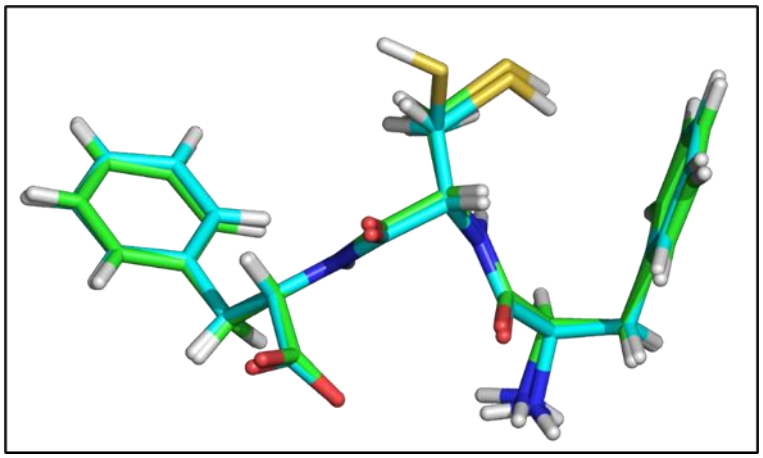

Figure 4.18. Comparison between crystallographically independent molecules of ^{D}Phe-Cys-Phe. The crystallographically independent molecules of ^{D}Phe-Cys-Phe show a similar backbone conformation and similar side chain rotamers for all three residues, considering the highest occupancy positions. For one of the peptides, the thiol group is statistically disordered in 2 positions, at 65% and 35% occupancy, respectively.

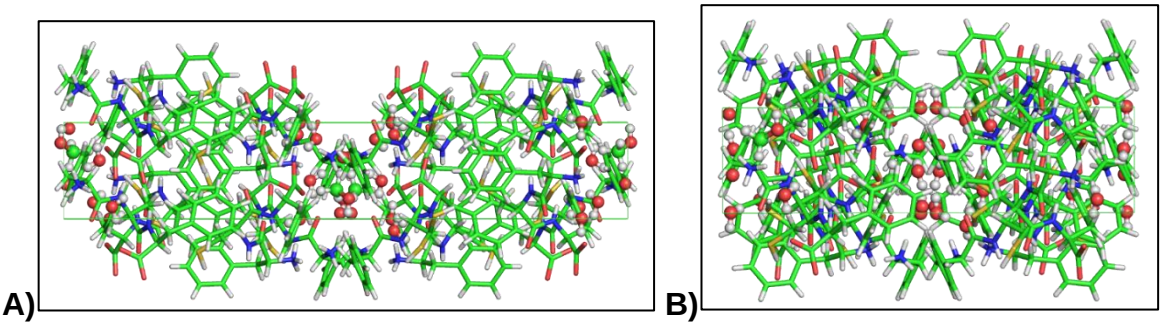

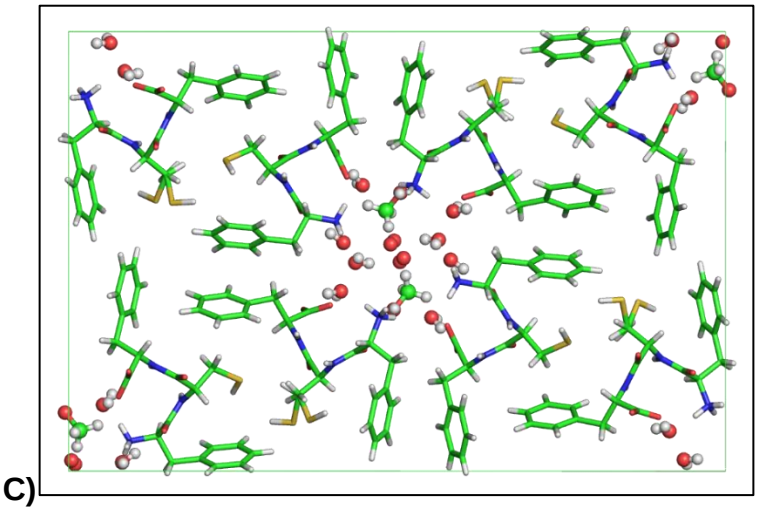

Figure 4.19. Unit cell of crystals of ^{D}Phe-Cys-Phe**.**

Crystal packing in the crystal of the peptide ^{D}Phe-Cys-Phe. Views along (**A**) the *a* crystallographic axis, (**B**) the *b* crystallographic axis and (**C**) the *c* crystallographic axis.

The crystal packing of ^{D}Phe-Cys-Phe (**Figure 4.20**) shows the formation of channels filled with solvent (methanol and water) along the *c* crystallographic direction. The channels have a circular shape with a diameter of about 8 Å.

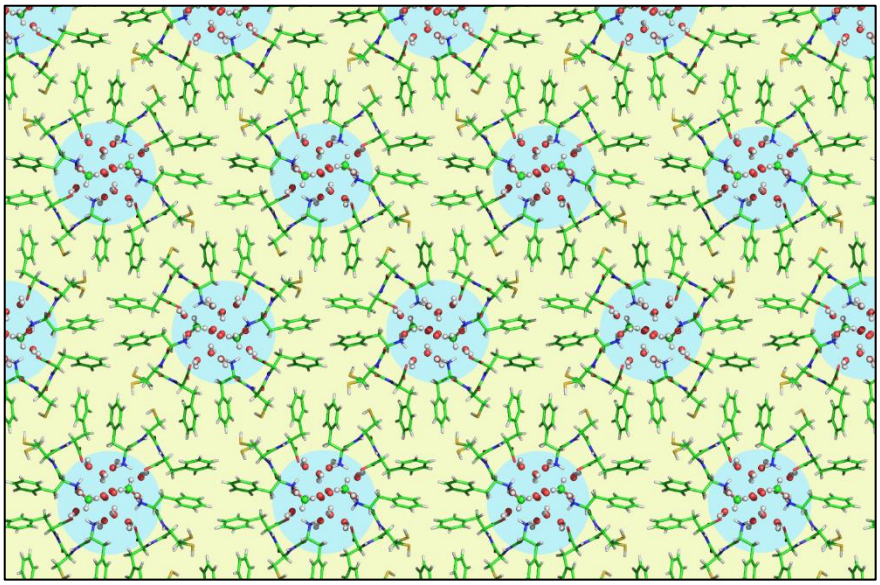

Figure 4.20. Hydrophobic and hydrophilic regions in the crystal packing of ^{D}Phe-Cys-Phe. When peptides ^{D}Phe-Cys-Phe pack forming the crystal, their arrangement leaves empty channels that are filled by solvent molecules (methanol and water). The walls of the channels, formed along the *c* crystallographic direction, are hydrophilic due to the presence of the backbone polar groups. Such groups interact with the solvent molecule through hydrophilic interactions.

The walls of the solvent-filled channels are constituted by the hydrophilic moieties of the peptides, held together by hydrophilic interactions (**Figure 4.21**, magenta dashes), while water molecules inside the channel interact with salt bridges and hydrogen bonds with peptide molecules (**Figure 4.21**, black dashes).

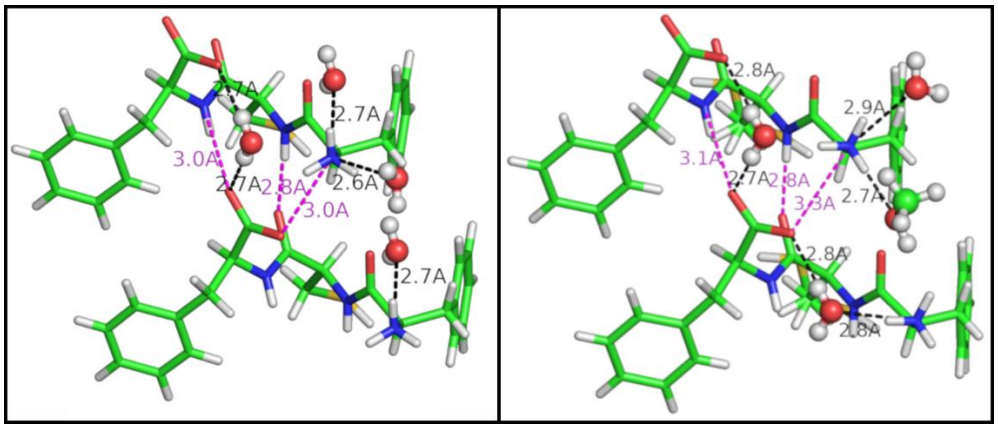

Figure 4.21. Hydrophilic interactions.
The two asymmetric peptides, represented in the two panels, have a similar pattern of hydrophilic interactions, namely hydrogen bonds and salt bridges. Peptide-peptide interactions are marked with magenta dashes and distances between the donor and the acceptor atom are reported. Peptide-solvent (water and methanol) interactions are marked with black dashes and donor-acceptor distances are reported.

The electron density of water molecules present in the channel is well defined, indicating that they interact with hydrogen bonds with peptides and other water molecules. In the structure, additional hydrophobic interactions are present between peptides, mainly CH-π interactions, contributing to the formation of the channels by holding the peptides in a suitable position (**Figure 4.22**, black dashes). There are also intramolecular SH-π interactions between the side chain of the cysteine residue and the side chain of the first phenylalanine residue (**Figure 4.22**, red dashes).[106]

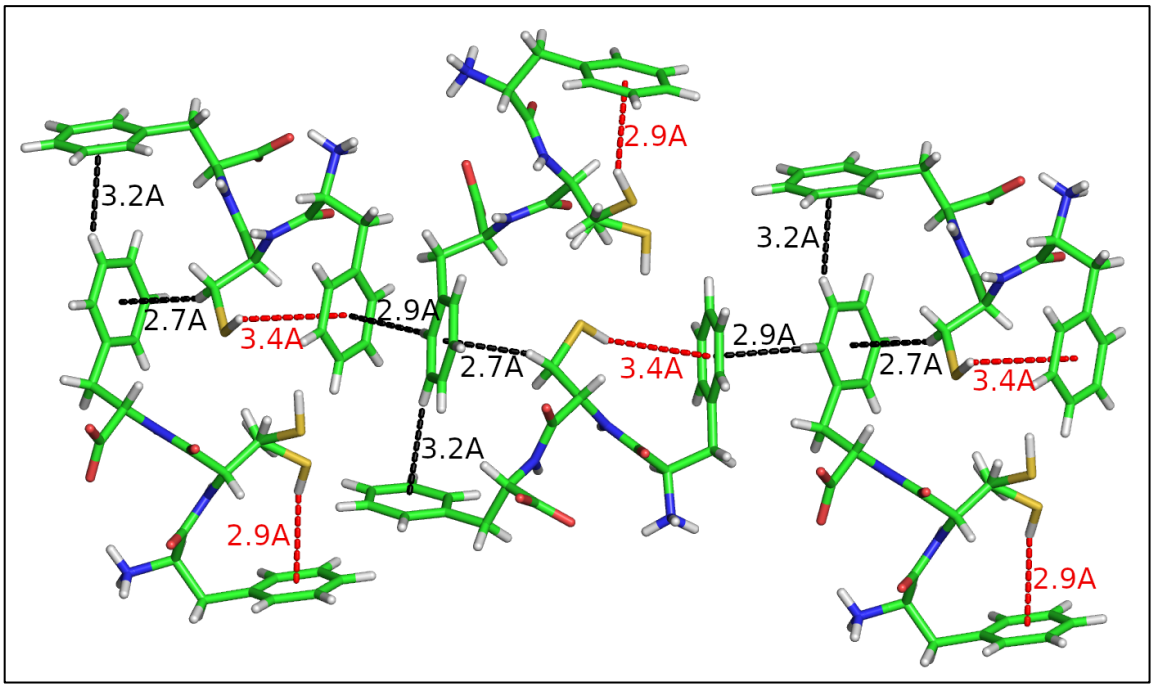

Figure 4.22. Hydrophobic interactions in the structure of ^{D}Phe-Cys-Phe. Intermolecular CH-π interactions (black dashes) and intramolecular SH-π interactions (red dashes) contribute to the formation of the channels by holding together the hydrophobic moieties of the peptides.

Crystallographic details are reported in ***Chapter 6*** **(Materials and Methods)** and supplementary data are reported in **Appendix** (**Tables A.3.1 and A.3.2**).

4.3. Conclusions

Four different stereoisomeric tripeptides sharing the same sequence (*i.e.*, Phe-Cys-Phe) have been synthesised and characterised for their ability to self-assemble at physiological conditions. In particular, 3 out of 4 peptides were able to form supramolecular hydrogels, whose viscoelastic properties strongly depended on the position of the D-amino acid along the sequence. Indeed, inversion tube test and oscillatory rheology data confirmed previously reported results whereby DLL and LDL heterochiral peptides showed superior gelling ability than the homochiral counterpart.[40, 43, 58]

In terms of nanomorphologies, chirality revealed its crucial importance since 3 different kinds of nano- and micro-structures have been observed by simply changing D-amino acid position. Chirality, thus, can be used as a main tool to tune different superstructure formations (*e.g.*, nanosheets, tube-like structures and thin nanofibrils) starting from the same amino acid sequence.

Finally, XRD data highlighted the importance of sulfhydryl groups for the self-assembly in ordered water channels due to their ability to establish useful interactions with aromatic moieties. In order to gain useful insight into this aspect, redox properties of cysteine can be in future exploited to investigate the impact of such interactions on self-assembly.

Chapter 5: Cysteine-Containing Peptides: Stimulus-Induced Disassembly of Nanostructured Hydrogels

5.1. Introduction

As depicted by Prof. Jean-Marie Lehn during is Nobel lecture in 1987, "*Supramolecular chemistry may be defined as "chemistry beyond the molecule," bearing on the organized entities of higher complexity that result from the association of two or more chemical species held together by intermolecular forces*",[107] one of the main advantages deriving from supramolecular materials is definitely their superior functional complexity that is possible to obtain from the highly ordered organisation of small molecules.

In the particular case of self-assembly of short peptides into supramolecular materials, new functional nanostructured hydrogels have shown a wide variety of possible bioapplications. Although several triggers have been studied to induce peptide self-assembly and gelation (including pH, temperature, ionic strength),[66] some issues relating to their lack of spatial and time dynamicity, which typically characterise natural self-assembling systems, are now arising. To overcome these concerns, new perspectives are moving towards bioinspired out-of-equilibrium systems, with the aim to create self-regulating, temporally patterned, dynamic, and functional nanomaterials.[108-110] Control of assembly kinetics provides great opportunity for the next generation of molecular materials with intelligent behaviour including programmed spatiotemporal organization. In order to achieve spatiotemporal control in nanostructured hydrogels, a first key step could be the design of new specific and selective stimuli that could induce smart and highly regulated disassembly.

Classical external stimuli that have been typically employed as reversible switches for controlled cycles of assembly/disassembly are based on temperature or pH changes or induced by chemical reactions. Since pH and chemical driven reversible disassemblies are achieved upon the addictions of reagents to assembled systems, their applicability could be challenging because of two main reasons: i) further additions of chemical entities induce unavoidably sample dilutions that, cycle by cycle, could bring gelator concentrations below minimum gelling concentrations, limiting the number of reversible cycles; ii) occurrence of physical phenomena, such as precipitation, could undesirably affects the availability of gelator molecules in solution necessary for the reassembly.

In this chapter, three different triggers (*i.e.*, physical, chemical, and photochemical) are investigated to induce selective disassembly of the hydrogels based on Cys-containing peptides described in ***Chapter 4***. Their reversible or irreversible nature has been discussed and tailored to implement smart functionalities of nanostructured hydrogels.

5.2. Results and Discussion

5.2.1. Physically Induced Disassembly

Temperature change is a physical switch that is generally employed to create dynamic hydrogels that can undergo reversible cycles of assembly. Thermoreversibility has been investigated as a useful tool to disassemble a hydrogel by heating it up. Hydrogels based on the assembly of cysteine-containing peptides described in ***Chapter 4*** revealed thermoreversible ability, as shown in **Table 5.1.** The re-assembly has been easily achieved by cooling down the system.

Peptide Sequence	Phe-Cys-Phe	^{D}**Phe**-Cys-Phe	Phe-^{D}**Cys**-Phe
Disassembled hydrogels at 60 °C			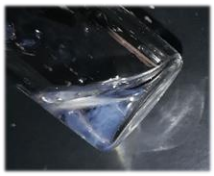
Thermoreversed hydrogel			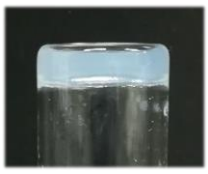

Table 5.1. Photographs of disassembling hydrogels at their melting temperatures and thermoreversed hydrogels.

Although it could be quite difficult to predict how a nanostructured hydrogel behaves when it is heated up, CD spectroscopy could be a useful technique to assess supramolecular

changes during heating and cooling processes. However, CD analyses performed on the samples didn't reveal meaningful information, due to the low signal intensity and the overall low variations that have been detected during heating processes. Evolution of CD spectra over a temperature ramp up to 85 °C of Phe-Cys-Phe, ^{D}Phe-Cys-Phe and Phe-^{D}Cys-Phe are reported in **Appendix** (**Figure A4.1 - A4.3**).

Considering that CD spectroscopy didn't allow to evaluate melting temperature of supramolecular nanostructured hydrogels based on Cys-containing peptides, further analyses need to be performed, such as differential scanning calorimetry (DSC) measurements to assess thermal stability.[44, 87]

5.2.2. Chemically Induced Disassembly

Sulfur-based chemistry has been exploited for reversible and selective assembly of hydrogels based on Cys-containing tripeptides. In order to obtain a selective chemically induced disassembly of a hydrogel based on a Cys-containing peptide, the use of reagents that can selectively react with cysteine is necessary. Considering the nucleophilic nature of this amino acid, it is widespread used in biological and biophysical studies as the easiest way for protein post-transcriptional modification, including alkylation, oxidation, and desulfurization reactions, and fluorescent labeling.[111]

Typically, reversible cysteine modifications can be easily achieved by the use of reagents that induce disulfide formation (such as methanethiosulfonates or alkaline agents), which can be then reduced by reducing agents (*e.g.*, DTT or TCEP, (tris(2-carboxyethyl)phosphine)). This classical approach has been largely employed to control self-assembling behaviour from two different kinds of nanostructures (*e.g.*, from nanospheres to fibrils and *vice versa*)[95] and to design transient supramolecular hydrogels for multiple assembling cycles.[112] However, redox based strategies could have limited scope of applications due to low stability and scrambling reactions of disulfides.

In the context of reversible and selective modification, Baker and co-workers developed an addition-elimination reaction based on the rapid and selective reaction between cysteine residues and mono-halomaleimides to form thiomaleimide conjugates, as reported in **Scheme 5.1**.[113] Reversibility of the reaction is based on the reactivity of thiomaleimide that,

retaining the double bond, could react with another nucleophile (such as DTT, TCEP, phosphines), which can cleave the cysteine residue. Noteworthy, the configuration of cysteine stereocentre (*i.e.*, α-carbon) remains unaltered. This protocol has been widely applied in solution on N-protected cysteine residues for polymer synthesis, protein labelling, fluorophore quenching and peptide synthesis as a mild and selective protecting and reversible modification of thiol groups.[114, 115]

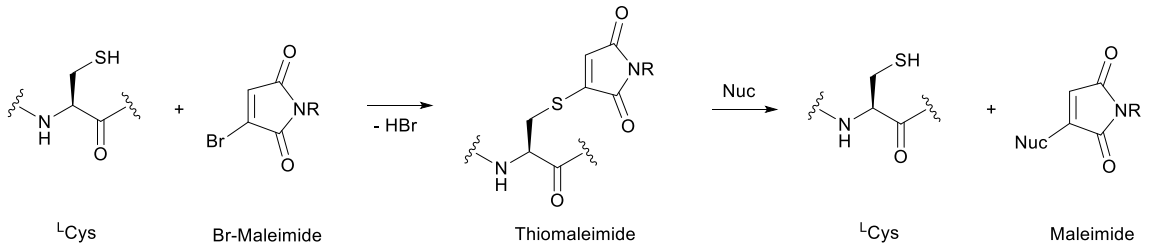

Scheme 5.1. Reversible reaction between a ᴸCys residue and Br-maleimide.

In this thesis, reversible reaction between gelling cysteinyl peptide and Br-maleimide has been exploited in hydrogel phase to disassemble it in a selective manner, since the involvement of peptide molecules within the reaction hindered their stacked organisation necessary for self-assembly. In particular, nanostructured hydrogel based on the unprotected heterochiral tripeptide containing ^{D}Cys has been selected because of its enhanced and superior viscoelastic properties relative to the other two reported in ***Chapter 4***. Its translucent nature, moreover, allowed to follow its disassembly behaviour by means of different analyses, which were challenging to perform on the other two opaque hydrogels. However, further studies and optimisation of protocol will be carried out to extend the scope of the reaction.

Br-maleimide reagent has been synthesised by Dr. Paolo Pengo (from the University of Trieste). Spectroscopic data are reported in the **Appendix**. After 1 hour of self-assembly of peptide Phe-^{D}Cys-Phe in PBS at neutral pH, 1 equivalent of Br-maleimide dissolved in DMF was added to the hydrogel. DMF was selected for a complete dissolution of Br-maleimide. Different ratio of DMF/hydrogel volumes have been investigated and minimised in order to avoid hydrogel disassembling processes due to dilution factors or solvent effect. As shown

in **Scheme 5.2**, Br-maleimide reacts with unprotected Cys-containing peptide forming the relating thiomaleimide.

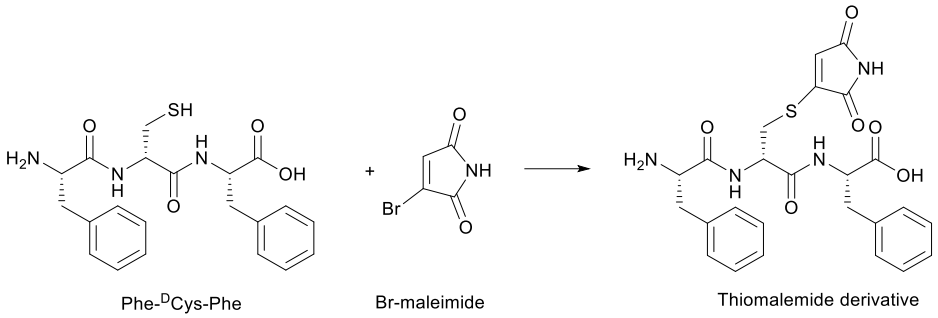

Scheme 5.2. Scheme of reaction between a Phe-^{D}Cys-Phe peptide residue and Br-maleimide in hydrogel phase.

First of all, disassembly process was monitored over time by visual observation, as reported in **Figure 5.1**. Although it has been reported that the reaction was really fast and occurred within few minutes in solution,[113] the disassembly of hydrogel phase needed more time. Indeed, only 1 hour after the addiction of Br-maleimide, the hydrogel started to disassemble, giving a heterogeneous mixture formed by clear solution, few precipitates and hydrogel. The hydrogel component appeared less present after 2 hours, and completely disassembled after 3 hours, when only yellowish precipitates were observed.

Figure 5.1. Gradual disassembly of the hydrogel induced by Br-maleimide.

Remarkably, 1 equivalent of Br-maleimide successfully induced complete hydrogel disassembly within 3 hours. Control experiments revealed that lower concentrations of maleimide derivative didn't affect hydrogel stability.

To validate the occurrence of reaction between cysteine and Br-maleimide derivative, two different analyses have been performed: Ellman's reagent test proved the involvement of thiol group during the reaction and LC-MS analyses demonstrated the formation of the thiomaleimide derivative.

5.2.2.1. Ellman's Reagent Test

In order to follow the reaction between Cys-peptide and Br-maleimide, the use of thiol reactive probes has been investigated. Several reagents and commercial kits are commonly used to monitor the presence of free thiol groups in proteins, including iodoacetamides, maleimides, benzylic halides, bromomethylketones, and many others.[116]

Amongst the many protocol that can be used, Ellman's reagent is one of the simplest and low-cost methodology for qualitative and quantitative analysis of thiol group in solution. It is the 5,5'-dithio-*bis*-(2-nitrobenzoic acid) (DTNB), a water-soluble compound that reacts with free sulfhydryl groups in solution forming a mixed disulfide and 2-nitro-5-thiobenzoic acid (TNB), a yellow-coloured product (**Scheme 5.3**). Occurrence of a yellow colour qualitatively indicates the presence of thiol group. For a quantitative analysis, measurements of TNB absorbance at 412 nm could be carried out.[117]

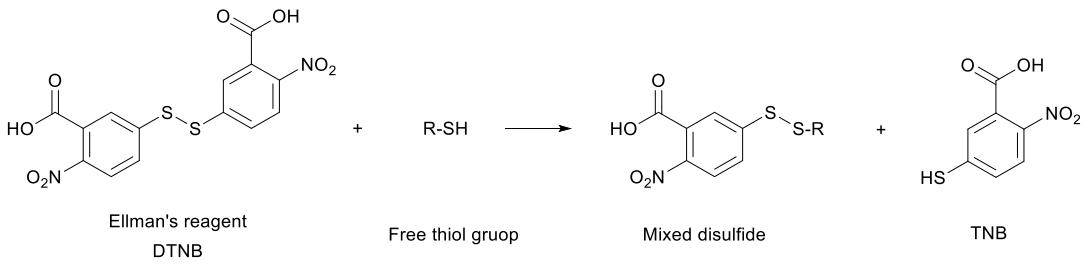

Figure 5.3. Reaction of Ellman's reagent with thiol.

The presence of free sulfhydryl groups has been followed before and after the self-assembly of peptide into the nanostructured hydrogels and after its disassembly triggered by reaction with Br-maleimide. First of all, the reaction protocol was applied on peptide Phe-^{D}Cys-Phe

in solution (*i.e.*, below the minimum gelling concentration) in order to check the presence of thiol groups and quantify possible cysteine oxidation in solution before the assembly. A calibration curve has been obtained measuring the absorbance at 412 nm of different concentration of ^{L}Cys, used as standard. Then values of absorbance of peptide in solution have been compared to those of the standard (as reported in **Figure 5.4**), revealing that no oxidation reactions occurred in solution, although few variations were observed due to experimental errors and the high sensitivity of the test. These results were also in agreement with LC-MS and ^{1}H-NMR analyses performed on peptide in solution (as reported in **Figures A.1.27- A.1.30** in **Appendix**).

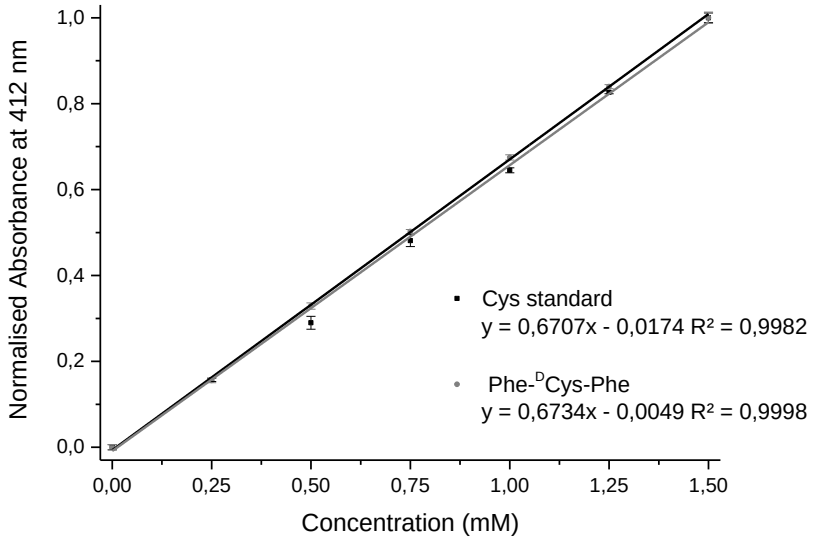

Figure 5.4. Calibration curve of peptide Phe-^{D}Cys-Phe with Ellman's reagent.

The reaction protocol reported to be applied in solution has been performed in hydrogel phase (before the addiction of Br-maleimide) to verify the presence of free sulfhydryl groups in the peptide assembled state. In this case, only a qualitative analysis was possible, since the measurement of absorbance on the hydrogel phase for a quantitative purpose led to not meaningful results, due to scattering phenomena and the availability of spectrophotometer optimised only for liquid samples. Ellman's reagent was added to the hydrogel after 1 hour and after 24 hours of self-assembly at air. The intense yellow colour showed in **Figure 5.5** demonstrated the presence of free thiol groups in the hydrogel phase, revealing that only minor oxidation reactions occurred, even if the hydrogel was exposed to air for 24 hours.

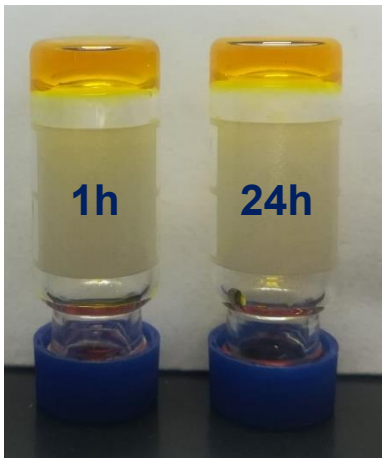

Figure 5.5. Ellman's reagent test on hydrogels derived from the assemlby of peptide Phe-^{D}Cys-Phe.

Once having confirmed the availability of free sulfhydryl groups in hydrogel phase, the reaction with 1 equivalent of Br-maleimide relative to peptide has been performed and, after 3 hours, Ellman's reagent was added. The absence of a yellow colour suggested that the thiol groups of cysteinyl peptide reacted with Br-maleimide to form thiomaleimide (**Figure 5.6A**). On the other hand, the test performed in presence of a lower amount of Br-maleimide, which was not able to disassemble the hydrogel, gave an intense yellow colour, demonstrating that reaction needed more Br-maleimide to be effective in hydrogel phase (**Figure 5.6B**).

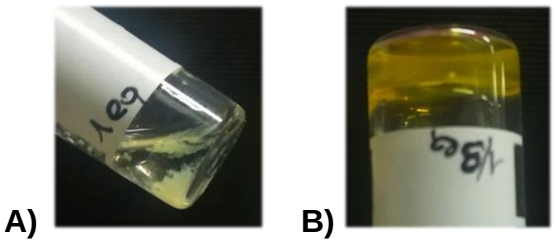

Figure 5.6. Ellman's reagent test on hydrogel in presence of (**A**) 1 equivalent and (**B**) 1/3 of equivalent of Br-maleimide relative to peptide.

Test with Ellman's reagent allowed to claim that hydrogel disassembly occurred in presence of Br-maleimide because of specific thiol involvement into the thiomaleimide derivative that detracted peptide molecules from supramolecular arrangement and broke the hydrogel network.

5.2.2.2. LC-MS Analyses

Thiomaleimide conjugates deriving from the reaction between Phe-^{D}Cys-Phe peptide and Br-maleimide in hydrogel state was crucial for the disassembly. LC-MS analysis have been carried out to verify thiomaleimide product formation. Confirming the results reported in literature, the reaction was really fast, although complete disassembly occurred after 3 hours. Indeed, immediately after Br-maleimide addiction to the hydrogel, a conjugate product (peak A in **Figure 5.7**) with a mass consistent with the thiomaleimide derivative was observed. Br-maleimide (peak B in **Figure 5.7**) and pristine peptide (peak C in **Figure 5.7**) were still present.

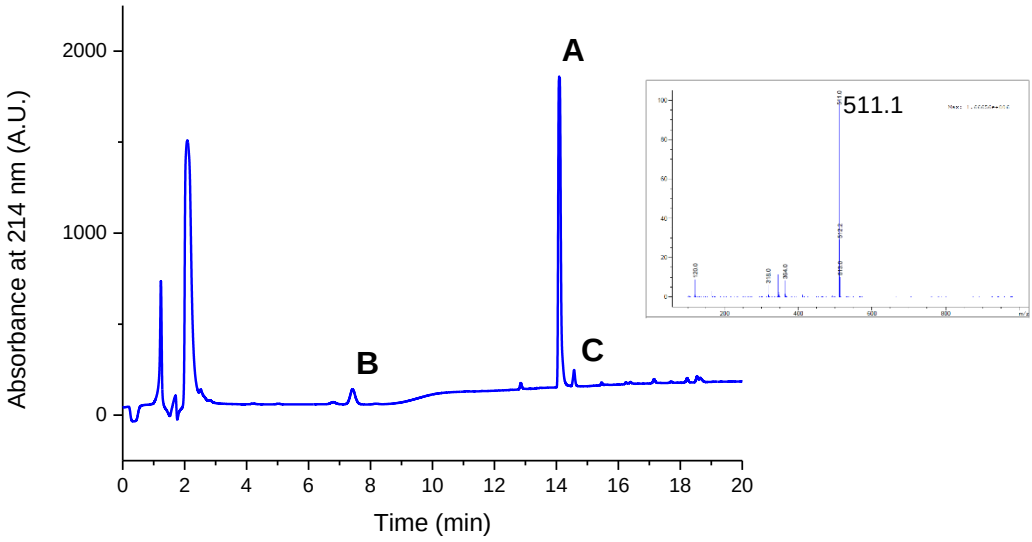

Figure 5.7. LC chromatogram of reaction mixture of peptide Phe-^{D}Cys-Phe immediately after Br-maleimide addition. Inset shows mass spectra of peak A, corresponding to thiomaleimide conjugate.

Considering the presence of another nucleophile in the peptide sequence (*i.e.*, unprotected amine group at the N-terminus) that could react with Br-maleimide, two possible conjugates with the same molecular weight can be formed, as showed in **Scheme 5.4**.

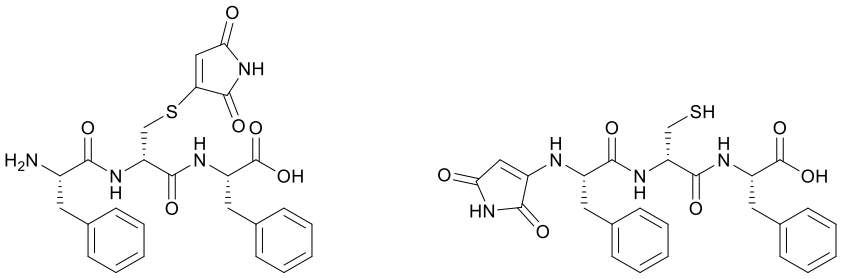

Thiomalimide
Chemical Formula: $C_{25}H_{26}N_4O_6S$
Exact Mass: 510,16
Molecular Weight: 510,57

Aminomaleimide
Chemical Formula: $C_{25}H_{26}N_4O_6S$
Exact Mass: 510,16
Molecular Weight: 510,57

Scheme 5.4. Possible conjugates that can be formed from the reaction between Cys-containing peptide and Br-maleimide

Of course, mass spectroscopy cannot distinguish between them. On the other hand, neither NMR analyses could give significant differences, since the reaction is performed in water, whereby signals related to thiol and amines cannot be observed. However, as discussed above, maleimides and in particular Br-maleimides preferentially react with thiol groups with high selectivity. It is also noteworthy that the nucleophile character of thiol groups is higher than that of amines at the neutral pH in which the reaction is carried out: in these conditions, amine groups (pKa 9.5) are protonated and hence less propense to react with maleimide derivatives, than thiol groups (pKa 7.3), as identified by titration curve of peptide in water (**Figure 5.8**). Finally, as discussed above, Ellman's reagent test clearly claimed the involvement of thiol groups during the reaction.

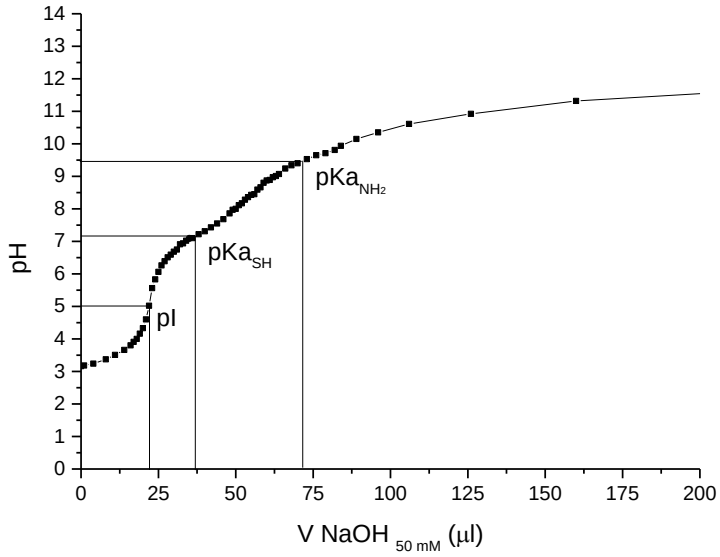

Figure 5.8. Titration curve of peptide Phe-^{D}Cys-Phe in water.

.

Comparison of LC-analyses performed over time reported in **Figure 5.9** revealed the complete consumption of Br-maleimide after 1 hour of reaction. Mass spectra of each peak is reported in **Appendix Figures** from **A.5.4** to **A.5.7**.

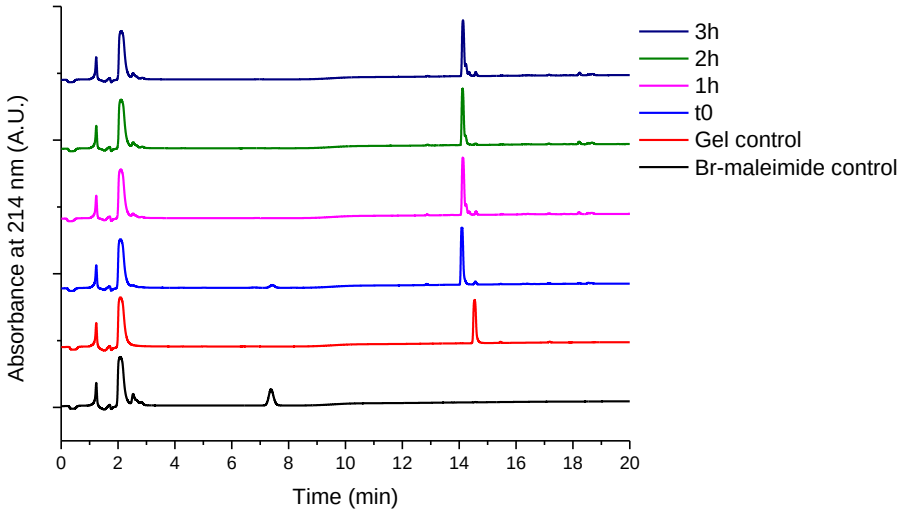

Figure 5.9. Comparison between LC analyses of reaction over 3 hours.

5.2.2.3. Reversibility Assay

As discussed above, reaction between peptides that contains Cys residues and Br-maleimide is reversible in solution upon the addition of nucleophile reagents, as phosphine derivatives.[113] This observation has been investigated as a possible strategy for reversible assembly of the hydrogel tested. After the complete disassembly, additions of different concentrations of water soluble triphenylphosphine-3,3′,3″-trisulfonic acid trisodium salt (TPPTS) have been carried out, but re-assembly process was not observed.

Many factors can be responsible for this result. First of all, in this case the disassembly process led to the formation of a precipitate containing peptide molecules engaged in thiomaleimide conjugates that are difficult to bring in solution, an essential condition for the assembly. Moreover, presence of other molecules in the same concentrations of gelator (*i.e.*, Br-maleimide, phosphine) could physically hinder peptide interactions and self-organisation. Overall dilution effects that could bring peptide concentration below minimum gelling concentration have to be taken in account, although additions of reagents have been carefully performed in order to limit them as much as possible. Further analyses, such as solid states NMR studies, are required to optimise the reversibility of this useful reaction also in hydrogel phase and obtain a smart material that could be selectively assembled and disassembled.

5.2.3. Photochemically Induced Disassembly

New generation of supramolecular functional materials are directed towards multi-stimuli responsive smart nanostructures. In this context, development of photo-responsive supramolecular hydrogels could be an interesting approach for diverse applications, as reported in **Figure 5.10**.

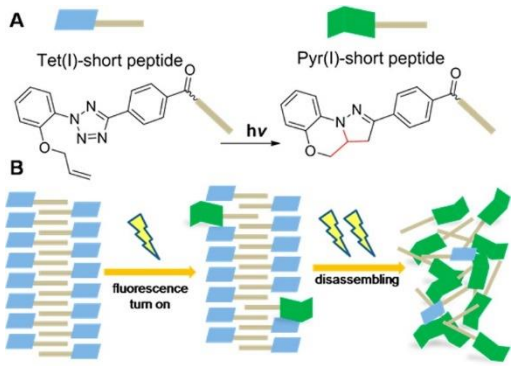

Figure 5.10. (**A**) Components of photoresponsive hydrogelator. (**B**) Photoresponse of the self-assembled hydrogels. Reprinted with permission from ref. 118 © 2013 American Chemical Society.[118]

Common photoswitches are reversible and typically based on photo-induced isomerization. Many examples have been reported, whereby peptide sequences have been covalently modified for this purpose with light sensitive hydrophobic groups, including azobenzene, diarylethene and spiropyran [64, 118-122] In those cases, one of the classical approaches is based on the fact that the *trans*-isomer has gelling ability, while the *cis*-isomer, deriving from photoisomerization, do not, as reported in **Scheme 5.5**.[122]

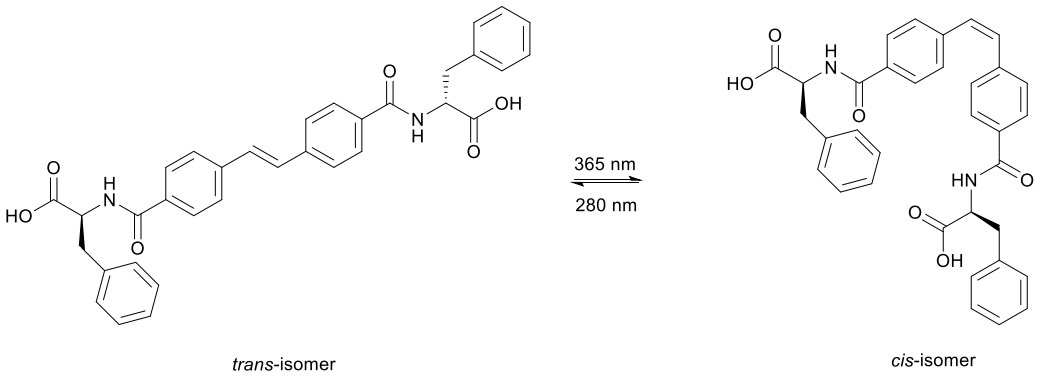

Scheme 5.5. *Trans-cis* reversible photoisomerization of a stilbene-based peptide gelator.[122]

Reversible processes, as discussed above, are fundamental to modulate supramolecular behaviour with spatiotemporal control. On the other hand, the possibility to disassemble in irreversible manner functional nanomaterials has to be recognised with the aim to definitely "switch off" functionalities related to assembled states, including catalytic activities, targeted delivery, and modulation of biological functions. Moreover, since environmental

issues are becoming more and more severe, an irreversible approach is necessary to dispose functional hydrogels as non-active peptide short sequences.

Herein, a rational design has been studied to obtain an innovative irreversible photo-triggered disassembly of a hydrogel based on Cys-containing tripeptide, avoiding the incorporation of any additional photosensitive moieties. The observation from our previous studies that the alanine-containing tripeptide Phe-^{D}Ala-Phe was not able to self-assemble into a hydrogel,[43] while its cysteine containing analogue Phe-^{D}Cys-Phe did (as described above), suggested that a cysteine-to-alanine conversion, through a photo-induced desulfurization, could be a good strategy to disassemble this nanostructured hydrogel in an irreversible manner. The irreversibility was achieved by the fact that the final product of the reaction, that is the alanyl peptide, is not able to self-assemble into a hydrogel anymore.

5.2.3.1. Desulfurization Reaction in Solution: LC-MS and NMR Analyses

In literature, several protocol of desulfurization reactions are reported in the context of native chemical ligation (NCL). The NCL reaction described by S. Kent and co-workers leads to the formation of a peptide bond between a C-terminal thioester residue and a N-terminal cysteine residue, by an intramolecular S-to-N acyl shift of thioester intermediate, as shown in **Scheme 5.6**.[123]

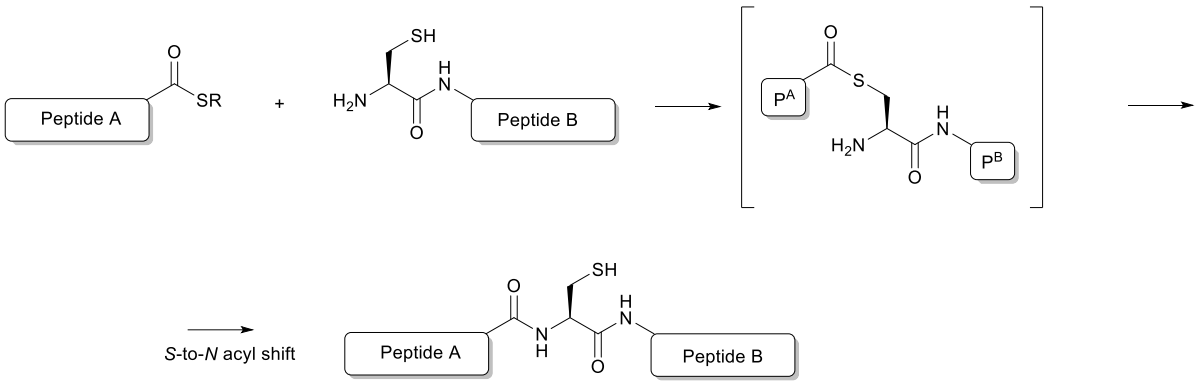

Scheme 5.6. Scheme of native chemical ligation.[123]

This useful reaction has extreme importance for the synthesis of long polypeptides and proteins, but the applications are traditionally related to the mandatory presence of cysteine in the final products. A good alternative to bypass cysteine dependence is the desulfurization

of the cysteine residue into an alanine residue, by means of, for example, a radical initiator[124] or UV irradiation.[125, 126] However, these reactions require harsher reaction conditions (including powerful and expensive UV reactors, organic solvents, thiol-based additives, inorganic photocatalysts)[127, 128] or they bring to the formation of several side products (*e.g.*, dehydroalanine derivatives).[129]

Herein, several attempts have been carried out to induce photodesulfurization of the gelling cysteine peptide in mild conditions. Indeed, different reaction conditions and UV lamps based on reported literature data have been tested, but all of them gave limited success when applied to unprotected cysteine tripeptide. After many efforts, finally, a mild procedure has been identified and optimised for cysteine tripeptide photo-desulfurization, inspired by a radical-based desulfurization protocol reported by Danishefsky and co-workers (reported in **Scheme 5.7**).[124]

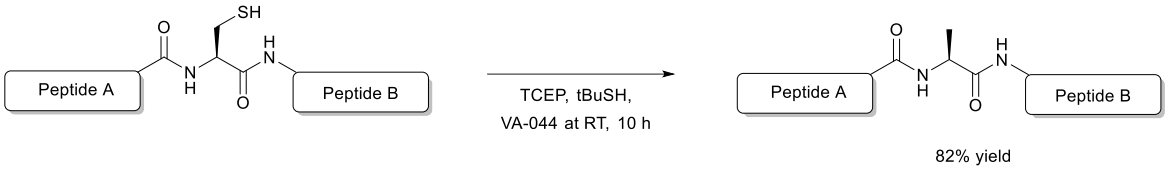

Scheme 5.7. Free-radical-mediated transformation of Cys to Ala.[124]

In particular, water soluble radical initiator 2,2'-azobis[2-(2-imidazolin-2-yl)propane]dihydrochloride (VA-044) has been substituted by UV light irradiation, using a *Hoefer UV-20 Transilluminator*, without the aid of tert-butylthiol (tBuSH). First, the reaction has been performed in solution dissolving peptide Phe-^{D}Cys-Phe in water at neutral pH in presence of 1 equivalent of an aromatic water-soluble phosphine as reducing agent (TPPTS instead of TCEP), at room temperature. Nearly quantitative conversion of cysteine residue into alanine occurred within 1 hour at neutral pH (as shown in **Scheme 5.8**), optimising, thus, Danishefsky' s protocol that needed 10 hours of reaction at room temperature or 2 hours at 37°C and a final purification step.

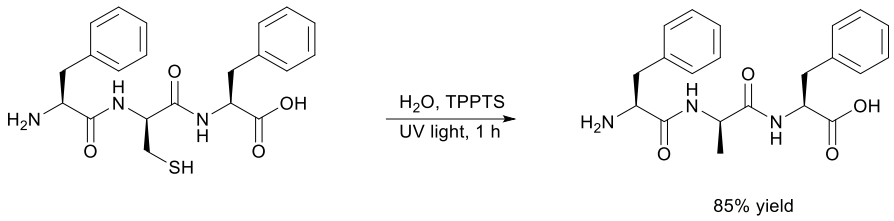

Scheme 5.8. UV-based desulfurization in mild conditions of Cys into Ala.

Reaction has been followed by means of ^{1}H-NMR, ^{31}P-NMR and LC-MS analysis. As reported in **Figure 5.11**, after 30 minutes of UV-irradiation of the sample, a doublet peak ascribed to the methyl groups of alanine appeared in ^{1}H-NMR spectrum, at 0.9 ppm. LC-MS analyses confirmed that result revealing the presence of a peak with mass related to the alanyl peptide (*i.e.*, Phe-^{D}Ala-Phe), although the peak of cysteine starting peptide was still present. After 60 minutes of UV irradiation, the reaction was complete: all the cysteinyl peptide was converted in its alanine analogue and, in small amount, in its dimer due to disulfide formation.

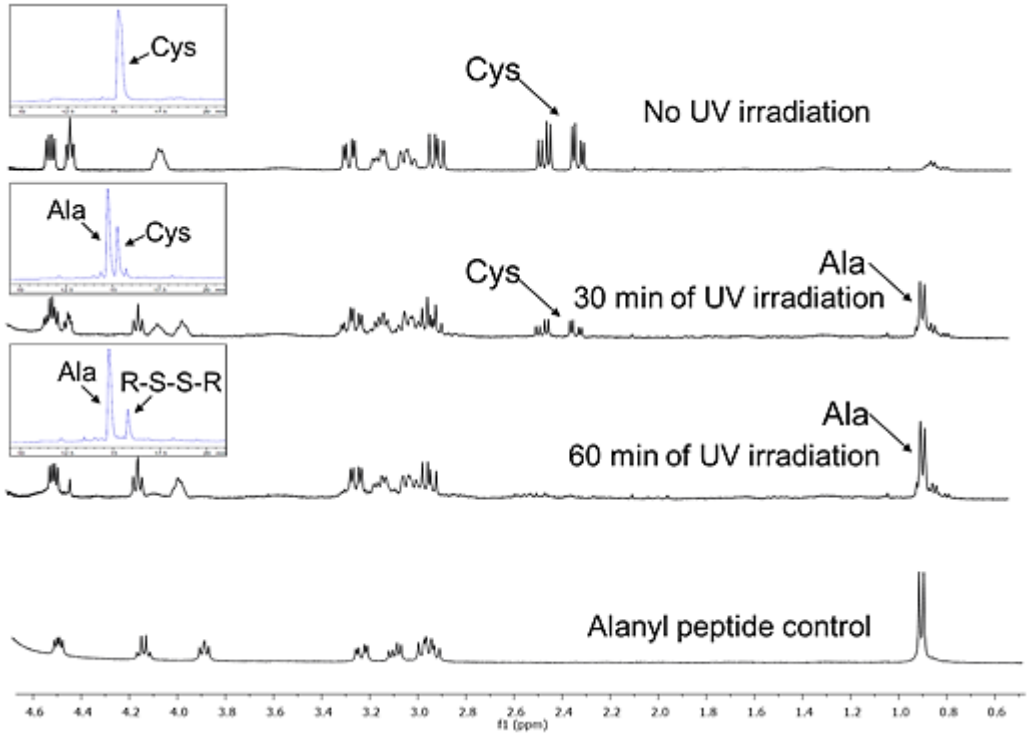

Figure 5.11. ^{1}H-NMR spectra of Phe-^{D}Cys-Phe photodesulfurization in D_2O at different time points. Insets show corresponding LC chromatograms.

Integration of peak areas revealed that less than 15% of conversion brought to the formation of the peptide dimer. Many considerations on diverse reducing agents have been done before finally selecting of TPPTS to guarantee the presence of thiol group in its reduced state. Addition of glutathione to keep a reduced environment was not considered because of the presence of Cys residue in its sequence that could compete for desulfurization reaction. Ascorbic acid and sodium hypophosphite[125] as reducing agents failed their attempts since the desired alanine product was not obtained. Finally, the use of TCEP, widely employed as disulfide reducing agent in peptide chemistry,[124, 130] brought to the formation of a small amount of desired product. Indeed, in radical based protocol, the authors envisaged that TCEP had a key role during dephosphorization reaction, since it mediated the removal of S atom,[124] as reported in **Scheme 5.9** and also confirmed by further DFT calculations.[131]

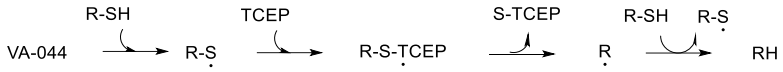

Scheme 5.9. Proposed mechanism of radical desulfurization reaction.

Considering the stated importance of phosphine but the low amount of product obtained in presence of TCEP, the decision to use TPPTS, an aromatic water-soluble phosphine, instead of the alkyl TCEP, derived from the purpose to introduce a UV light sensitizer in this context. In order to assess the abstraction of S atom by phosphine during the reaction, ^{31}P-NMR analyses have been carried out. As shown in **Figure 5.11**, after 1 hour of UV irradiation, the starting phosphine was completely consumed to form phosphine oxide and phosphine sulphide (chemical structures are reported in **Scheme 5.10**).[132, 133] These result confirmed the removal of the S atom by the phosphine, which followed the attack of the sulfur on the phosphorus of the phosphine.

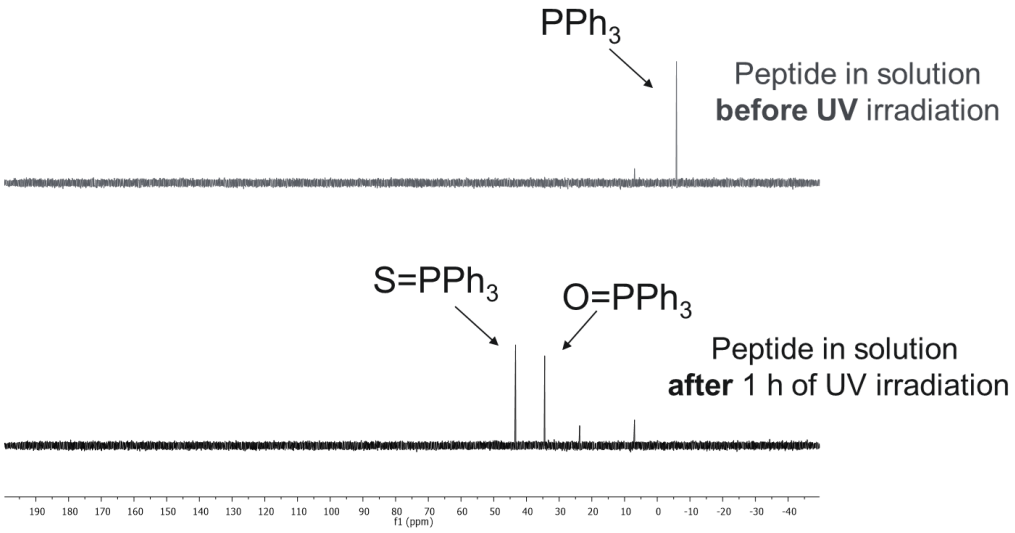

Figure 5.11. ^{31}P-NMR spectra of reaction mixture of Phe-^{D}Cys-Phe photodesulfurization in D_2O before and after 1 hour of UV irradiation.

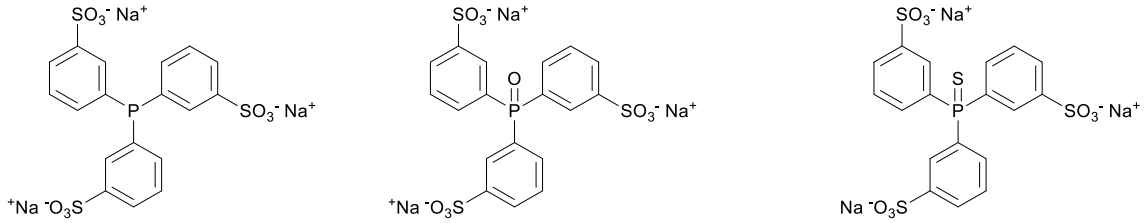

Scheme 5.10. Chemical structures of starting phosphine (TPPTS) and its oxide and sulfide derivatives.

As mentioned above, a radical mechanism was envisaged, whereby the UV light induced the radical formation (instead of the radical initiator used in previously reported protocol). This mechanism was further corroborated by experiments performed in presence of 2,2,6,6-tetramethyl-1-piperidinyloxy (TEMPO, 1 equivalent), because the desired alanine product was not obtained. Proposed radical mechanism for UV light induced desulfurization of peptide Phe-^{D}Cys-Phe in presence of TPPTS is reported in **Scheme 5.11**.

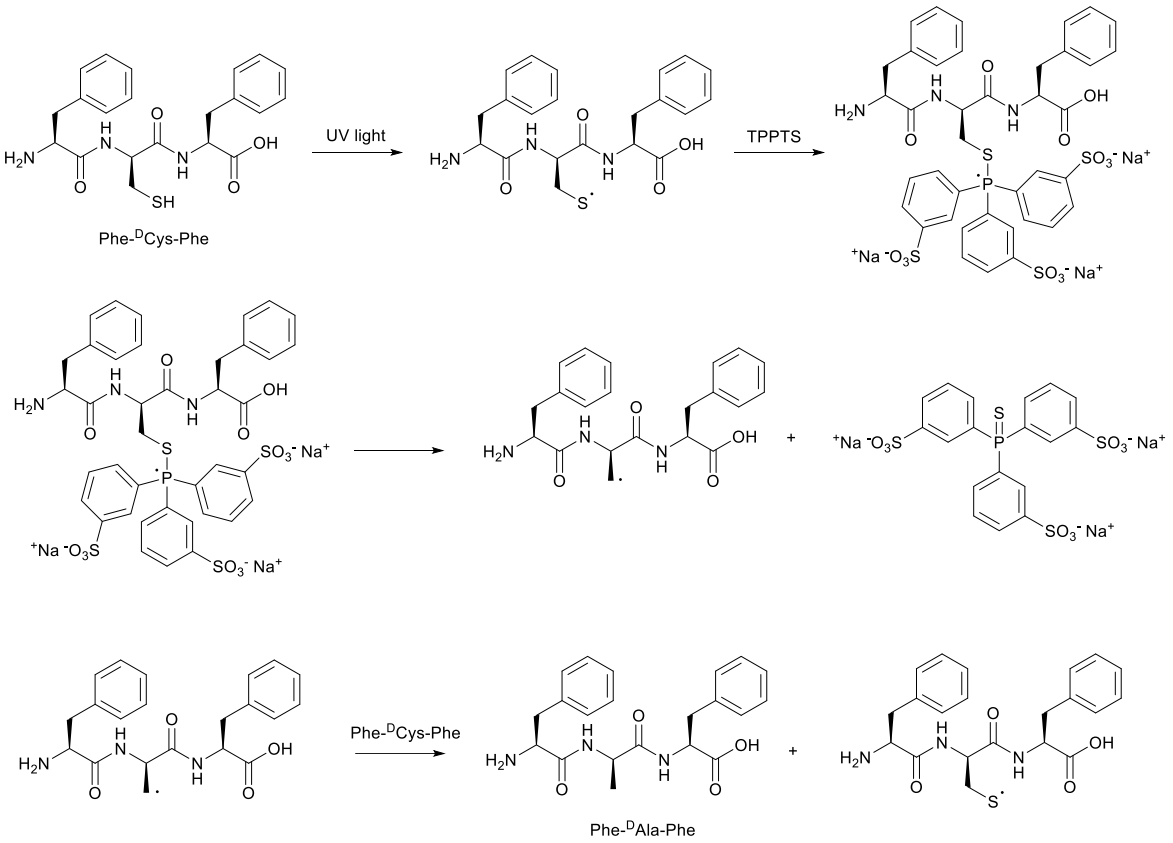

Scheme 5.11. Proposed mechanism of UV-induced desulfurization reaction.

Once optimised desulfurization reaction in solution, it was performed on hydrogel phase with the aim to induce a selective and irreversible disassembly of hydrogel based on peptide Phe-^{D}Cys-Phe.

5.2.3.2. Desulfurization Reaction in Hydrogel: TEM and Raman Analyses

Hydrogel was prepared following the protocol reported in ***Chapter 4***, **Section 4.2.3**, in an *Ibidi* uncoated dish that allowed high UV light transmission. In hydrogel phase, 2 hours and 30 minutes were required to induce a visible disassembly. In order to get a spatial control over hydrogel rheological properties, a triangle shaped UV-photo mask was employed. As reported in **Figure 5.12B**, a solution was obtained after UV-irradiation, surrounded by the hydrogel on the edge of the mask.

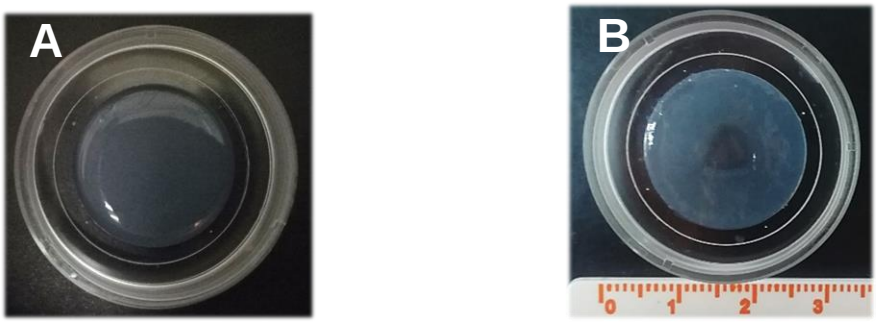

Figure 5.12. Photographs of hydrogel (**A)** before and (**B**) after UV irradiation using a mask.

TEM analyses of dried samples taken in the centre and on the edge of the irradiated gel were performed in order to investigate the effect of UV irradiation on nanostructures. The hydrogel not exposed to UV light (**Figure 5.13A**) maintained its well organised network of nanofibrils, whilst the irradiated sample (**Figure 5.13B**) showed few broken and short fibrils, which were not able to entrap water molecules. Hence, the disassembly occurred on nanoscale level.

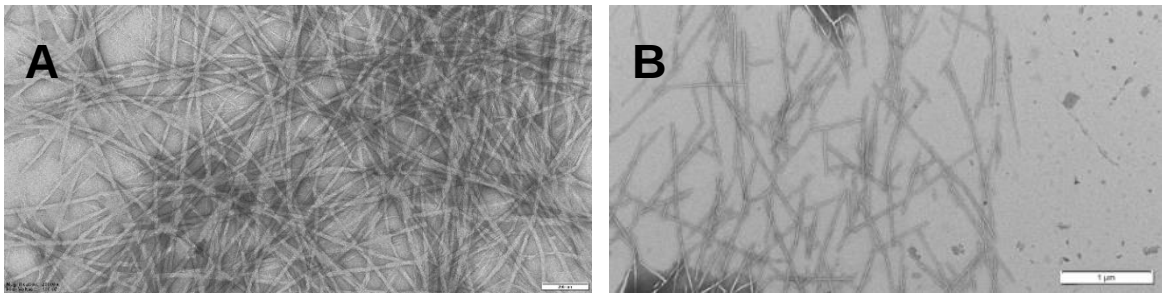

Figure 5.13. TEM images of hydrogel (**A**) before and (**B**) after UV irradiation using a mask.

As described above, Ellman test is an elegant assay to perform for checking the presence of thiol groups. However, in this case, the presence of phosphine as reducing agent that can react with Ellman's reagent interfered with the results, making the test not meaningful. Vibrational techniques, such as IR and Raman spectroscopies, can be employed to follow the presence of thiol group before and after the UV- mediated disassembly. Since the stretching of S-H bond is reported to give only weak IR bands, Raman spectroscopy has been exploited in this case.

Raman is a vibrational spectroscopic technique discovered in 1928 by C. V. Raman, who gave his name to the technique being awarded with Nobel Prize in 1930.[134] Development of Raman is highly related to the development of laser source by T. H. Maiman, A. L. Schawlow and others. Considering vibrational excitation, in IR spectroscopy photons can be absorbed and induce a transition from the vibrational ground state to higher vibrational energy levels. In Raman, instead, the laser brings molecules from the vibrational ground state to a transient virtual state, and from this level they can scatter the light back in three different ways:

- to the ground state: this is Rayleigh scatter that has the same energy of the laser and no changes in energy are noticed (elastic scattering);
- to an excited vibrational state, taking out some energy: in this case Stokes scattering is observed (inelastic scattering);
- from an even higher virtual states to the ground state: anti-Stokes photons with higher energy than laser energy are scattered (inelastic scattering) and they are related to fluorescence phenomena.

Stokes scattering is the most common studied by Raman instruments, since the different frequency returning from the sample corresponds to the vibrational frequency of the molecule bonds and it is measured in Raman shift that is the shift in wavenumbers with respect to the exciting laser. The overall intensity of Raman bands depends on the laser colour (*i.e.,* laser frequency).

Micro-Raman instrument has been herein employed on dried samples before and after UV irradiation. A band at 2621 cm^{-1} Raman shift identified on the dried sample not exposed to UV light (black spectrum in **Figure 5.14**) confirmed once again the presence of the free sulfhydryl groups of gelling cysteine peptide into the assembled state. After 2 hour and 30 minutes of UV irradiation, such band disappeared, proving the occurrence of desulfurization reaction also in hydrogel phase.

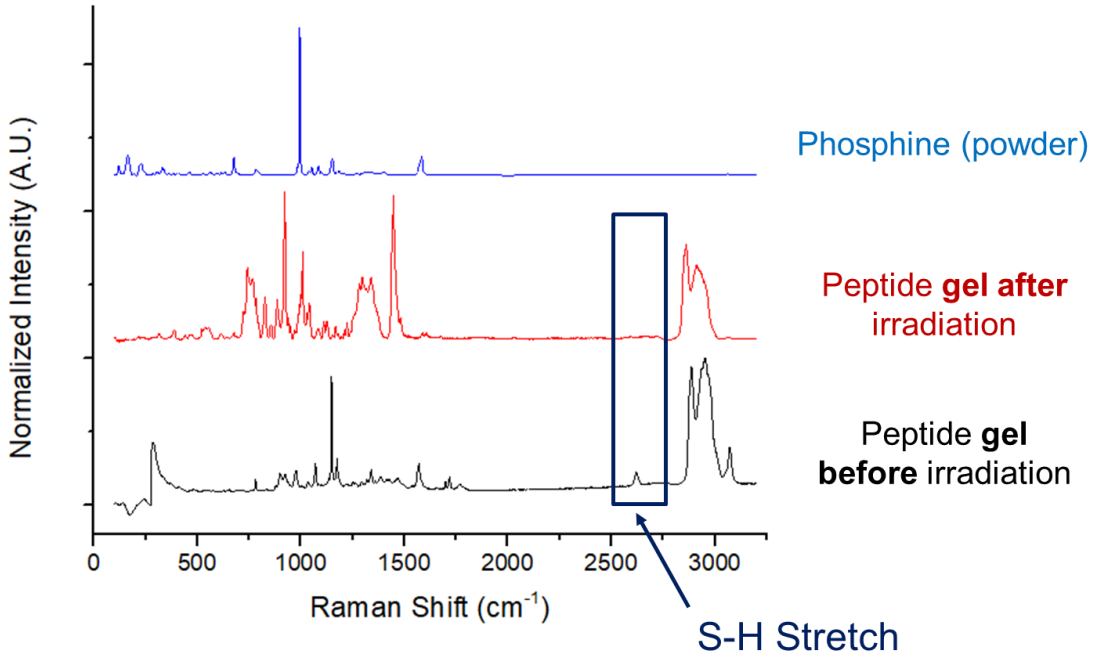

Figure 5.14. Raman spectra of hydrogel before and after UV-induced disassembly.

5.3. Conclusions

Three different protocols have been reported to induce disassembly of unreported gelling systems based on cysteine containing peptides. Thermostability has been investigated as a reversible and not specific tool to control assembled/disassembled states of supramolecular nanostructured materials, obtaining different cycles of assembly. Reversible sulfur-based chemistry has been successfully exploited for the disassembly of a hydrogel, although the reversibility of the process faced some obstacles due to precipitation phenomena. Additional investigations based on NMR studies will be performed towards the optimisation of reaction conditions in order to achieve reversible assembly. This protocol, useful for a time-controlled disassembly, will be then applied to other hydrogels based on cysteine containing peptide to extend the scope of the reaction. Finally, a UV-based desulfurization of cysteine residue in water has been achieved in milder conditions than those previously reported, avoiding the use of organic solvent and expensive photoreactors. This protocol has been applied for the irreversible UV-triggered disassembly of a nanostructured hydrogel in a spatially resolved manner using a photo mask. Future perspectives will focus on the investigations of the applicability towards functional materials.

Chapter 6: Materials and Methods

6.1. Peptide Synthesis

The selected peptides were synthesised according to solid phase peptide synthesis (SPPS) based on Fmoc protection and HBTU activation, using 2-chlorotrityl chloride resin as solid support.

All Fmoc-protected amino acids and the resin were from *IRIS Biochem*, HBTU and HOAt were from *GL Biochem*. All the other reagents and solvents were purchased of analytical grade from *Merck*.

6.1.1. Loading of the C-Terminally Amino Acid on the Resin

For each peptide, 1 g of resin was put into a fritted glass reactor where it has been swollen in DCM under argon flow for 30 minutes. Then, resin was activated by addition of 100 μL of thionyl chloride ($SOCl_2$) for 1 hour. After that time, the resin has been accurately washed with DCM and DMF. 1.6 mmol of the C-terminus amino acid have been dissolved in DMF/DCM mixture and 0.9 mL of DIPEA. This solution was added to the resin and left under argon flow for 1.5 hour. Then, eventually unreacted resin has been capped by addition of 0.5 mL of methanol to avoid formation of truncated peptides. The resin has been filtered and accurately washed with DMF and DCM.

The amount of amino acid loaded on the resin has been measured. Three samples of few mg (around 5 mg) of resin after the loading (before Fmoc- deprotection) were taken, put in three Eppendorf tubes and weighted. 1 mL of a Piperidine 20% solution in DMF was added in each Eppendorf tube to remove Fmoc group from the loaded amino acid. After being shaken for 20 minutes and centrifuged for 5 minutes, 100 μL of supernatant from each Eppendorf tube were put it in three vials containing 10 mL of DMF (dilution 1:100). The absorbance at 301 nm of this solution containing the fluorophore dibenzofulvene-piperidine adduct have been measured in 1 cm cuvette by means of a UV spectrophotometer. Absorbance measurements have been performed three times for each samples and average values were used to calculate loading. Substitution of Fmoc-amino acid loaded on the resin was calculated for each sample using the following formula: [135]

$$\text{Substitution (mmol/g)} = (101 * Abs_{301nm}) / (7.8 * m_{resin})$$

Derived from:

$$SFmoc\ (mmol/g) = (Abs_{301nm} * 10^6 mmol * mol^{-1} * mg * g^{-1} * V * D) / \varepsilon\ m_{resin} * l$$

Whereby,

SFmoc = Fmoc substitution (mmol/g)

ε = Molar absorption coefficient of dibenzofulvene–piperidine adduct at 301 nm: = 7800 L mol^{-1} cm^{-1}

$Abs_{301\ nm}$ = Absorption of the sample solution at 301 nm

m_{Resin} = Sample weight of the resin (in mg)

10^6 mmol mol^{-1} mg g^{-1} = Factor for conversion of mol to mmol and mg^{-1} to g^{-1}

V = Sample volume (in L)

l = Optical path length of the cell in cm (1 cm)

D = Dilution factor

6.1.2. Fmoc Cleavage

N-protecting Fmoc group was removed from the loaded amino acid by treating the resin with 20 % piperidine solution in DMF for 10 minutes twice. After that, the resin was filtered again and finally washed with DMF and DCM. The same protocol has been followed after coupling reaction of each amino acid during peptide elongation.

6.1.3. Colourimetric Tests

The occurrence of both Fmoc removal from loaded amino acid and coupling reactions of the following ones were monitored performing two colourimetric assays that detected unreacted amino groups: bromophenol blue and chloranil assays.

For bromophenol blue test, few drops of a 0.05% bromophenol blue solution in DMF were added in a test tube containing few resin beads: the presence of amine groups is noticed by the presence of blue beads.[136]

In case of acetaldehyde/chloranil test, few drops of a 2% acetaldehyde solution in DMF were added to few resin beads in a test tube, followed by few drops of 2% chloranil in DMF. The test tube was gently shacked and after 5 minutes the result of the test was observed: blue beads indicated the presence of secondary or primary amines.[137]

6.1.4. Couplings of the Following Amino Acids

Sequences were then elongated by following steps of Fmoc-protected amino acid couplings, washings, filtrations and Fmoc-cleavages. 3 equivalents of Fmoc-amino acids were dissolved in DMF in presence of 2 equivalents of both HOAT and HBTU and 2 mL of a 1 M DIPEA solution in DMF for every equivalent of loaded amino acid on resin. After 3 minutes of pre-activation step, the mixture was added to the resin and stirred under argon flow until completeness was confirmed by negative colorimetric tests (typically 1.5 hours). In case of Fmoc protected cysteine couplings, 0.5 M collidine solution in DMF was used instead of DIPEA and pre-activation step was avoided.

6.1.5. Cleavage of the Tripeptide from the Resin

The purpose of the step is to cleave the peptide from resin as well as remove sidechain protecting groups (*i.e.*, trityl from cysteine thiol group in cysteine containing peptides).

10 mL of selected cleavage cocktail Reagent L were prepared fresh prior to use by mixing TFA (88%), DTT (5%), H_2O (5%), and TIPS (2%). The cleavage solution was added to the resin and left under gentle argon stirring for 1.5 hours. After that time, the solution containing the crude peptide was filtered from the resin in a round flask and the resin washed twice with fresh cleavage cocktail. Filtrate was recovered. TFA was then removed by evaporation with argon flow (3 hours). After TFA evaporation, a yellowish precipitate was obtained.

6.2. Peptide Purification

Precipitate obtained from TFA evaporation was dissolved in 7 mL of a mixture water/acetonitrile (H_2O/MeCN) 70/30 containing 0.05% of TFA and filtered with 0.45 μm PTFE filter. All peptides were purified through RP-HPLC (*1260 Agilent Infinity system*)

equipped with a preparative gradient pump (*G1311B*), semipreparative C-18 column (*Kinetex*, 5 μm, 100 Å, 250 x 10 mm, *Phenomenex*) and photodiode array detector (*G1315C*). The gradient used consisted of MeCN/ H_2O with 0.05% TFA with a flow rate of 3 mL/min and the following program:

- t = 0 - 2 min, 25% MeCN;
- t = 8 min, 45% MeCN;
- t = 10 min, 95% MeCN;
- t = 15 min, 95% MeCN.

Collected fractions were then freeze-dried to yield the corresponding peptide as a white fluffy powder.

6.3. Peptide Characterisation

Electron Ionisation-Mass Spectroscopy (ESI-MS) and Nuclear Magnetic Resonance Spectroscopy (^{1}H-NMR and ^{13}C-NMR) have been performed for all the selected peptides to verify their identity and purity.

In particular, LC-MS samples have been prepared by dissolving each peptide at 1 mg/mL concentration in a mixture H_2O/MeCN 50/50 with the addiction of 0.1% of formic acid. Samples were filtered with 0.2 μm PTFE filters and analyses were performed on quadrupole LC/MS (*6120*) using an analytic C-18 column (*Luna*, 5 μm, 100 Å, 150 x 2 mm, *Phenomenex*) at 35 °C. The gradient used consisted of MeCN/ H_2O with 0.1% of formic acid with a flow rate of 0.3 mL/min and the following program:

- t =0 min, 5% MeCN;
- t = 20 min, 95% MeCN;
- t = 21 min, 95% MeCN.

The ^{1}H-NMR and ^{13}C-NMR spectra were recorded in dimethyl sulfoxide (DMSO-d_6), using tetramethylsilane (TMS) as internal standard, with a *Varian Innova* spectrometer at the frequency of 400 and 100 MHz, respectively.

6.4. Peptide Self-Assembly

6.4.1. Methionine Containing Peptide Self-Assembly

A pH trigger was used to study self-assembling ability of methionine containing peptides. Peptides were dissolved in alkaline sodium phosphate buffer (0.1 M pH 11.8) in ultrasonic bath for 15 minutes at 30°C, and then diluted 1:1 by addition of an acidic sodium phosphate buffer (0.1 M pH 5.5) in order to reach final concentration of 15 mM for peptide ^{D}Met-Phe-Phe and 10 mM for both Phe-^{D}Met-Phe and ^{D}Phe-Phe-Met. Samples were left to self-assemble without shaking or sonication at room temperature for 1 hour, when final pH was measured to be 7.2 ± 0.2.

6.4.2. Cysteine Containing Peptide Self-Assembly

A temperature switch was used to study self-assembling ability of cysteine containing peptides. Each peptide was dissolved in a phosphate buffer saline (0.1 M pH 7.7) by heating the sample to get a final concentration of 15 mM. Samples were left to gradually reach room temperature and self-assemble without shaking or sonication for 1 hour, when final pH was measured to be 7.2 ± 0.2.

6.5. Rheological Analyses

Dynamic time sweep rheological analyses were performed for all samples on a *Malvern Kinexus Ultra Plus* oscillatory rheometer with a 20 mm stainless steel parallel plate geometry. The temperature was maintained at 25 °C using a Peltier temperature controller. Samples were prepared *in situ* and immediately analysed with a gap of 1.00 mm. Time sweeps were recorded for 1 hour using frequency and stress values that allowed to operate in a linear viscoelastic regime, that is 1.00 Hz frequency and controlled stress of 0.10, 1.00, 4.00, or 5.00 Pa (depending from the sequence). After 1 hours, frequency sweeps were recorded using a controlled stress of 0.10, 1.00, 4.00, or 5.00 Pa (depending from the sequence) and frequency values from 0.1 to 10 Hz. Finally, stress sweeps were recorded using a frequency of 1.00 Hz and stress from 0.1 Pa until the breaking point typical for every hydrogel, detectable by the inversion of G’ and G” values. Measurements were repeated at least 3 times.

6.6. Transmission Electron Microscopy (TEM) Analyses

TEM micrographs were acquired at 100 kV by Dr. Slavko Kralj from Jožef Stefan Institute in Ljubljana (Slovenia) on a *Jeol, JEM 2100* instrument (Japan) and by Dr. Daniel Iglesias on a *TEM FEI EM208*, digital camera *Quemesa*, acquisition software *Radius Emsis*, at the Center of Electron Microscopy, Department of Live Science, University of Trieste.

TEM grids (either copper-grid-supported lacey carbon film or carbon-coated copper grid) were first exposed to a UV-ozone cleaner (*UV-Ozone Procleaner Plus*) for 5 minutes to make their surface more hydrophilic. Then, a small amount of both 1 hour and 24 hours-aged gels were precisely deposited on a TEM grid, dried for 10 minutes at room temperature, and stained by addition of one drop of a 2% sodium phosphotungstate aqueous solution pH 7.5. Grids were dried under vacuum before their visualisation. Average size or cross-section diameter of the nanostructures was determined by taking into account at least 100 individual nanostructures.

6.7. Scanning Electron Microscopy (SEM) Analyses

Hydrogels derived from the self-assembly of gelling cysteine containing peptides were analysed using a *FEI SEM Helios Nanolab 600*, at the Institute of Physics, University of Tartu (Estonia) in collaboration with Prof. Sergei Vlassov. Samples were prepared by depositing a small amount of hydrogels after 1 hour and 24 hours of self-assembly on a small piece (1 cm x 1 cm) of silicon wafer and dried under vacuum. Samples were coated with gold by means of sputtering device *Emitech Sputter Coater* and then visualised under 10 kV electron beam.

6.8. Circular Dichroism Spectroscopy (CD)

A 0.1 mm pathlength quartz cuvette was used on a *Jasco J815 spectropolarimeter*, with 1 s integration time, 1 accumulation, and a step size of 1 nm with a bandwidth of 1 nm over a wavelength range of 200–280 nm. The samples were freshly prepared directly in the CD cell and the spectra were immediately recorded. All buffer solutions were filtered (0.45 µm filter) prior to use. To follow the self-assembly kinetics, the CD signal was monitored at 25 °C (*Peltier*) every 2.5 minutes for one hour. After one hour of kinetics, a heating ramp of 5 ºC/min from 25 ºC to 85 ºC with 5 °C steps was applied to the self-assembled samples, followed by a cooling ramp from 85 °C to 25 °C and 5 °C steps. To monitor the CD signal of the samples in solution (below the minimum gelling concentration), methionine

containing peptides were dissolved at a concentration of 1 mM in phosphate buffer (pH 11.80), whilst cysteine containing peptides were dissolved at 1 mM in phosphate buffer saline (pH 7.7). Measurements were repeated at least 3 times.

6.9. Fourier-Transformed Infrared Spectroscopy (FT-IR)

FT-IR spectra were collected on a *Perkin Elmer System 2000* operating in transmission mode using KBr pellets method. The scanned wavenumber range was from 4000 to 400 cm^{-1} with 128 accumulations at a resolution of 1 cm^{-1}. Freshly prepared samples were left to settle for 24 hours in a glass vial and then dried under vacuum over 48 hours. A small portion of dried samples was mixed with KBr powder and then pressed to obtain pellets.

6.10. Amyloid Fluorescence Assays

100 μL hydrogels were prepared inside wells of *Greiner 96 U Bottom Black Polystyrene in situ*, accordingly to protocols described above. Negative controls experiments consisted of 100 μL of buffer solutions. After 1 hour of self-assembly, 20 μL of a solution of either Thioflavin T (28 μM in 20 mM glycine/NaOH buffer pH 7.5, filtered with a 0.2 μm filter) or Nile blue A (0.3 mM in water) were added in each well. Within 10 minutes, fluorescence emission was measured at 25 °C using a *Tecan Infinite M1000 pro*, selecting for ThT analyses an excitation wavelength of 446 nm and an emission wavelength of 490 nm and 20 nm bandwidth. For Nile blue A analyses, a 636 nm excitation wavelength and an emission wavelength range from 660 nm to 800 nm were used with a bandwidth of 20 nm. Each condition was repeated at least twice in triplicate. The average and standard deviations were calculated and plotted.

6.11. X-Ray Diffraction (XRD) Single Crystal Analyses

6.11.1. Single-Crystal XRD Data of ^{D}Met-Phe-Phe

A stick-shaped single crystal of the peptide was collected with a loop, cryoprotected by dipping the crystal in glycerol and stored frozen in liquid nitrogen. The crystal was mounted on the diffractometer at the synchrotron Elettra, Trieste (Italy), beamline XRD1, using the robot present at the facility. Temperature was kept at 100 K by a stream of nitrogen on the crystal. Diffraction data were collected by the rotating crystal method using synchrotron radiation, wavelength 0.70 Å, rotation interval 1°/image, crystal-to-detector distance of 85 mm. A total of 270 images were collected to increase redundancy of data. Reflections were

indexed and integrated using the XDS package,[138] space group $P2_1$ was determined using POINTLESS,[139] and the resulting data set was scaled using AIMLESS.[140] Phase information were obtained by direct methods using the software SHELXT.[141] Refinements cycles were conducted with SHELXL-14,[142] operating through the WinGX GUI,[143] by full-matrix least-squares methods on F^2. Unit cell parameters and scaling statistics are reported in **Table A.3.1**. The asymmetric unit contains a molecule of the peptide, a molecule of ethanol, and two water molecules. Hydrogen atoms of the peptide and the alcohol molecule were added at geometrically calculated positions and refined isotropically, with thermal parameters dependent on those of the attached atom. Hydrogen atoms of the water molecules were added in the electron density considering the hydrophilic interactions with peptide and solvent molecules and refined with geometric restraints on O-H distances (0.84 ± 0.02 Å) and H-H distance (1.34 ± 0.04 Å). During refinement, no restraints were applied on distances, angles or thermal parameters of the peptide. All the atoms, except the hydrogen atoms, within the asymmetric unit have been refined with anisotropic thermal parameters. Refinement statistics are reported in **Table A.3.1**.

6.11.2. Single-Crystal XRD Data of ^{D}Phe-Phe-Met

A plate-shaped single crystal of the peptide was collected with a loop, cryoprotected by dipping the crystal in glycerol and stored frozen in liquid nitrogen. The crystal was mounted on the diffractometer at the synchrotron Elettra, Trieste (Italy), beamline XRD1, using the robot present at the facility. Temperature was kept at 100 K by a stream of nitrogen on the crystal. Diffraction data were collected by the rotating crystal method using synchrotron radiation, wavelength 0.70 Å, rotation interval 1°/image, crystal-to-detector distance of 85 mm. A total of 180 images were collected. Reflections were indexed and integrated using the XDS package,[138] space group *C2* was determined using POINTLESS,[139] and the resulting data set was scaled using AIMLESS.[140] Phase information were obtained by direct methods using the software SHELXT.[141] Refinements cycles were conducted with SHELXL-14,[142] operating through the WinGX GUI,[143] by full-matrix least-squares methods on F^2. Unit cell parameters and scaling statistics are reported in **Table A.3.1**. The asymmetric unit contains three molecules of the peptide and 7 molecules of water (crystallization solvent). Hydrogen atoms of the peptide molecules were added at geometrically calculated positions and refined isotropically. Hydrogen atoms of the water molecules were manually added in the residual electron density and their position was confirmed by the analysis of the

geometry of interactions. Restrains on distance (O-H distance of 0.84 ± 0.02Å) and angles (H-H distance of 1.34 ± 0.04Å) of the water molecules were added during refinement, using the cards DFIX and DANG of the program SHELXL-14.[142] All the atoms, except the hydrogen atoms, within the asymmetric unit have been refined with anisotropic thermal parameters. Refinement statistics are reported in **Table A.3.1**.

6.11.3. Single-Crystal XRD Data of ^{D}Phe-Cys-Phe

A needle-shaped single crystal of the peptide was collected with a loop, cryoprotected by dipping the crystal in glycerol and stored frozen in liquid nitrogen. The crystal was mounted on the diffractometer at the synchrotron Elettra, Trieste (Italy), beamline XRD1, using the robot present at the facility. Temperature was kept at 100 K by a stream of nitrogen on the crystal. Diffraction data were collected by the rotating crystal method using synchrotron radiation, wavelength 0.70 Å, rotation interval 1°/image, crystal-to-detector distance of 85 mm. A total of 270 images were collected. Reflections were indexed and integrated using the XDS package,[138] space group $P2_12_12$ was determined using POINTLESS,[139] and the resulting data set was scaled using AIMLESS.[140] Phase information were obtained by direct methods using the software SHELXT.[141] Refinements cycles were conducted with SHELXL-14,[142] operating through the WinGX GUI,[143] by full-matrix least-squares methods on F^2. Unit cell parameters and scaling statistics are reported in **Table A.3.1**. The asymmetric unit contains two molecules of the peptide, a molecule of methanol at 50% occupancy, 2 water molecules in positions at 100% occupancy, a water molecule in a position at 70% occupancy, and 3 water molecules at 50% occupancy. The thiol group of one of the peptides is statistically disordered in two positions at 65% and 35% occupancy, respectively. Hydrogen atoms of the peptide and the methanol molecule were added at geometrically calculated positions and refined isotropically. The thiol group of the cysteine residue is in its reduced form in both the independent molecules present in the crystal structure. Hydrogen atoms of the water molecules were added considering the residual electron density and the hydrophilic interactions with neighbouring groups, except for 2 water molecules at 50% occupancy, for which hydrogen atoms could not be located. During refinement, restrains were applied to distances and angles of the water molecules. All the atoms, except the hydrogen atoms, within the asymmetric unit have been refined with anisotropic thermal parameters. Refinement statistics are reported in **Table A.3.1**.

6.12. Cytocompatibility Tests

6.12.1. Preparation of Hydrogels for Cytocompatibility Tests

Each peptide hydrogel was prepared according to the protocol described above inside microwells of *μ-slide Angiogenesis uncoated (Ibidi*) in a laminar-flow cabinet and left for 24 hours before the addition of cells. Control wells contained 20 μL of hydrogel and 30 μL of specifically prepared medium for fibroblast cells or 20 μL of hydrogel and 30 μL of water, while sample wells contained 20 μL of hydrogel and 30 μL of cells appropriately counted in their medium. Each sample was prepared in triplicate. Cells were left free to spread and growth on the hydrogels inside the microwells for 24 hours at 37 °C in a humidified incubator.

6.12.2. Cell Count

Number of cells in each microwell was fixed at 15,000 cells for 112 microwells. Cell count was performed before every cell transfer from their growth plates (maintained for the whole period of all experiments at 37 °C in humidified incubator) through trypan blue exclusion test of cell viability using a *Countess™ Automated Cell Counter*. This dye exclusion test is based on the principle that dead cells cannot exclude dyes (*e.g.*, trypan blue) while live cells with intact cell membranes can. In the adopted procedure a small volume of cell suspension was mixed 1:1 with the dye, moved inside a countess slide and measured through the *Countess™ Automated Cell Counter*. Once counted, an average of 15,000 cells were placed on hydrogels after 24 hours from their preparations and left to spread at 37 °C in the humidified incubator for 24 hours before performing the cytotoxicity assays described in the next sections.

6.12.3. LIVE/DEAD Viability/Cytotoxicity Assay

Peptide self-assembled hydrogels were prepared as described above by using 10 μL of each precursor solution which were filtered with 0.2 mm filters and added to each microwell of a μ-slide *Angiogenesis uncoated (Ibidi)* in a laminar-flow cabinet (final gel volume was 20 μL). Hydrogels were left to settle at room temperature for 24 hours. 30 μL of milli-Q filtered 0.2 mm water for control wells and fresh DMEM/glutamax (*Invitrogen*) medium containing 10% foetal bovine serum incubated for 30 minutes at room temperature were gently added on top of gels. The solution was then replaced with media containing L929 fibroblasts (mouse C3H/An connective tissue from *Sigma*) at 15,000 cells per well. These were cultured

at 37 °C in a humidified incubator for up to 3 days, exchanging the media with fresh (30 μL) after 48 hours. Few drops of sterile PBS were carefully placed between the microwells to reduce evaporation. Live/dead assays were performed at 24, 48, or 72 hours by replacing 30 μL of media with 15 μL of freshly prepared live/dead solution containing calcein (live) and ethidium homodimer (dead) (Viability/Cytotoxicity kit for mammalian cell, Invitrogen by Thermo Fisher Scientific) prepared according to the manufacturers' instructions. Following 20 minutes incubation, cells were imaged on an inverted widefield fluorescence microscope (*EVO FL Microscope*). Each condition was repeated twice in triplicates.

6.12.4. MTS Assay

Microwells containing hydrogels and cells, cells only (control), hydrogel only with media or milliQ water filtered 0.2 mm were prepared as described above and incubated for 24 hours. 25 μL of media were replaced with 25 μL of an MTS solution (ab197010 from *Abcam*). Absorbance at 490 nm was read by placing 5 μL samples on a *Nanodrop ND-2000c Spectrophotometer (Thermo Scientific)*. Each measurement was repeated at least three times per sample, and each condition was repeated twice in quintuplicate. Absorbance at 490 nm of the blanks was subtracted to the absorbance at 630 nm of the samples and controls. Data are represented as means and standard deviation (SD).

6.13. Synthesis of 3-Bromomaleimide

A 50 mL three neck round bottom was charged with 1.0 g (10.3 mmol) of maleimide and 7.5 mL of chloroform. A solution obtained by diluting 0.65 mL of bromine (12.7 mmol) in 7.5 of chloroform was added dropwise to the maleimide suspension in a 2 hours timespan. When the addition of bromine was completed, the reaction mixture was brought to reflux and kept at this temperature for three hours. After allowing the mixture to cool to room temperature, the solvent was removed under reduced pressure obtaining a yellow precipitate that was washed with ice-cold chloroform (4 x 5 mL) obtaining a first crop of crude 2,3-dibromosuccinimide (1.4 g). A second crop of 2,3-bromosuccinimide could be obtained from the chloroform phases after solvent removal (0.4 g) and washing of the residue with chloroform (4 x 2 ml). Overall 1.8 g (7 mmol) of crude 2,3-dibromosuccinimide were obtained and this was used in the second step of the reaction without further purification, yield 68%.[113, 144, 145]

In a 50 mL round bottom flask were introduced 1.5 g (5.84 mmol) of crude 2,3-dibromosuccinimide and 15 mL of THF and the solution was brought to 0 °C with a melting ice bath. To this solution were added dropwise 0.82 mL (5.9 mmol) of triethylamine diluted in 9 mL of THF. Upon addition a white precipitate formed immediately, the mixture was left stirring in the dark at room temperature for 24 hours. The precipitate was filtered off and the solution was brought to dryness obtaining a faint yellow solid which was purified by flash chromatography on silica gel using hexane/ethyl acetate 5/1 as eluent obtaining 760 mg of product as a faint yellow solid, yield 74%.[113, 144, 145] Melting points were obtained with a *Gallenkamp* melting point apparatus. Maleimide was a product of *Merck*, bromine was a product of *Alfa Aesar*.

6.14. Hydrogel Chemically Disassembled

A 200 μL volume hydrogel based on the assembly of peptide Phe-^{D}Cys-Phe was prepared in a glass vial. After 1 hour of self-assembly, 5 μL of a stock solution of Br-maleimide in DMF was added to the hydrogel to get 1 equivalent of Br-maleimide relative to peptide. Disassembly was monitored by visual observation.

6.15. Ellman's Reagent Assays

To quantify peptide sulfhydryl groups present in PBS solution, 7 standard solutions of cysteine at fixed concentrations (0.0, 0.25, 0.50, 0.75, 1.00, 1.25, 1.50 mM) were prepared. 10 mL of these solutions were put into microwells of multiwell plate *Grainer 96 U* transparent and diluted with 100 μL of reaction buffer (PBS 0.1 M pH 7.7 containing 1 mM ethylenediaminetetraacetic acid - EDTA). 2 μL of a freshly prepared Ellman's reagent solution (4 mg/mL Ellman's reagent in reaction buffer) were added in each well and absorbance was measured at 412 nm by means of multiplate reader *Tecan Infinity pro 1000*. Experiment was repeated three times and average data were plotted to obtain the linear standard curve.

The same protocol was used to create a standard curve of peptide, using 7 standard solutions of Phe-^{D}Cys-Phe at fixed concentrations.

Ellman's reagent test was performed in hydrogel phase, adding 40 μL of Ellman's reagent solution freshly prepared to 200 μL of both 1 hour and 24 hours aged hydrogel.

6.16. Titration of Peptide Phe-^{D}Cys-Phe in Water

A 1 mM solution of peptide Phe-^{D}Cys-Phe in MilliQ water was titrated by addition of constant volumes of NaOH 50 mM until a pH value plateau was reached (pH 12). pH was measured by means of *SensION*$^{+}$ pHmeter equipped with *Crison 5028* micro-electrode.

6.17. Desulfurization Reaction

For the reaction in solution, 4.10 mg of TPPTS were dissolved in 0.750 mL of D_2O in a glass vial, and this solution was used to dissolve 2 mg of peptide. pH was adjusted by addition of NaOH 1M to reach the final value of pH 7.4. Sample was put in the middle of an *IBIDI μDish 35mm* low uncoated and irradiated on transilluminator *Hoefer UV-20-230v Macrovue-UV-20*. LC-MS samples were prepared by diluting samples at different time points 1:1 with a mixture H_2O/MeCN containing 0.01% formic acid. NMR and LC-MS analyses were carried out as described above.

For reaction in hydrogel phase, 750 μL of hydrogel containing 1 equivalent of TPPTS relative to peptide were directly prepared, as described above, in an *IBIDI μDish 35mm* low uncoated and after 1 hour of self-assembly it was irradiated on transilluminator *Hoefer UV-20-230v Macrovue-UV-20* for 3 hours. A black printed acetate sheet with triangle shape was put between samples and lamp as photomask to get spatial resolved disassembly.

6.18. Raman Spectroscopy

Dried samples prepared as described above were analysed by Raman spectroscopy with an *Invia Renishaw microspectrometer* (50) equipped with a 785 nm diode laser. Laser was focused on the sample using the 50× microscope, and the power was set at 0.18 mW. Analysed range was 4000-100 cm^{-1}. At least 20 accumulations were carried out on three different areas of the samples with an acquisition exposure time of 10s for each accumulation.

Appendix

A.1. Tripeptides Spectroscopy Data

a. ^{D}Met-Phe-Phe

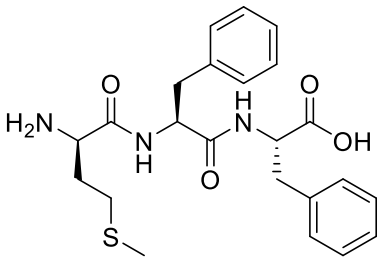

Chemical Formula: $C_{23}H_{29}N_3O_4S$
Exact Mass: 443,19
Molecular Weight: 443,56

Figure A.1.1. Chemical structure of ^{D}Met-Phe-Phe.

^{1}H-NMR (400 MHz, DMSO-*d_6*, TMS)

^{1}H-NMR (400 MHz, DMSO-d_6, TMS), δ (ppm): 8.64 (d, J = 9.0 Hz, 1H, NH), 8.54 (d, J = 7.7 Hz, 1H, NH), 7.30 – 7.16 (m, 10H, Ar), 4.71 (m, 1H, αCH), 4.44 (m, 1H, αCH), 3.66 (m, 1H, αCH), 3.14 – 3.06 (m, 2H, βCH_2), 2.94 (dd, J = 13.9, 9.0 Hz, 1H, βCH_2), 2.68 (dd, J = 13.8, 11.1 Hz, 1H, βCH_2), 2.08 (m, 1H, βCH_2), 2.01 – 1.90 (m, 4H, 1 x βCH_2 , 3 x δCH_3), 1.64 (m, 1H, γCH_2), 1.59 – 1.49 (m, 1H, γCH_2).

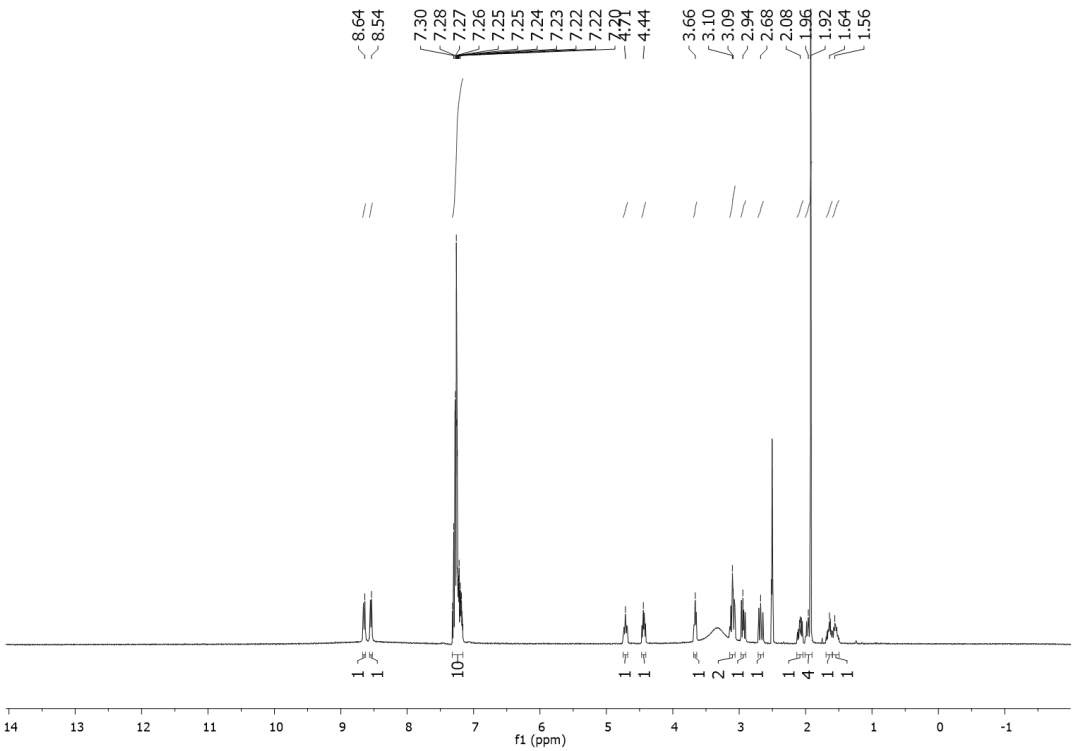

Figure A.1.2. ^{1}H-NMR spectrum of ^{D}Met-Phe-Phe.

^{13}C-NMR (100MHz, DMSO-d_6, TMS)

^{13}C-NMR (100 MHz, DMSO-d_6, TMS), δ (ppm): 172.78, 171.11, 167.79 (3 x CO); 137.56, 137.37, 129.20, 129.14, 128.31, 128.01, 126.55, 126.48 (Ar); 53.80, 53.41, 51.58 (3 x αC); 38.18, 36.59, 30.97 (3 x βC); 27.69 (γC); 14.30 (δC).

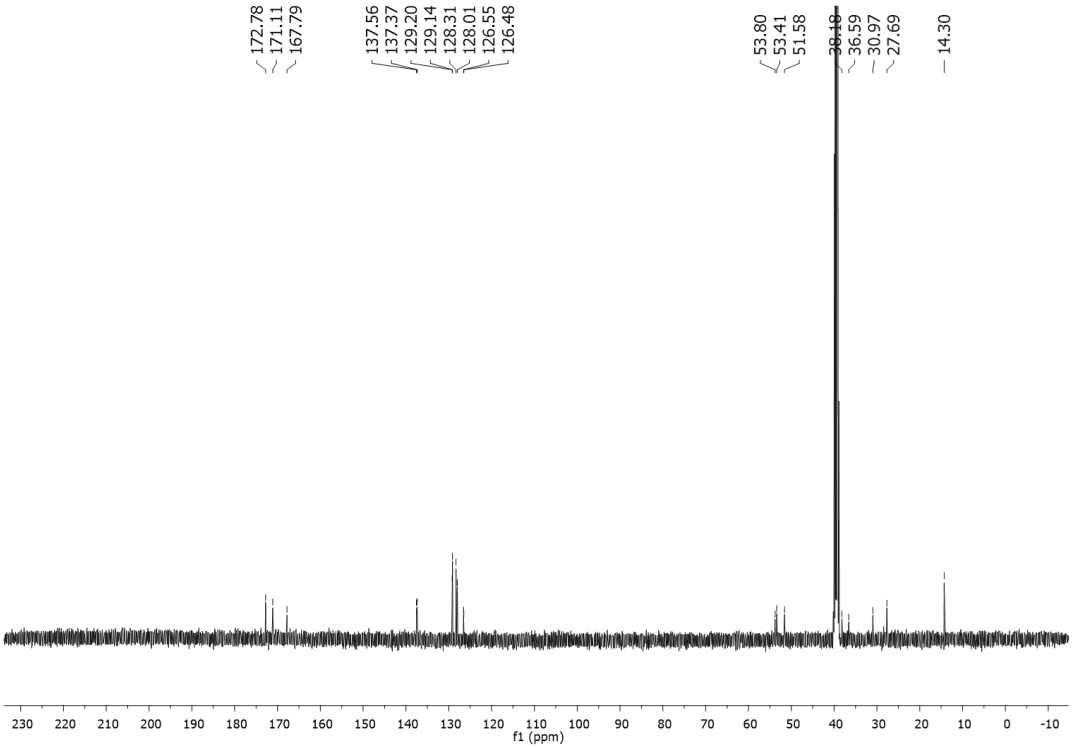

Figure A.1.3. ^{13}C-NMR spectrum of ^{D}Met-Phe-Phe.

MS (ESI)

$C_{23}H_{29}N_3O_4S$ requires 443.2: m/z 443.7 $[M+H]^+$, m/z 886.5 $[2M+H]^+$; m/z 441.7 $[M-H]^-$, m/z 886.5 $[2M-H]^-$.

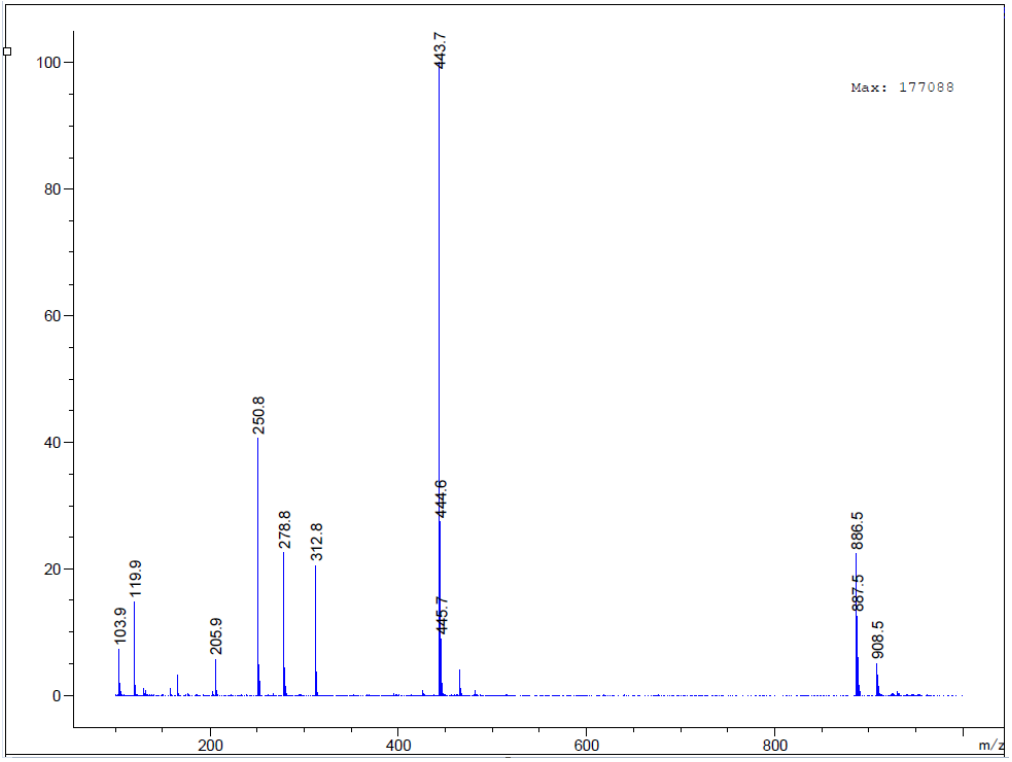

Figure A.1.4. ESI-MS spectrum of ^{D}Met-Phe-Phe in positive mode.

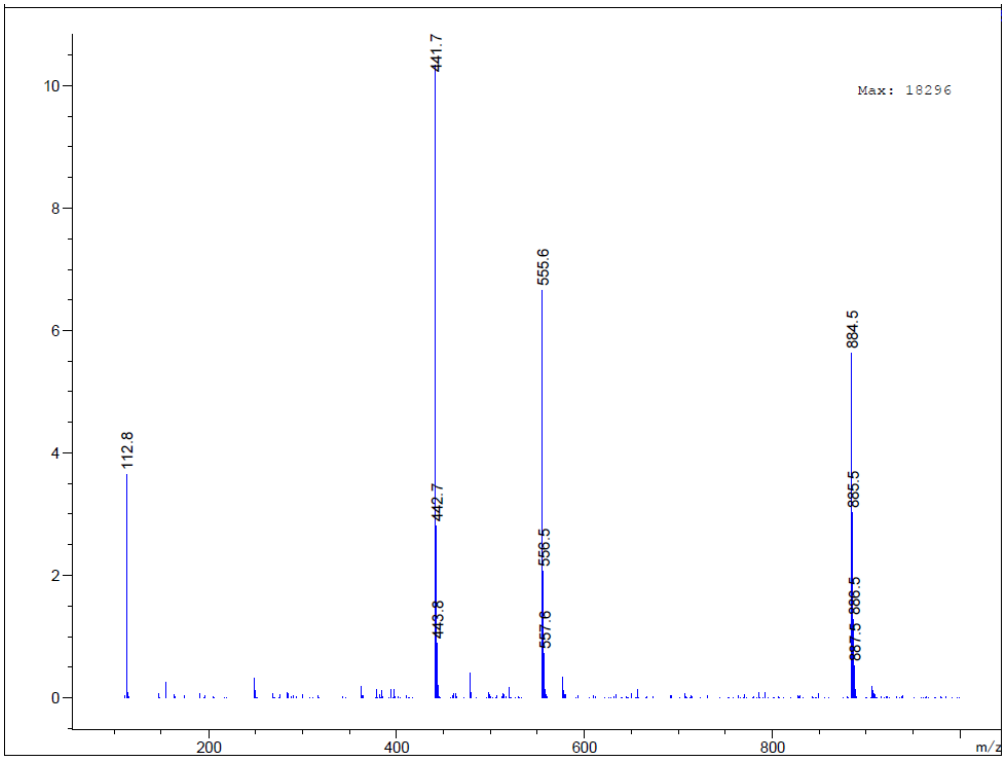

Figure A.1.5. ESI-MS spectrum of ^{D}Met-Phe-Phe in negative mode.

b. Phe-^{D}Met-Phe

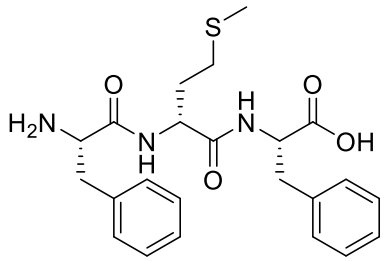

Chemical Formula: $C_{23}H_{29}N_3O_4S$
Exact Mass: 443,19
Molecular Weight: 443,56

Figure A.1.6. Chemical structure of Phe-^{D}Met-Phe.

^{1}H-NMR (400 MHz, DMSO-*d_6*, TMS)

^{1}H-NMR (400 MHz, DMSO-*d_6*, TMS), δ (ppm): 8.53 (d, J = 8.4 Hz, 2H, 2 x NH), 7.31 – 7.21 (m, 10H, Ar), 4.48 (m, 1H, αCH), 4.39 (m, 1H, αCH), 4.10 (m, 1H, αCH), 3.10 (m, 1H, βCH_2), 2.98 - 2.95 (m, 2H, βCH_2), 2.81 (m, 1H, βCH_2), 1.87 (s, 3H, 3 x δCH_3), 1.84 - 1.80 (m, 2H, βCH_2), 1.45 – 1.33 (m, 2H, 1H, γCH_2).

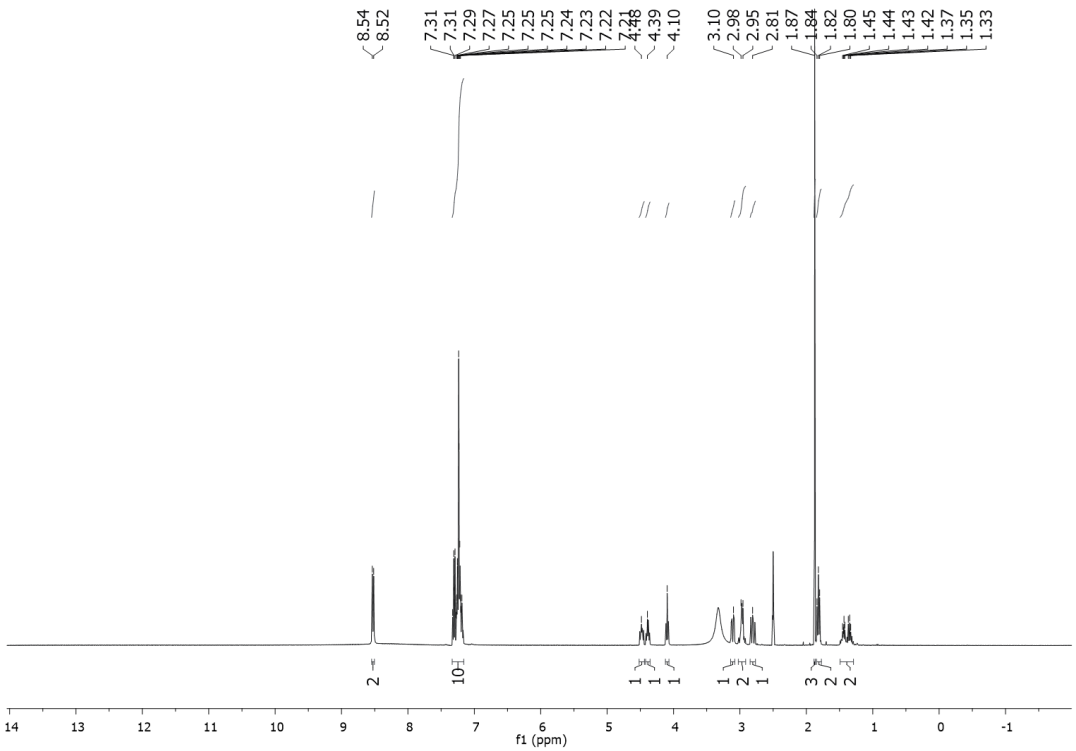

Figure A.1.7. ^{1}H-NMR spectrum of Phe-^{D}Met-Phe.

^{13}C-NMR (100MHz, DMSO-d_6, TMS)

^{13}C-NMR (100 MHz, DMSO-d_6, TMS), δ (ppm): 172.86, 170.09, 167.72 (3 x CO); 137.44, 134.85, 129.44, 129.10, 128.43, 128.10, 118.92, 115.85 (Ar); 53.22, 53.12, 51.54 (3 x αC); 32.33, 32.28, 28.70 (3 x βC); 22.87 (γC); 14.35 (δC).

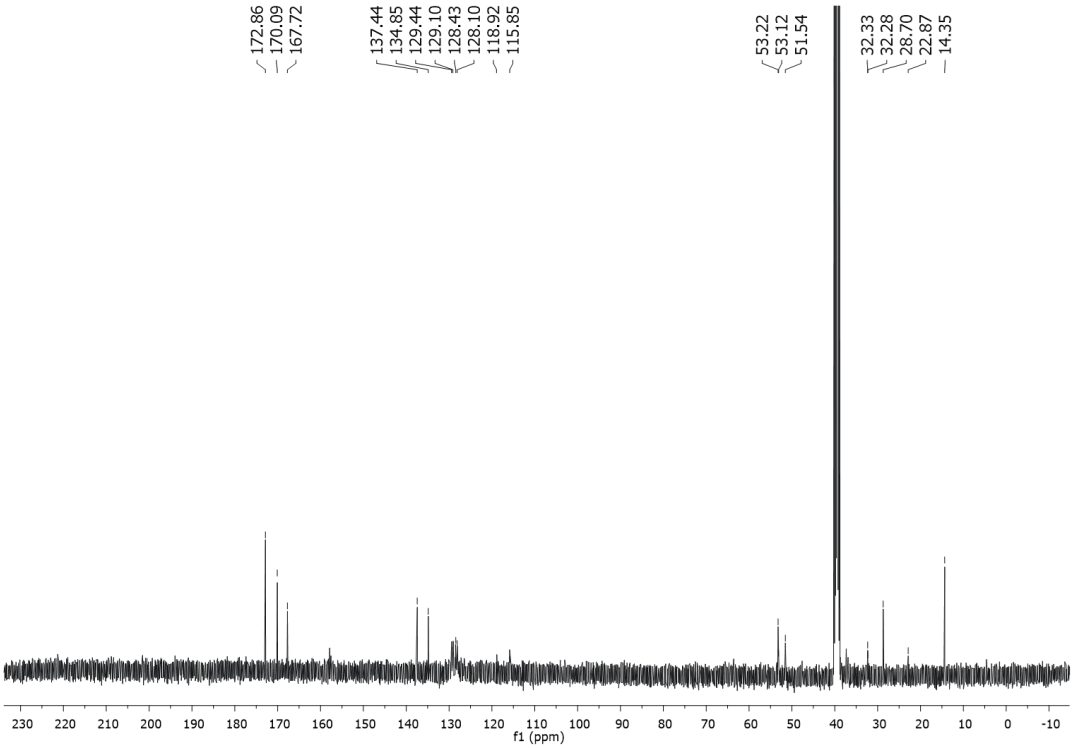

Figure A.1.8. ^{13}C-NMR spectrum of Phe-^{D}Met-Phe.

MS (ESI)

$C_{23}H_{29}N_3O_4S$ requires 443.2: m/z 444.2 $[M+H]^+$, m/z 887.4 $[2M+H]^+$; m/z 442.2 $[M-H]^-$, m/z 885.4 $[2M-H]^-$.

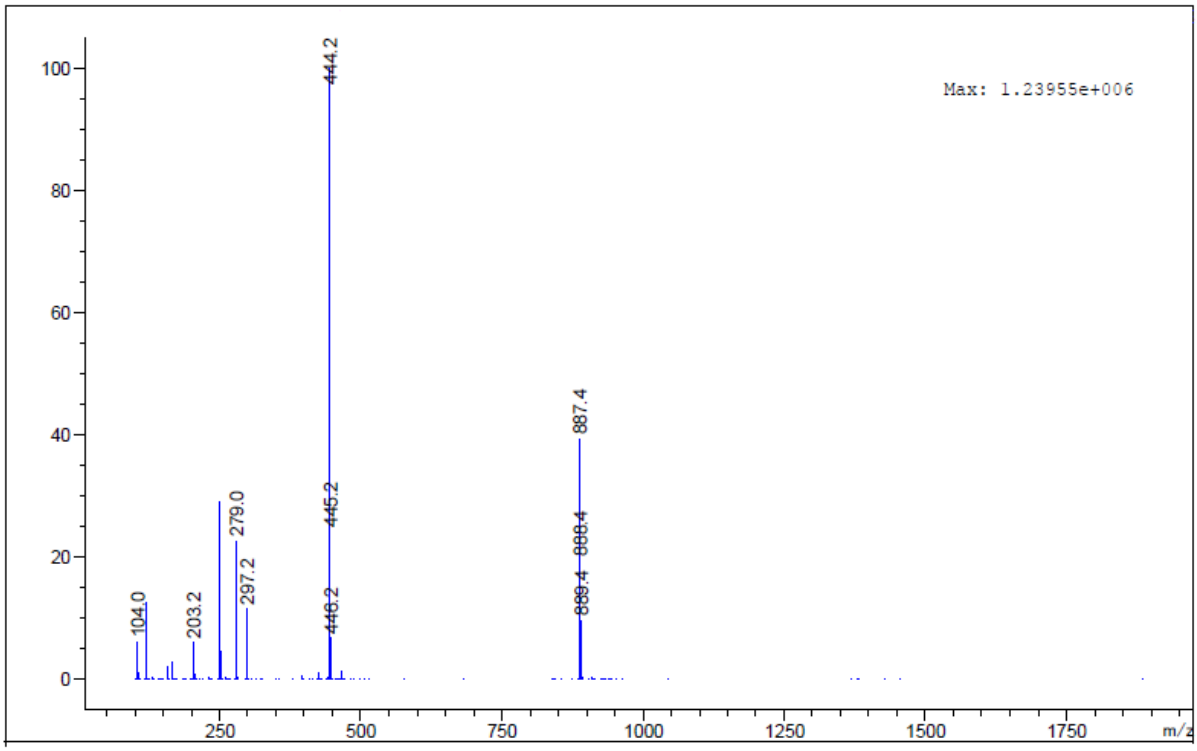

Figure A.1.9. ESI-MS spectrum of Phe-^{D}Met-Phe in positive mode.

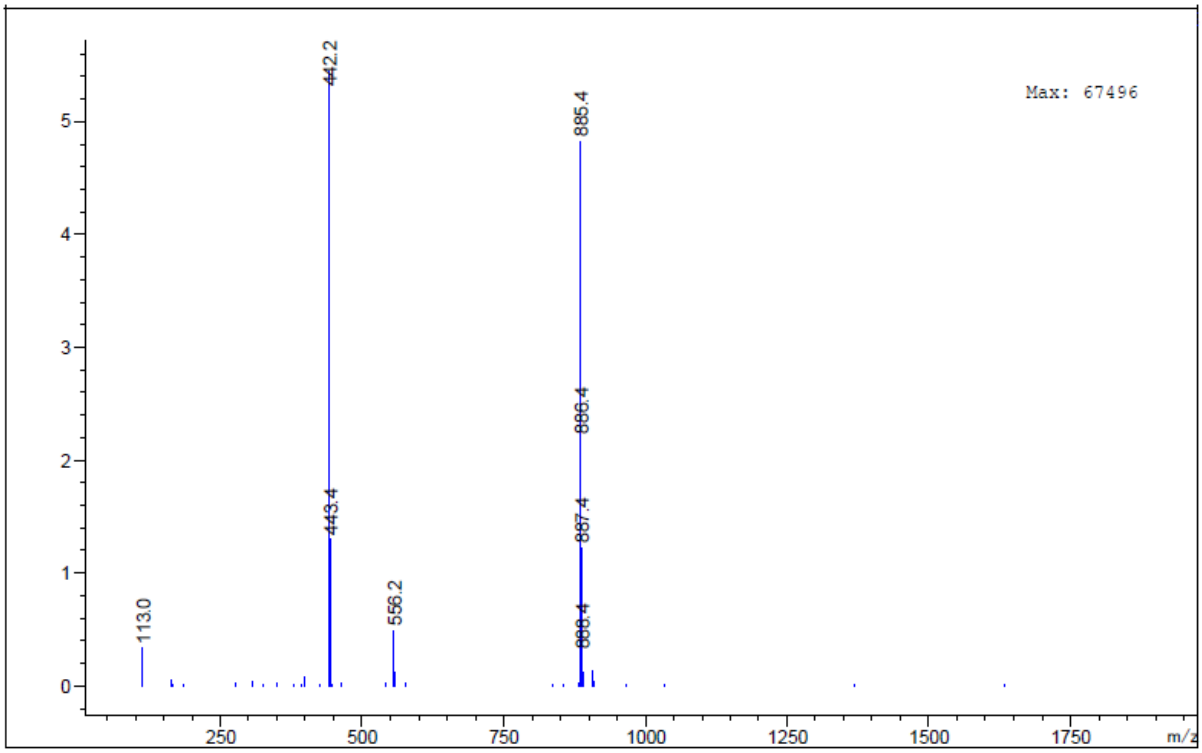

Figure A.1.10. ESI-MS spectrum of Phe-^{D}Met-Phe in negative mode.

c. ^{D}Phe-Phe-Met

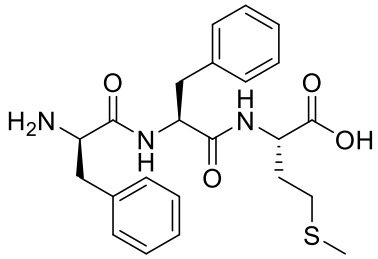

Chemical Formula: $C_{23}H_{29}N_3O_4S$
Exact Mass: 443,19
Molecular Weight: 443,56

Figure A.1.11. Chemical structure of peptide ^{D}Phe-Phe-Met.

^{1}H-NMR (400 MHz, DMSO-*d*$_6$, TMS)

^{1}H-NMR (400 MHz, dmso-*d*$_6$) δ (ppm): 8.89 (d, J = 8.7 Hz, 1H, NH), 8.59 (d, J = 7.8 Hz, 1H, NH), 7.33 – 7.26 (m, 4H, Ar), 7.22 – 7.20 (m, 4H, Ar), 6.92-6.90 (m, 2H, Ar), 4.72 (m, 1H, αCH), 4.34 (m, 1H, αCH), 4.00 (m, 1H, αCH), 3.07 (m, 1H, βCH_2), 2.78 – 2.72 (m, 3H, βCH_2), 2.53 (m, 1H, βCH_2), 2.47 (m, 1H, βCH_2), 2.06 – 1.97 (m, 4H, γCH_2, δCH_3), 1.89 (m, 1H, γCH_2).

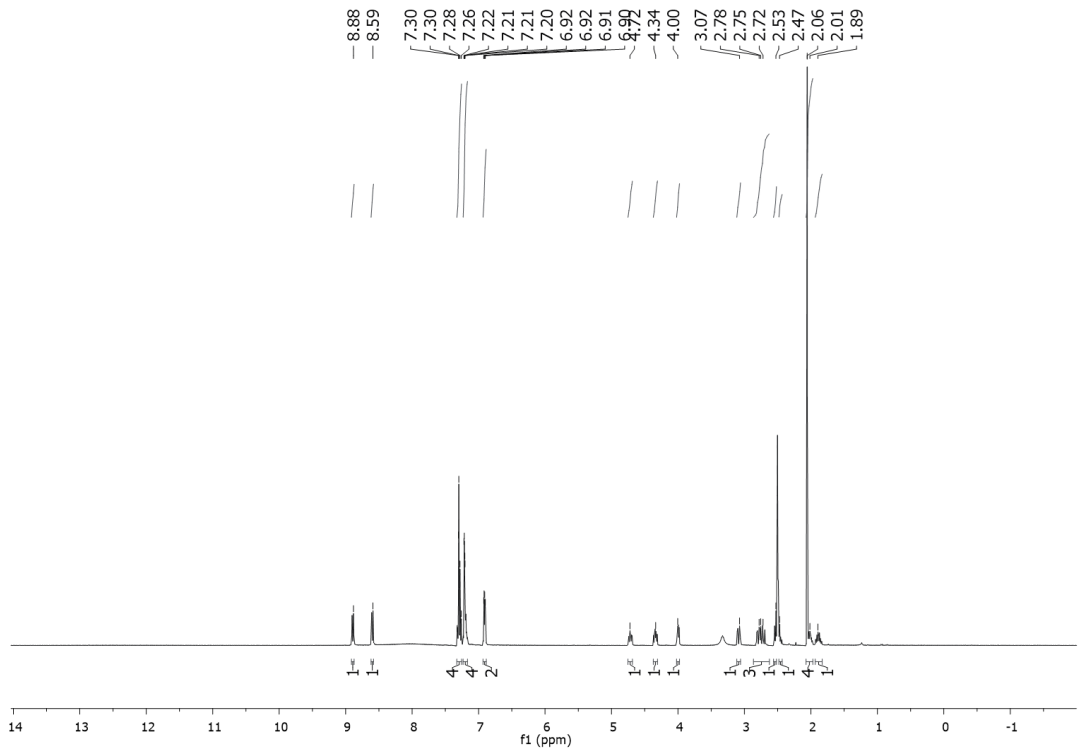

Figure A.1.12. ^{1}H-NMR spectrum of ^{D}Phe-Phe-Met.

^{13}C-NMR (100MHz, DMSO-d_6, TMS)

^{13}C-NMR (100 MHz, DMSO-d_6, TMS), δ (ppm): 173.03, 171.05, 167.84 (3 x CO); 137.42, 134.64, 129.45, 129.40, 128.40, 128.11, 127.02, 126.55 (Ar); 53.78, 53.27, 51.05 (3 x αC); 38.16, 36.98, 30.64 (3 x βC), 29.65 (γC), 14.51 (δC).

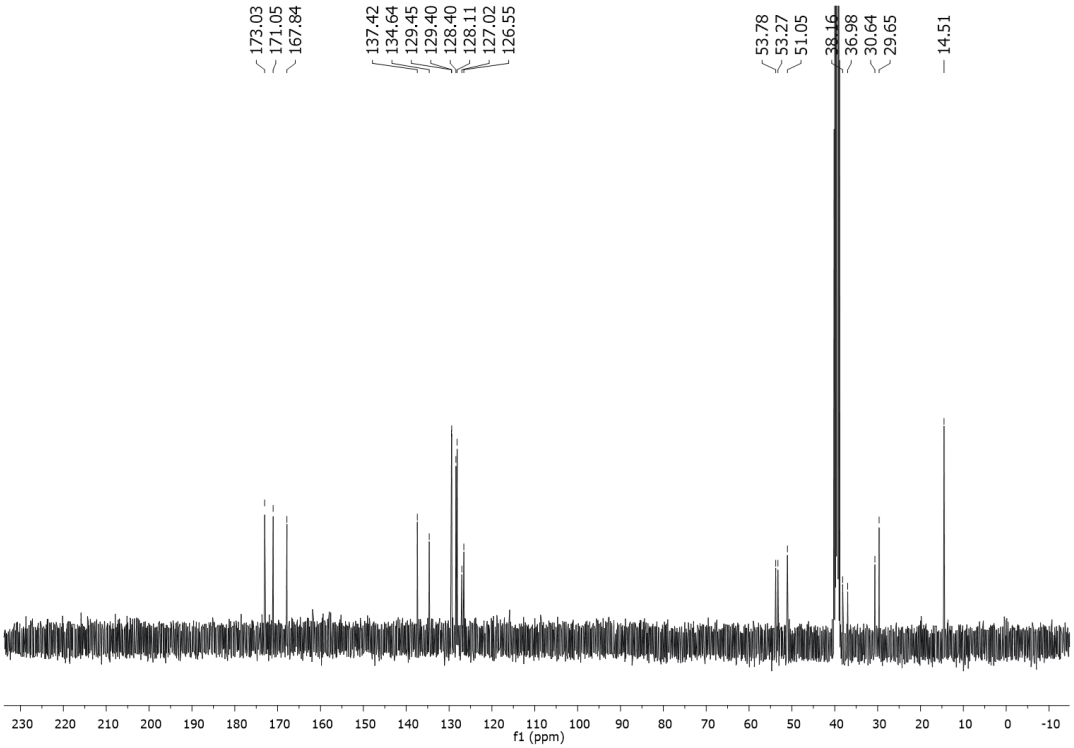

Figure A.1.13. ^{13}C-NMR spectrum of ^{D}Phe-Phe-Met.

MS (ESI)

$C_{23}H_{29}N_3O_4S$ requires 443.2: m/z 443.7 $[M+H]^+$, m/z 886.5 $[2M+H]^+$; m/z 442.2 $[M-H]^-$, m/z 884.5 $[2M-H]^-$.

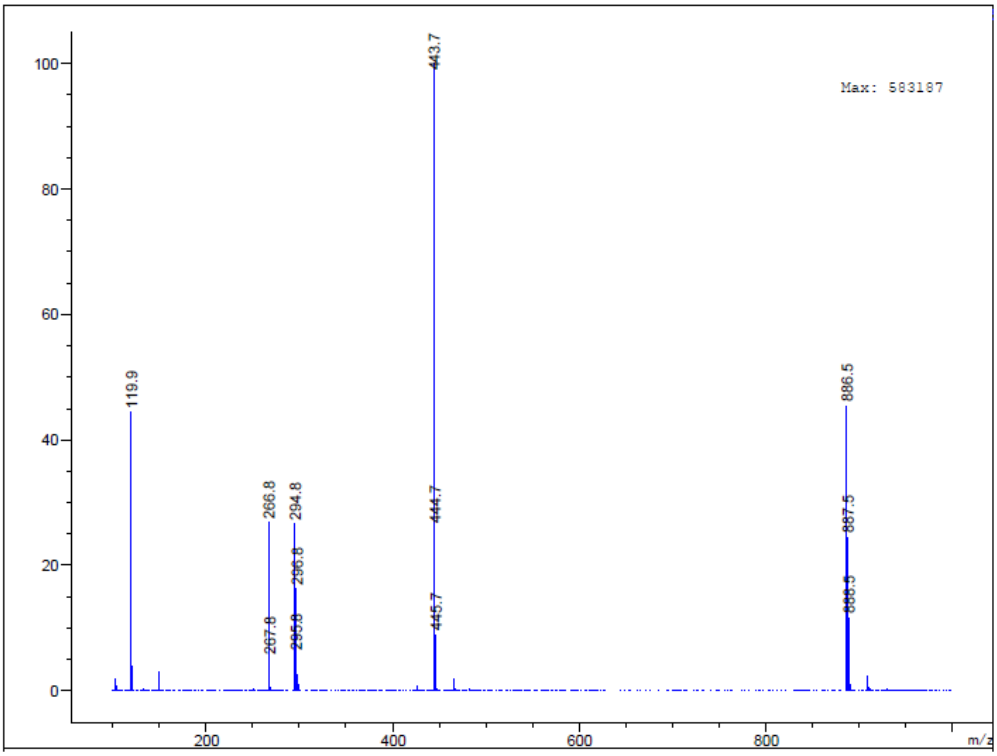

Figure A.1.14. ESI-MS spectrum of ^{D}Phe-Phe-Met in positive mode.

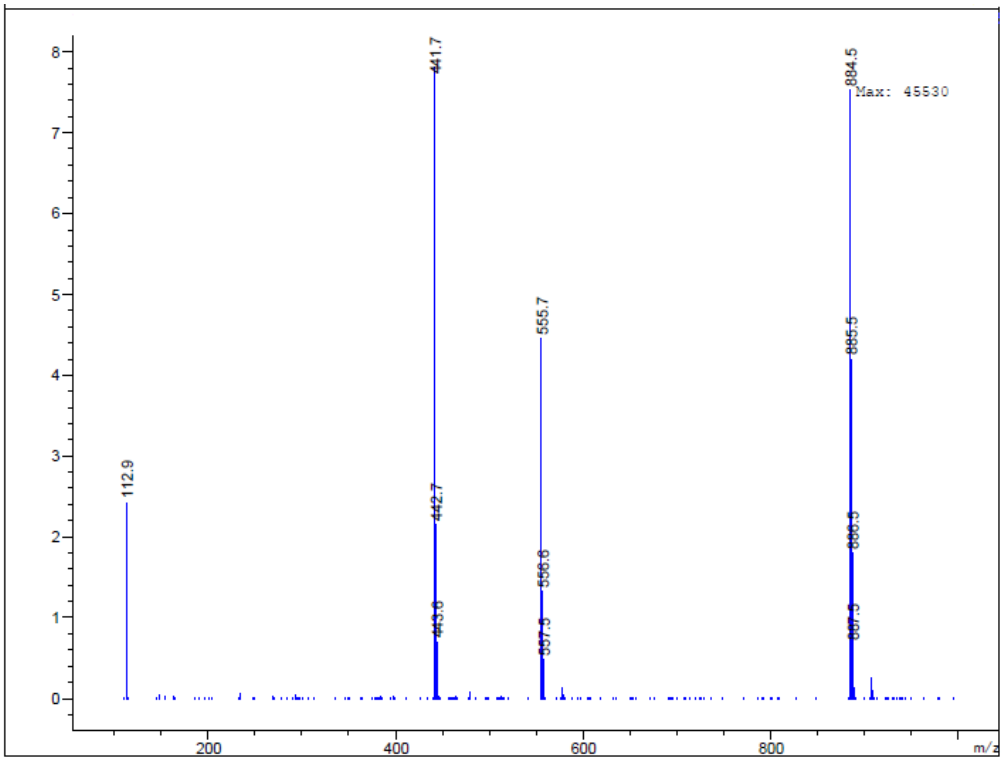

Figure A.1.15. ESI-MS spectrum of ^{D}Phe-Phe-Met in negative mode.

d. Phe-Cys-Phe

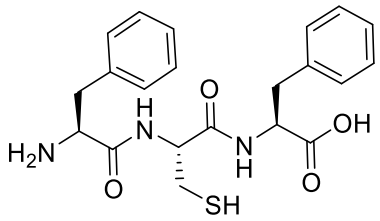

Chemical Formula: $C_{21}H_{25}N_3O_4S$
Exact Mass: 415,16
Molecular Weight: 415,51

Figure A.1.16. Chemical structure of peptide Phe-Cys-Phe.

^{1}H-NMR (400 MHz, DMSO-*d_6*, TMS)

^{1}H-NMR (400 MHz, DMSO-*d_6*, TMS), δ (ppm): 8.70 (s, 1H, NH), 8.46 (s, 1H, NH), 7.25 – 7.15 (m, 10H, Ar), 4.51 – 4.41 (m, 2H, 2 x αCH), 4.07 (m, 1H, αCH), 3.10 – 2.99 (m, 2H, βCH_2), 2.93 – 2.82 (m, 2H, βCH_2), 2.79 – 2.65 (m, 2H, βCH_2), 2.28 (t, J= 7.76 Hz, 1H, SH).

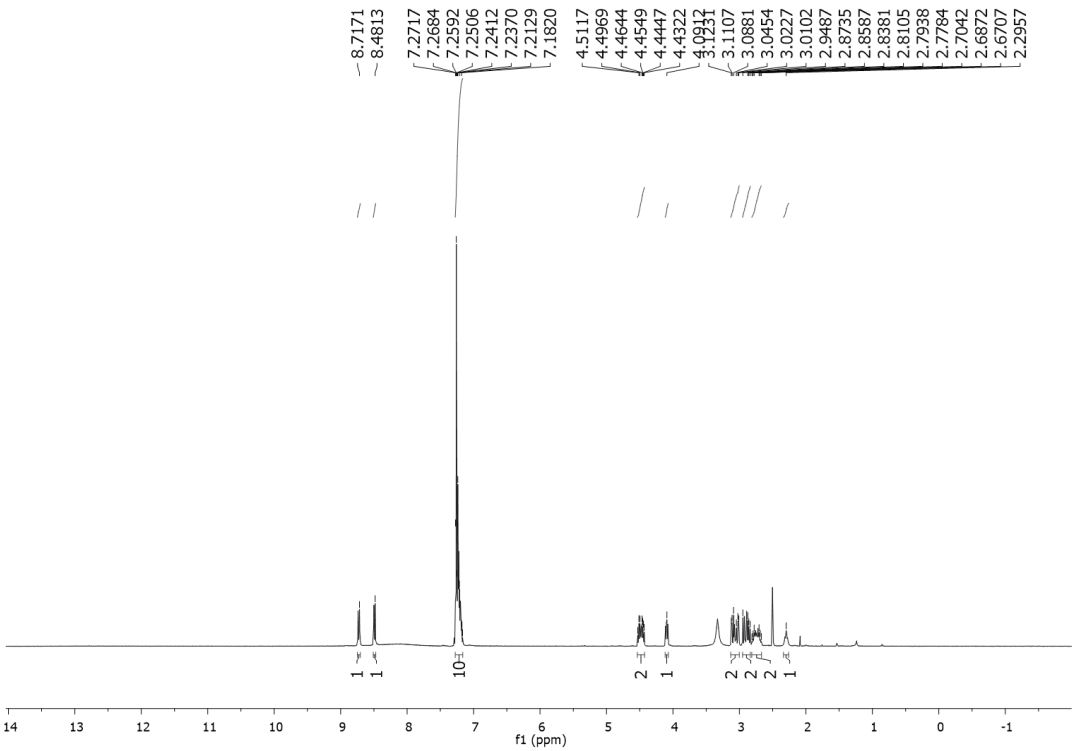

Figure A.1.17. ^{1}H-NMR spectrum of Phe-Cys-Phe.

^{13}C-NMR (100MHz, DMSO-d_6, TMS)

^{13}C-NMR (100 MHz, DMSO-d_6, TMS), δ (ppm): 172.65, 169.03, 168.14 (3 x CO); 137.43, 134.79, 129.46, 129.09, 128.49, 128.19, 127.10, 126.45 (Ar); 54.78, 53.67, 53.27 (3 x αC); 37.05, 36.46, 26.55 (3 x βC).

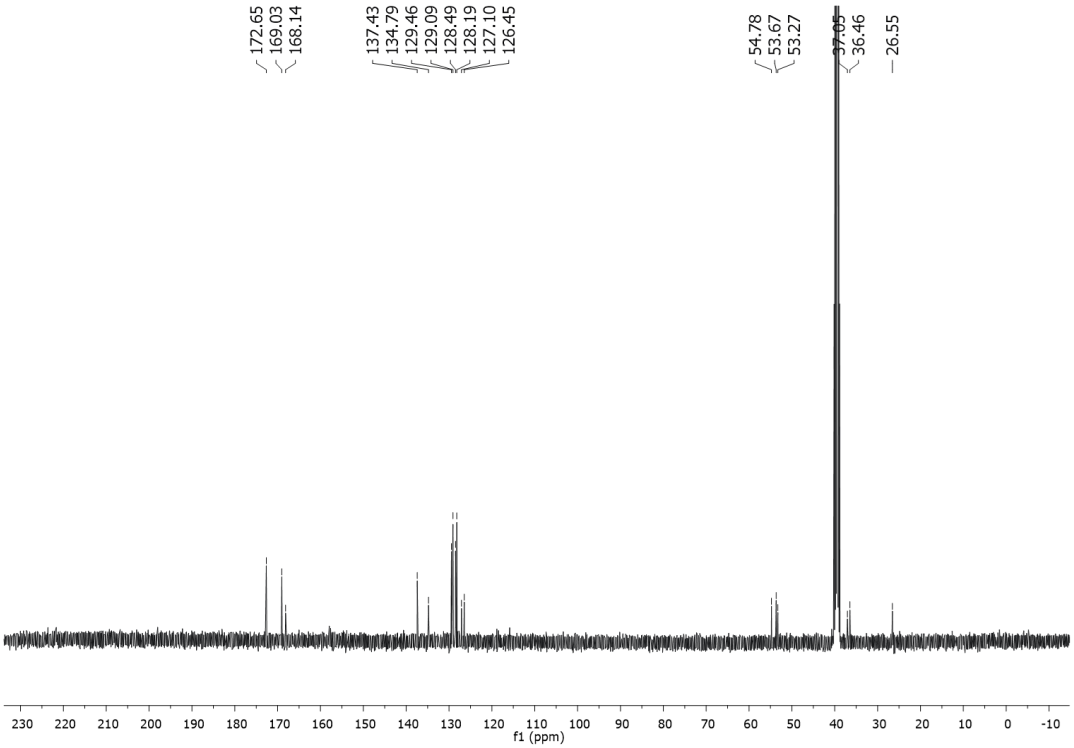

Figure A.1.18. ^{13}C-NMR spectrum of Phe-Cys-Phe.

MS (ESI)

$C_{21}H_{25}N_3O_4S$ requires 415.2: m/z 416.1 $[M+H]^+$, m/z 831.3 $[2M+H]^+$; m/z 414.1 $[M-H]^-$, m/z 829.2 $[2M-H]^-$.

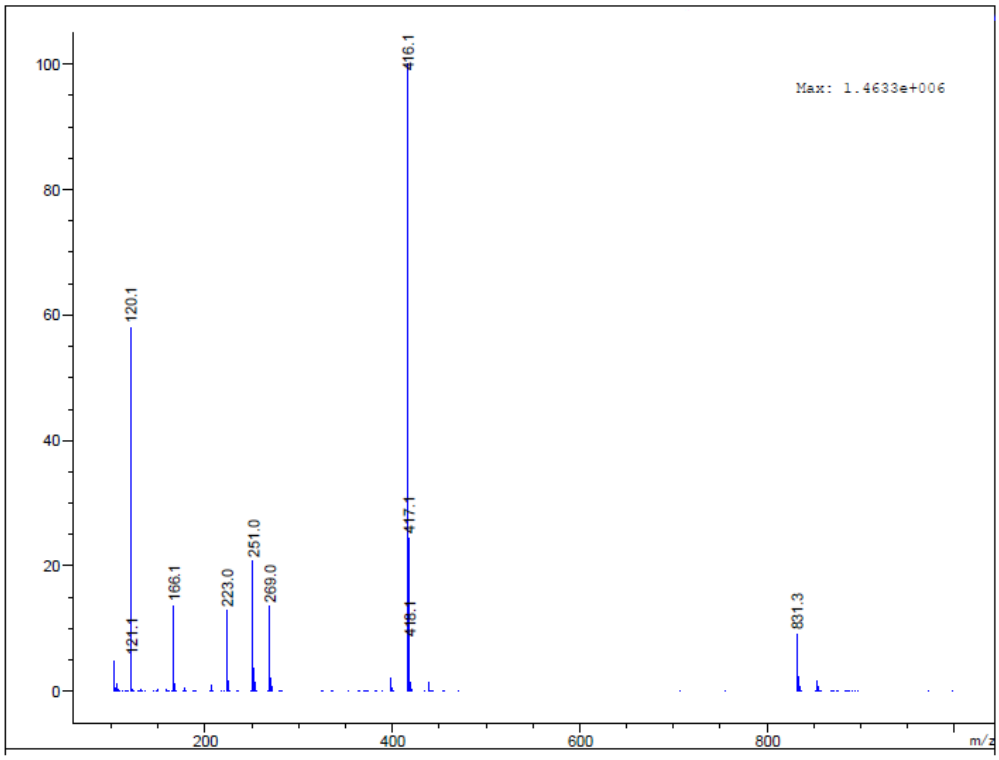

Figure A.1.19. ESI-MS spectrum of Phe-Cys-Phe in positive mode.

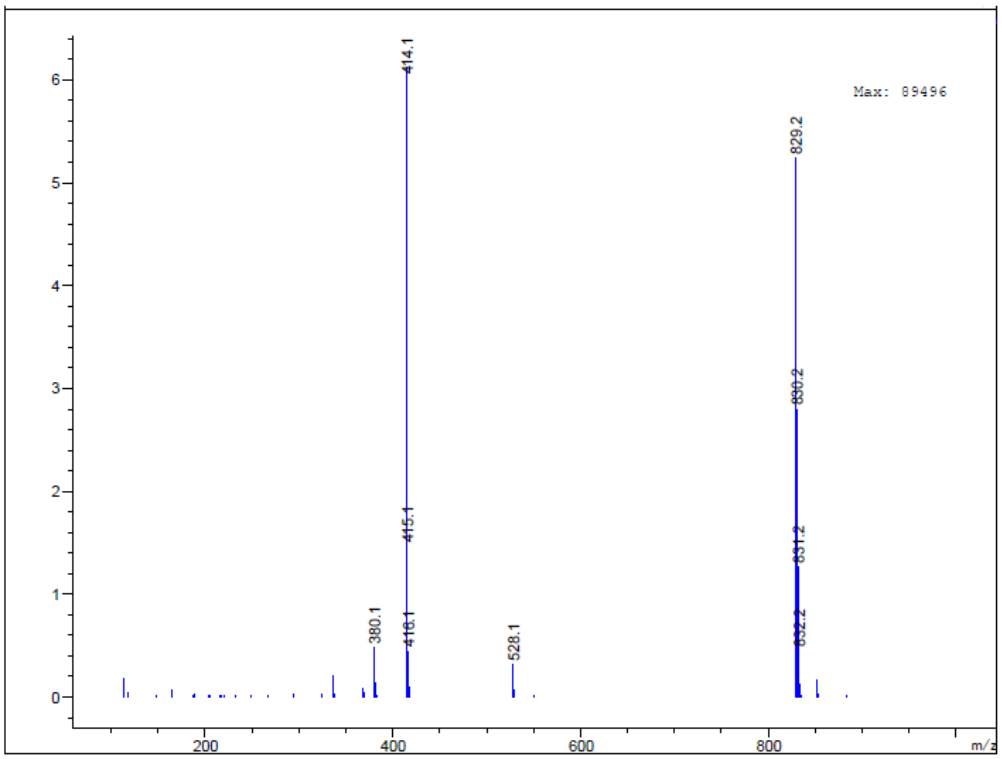

Figure A.1.20. ESI-MS spectrum of Phe-Cys-Phe in negative mode.

e. ^{D}Phe-Cys-Phe

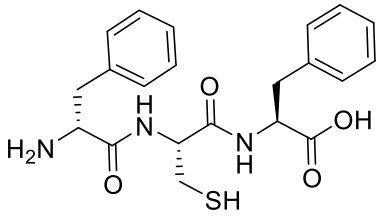

Chemical Formula: $C_{21}H_{25}N_3O_4S$
Exact Mass: 415,16
Molecular Weight: 415,51

Figure A.1.21. Chemical structure of peptide ^{D}Phe-Cys-Phe.

^{1}H-NMR (400 MHz, DMSO-*d_6*, TMS)

^{1}H-NMR (400 MHz, DMSO-d_6, TMS), δ (ppm): 12.85 (s, 1H, COOH), 8.66 (s, 1H, NH), 8.48 (s, 1H, NH), 8.12 (s, 3H, NH_3^+), 7.32 – 7.16 (m, 10H, Ar), 4.47 (s, 1H, αCH), 4.39 (s, 1H, αCH), 4.13 (s, 1H, αCH), 3.08 – 3.03 (m, 2H, βCH_2), 2.96 - 2.83 (m, 8.6 Hz, 2H, βCH_2), 2.59 – 2.55 (m, 2H, βCH_2), 1.93 (t, J= 8.64 Hz, 1H, SH).

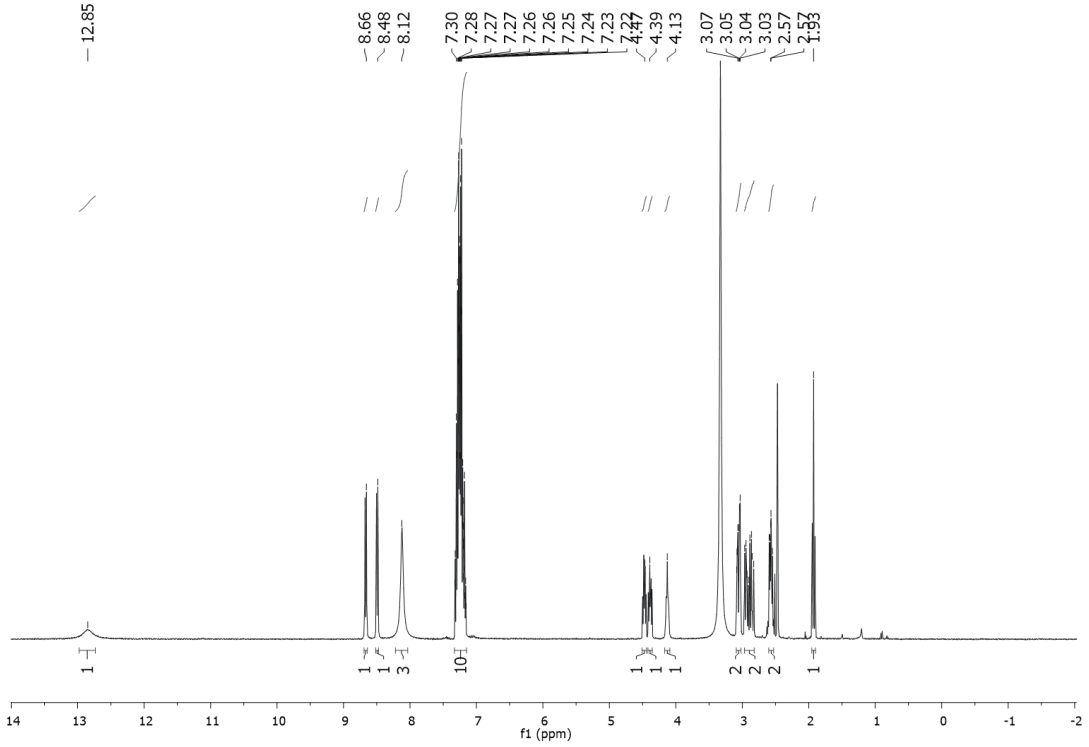

Figure A.1.22. ^{1}H-NMR spectrum of ^{D}Phe-Cys-Phe.

^{13}C-NMR (100MHz, DMSO-*d_6*, TMS)

^{13}C-NMR (100 MHz, DMSO-*d_6*, TMS), δ (ppm): 172.68, 169.16, 167.95 (3 x CO); 137.47, 134.82, 129.59, 129.07, 128.54, 128.27, 127.20, 126.52 (Ar), 54.27, 53.81, 53.15 (3 x αC); 37.32, 36.41, 26.88 (3 x βC).

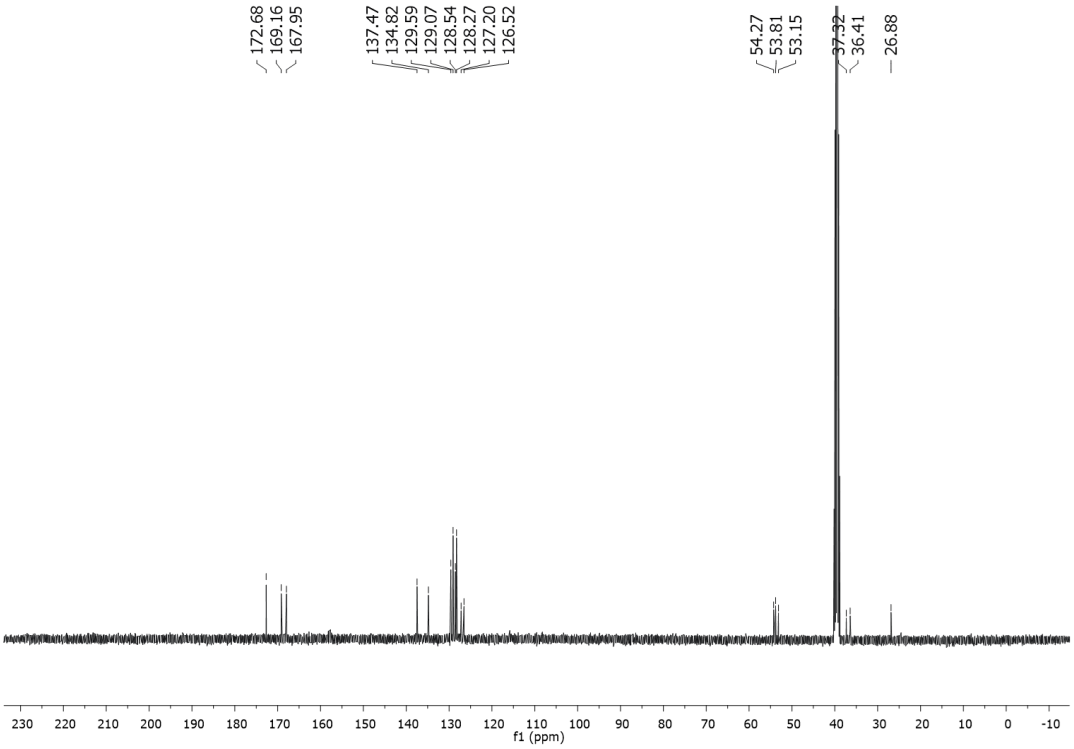

Figure A.1.23. ^{13}C-NMR spectrum of ^{D}Phe-Cys-Phe.

MS (ESI)

$C_{21}H_{25}N_3O_4S$ requires 415.2: m/z 416.1 $[M+H]^+$, m/z 831.3 $[2M+H]^+$; m/z 414.1 $[M-H]^-$, m/z 829.2 $[2M-H]^-$.

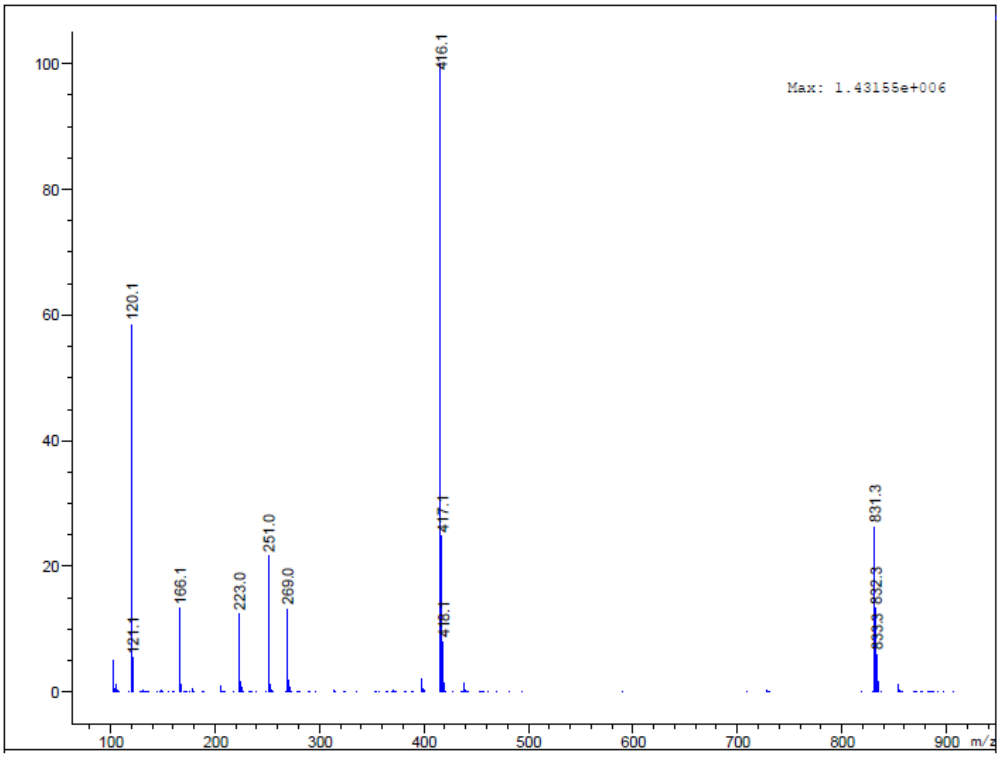

Figure A.1.24. ESI-MS spectrum of ^{D}Phe-Cys-Phe in positive mode.

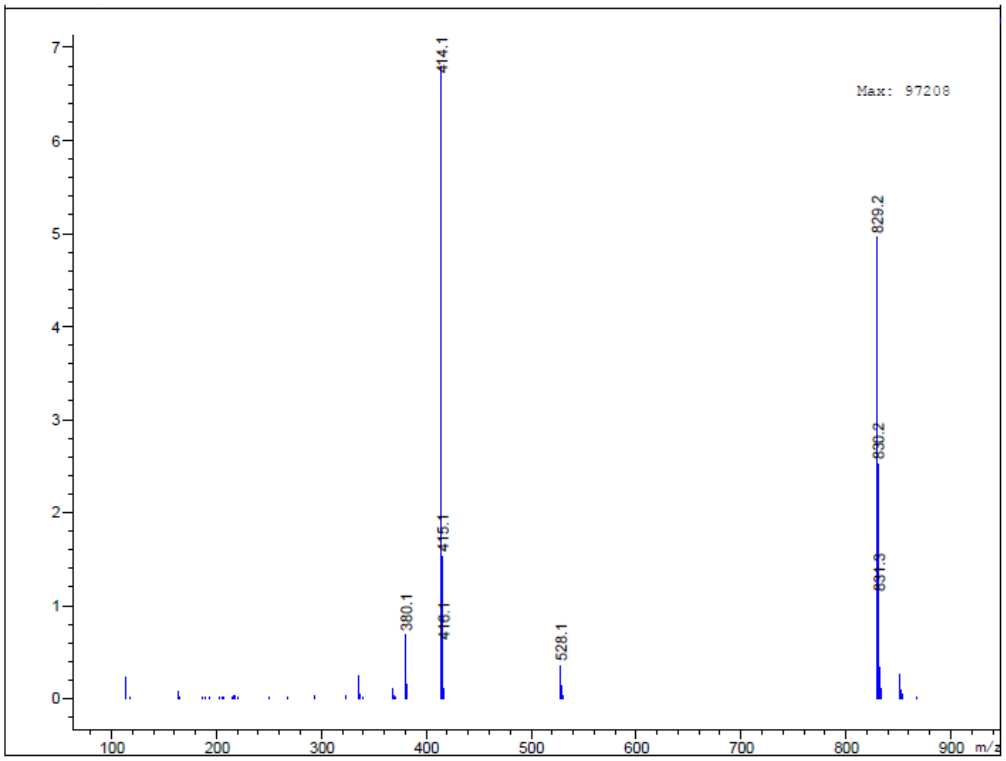

Figure A.1.25. ESI-MS spectrum of ^{D}Phe-Cys-Phe in negative mode.

f. Phe-^{D}Cys-Phe

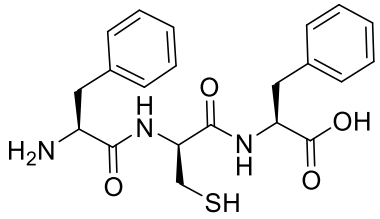

Chemical Formula: $C_{21}H_{25}N_3O_4S$
Exact Mass: 415,16
Molecular Weight: 415,51

Figure A.1.26. Chemical structure of peptide Phe-^{D}Cys-Phe.

^{1}H-NMR (400 MHz, DMSO-d_6, TMS)

^{1}H-NMR (400 MHz, DMSO-d_6, TMS), δ (ppm): 8.65 (s, 1H, NH), 8.55 (s, 1H, NH), 7.34 – 7.17 (m, 10H, Ar), 4.54 – 4.46 (m, 2H, 2 x αCH), 4.15 (m, 1H, αCH), 3.10 – 3.04 (m, 2H, βCH_2), 2.96 (m, 1H, βCH_2), 2.83 (m, 1H, βCH_2), 2.33 (m, 2H, βCH_2), 1.46 (t, J= 6.5 Hz, 1H, SH).

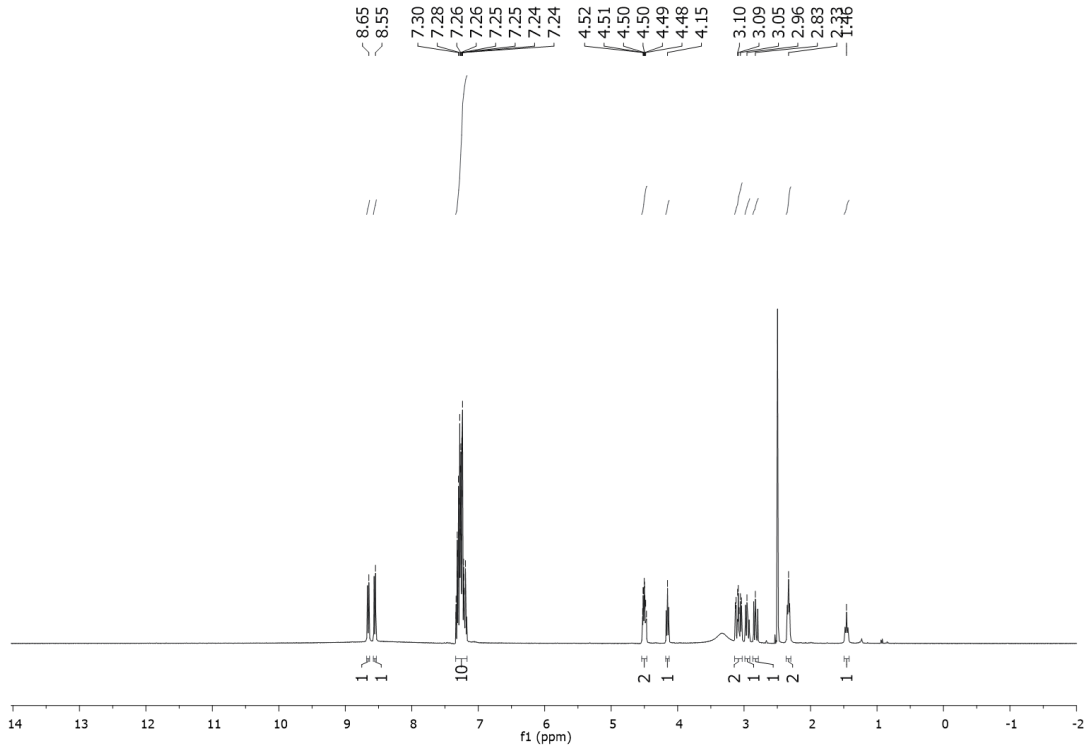

Figure A.1.27. ^{1}H-NMR spectrum of Phe-^{D}Cys-Phe.

^{13}C-NMR (100MHz, DMSO-d_6, TMS)

^{13}C-NMR (100 MHz, DMSO-d_6, TMS), δ (ppm): 172.70, 168.62, 168.06 (3 x CO); 137.37, 134.92, 129.57, 129.17, 128.51, 128.18, 127.16, 126.50 (Ar); 54.17, 53.32, 53.21 (3 x αC); 37.40, 36.96, 26.84 (3 x βC).

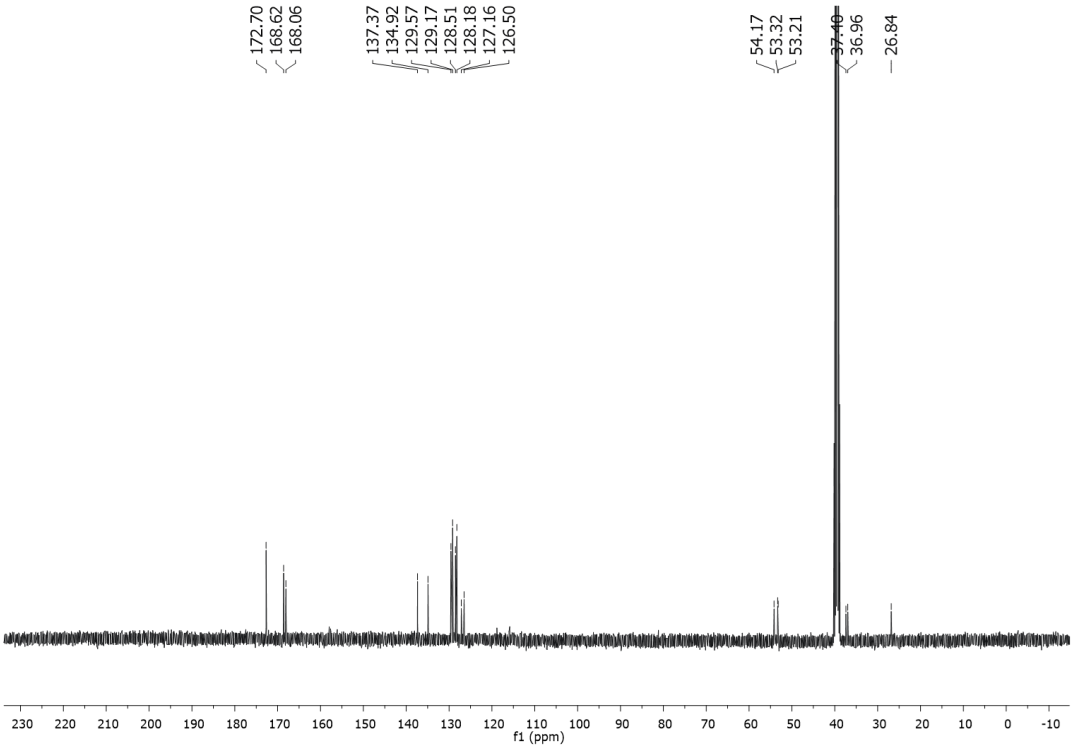

Figure A.1.28. ^{13}C-NMR spectrum of Phe-^{D}Cys-Phe.

MS (ESI)

$C_{21}H_{25}N_3O_4S$ requires 415.2: m/z 416.1 $[M+H]^+$, m/z 831.3 $[2M+H]^+$; m/z 414.1 $[M-H]^-$, m/z 829.3 $[2M-H]^-$.

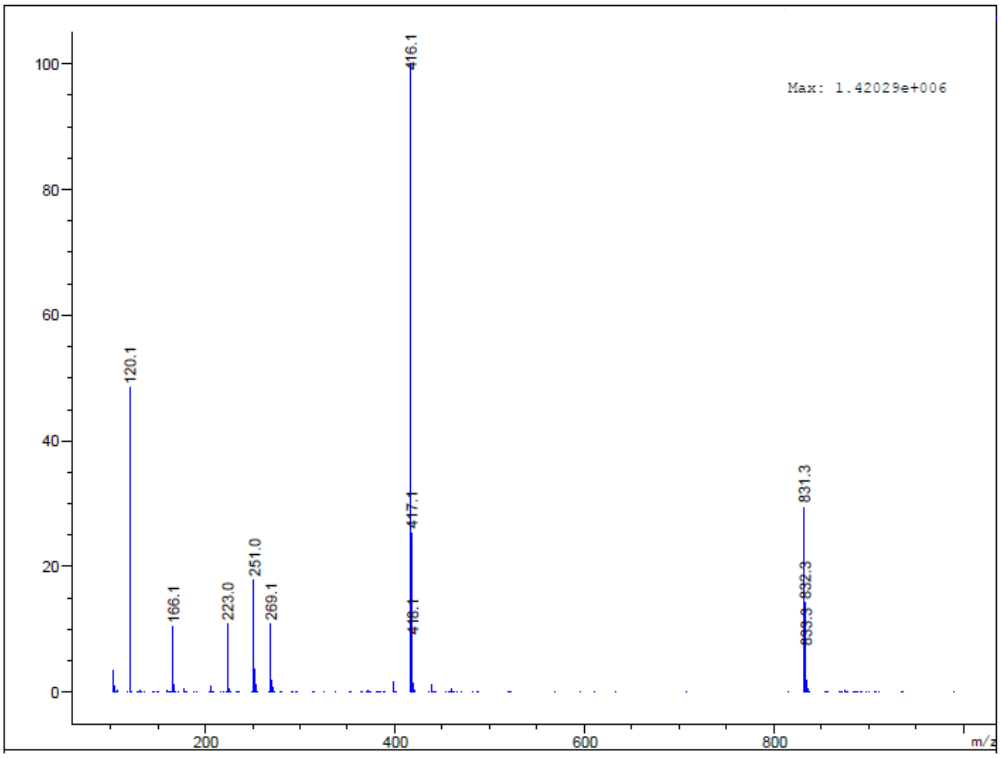

Figure A.1.29. ESI-MS spectrum of Phe-^{D}Cys-Phe in positive mode.

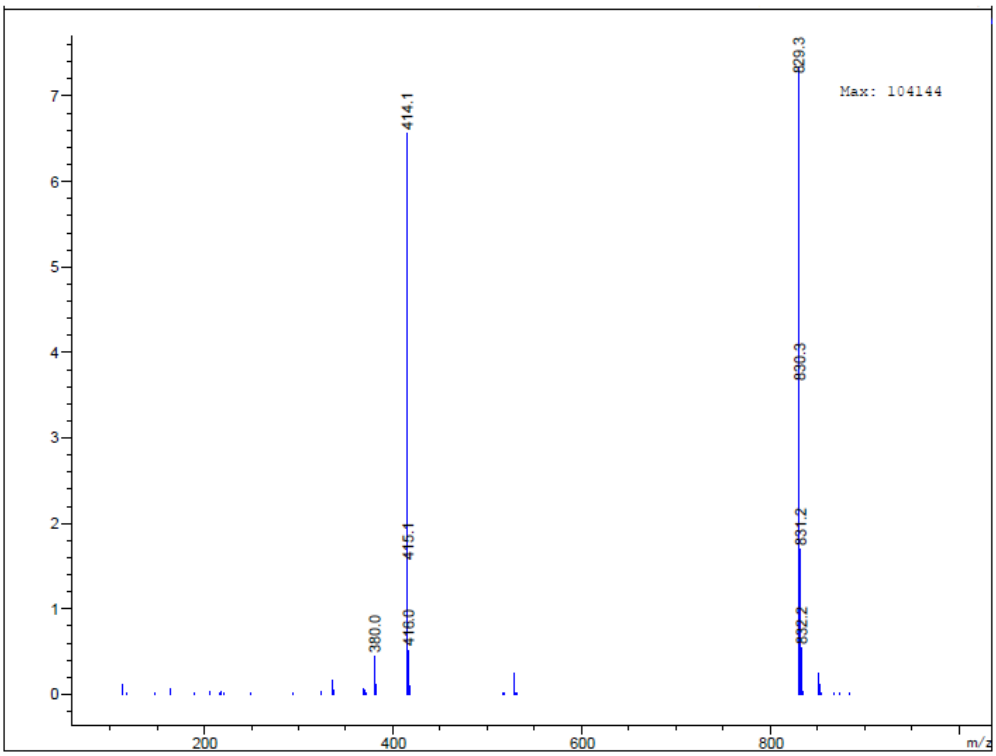

Figure A.1.30. ESI-MS spectrum of Phe-^{D}Cys-Phe in negative mode.

g. Phe-Cys-^{D}Phe

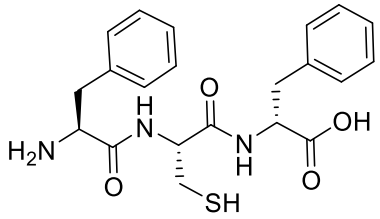

Chemical Formula: $C_{21}H_{25}N_3O_4S$
Exact Mass: 415,16
Molecular Weight: 415,51

Figure A.1.31. Chemical structure of peptide Phe-Cys-^{D}Phe.

^{1}H-NMR (400 MHz, DMSO-d_6, TMS)

^{1}H-NMR (400 MHz, DMSO-d_6, TMS), δ (ppm): 12.92 (s, 1H, COOH), 8.71 (s, 1H, NH), 8.53 (s, 1H, NH), 8.11 (s, 3H, NH_3^+), 7.31 – 7.16 (m, 10H, Ar), 4.53 – 4.47 (m, 2H, 2 x αCH), 4.10 (s, 1H, αCH), 3.14 – 3.04 (m, 2H, βCH_2), 2.90 - 2.82 (m, 2H, βCH_2), 2.54 - 2.46 (m, 2H, βCH_2), 1.87 (t, J= 8Hz, 1H, SH).

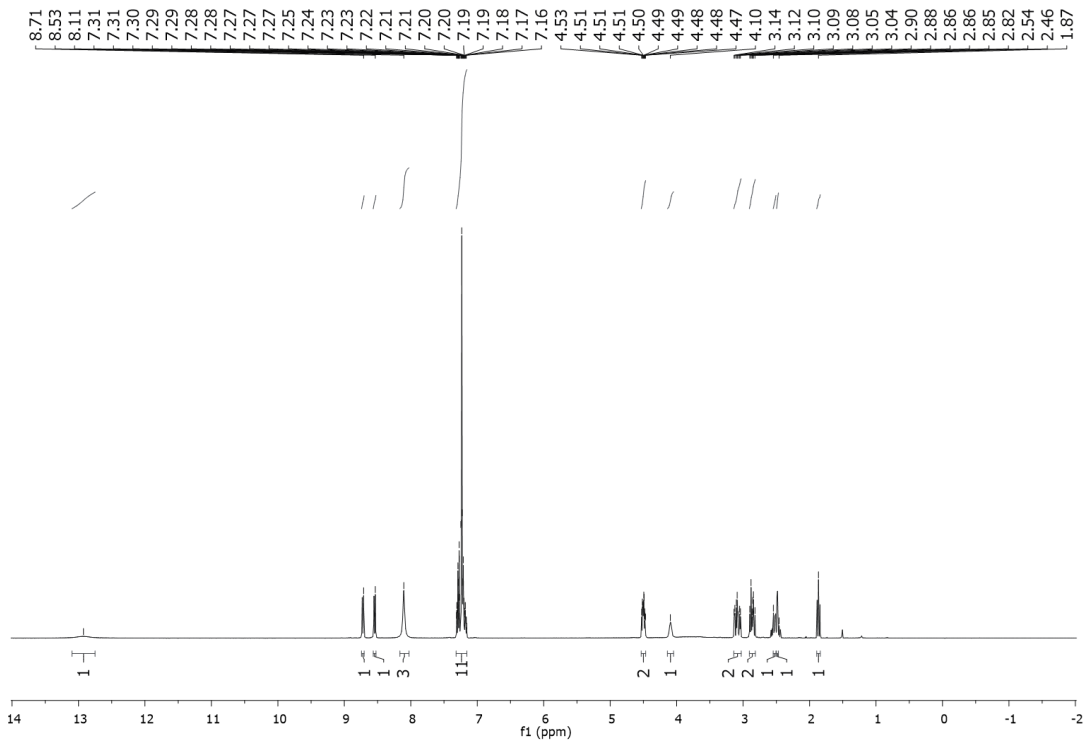

Figure A.1.32. ^{1}H-NMR spectrum of Phe-Cys-^{D}Phe.

^{13}C-NMR (100MHz, DMSO-*d*$_6$, TMS)

^{13}C-NMR (100 MHz, DMSO-*d*$_6$, TMS), δ (ppm): 172.69, 168.72, 167.99 (3 x CO); 137.42, 134.73, 129.52, 129.19, 128.55, 128.18, 127.12, 126.50 (Ar), 54.65, 53.39, 53.23 (3 x αC); 36.94, 36.87, 26.60 (3 x βC).

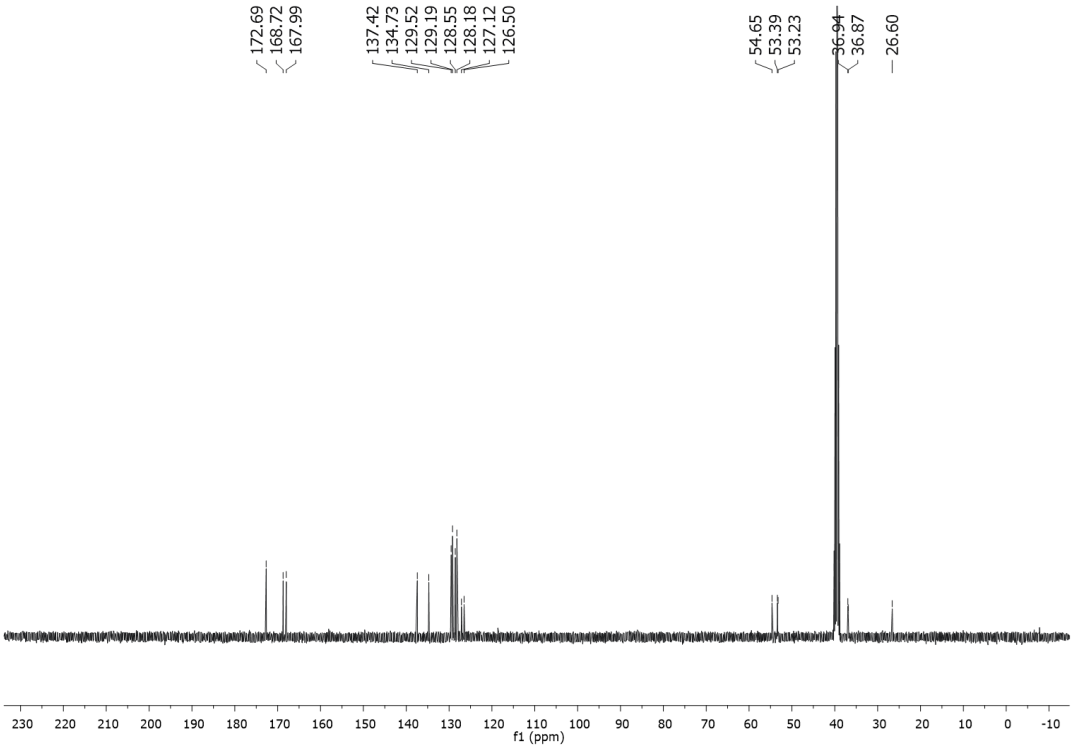

Figure A.1.33. ^{13}C-NMR spectrum of Phe-Cys-^{D}Phe.

MS (ESI)

$C_{21}H_{25}N_3O_4S$ requires 415.2: m/z 416.1 $[M+H]^+$, m/z 832.3 $[2M+2H]^+$; m/z 414.1 $[M-H]^-$, m/z 829.3 $[2M-H]^-$;

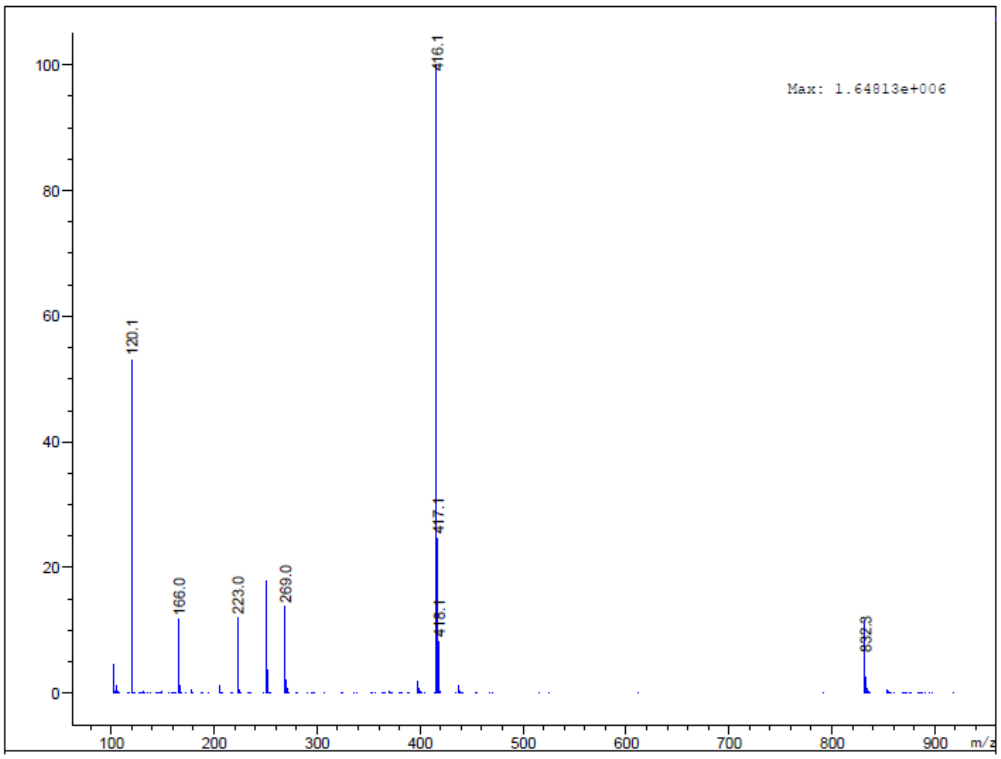

Figure A.1.34. ESI-MS spectrum of Phe-Cys-^{D}Phe in positive mode.

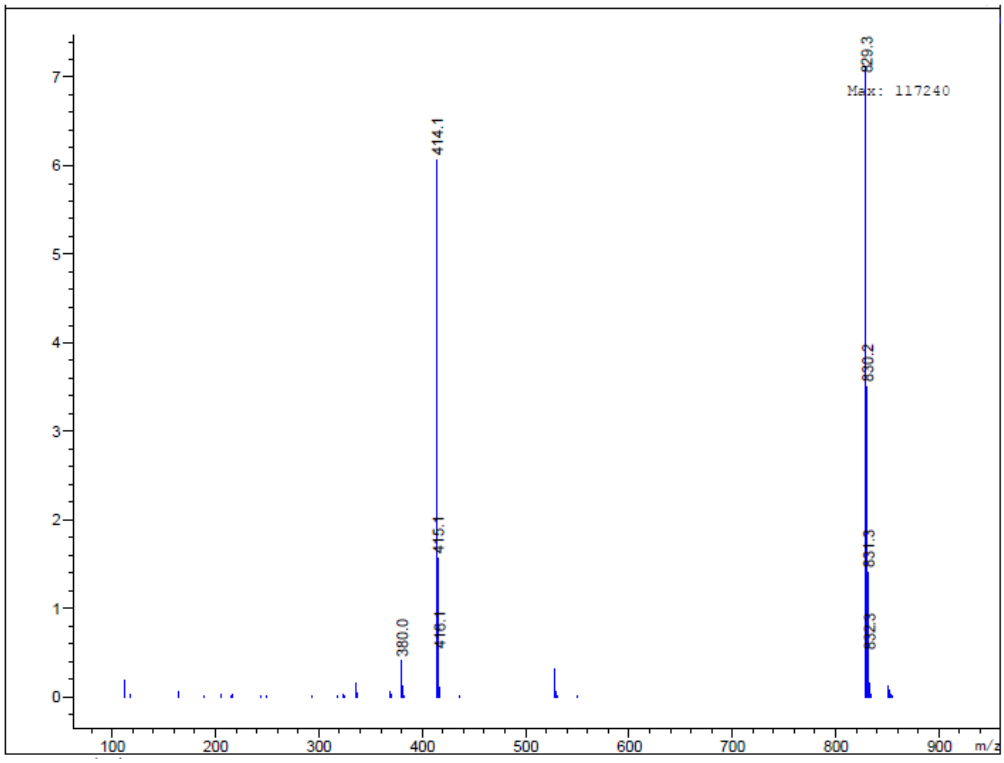

Figure A.1.35. ESI-MS spectrum of Phe-Cys-^{D}Phe in negative mode.

A.2. Tripeptides HPLC Traces

Peptide Sequence	***LogP***	***Retention time (min)***	***Gel***
^{D}**Met**-Phe-Phe	1.6 ± 0.2	14.9	✓
Phe-^{D}**Met**-Phe	1.6 ± 0.2	15.0	✓
^{D}Phe-Phe-**Met**	1.6 ± 0.2	14.7	✓

Table A.2.1. Hydrophobicity, based on logP and experimental HPLC retention time, and gelling ability for Met-containing tripeptides.

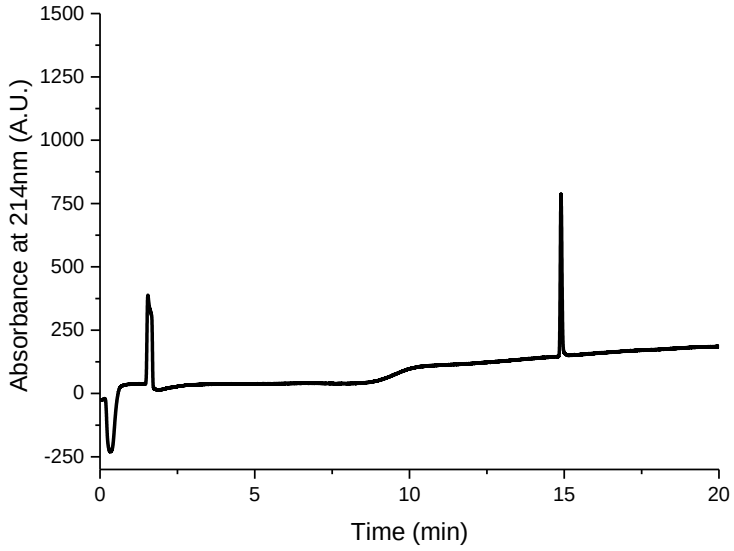

Figure A.2.1. Analytical HPLC chromatogram of tripeptide ^{D}Met-Phe-Phe. Retention time: 14.9 minutes.

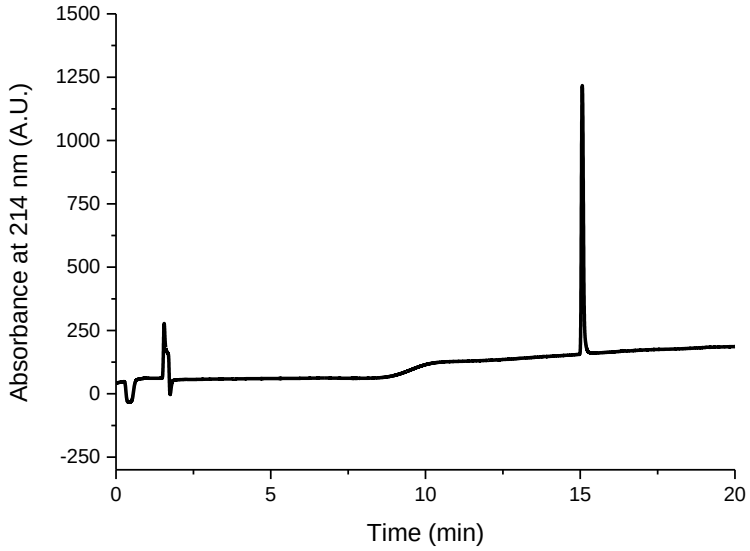

Figure A.2.2. Analytical HPLC chromatogram of tripeptide Phe-^{D}Met-Phe. Retention time: 15.0 minutes.

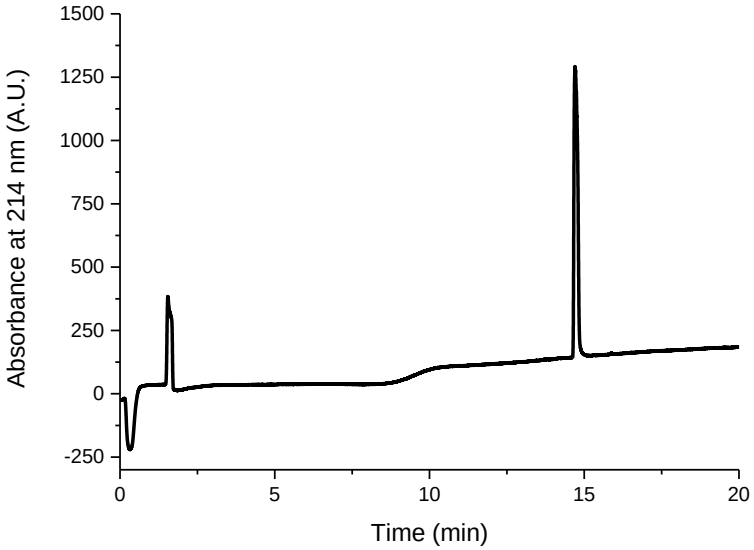

Figure A.2.3. Analytical HPLC chromatogram of tripeptide ^{D}Phe-Phe-Met. Retention time: 14.7 minutes.

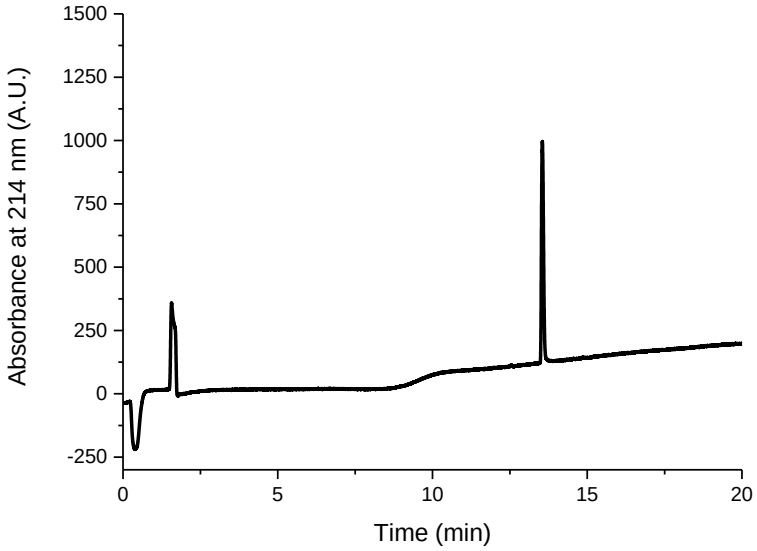

Figure A.2.4. Analytical HPLC chromatogram of tripeptide Phe-Cys-Phe. Retention time: 13.6 minutes.

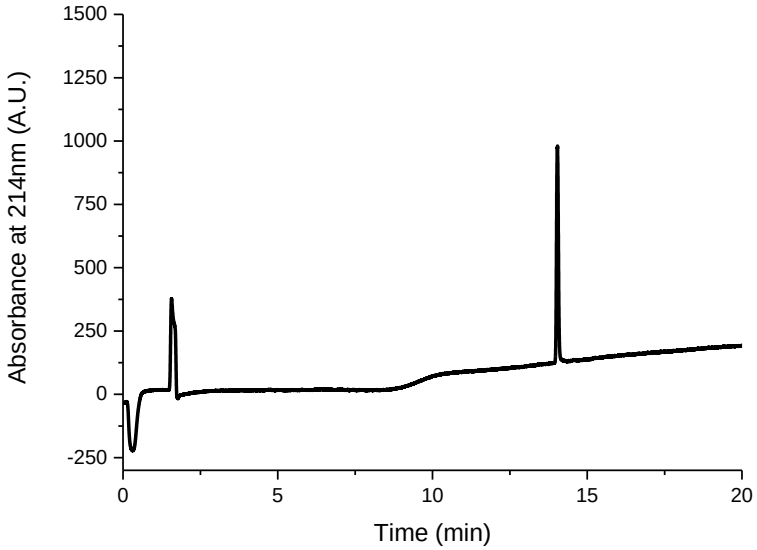

Figure A.2.5. Analytical HPLC chromatogram of tripeptide ^{D}Phe-Cys-Phe. Retention time: 14.1 minutes.

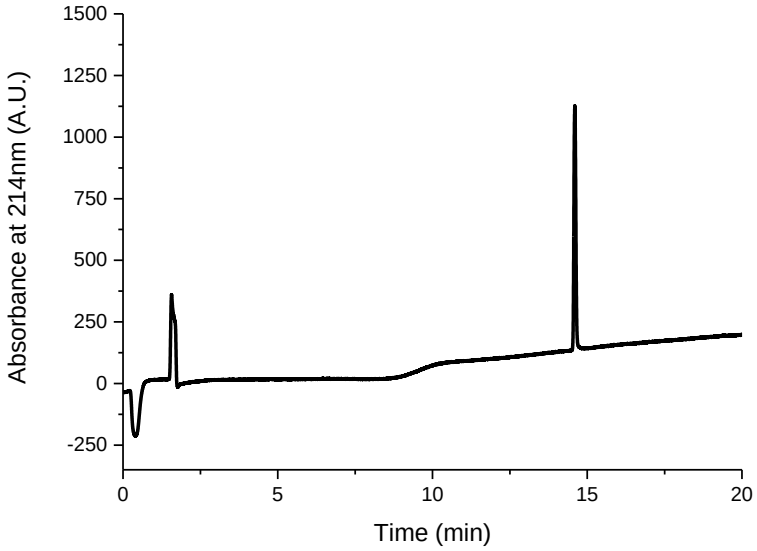

Figure A.2.6. Analytical HPLC chromatogram of tripeptide Phe-^{D}Cys-Phe. Retention time: 14.6 minutes.

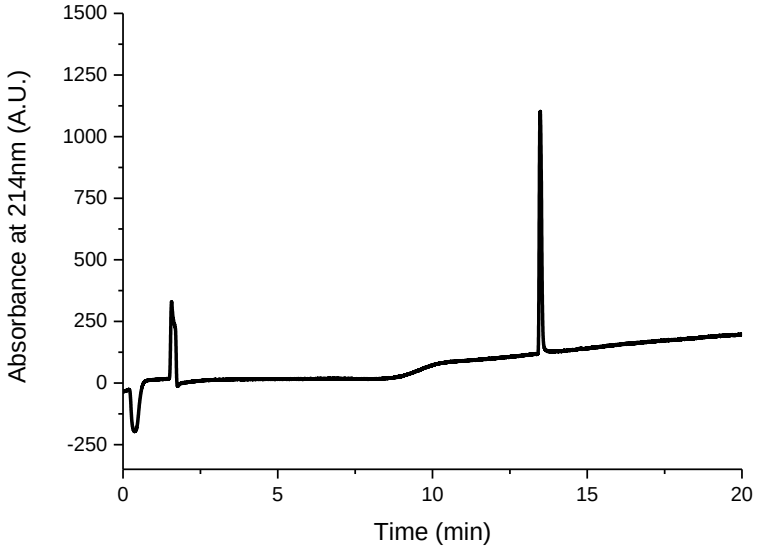

Figure A.2.7. Analytical HPLC chromatogram of tripeptide Phe-Cys-^{D}Phe. Retention time: 13.5 minutes.

A.3. Crystallographic Data

	^{D}Met-Phe-Phe	^{D}Phe-Phe-**Met**	^{D}Phe-**Cys**-Phe
Formula	$C_{23}H_{29}N_3O_4S \cdot C_2H_6O \cdot 2H_2O$	$3C_{23}H_{29}N_3O_4S \cdot 7H_2O$	$2C_{21}H_{25}N_3O_4S \cdot 0.5CH_4O \cdot 4.2H_2O$
Temperature (K)	100	100	100
Wavelength (Å)	0.7	0.7	0.7
Crystal system	Monoclinic	Monoclinic	Orthorhombic
Space group	*P 2₁*	*C 2*	*P 2₁ 2₁ 2*
a (Å)	13.301(3)	33.240(7)	22.953(5)
b (Å)	5.938(1)	5.890(1)	34.327(7)
c (Å)	19.840(4)	37.130(7)	5.869(1)
α (°)	90	90	90
β (°)	105.79(3)	92.20(3)	90
γ (°)	90	90	90
V (Å^3)	1394.5(5)	7264(3)	4624(2)
Z, ρcalc (g/cm^3)	2, 1.252	4, 1.332	4, 1.327
μ (mm^{-1})	0.137	0.136	0.161
F (000)	472	3112	1966
Data collection θ range	1.05 - 28.397	1.081 - 25.374	1.459 – 22.996
Refl. Collected / unique	17602 / 7110	22408 / 12662	18759 / 6580
Rint	0.0704	0.0952	0.0868
Completeness (%)	99.9	98.5	98.3
Data/Restraints/Parameters	7110 / 7 / 346	12662 / 113 / 963	18759 / 64 / 644
GooF	1.026	1.001	1.012
R1, wR2 [I>2σ(I)]	0.0592 / 0.1461	0.0656 / 0.1426	0.0575 / 0.1391
R1, wR2 all data	0.0877 / 0.1654	0.1203 / 0.1724	0.1004 / 0.1643

Table A.3.1. Crystallographic data for tripeptides ^{D}Met-Phe-Phe, ^{D}Phe-Phe-Met, and ^{D}Phe-Cys-Phe.

	n=1	n=2		n=3
	ψ:N_n-Cα_n-C_n-N_{n+1}	φ:C_{n-1}-N_n-Cα_n-C_n	ψ:N_n-Cα_n-C_n-N_{n+1}	φ:C_{n-1}-N_n-Cα_n-C_n
^{D}Met-Phe-Phe	-138.52	-79.52	-26.87	-76.65
^{D}Phe-Phe-Met	-128.47	-68.35	-38.41	-65.58
	-134.26	-68.18	-40.99	-65.58
	-135.85	-73.15	-30.36	-76.72
^{D}Phe-Cys-Phe	-129.11	-66.32	-37.87	-65.07
	-137.55	-69.05	-40.23	-61.61

Table A.3.2. Torsion angles in the structures of tripeptides ^{D}Met-Phe-Phe, ^{D}Phe-Phe-Met, and ^{D}Phe-Cys-Phe

A.4. CD over a Temperature Ramp

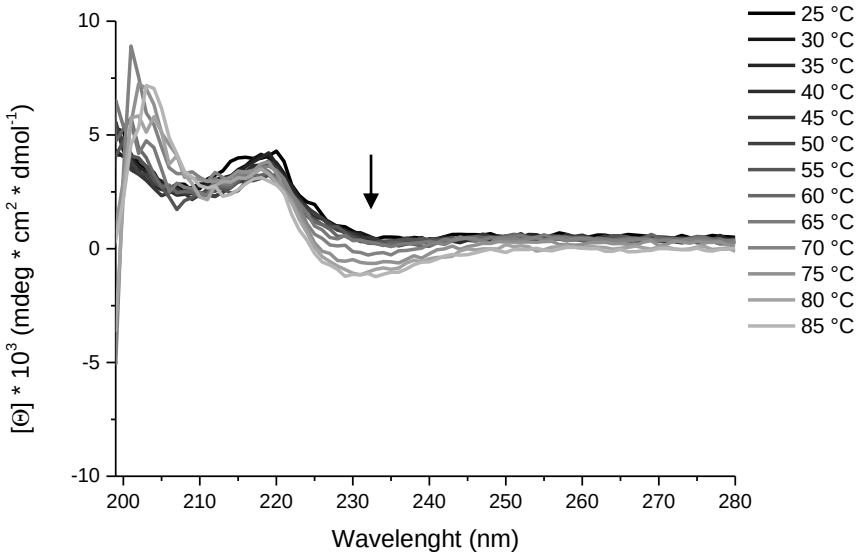

Figure A.4.1. Evolution of CD spectra of tripeptide Phe-Cys-Phe during a heating ramp. Arrow indicates direction of signal evolution over temperature.

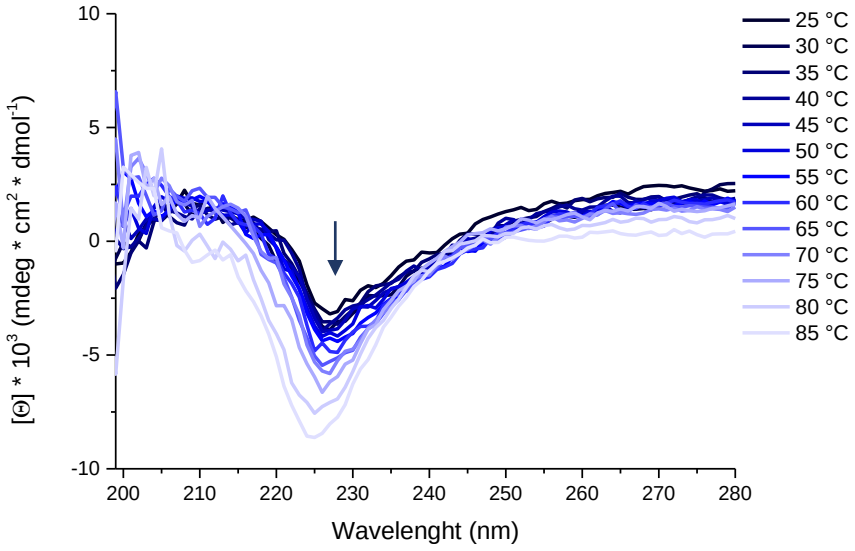

Figure A.4.2. Evolution of CD spectra of tripeptide ^{D}Phe-Cys-Phe during a heating ramp. Arrow indicates direction of signal evolution over temperature.

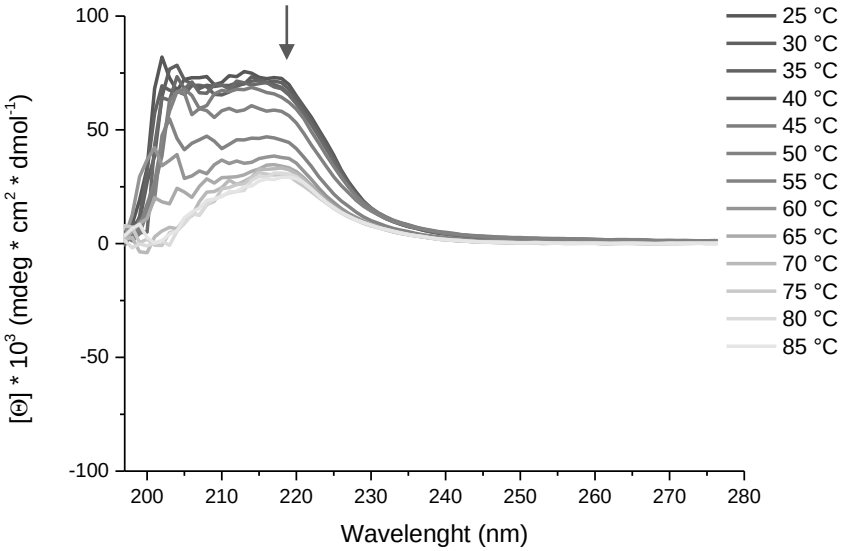

Figure A.4.3. Evolution of CD spectra of tripeptide Phe-^{D}Cys-Phe during a heating ramp. Arrow indicates direction of signal evolution over temperature.

A.5. Spectroscopic Data of 3-Bromomaleimide

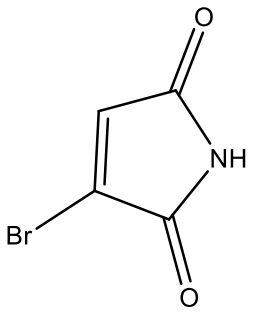

Chemical Formula: $C_4H_2BrNO_2$
Exact Mass: 174,93
Molecular Weight: 175,97

Figure A.5.1. Chemical structure of 3-bromomaleimide.

TLC (SiO_2, EP/AcOEt 5/1) R_f: 0.25.

TLC (SiO_2, EP/AcOEt 3/1) R_f: 0.48.

TLC (SiO_2, EP/AcOEt 1/1) R_f: 0.78.

m.p.: 151 °C (lit: 152 °C,[145] lit: 148-151 °C [113]).

^{1}H-NMR (400 MHz, $CDCl_3$) δ (ppm): 7.59 (br, 1H, NH), 6.89 (d, 1H, *J* =1.6, CH).

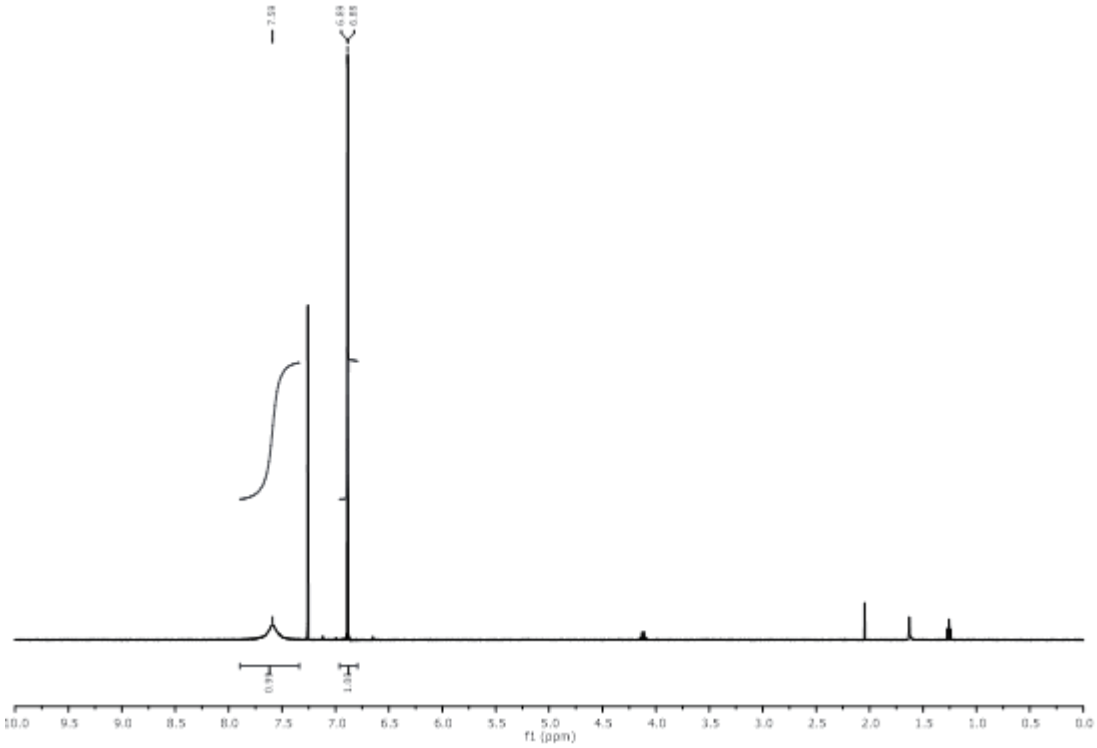

Figure A.5.2. ^{1}H-NMR of 3-bromomaleimide in $CDCl_3$.

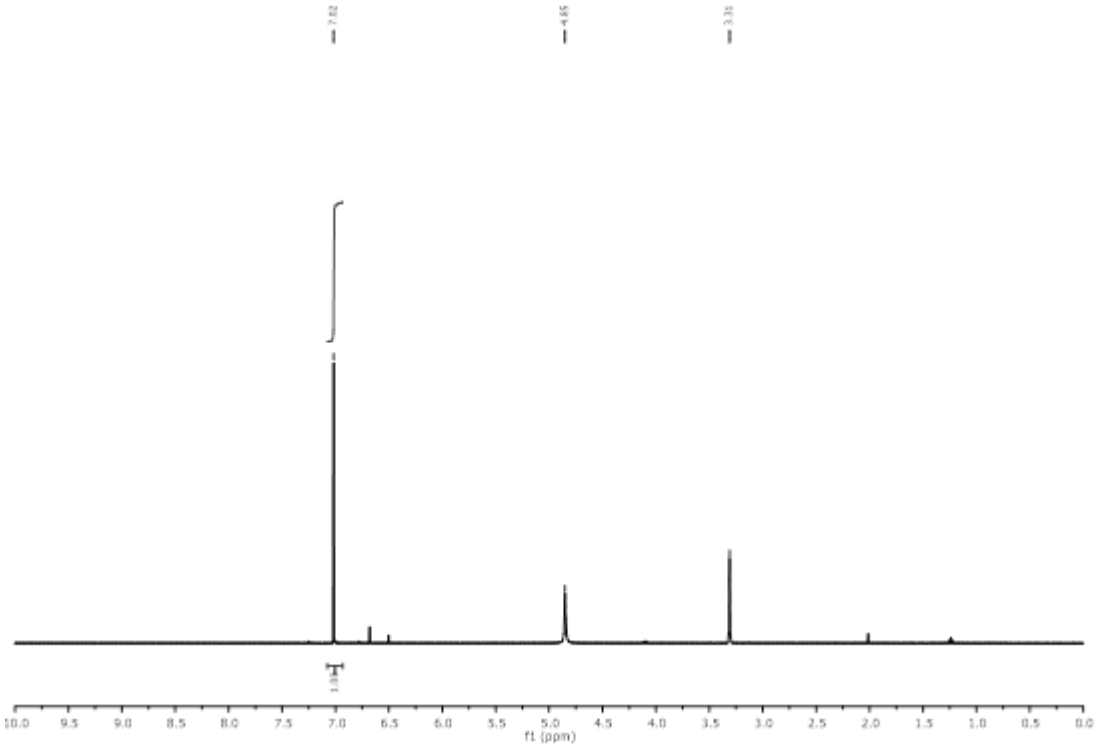

Figure A.5.3. ^{1}H-NMR of 3-bromomaleimide in CD_3OD.

MS (ESI) spectra of peaks obtained during LC analyses.

Peak A: thiomaleimide conjugate: $C_{25}H_{25}N_4O_6S$ requires 510.1: m/z 511.0 $[M+H]^+$; m/z 509.0 $[M-H]^-$.

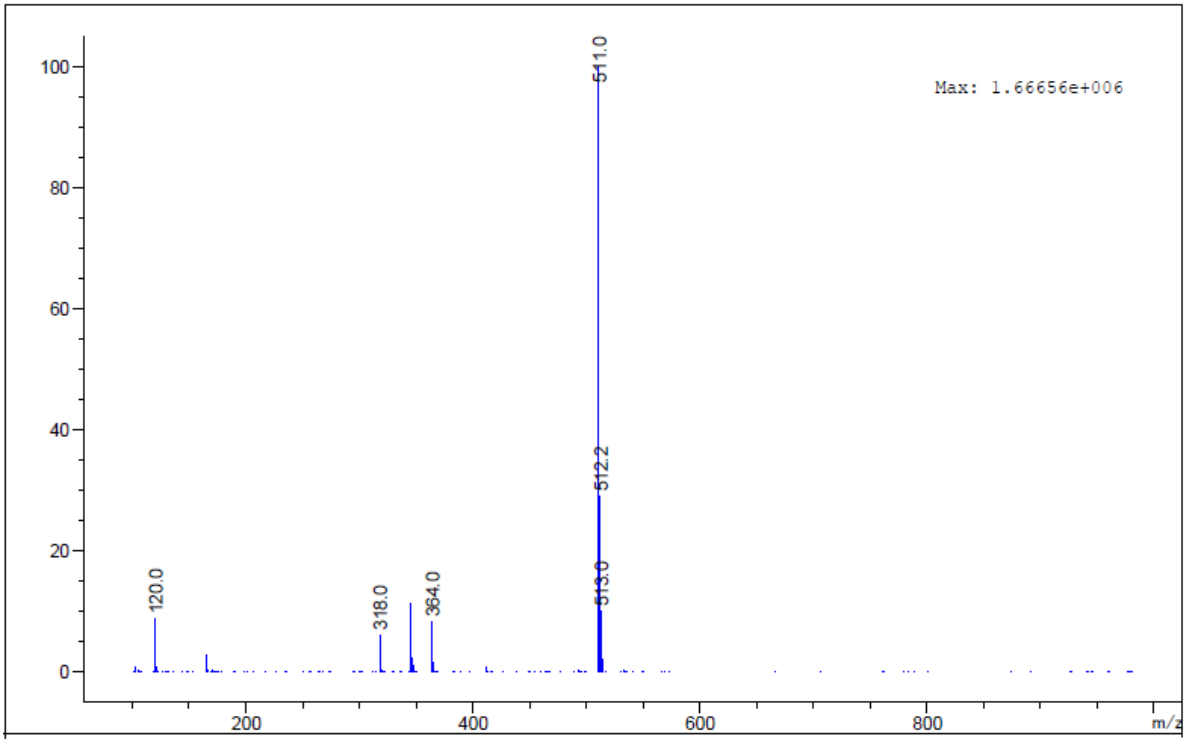

Figure A.5.4. MS spectrum of peak A in positive mode.

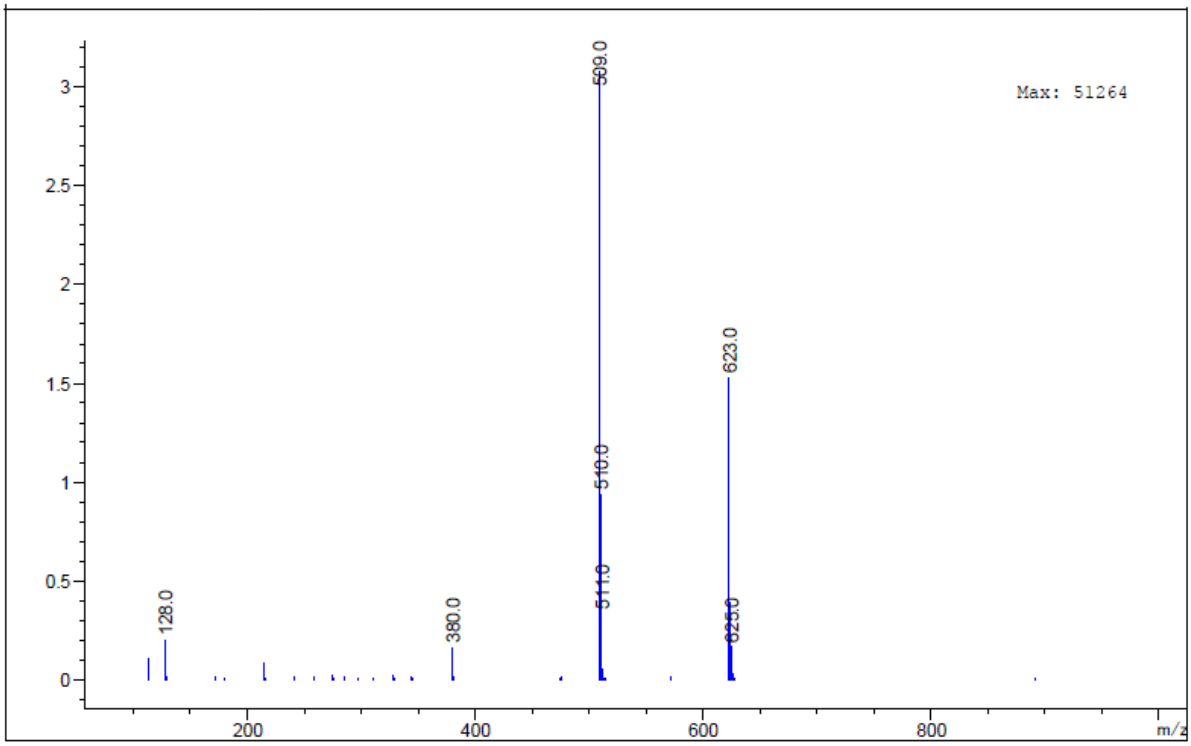

Figure A.5.5. MS spectrum of peak A in negative mode.

Peak B: Bromomaleimide: $C_4H_2BrNO_2$ requires 174.9: ESI-MS was attempted using a solution of the product in acetonitrile but no signals could be observed; in the literature[113, 146] high resolution mass spectra of similar compounds were obtained by either Electron impact ionization or Chemical ionization, neither of which are available in the department.

Peak C: Peptide Phe-^{D}Cys-Phe: $C_{21}H_{25}N_3O_4S$ requires 415.2: m/z 416.0 $[M+H]^+$; m/z 414.0 $[M-H]^-$.

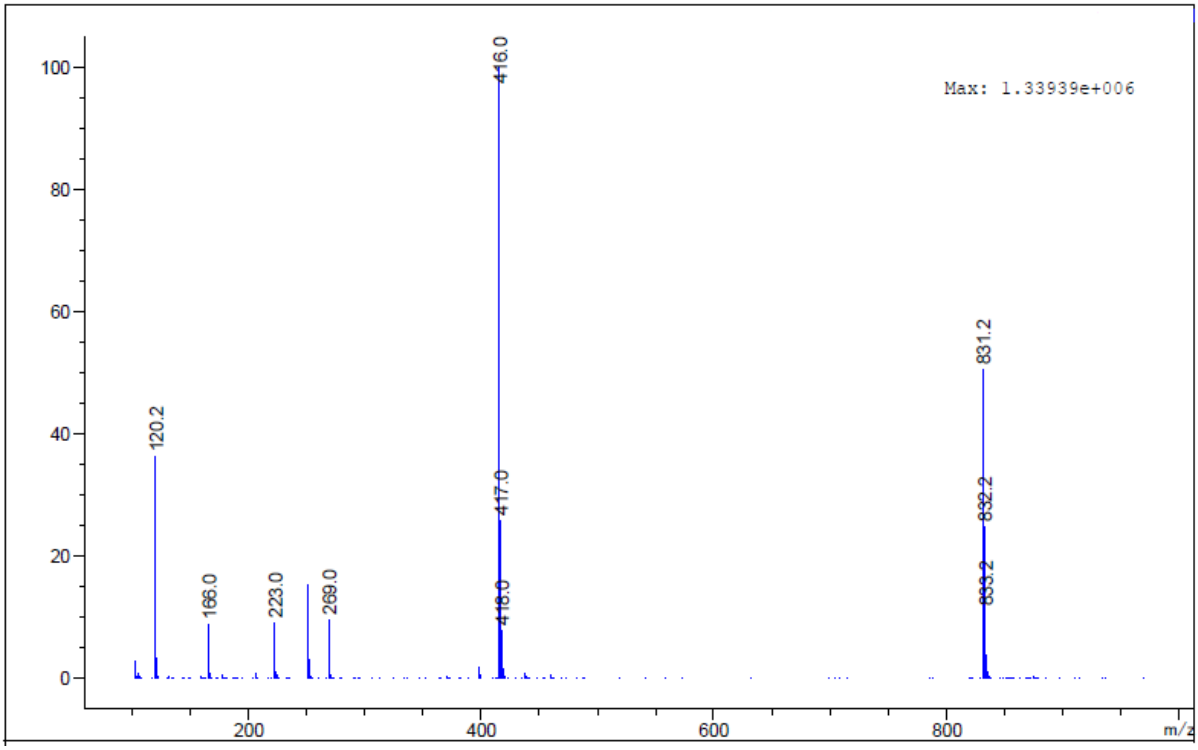

Figure A.5.6. MS spectrum of peak C in positive mode.

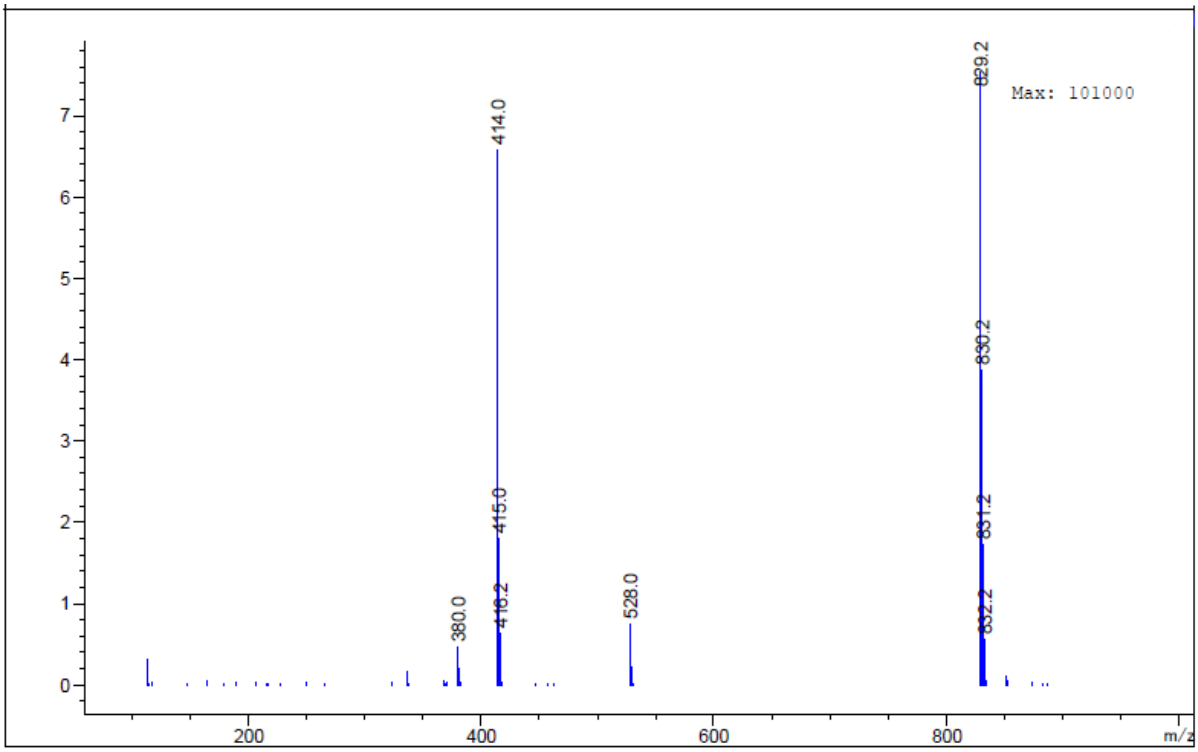

Figure A.5.7. MS spectrum of peak C in negative mode.

References

1. L. Pasteur, *Ann. Chim. Phys.*, **1848**, *24*, 442-459.
2. M. Liu, L. Zhang and T. Wang, *Chem. Rev.*, **2015**, *115*, 7304-7397.
3. G. Genchi, *Amino Acids*, **2017**, *49*, 1521-1533.
4. E. Fischer, *Ber. Dtsch. Chem. Ges.*, **1891**, *24*, 2683-2687.
5. X. Dai, E. Zhou, W. Yang, X. Zhang, W. Zhang and Y. Rao, *Nat. Commun.*, **2019**, *10*, 1986.
6. K. Hamase, A. Morikawa and K. Zaitsu, *J. Chromatogr. B*, **2002**, *781*, 73-91.
7. D. A. Reaveley and R. E. Burge, in *Advances in Microbial Physiology*, eds. A. H. Rose and D. W. Tempest, Academic Press, **1972**, vol. 7, pp. 1-81.
8. J. Csapó, Z. Csapó-Kiss, J. Schmidt and T. G. Martin, *TrAC, Trends Anal. Chem.*, **2001**, *20*, 42-48.
9. S. Kanie, T. Nishikawa, M. Ojika and Y. Oba, *Sci. Rep.*, **2016**, *6*, 24794.
10. J. J. Corrigan, *Science*, **1969**, *164*, 142-149.
11. A. D'Aniello and A. Giuditta, *J. Neurochem.*, **1978**, *31*, 1107-1108.
12. H. Felbeck, *J. Exp. Zool.*, **1985**, *234*, 145-149.
13. H. Brückner and T. Westhauser, *Chromatographia*, **1994**, *39*, 419-426.
14. P. C. Montecucchi, R. De Castiglione, S. Piani, L. Gozzini and V. Erspamer, *Int. J. Pept. Protein Res.*, **1981**, *17*, 275-283.
15. V. Erspamer, G. F. Erspamer, C. Severini, R. L. Potenza, D. Barra, G. Mignogna and A. Bianchi, *Toxicon*, **1993**, *31*, 1099-1111.
16. H. Wolosker, S. Blackshaw and S. H. Snyder, *Proc. Natl. Acad. Sci.*, **1999**, *96*, 13409-13414.
17. N. Shibuya, S. Koike, M. Tanaka, M. Ishigami-Yuasa, Y. Kimura, Y. Ogasawara, K. Fukui, N. Nagahara and H. Kimura, *Nat. Commun.*, **2013**, *4*, 1366.
18. C. Ollivaux, D. Soyez and J.-Y. Toullec, *J. Pept. Sci.*, **2014**, *20*, 595-612.
19. M. Qin, J. Zhang and W. Wang, *Biophys. J.*, **2006**, *90*, 272-286.
20. T. Handel, S. Williams and W. DeGrado, *Science*, **1993**, *261*, 879-885.

21. V. J. Hruby, *Nat. Rev. Drug Discov.*, **2002**, *1*, 847-858.

22. B. Imperiali, R. A. Moats, S. L. Fisher and T. J. Prins, *J. Am. Chem. Soc.*, **1992**, *114*, 3182-3188.

23. M. D. Struthers, R. P. Cheng and B. Imperiali, *Science*, **1996**, *271*, 342-345.

24. I. Karle, H. N. Gopi and P. Balaram, *Proc. Natl. Acad. Sci.*, **2002**, *99*, 5160-5164.

25. C. Xie, A. Prahl, B. Ericksen, Z. Wu, P. Zeng, X. Li, W.-Y. Lu, J. Lubkowski and W. Lu, *J. Biol. Chem.*, **2005**.

26. J. P. Schneider, D. J. Pochan, B. Ozbas, K. Rajagopal, L. Pakstis and J. Kretsinger, *J. Am. Chem. Soc.*, **2002**, *124*, 15030-15037.

27. J. K. Kretsinger, L. A. Haines, B. Ozbas, D. J. Pochan and J. P. Schneider, *Biomaterials*, **2005**, *26*, 5177-5186.

28. D. A. Salick, J. K. Kretsinger, D. J. Pochan and J. P. Schneider, *J. Am. Chem. Soc.*, **2007**, *129*, 14793-14799.

29. P. Worthington, S. Langhans and D. Pochan, *Adv. Drug Deliv. Rev.*, **2017**, *110-111*, 127-136.

30. P. Worthington, K. M. Drake, Z. Li, A. D. Napper, D. J. Pochan and S. A. Langhans, *Anal. Biochem.*, **2017**, *535*, 25-34.

31. K. M. Makwana and R. Mahalakshmi, *Pep. Sci.*, **2016**, *106*, 260-266.

32. S. Prusiner, *Science*, **1991**, *252*, 1515-1522.

33. L. C. Serpell, *BBA-Mol. Basis. Dis.*, **2000**, *1502*, 16-30.

34. G. Liang, Z. Yang, R. Zhang, L. Li, Y. Fan, Y. Kuang, Y. Gao, T. Wang, W. W. Lu and B. Xu, *Langmuir*, **2009**, *25*, 8419-8422.

35. Z. Luo, S. Wang and S. Zhang, *Biomaterials*, **2011**, *32*, 2013-2020.

36. S. Chen, A. Zhou, B. He, W. Zhao, X. Chen and D. Jiang, *Int J Mol Med*, **2017**, *40*, 679-688.

37. Z. Ye, X. Zhu, S. Acosta, D. Kumar, T. Sang and C. Aparicio, *Nanoscale*, **2019**, *11*, 266-275.

38. R. J. Swanekamp, J. T. M. DiMaio, C. J. Bowerman and B. L. Nilsson, *J. Am. Chem. Soc.*, **2012**, *134*, 5556-5559.

39. T. Koga, M. Matsuoka and N. Higashi, *J. Am. Chem. Soc.*, **2005**, *127*, 17596-17597.

40. S. Marchesan, C. D. Easton, K. E. Styan, L. J. Waddington, F. Kushkaki, L. Goodall, K. M. McLean, J. S. Forsythe and P. G. Hartley, *Nanoscale*, **2014**, *6*, 5172-5180.

41. A. M. Almeida, R. Li and S. H. Gellman, *J. Am. Chem. Soc.*, **2012**, *134*, 75-78.

42. Z. Shlomo, T. P. Vinod, R. Jelinek and H. Rapaport, *Chem. Commun.*, **2015**, *51*, 3154-3157.

43. A. M. Garcia, D. Iglesias, E. Parisi, K. E. Styan, L. J. Waddington, C. Deganutti, R. De Zorzi, M. Grassi, M. Melchionna, A. V. Vargiu and S. Marchesan, *Chem*, **2018**, *4*, 1862-1876.

44. A. V. Vargiu, D. Iglesias, K. E. Styan, L. J. Waddington, C. D. Easton and S. Marchesan, *Chem. Commun.*, **2016**, *52*, 5912-5915.

45. R. Fairman, S. J. Anthony-Cahill and W. F. DeGrado, *J. Am. Chem. Soc.*, **1992**, *114*, 5458-5459.

46. E. Krause, M. Bienert, P. Schmieder and H. Wenschuh, *J. Am. Chem. Soc.*, **2000**, *122*, 4865-4870.

47. G. H. Zerze, M. N. Khan, F. H. Stillinger and P. G. Debenedetti, *J. Phys. Chem. B*, **2018**, *122*, 6357-6363.

48. U. Orcel, M. De Poli, M. De Zotti and J. Clayden, *Chem.: Eur. J.*, **2013**, *19*, 16357-16365.

49. C. D. Vacogne, C. Wei, K. Tauer and H. Schlaad, *J. Am. Chem. Soc.*, **2018**, *140*, 11387-11394.

50. L. Ruckthong, A. F. A. Peacock, C. E. Pascoe, L. Hemmingsen, J. A. Stuckey and V. L. Pecoraro, *Chem.: Eur. J.*, **2017**, *23*, 8232-8243.

51. J. Zhou, J. Li, X. Du and B. Xu, *Biomaterials*, **2017**, *129*, 1-27.

52. S. Fleming and R. V. Ulijn, *Chem. Soc. Rev.*, **2014**, *43*, 8150-8177.

53. A. M. Smith, R. J. Williams, C. Tang, P. Coppo, R. F. Collins, M. L. Turner, A. Saiani and R. V. Ulijn, *Adv. Mater.*, **2008**, *20*, 37-41.

54. S. Marchesan, A. V. Vargiu and K. E. Styan, *Molecules*, **2015**, *20*, 19775-19788.

55. H. M. Werner, C. C. Cabalteja and W. S. Horne, *ChemBioChem*, **2016**, *17*, 712-718.

56. S. Marchesan, L. Waddington, C. D. Easton, D. A. Winkler, L. Goodall, J. Forsythe and P. G. Hartley, *Nanoscale*, **2012**, *4*, 6752-6760.

57. S. Marchesan, C. D. Easton, F. Kushkaki, L. Waddington and P. G. Hartley, *Chem. Commun.*, **2012**, *48*, 2195-2197.

58. S. Marchesan, K. E. Styan, C. D. Easton, L. Waddington and A. V. Vargiu, *J. Mater. Chem. B*, **2015**, *3*, 8123-8132.

59. A. Méndez-Ardoy, J. R. Granja and J. Montenegro, *Nanoscale Horiz.*, **2018**, *3*, 391-396.

60. H. Shaikh, J. Y. Rho, L. J. Macdougall, P. Gurnani, A. M. Lunn, J. Yang, S. Huband, E. D. H. Mansfield, R. Peltier and S. Perrier, *Chem.: Eur. J.*, **2018**, *24*, 19066-19074.

61. C. Ou, J. Zhang, Y. Shi, Z. Wang, L. Wang, Z. Yang and M. Chen, *RSC Adv.*, **2014**, *4*, 9229-9232.

62. K. McAulay, B. Dietrich, H. Su, M. T. Scott, S. Rogers, Y. K. Al-Hilaly, H. Cui, L. C. Serpell, Annela M. Seddon, E. R. Draper and D. J. Adams, *Chem. Sci.*, **2019**, *10*, 7801-7806.

63. C. Ren, Y. Gao, J. Liu, Y. Zhang, G. Pu, L. Yang, F. Huang, C. Yang, Z. Yang and J. Liu, *J. Biomed. Nanotechnol.*, **2018**, *14*, 1125-1134.

64. Y. Huang, Z. Qiu, Y. Xu, J. Shi, H. Lin and Y. Zhang, *Org. Biomol. Chem.*, **2011**, *9*, 2149-2155.

65. Z. Chen, Z. Lv, G. Qing and T. Sun, *J. Mater. Chem. B*, **2017**, *5*, 3163-3171.

66. E. R. Draper and D. J. Adams, *Chem*, **2017**, *3*, 390-410.

67. S. G. Lipson, H. Lipson and D. S. Tannhauser, *Optical Physics*, 3 edn., Cambridge University Press, Cambridge, **1995**.

68. D. Cressey and E. Callaway, *Nature*, **2017**, *550*, 167-167.

69. D. Iglesias and S. Marchesan, in *Nanostructures for Novel Therapy*, eds. D. Ficai and A. M. Grumezescu, Elsevier, **2017**, pp. 227-250.

70. A. Zengin, G. Cinar and M. O. Guler, *Curr. Appl. Phys.*, **2017**, *17*, 785-792.

71. J. Liu, J. Liu, L. Chu, Y. Zhang, H. Xu, D. Kong, Z. Yang, C. Yang and D. Ding, *ACS Appl. Mater. Interfaces*, **2014**, *6*, 5558-5565.

72. E. Parisi, A. M. Garcia, D. Marson, P. Posocco and S. Marchesan, *Gels*, **2019**, *5*, 5.

73. G. A. Hudalla, T. Sun, J. Z. Gasiorowski, H. Han, Y. F. Tian, A. S. Chong and J. H. Collier, *Nat. Mater.*, **2014**, *13*, 829.

74. H. Wang, Z. Luo, Y. Wang, T. He, C. Yang, C. Ren, L. Ma, C. Gong, X. Li and Z. Yang, *Advanced Functional Materials*, **2016**, *26*, 1822-1829.

75. Z. Wang, Y. Cai, L. Yi, J. Gao and Z. Yang, *Chin. J. Chem.*, **2017**, *35*, 1057-1062.

76. Y. Wang, X. Li, Y. Zhang, L. Wang and Z. Yang, *Chem. Commun.*, **2019**.

77. Z. Luo, Q. Wu, C. Yang, H. Wang, T. He, Y. Wang, Z. Wang, H. Chen, X. Li, C. Gong and Z. Yang, *Adv. Mater.*, **2017**, *29*, 1601776.

78. R. Appavu, C. B. Chesson, A. Y. Koyfman, J. D. Snook, F. J. Kohlhapp, A. Zloza and J. S. Rudra, *ACS Biomater. Sci. Eng.*, **2015**, *1*, 601-609.

79. Z. Luo, Y. Yue, Y. Zhang, X. Yuan, J. Gong, L. Wang, B. He, Z. Liu, Y. Sun, J. Liu, M. Hu and J. Zheng, *Biomaterials*, **2013**, *34*, 4902-4913.

80. H. Zheng, T. Yoshitomi and K. Yoshimoto, *ACS App. Bio. Mater.*, **2018**, *1*, 538-543.

81. K. Baranes, H. Moshe, N. Alon, S. Schwartz and O. Shefi, *ACS Chem. Neurosci.*, **2014**, *5*, 370-376.

82. J. C. Heiby, B. Goretzki, C. M. Johnson, U. A. Hellmich and H. Neuweiler, *Nat. Commun.*, **2019**, *10*, 4378.

83. R. Otter, C. M. Berac, S. Seiffert and P. Besenius, *Eur. Polym. J.*, **2019**, *110*, 90-96.

84. J. T. Rubino, P. Riggs-Gelasco and K. J. Franz, *J. Biol. Inorg. Chem.*, **2010**, *15*, 1033-1049.

85. S. Pellegrino, G. Facchetti, A. Contini, M. L. Gelmi, E. Erba, R. Gandolfi and I. Rimoldi, *RSC Adv.*, **2016**, *6*, 71529-71533.

86. H. Huang and D. L. Rabenstein, *J. Pept. Res.*, **1999**, *53*, 548-553.

87. M. C. Cringoli, S. Kralj, M. Kurbasic, M. Urban and S. Marchesan, *Beilstein J. Nanotechnol.*, **2017**, *8*, 1553-1562.

88. P. J. Stephens, F. J. Devlin and J.-J. Pan, *Chirality*, **2008**, *20*, 643-663.

89. A. G. de Brevern, *Sci. Rep.*, **2016**, *6*, 33191.

90. C. Wu, M. Biancalana, S. Koide and J.-E. Shea, *J. Mol. Biol.*, **2009**, *394*, 627-633.

91. N. Amdursky, Y. Erez and D. Huppert, *Acc. Chem. Res.*, **2012**, *45*, 1548-1557.

92. M. Biancalana and S. Koide, *BBA-Proteins Proteom.*, **2010**, *1804*, 1405-1412.

93. E. Awoonor-Williams and C. N. Rowley, *J. Chem. Theory Comput.*, **2016**, *12*, 4662-4673.

94. K. G. Reddie and K. S. Carroll, *Curr. Opin. Chem. Biol.*, **2008**, *12*, 746-754.

95. M. A. Sequeira, M. G. Herrera and V. I. Dodero, *Phys. Chem. Chem. Phys.*, **2019**, *21*, 11916-11923.

96. A. K. Nowinski, F. Sun, A. D. White, A. J. Keefe and S. Jiang, *J. Am. Chem. Soc.*, **2012**, *134*, 6000-6005.

97. I. Russier-Antoine, F. Bertorelle, A. Kulesza, A. Soleilhac, A. Bensalah-Ledoux, S. Guy, P. Dugourd, P.-F. Brevet and R. Antoine, *Prog. Nat. Sci.- Mater.*, **2016**, *26*, 455-460.

98. A. D. Malay, N. Miyazaki, A. Biela, S. Chakraborti, K. Majsterkiewicz, I. Stupka, C. S. Kaplan, A. Kowalczyk, B. M. A. G. Piette, G. K. A. Hochberg, D. Wu, T. P. Wrobel, A. Fineberg, M. S. Kushwah, M. Kelemen, P. Vavpetič, P. Pelicon, P. Kukura, J. L. P. Benesch, K. Iwasaki and J. G. Heddle, *Nature*, **2019**, *569*, 438-442.

99. S. Scintilla, C. Bonfio, L. Belmonte, M. Forlin, D. Rossetto, J. Li, J. A. Cowan, A. Galliani, F. Arnesano, M. Assfalg and S. S. Mansy, *Chem. Commun.*, **2016**, *52*, 13456-13459.

100. Y. Han, F. Albericio and G. Barany, *J. Org. Chem.*, **1997**, *62*, 4307-4312.

101. V. N. Viswanadhan, A. K. Ghose, G. R. Revankar and R. K. Robins, *J. Chem. Inf. Comput. Sci.*, **1989**, *29*, 163-172.

102. A. K. Ghose and G. M. Crippen, *J. Chem. Inf. Comput. Sci.*, **1987**, *27*, 21-35.

103. Y. Fu, B. Li, Z. Huang, Y. Li and Y. Yang, *Langmuir*, **2013**, *29*, 6013-6017.

104. M. Wang, P. Zhou, J. Wang, Y. Zhao, H. Ma, J. R. Lu and H. Xu, *J. Am. Chem. Soc.*, **2017**, *139*, 4185-4194.

105. N. A. Dudukovic and C. F. Zukoski, *Soft Matter*, **2014**, *10*, 7849-7856.

106. C. R. Forbes, S. K. Sinha, H. K. Ganguly, S. Bai, G. P. A. Yap, S. Patel and N. J. Zondlo, *J. Am. Chem. Soc.*, **2017**, *139*, 1842-1855.

107. J.-M. Lehn, *Angew. Chem. Int. Ed.*, **1988**, *27*, 89-112.

108. R. Merindol and A. Walther, *Chem. Soc. Rev.*, **2017**, *46*, 5588-5619.

109. L. Heinen and A. Walther, *Soft Matter*, **2015**, *11*, 7857-7866.

110. G. M. Whitesides and B. Grzybowski, *Science*, **2002**, *295*, 2418-2421.

111. J. M. Chalker, G. J. L. Bernardes, Y. A. Lin and B. G. Davis, *Chem. Asian J.*, **2009**, *4*, 630-640.

112. J. P. Wojciechowski, A. D. Martin and P. Thordarson, *J. Am. Chem. Soc.*, **2018**, *140*, 2869-2874.

113. L. M. Tedaldi, M. E. B. Smith, R. I. Nathani and J. R. Baker, *Chem. Commun.*, **2009**, 6583-6585.

114. X. Li, H. Li, W. Yang, J. Zhuang, H. Li and W. Wang, *Tetrahedron Lett.*, **2016**, *57*, 2660-2663.

115. J. Youziel, A. R. Akhbar, Q. Aziz, M. E. B. Smith, S. Caddick, A. Tinker and J. R. Baker, *Org. Biomol. Chem.*, **2014**, *12*, 557-560.

116. G. Y. Wiederschain, *Biochemistry (Moscow)*, **2011**, *76*, 1276-1276.

117. G. L. Ellman, *Arch. Biochem. Biophys.*, **1959**, *82*, 70-77.

118. M. He, J. Li, S. Tan, R. Wang and Y. Zhang, *J. Am. Chem. Soc.*, **2013**, *135*, 18718-18721.

119. M. E. Roth-Konforti, M. Comune, M. Halperin-Sternfeld, I. Grigoriants, D. Shabat and L. Adler-Abramovich, *Macromol. Rapid Commun.*, **2018**, *39*, 1800588.

120. D. Wu, X. Xie, A. A. Kadi and Y. Zhang, *Chin. Chem. Lett.*, **2018**, *29*, 1098-1104.

121. Z. Zhou, Q. Yi, T. Xia, W. Yin, A. A. Kadi, J. Li and Y. Zhang, *Org. Biomol. Chem.*, **2017**, *15*, 2191-2198.

122. E. R. Draper, E. G. B. Eden, T. O. McDonald and D. J. Adams, *Nat. Chem.*, **2015**, *7*, 848-852.

123. P. Dawson, T. Muir, I. Clark-Lewis and S. Kent, *Science*, **1994**, *266*, 776-779.

124. Q. Wan and S. J. Danishefsky, *Angew. Chem. Int. Ed.*, **2007**, *46*, 9248-9252.

125. C. Bonfio, L. Valer, S. Scintilla, S. Shah, D. J. Evans, L. Jin, J. W. Szostak, D. D. Sasselov, J. D. Sutherland and S. S. Mansy, *Nat. Chem.*, **2017**, *9*, 1229-1234.

126. T. S. Chisholm, D. Clayton, L. J. Dowman, J. Sayers and R. J. Payne, *J. Am. Chem. Soc.*, **2018**, *140*, 9020-9024.

127. M. Lee, S. Neukirchen, C. Cabrele and O. Reiser, *J. Pept. Sci.*, **2017**, *23*, 556-562.

128. W. A. Pryor and E. G. Olsen, *J. Am. Chem. Soc.*, **1978**, *100*, 2852-2856.

129. O. Mozziconacci, B. A. Kerwin and C. Schöneich, *J. Phys. Chem. B*, **2011**, *115*, 12287-12305.

130. I. S. Alferiev, J. M. Connolly and R. J. Levy, *J. Organomet. Chem.*, **2005**, *690*, 2543-2547.

131. Y. Tian, L. Wang, J. Shi and H.-z. Yu, *Chinese J. Chem. Phys.*, **2015**, *28*, 269-276.

132. M. Zeldin, P. Mehta and W. D. Vernon, *Inorg. Chem.*, **1979**, *18*, 463-466.

133. R. Alan Aitken, M. J. Drysdale and B. M. Ryan, *J. Chem. Soc., Perkin Trans. 1*, **1998**, 3345-3348.

134. C. V. Raman, *Nature*, **1928**, *121*, 619-619.

135. S. Eissler, M. Kley, D. Bächle, G. Loidl, T. Meier and D. Samson, *J. Pept. Sci.*, **2017**, *23*, 757-762.

136. V. Krchňák, J. Vágner and M. Lebl, *Int. J. Pept. Protein Res.*, **1988**, *32*, 415-416.

137. T. Vojkovsky, *Pept. Res.*, **1995**, *8*, 236-237.

138. W. Kabsch, *Acta Cryst. D.*, **2010**, *66*, 125-132.

139. P. Evans, *Acta Cryst. D.*, **2006**, *62*, 72-82.

140. P. R. Evans and G. N. Murshudov, *Acta Cryst. D.*, **2013**, *69*, 1204-1214.

141. G. Sheldrick, *Acta Cryst. A*, **2008**, *64*, 112-122.

142. G. Sheldrick, *Acta Cryst. C*, **2015**, *71*, 3-8.

143. L. Farrugia, *J. Appl. Crystallogr.*, **2012**, *45*, 849-854.

144. J.-J. Yan, D. Wang, D.-C. Wu and Y.-Z. You, *Chem. Commun.*, **2013**, *49*, 6057-6059.

145. A. Tourteau, E. Merlet, A. Bontemps, M. Leland, P. Helissey, S. Giorgi-Renault and S. Desbène-Finck, *Eur. J. Org. Chem.*, **2015**, *2015*, 7028-7035.

146. L. Castañeda, Z. V. F. Wright, C. Marculescu, T. M. Tran, V. Chudasama, A. Maruani, E. A. Hull, J. P. M. Nunes, R. J. Fitzmaurice, M. E. B. Smith, L. H. Jones, S. Caddick and J. R. Baker, *Tetrahedron Lett.*, **2013**, *54*, 3493-3495.